International Mine Water Association Congress New Zealand 2020 Proceedings

James Pope, Christian Wolkersdorfer
Lotta Sartz, Anne Weber
Karoline Wolkersdorfer


MINE WATER
SOLUTIONS

MINE WATER SOLUTIONS

Proceedings of the postponed 14th IMWA Congress – "Mine Water Solutions"

9–13 November 2020

Christchurch, New Zealand

Editors

James Pope

Christian Wolkersdorfer

Lotta Sartz

Anne Weber

Karoline Wolkersdorfer

International Mine Water Association

Mine Water Solutions
2020, Christchurch, New Zealand

ISBN 978-3-00-067297-2

Editors
James Pope, Christian Wolkersdorfer, Lotta Sartz, Anne Weber, Karoline Wolkersdorfer

Cover Design
Karoline Wolkersdorfer

Layout and Typesetting
Jigsaw Graphic Design

Cover Photographs
Yoal Desurmont on Unsplash – Mount Cook Road in Canterbury, New Zealand

Foreword Image
Daniel Campos on Vecteezy – Kiwi Bird

All abstracts were reviewed by 2–3 experts of the International Scientific Committee

www.IMWA.info

Organizers

Verum Group

Verum Group

International Mine Water Association

14TH IMWA CONGRESS
MINE WATER SOLUTIONS
CHRISTCHURCH TOWN HALL
9-13 NOVEMBER 2020

International Scientific Committee (ISC)

Lena Alakangas, Sweden
Bert Allard, Sweden
John George Annandale, South Africa
Margarida Horta Antunes, Portugal
Carlos Felipe Aravena, Chile
Tim Aubel, Germany
Mattias Bäckström, Sweden
Jeff Bain, Canada
Selina Mary Bamforth, United Kingdom
Andre Banning, Germany
Maria Dolores Basallote, Spain
Sod-Erdene Bazardorj, Mongolia
Melanie Lise Blanchette, Australia
David Blowes, Canada
Andrey Bogomolov, Russia
Anna Bogush, United Kingdom
Rob Bowell, United Kingdom
Jo Burgess, South Africa
Manuel Antonio Caraballo Monge, Chile
Rosa Cidu, Italy
Henk Coetzee, South Africa
David Craw, New Zealand
Andy Davs, United States
Camilo Raul de los Hoyos, Argentina
Gareth Digges La Touche, United Kingdom
Wenfeng Du, China
Lee Evans, Australia
Marlese Fairgray, Australia
Nuria Fernandez Castro, Brazil
Rafael Fernandez-Rubio, Spain
Adriano Fiorucci, Italy
Elvis Fosso-Kankeu, South Africa
Silvia Cristina Alves França, Brazil
Rudy Sayoga Gautama, Indonesia
Cleber Jose Baldoni Gomes, Brazil
William Mario Goodman, United States
Jabulani Gumbo, South Africa
Robert S. Hedin, United States
Altus Huisamen, South Africa
Andrei Ivanets, Belarus
Ryan Thomas Jakubowski, United States
Sajjad Jannesar Malakooti, Iran
Adam Paul Jarvis, United Kingdom
Lucinda Johnson, United States
Raymond H. Johnson, United States
Andrew Clifford Johnstone, South Africa
David Richard Jones, Australia
Margarete Maria Kalin, Switzerland
Päivi M. Kauppila, Finland
Anu Kettunen, Finland
Elena Khayrulina, Russia
Lisa Bithell Kirk, United States
Robert Lawrence Kleinmann, United States
Frans Knops, Netherlands
Konstantinos Kollias, Greece
Oleg Kovin, Russia
Natalie A. S. Kruse, United States
Olga Kudryashova, Russia
Morten Birch Larsen, Denmark
Ulla Lassi, Finland
Anthony Le Beux, France
Simon Antony Lorentz, South Africa
Michael Losavio, United States
Paul Joel Lourens, South Africa
Mark Lund, Australia
Rudzani Lusunzi, South Africa
Tatyana Lyubimova, Russia
Justin Kambale Maganga, Kenya
Maria Mamelkina, Finland
Malibongwe Shadrach Manono, South Africa
Cherie McCullough, Australia
Matthew P. McGann, Peru
Broder Merkel, Germany
Thomas Metschies, Germany
Michael Arthur Milczarek, United States
Jacek Motyka, Poland
Kevin Myers, United States
Robert W. Nairn, United States
Carmen Mihaela Neculita, Canada
Darrell Kirk Nordstrom, United States
Damian Onwudiwe, South Africa
Iuliia Ozarian, Russia
Michael Paul, Germany
Steven Richard Pearce, United Kingdom

Tobias Merlijn Pinkse, Germany
Walter L. Pohl, Austria
James Pope, New Zealand
Xunchi Pu, China
Nada Rapantova, Czech Republic
Pierre Rousseau, Australia
Carlos Ruiz Cánovas, Spain
David Anthony Salmon, Australia
Lotta Sartz, Sweden
Christopher James Satterley, United Kingdom
Ivo André Homrich Schneider, Brazil
Ralph Schöpke, Germany
Martin Schultze, Germany
Robert R. Seal, United States
Alison Sinclair, Australia
Abhay Soni, India
Peter Clive Stanley, United Kingdom
Wanghua Sui, China
Jacek Szczepiński, Poland
Esther Takaluoma, Finland
Teresa Maria Valente, Portugal
Danie Vermeulen, South Africa
Denys Villa Gomez, Australia
Wolf von Igel, Chile
Changshen Wang, China
John Douglass Waterhouse, Australia
Anne Weber, Germany
Paul Weber, New Zealand
Jenny Webster-Brown, New Zealand
Holger Weiß, Germany
Phil Whittle, Australia
Christian Wolkersdorfer, South Africa
Peter Woods, Australia
Dongjing Xu, China
Jorge Zafra, Peru
Sergey Zhdanov, Russia

Local Organizing Committee (LOC)

Champion

James Pope	*Verum Group*

Members

Dave Trumm	*Verum Group*
Hana Christenson	*Verum Group*
Paul Weber	*Mine Waste Management*
Jenny Webster-Brown	*Lincoln University*

Administration

Karoline Wolkersdorfer	*wolke events*
Mandy Train	*conference innovators*

IMWA 2020 Sponsors & Partners

Verum Group

BATHURST RESOURCES LIMITED

MINE WASTE MANAGEMENT

NZCC NEW ZEALAND COAL & CARBON LTD

14TH IMWA CONGRESS
MINE WATER SOLUTIONS
CHRISTCHURCH TOWN HALL
9-13 NOVEMBER 2020

Kia ora koutou – Greetings dear Delegate for the 14th IMWA Congress,

"Welcome to IMWA 2020 New Zealand!", that's how we intended to greet you in Christchurch, the largest city on the South Island of New Zealand. We're sure many of you had planned an itinerary before or after IMWA 2020 to explore our islands and make the most of your time in our remote part of the globe. Sadly, we had to inform our delegates that IMWA 2020 in New Zealand has been postponed in response to disruption by the COVID-19 pandemic on global travel and economic conditions. This was a difficult decision several months ago as the trajectory of the COVID-19 pandemic was less clear than now, but the right decision was made. The New Zealand based Organizing Committee has agreed with the IMWA Executive Committee that another IMWA Conference in New Zealand at a similar time of year and with similar offerings of short courses, field trips and keynote speakers will happen. We hope that the delay, though frustrating, only builds your anticipation and desire to visit New Zealand and participate in IMWA 2022 in Christchurch.

We discussed holding IMWA 2020 online but withdrew from this type of format, because all of us had negative experience with online meetings, and IMWA is a truly international organisation with delegates in every time zone around the globe. We are almost a year into the Pandemic, and electronic ways to communicate and hold online meetings have substantially improved, but we still think that the IMWA family is only a family when we can see and chat with each other face to face. Presentations online are a useful tool, but simply don't replace live speakers' attentive audiences, insightful questions, or subsequent discussions over coffee, food or great beer and wine. So, we believe we made the correct decision.

All of us were looking forward to a fantastic IMWA Congress in New Zealand this year. 223 abstracts were accepted for presentation, and 40 of them are now published in these proceedings. They cover the full range of mine water related topics by experts from all around the world. Though you can't listen to the presentations, we hope that you still can enjoy reading the related papers. Especially because of these unintended changes, the authors did a great job to compile and write their papers for these proceedings. It shows us that a Pandemic like that can interrupt face to face communication, but it can't beat our enthusiasm for mine water and our international friendship.

We want to thank all our reviewers from the International Scientific Committee (ISC), the people behind the scenes who partially organised IMWA 2020, and our collaborators and sponsors. It was fantastic to work together with you to share a vision and we look forward to working together again to deliver IMWA 2022.

Stay tuned, dear friends all around the world, and let's work on IMWA 2021 in Wales and IMWA 2022 in New Zealand. Let's keep in contact through e-mail and social media and online meetings. And let's look positively into the future. There will be a time when the Pandemic is over, we will have a vaccine and we will be able to see each other again.

Keep healthy and with the German miner's greeting "Glückauf" we are wishing you all the best!

Christian Wolkersdorfer – IMWA President

James Pope – IMWA 2020 Chair

Contents

1 Mine Drainage Chemistry

2 Passive Treatment Innovation

Ayanda Nomaswazi Shabalala
Efficacies of Pervious Concrete and Zero-Valent Iron as Reactive Media for Treating Acid Mine Drainage 83

3 Bio-geochemical Systems

Nikolay Maksimovich, Vadim Khmurchik, Olga Meshcheriakova, Artem Demenev, Olga Berezina
The Use of Industrial Alkaline Wastes to Neutralise Acid Drain Water from Waste Rock Piles 117

Robert W. Nairn, Julie A. LaBar, Leah R. Oxenford, Nicholas L. Shepherd, Brandon K. Holzbauer-Schweitzer, Juan G. Arango, Zepei Tang, Dayton M. Dorman, Carlton A. Folz, Justine I. McCann, JD Ingendorf, Harper T. Stanfield, Robert C. Knox
Toward Sustainability of Passive Treatment in Legacy Mining Watersheds: Operational Performance and System Maintenance 123

4 Waste Rock Storage

5 Tailings Storage

6 Rehabilitation

7 Conventional Water Treatment

11 Legacy Mine Impacts and Clean Up

12 Mine Catchment Assessments

REE Enrichment Pattern in Acid Mine Drainage and Overburden from Coal Mine in Indonesia

Abie Badhurahman[1], Rudy Sayoga Gautama[1], Ginting Jalu Kusuma[1]

[1]*Department of Mining Engineering, Institut Teknologi Bandung, Jl. Ganesha I0, Bandung 40132, Indonesia*

Abstract

Acid mine drainage (AMD) is one of main negative environmental impact from mining activities. AMD is resulted from reaction between sulfide mineral, mainly pyrite, with oxygen and water. AMD characterized as high-acidic water with elevated sulfate, iron and other dissolved metals concentration, including rare earth elements (REE). REE is used as an indicator in water-rock interaction and pollution of AMD and as a source of REE. Studies show that North American Shale Composite (NASC) normalized REE concentration in AMD has pattern or enrichment, i.e. medium rare earth elements enrichment (MREE) or light rare earth elements (LREE), despite the processes controlling this enrichment are still unknown and unclear whether related to sources or aqueous process.

This study is conducted in PT Bukit Asam coal mine in Indonesia, which consist of 3 main coal mines namely Banko Barat, Tambang Air Laya and Muara Tiga Besar. Those mines show varieties in geochemical characteristics of water and overburden. Previous studies showed that there is indication of REE-enrichments in AMD from PT Bukit Asam, Indonesia. This study aims to characterize REE enrichment in AMD and overburden samples from PT Bukit Asam coal mine, Indonesia.

Geochemical characteristics of REE in AMD and overburden from PT Bukit Asam coal mine, Indonesia were investigated by determining concentration of dissolved REE and other geochemical parameters of 11 AMD samples and concentration of REE from 24 overburden samples. The REE concentration is normalized using) to determine the enrichment pattern of REE of both type of sample. Those samples are representing 3 main mines in PT Bukit Asam coal mine. AMD samples have varying pH value, dissolved Fe and dissolved Mn of 2.74 – 5.91, 0.11 – 29,78 mg/L and 2.83 – 16.35 mg/L, respectively. AMD samples shows elevated dissolved ΣREE concentration varying from 5.54 – 261.05 µg/L. The overburden samples have varying ΣREE concentration from 14.95 mg/kg to 106.95 mg/kg. NASC-normalized REE concentration of all AMD samples shows distinctive MREE (medium rare earth elements) enrichment pattern. In the other hand, overburden samples show variety of enrichment pattern, mostly MREE.

Similarity between enrichment type of AMD and overburden samples shows that processes controlling REE enrichment in AMD is somewhat relate to the source of REE. Further study on the mechanism of REE enrichment from overburden to AMD to determine whether the mechanism is controlled by the source of REE or the geochemical characteristics of AMD is needed to obtain more information of processes of REE enrichment in AMD.

Keywords: acid mine drainage (AMD), overburden, rare earth elements (REE), enrichment

Introduction

Mining activities potentially cause substantial environmental impacts. Excavation and dumping activities might expose sulfide minerals that previously confined in rocks beneath the surface to the open air. Contact between oxygen, sulfide and water minerals will lead to oxidation reactions that produce acid mine drainage (AMD). AMD is an acidic water formed by oxidation of sulphide minerals and characterised by a low pH or below pH value of 5 (Gautama 2014).

Acid mine drainage due to its characteristic, is able to leach hard metals (including REE) from rocks. Research on the leaching process and accumulation of hard rocks are widely available, but leaching process and accumulation of REE by AMD especially which of that related to coal mine is still scarce. This study aims to demonstrate the REE enrichment patterns in water and overburden samples from PTBA which served as an initial indication of REE-enrichment process from overburden to water in coal mine.

General Information

This study is conducted in PT Bukit Asam (PTBA) coal mine in Indonesia PTBA is one of major coal producers, located at Tanjung Enim, South Sumatra Province. There are 3 main mining sites that are still active, namely Muara Tiga Besar (MTB), Bangko Barat (BB) and Tambang Air Laya (TAL). Previous work by Gautama (1994) and Gautama and Hartaji (2004) has shown that acid mine drainage is an important issue at the Tanjung Enim mine. Gautama and Hartaji (2004) demonstrated that the source of the AMD is predominantly from the overburden and inter-seam rocks (interburden) and they were able to differentiate between potentially acid forming (PAF) and non-acid forming (NAF) rocks by the application of both static and kinetic testing procedures. The PTBA pits yield different mine water quality, as reported by Gautama (2018), due to different geochemical characteristic of rocks, spatially and stratigraphically. It is evident also that there is elevated concentration of Fe and Mn, as well as REE, which also varying for each pit (Gautama 2018).

Sample Information

11 samples of AMD samples are sampled from various pit sumps otherwise from detention pond if not accessible. 24 samples of overburden are taken from various lithology and stratigraphy from all three mining sites.

Methods

Measurements of pH is conducted in the field using Lutron WA-2017 SD. AMD samples are filtered with 45 μm filter disc and stored in 2 different bottles for each sample. One bottle of sample is acidified using HNO3 for measurements of cation and REE. Cation (Fe and Mn) are measured using Perkin Elmer Atomic Absorption Spectrometer (AAS) analyst 400S and REE concentration is measured using Inductively Coupled Plasma Mass Spectrometer (ICP-MS) Agilent 7000. All instruments are calibrated prior measurements. Overburden samples are pulverized into size less than 75 μm, measured ±500 mg and digested using ultrapure concentrated acid (HF + aqua regia) in Teflon digestion crucibles at 180 °C. After cooling, the vessel contents centrifuged then discharging, diluted to volume of 10 mL. REE concentration then is measured using Inductively-Coupled Plasma Mass Spectrometer (ICP-MS) Agilent 7000. Standard and blanks are also measured alongside the AMD and overburden samples. REE concentration of water and overburden samples are then normalized using North American Shale Composites (NASC) value (McLennan et al., 1980) to determine the REE enrichment pattern of those samples.

Results

The result of REE concentration and water geochemical characteristic (pH, Total Fe and Mn) for water samples are shown in Table 1. REE concentration for overburden samples are shown in Table 2, Table 3 and Table 4. (on the next page).

REE enrichment pattern

REE enrichment parameters are calculated to determine the enrichment pattern of REE concentration in water and overburden samples. There are mainly 3 types of REE-enrichment patterns, i.e. LREE/Light REE, MREE/Medium REE and HREE/heavy REE. Common calculations used in determining enrichment pattern of REE are shown in Table 5. The calculation result of REE enrichment pattern parameter for water samples and overburden samples is shown in Table 6.

AMD samples have varying pH value, dissolved Fe and dissolved Mn of 2.74 – 5.91, 0.11 – 29,78 mg/L and 2.83 – 16.35 mg/L, respectively. AMD samples shows elevated dissolved ΣREE concentration varying from 5.54 – 261.05 μg/L. In the other hand, overburden samples have varying ΣREE concentration from 14.95 mg/kg to 106.95 mg/kg.

Table 1 REE Concentration in Water Samples (Sample ID SW1 – SW8).

Sample ID	SW1	SW2	SW3	SW4	SW5	SW6	SW7	SW8	SW9	SW10	SW11
Mining Site	BB	BB	TAL	TAL	BB	MTB	TAL	TAL	BB	TAL	TAL
pH	2.74	2.84	5.23	4.85	3.05	4.05	5.82	5.18	3.87	4.05	5.91
ΣFe (mg/L)	0.76	1.07	0.00	0.01	0.13	0.01	0.01	0.04	0.01	0.01	0.00
Mn (mg/L)	0.40	0.39	0.22	0.10	0.27	0.25	0.37	0.60	0.36	0.39	0.22
					concentration in µg/L						
La	42.09	37.14	1.54	6.91	24.40	7.77	1.82	9.25	13.96	11.71	1.17
Ce	96.34	67.11	2.68	11.55	47.77	16.55	1.96	16.64	21.29	28.31	1.81
Pr	11.69	6.71	0.20	1.26	5.59	1.84	0.18	1.81	2.57	3.20	0.18
Nd	47.24	24.46	0.75	4.50	22.49	7.22	0.69	7.12	9.73	13.22	0.71
Sm	12.15	4.73	0.17	0.89	5.80	1.70	0.14	1.69	2.16	3.61	0.15
Eu	3.24	1.18	0.05	0.27	1.54	0.47	0.05	0.46	0.55	1.01	0.05
Gd	14.81	5.67	0.23	1.19	7.07	2.22	0.27	2.30	2.62	4.90	0.23
Tb	2.34	0.83	0.04	0.17	1.12	0.34	0.04	0.32	0.38	0.79	0.03
Dy	13.94	4.63	0.20	0.93	6.60	2.01	0.19	1.92	2.30	4.76	0.20
Ho	2.68	0.94	0.05	0.19	1.25	0.39	0.04	0.38	0.45	0.95	0.04
Er	7.15	2.50	0.11	0.49	3.25	1.03	0.10	0.95	1.20	2.53	0.11
Tm	0.95	0.33	0.02	0.06	0.42	0.13	0.01	0.12	0.14	0.33	0.01
Yb	5.61	1.80	0.08	0.32	2.49	0.78	0.05	0.70	0.87	1.89	0.07
Lu	0.82	0.27	0.02	0.05	0.35	0.11	0.01	0.11	0.13	0.27	0.01
ΣREE	261.05	158.28	6.14	28.79	130.16	42.56	5.54	43.78	58.33	77.48	4.78

Table 2 REE Concentration in Overburden Samples (Sample ID S1 – S8).

Sample ID	S1	S2	S3	S4	S5	S6	S7	S8
Mining Site	BB	MTB	BB	BB	TAL	TAL	TAL	TAL
				concentration in mg/kg				
La	17.53	15.51	17.85	18.05	3.3	4.37	1.51	21.16
Ce	33.67	37.18	34.37	43.83	8.03	10	4.32	46.81
Pr	3.43	4.15	3.52	4.74	1.01	1.27	0.64	5.01
Nd	12.06	16.54	12.16	18.69	4.14	5.06	3.18	17.92
Sm	2.45	3.71	2.55	4.15	1.02	1.2	1.17	3.72
Eu	0.22	0.9	0.21	1.02	0.26	0.31	0.33	0.47
Gd	2.52	3.47	2.47	3.92	1.05	1.18	1.59	3.28
Tb	0.42	0.52	0.42	0.59	0.17	0.17	0.24	0.46
Dy	2.69	2.98	2.59	3.31	1	0.95	1.13	2.27
Ho	0.57	0.57	0.54	0.63	0.21	0.18	0.18	0.36
Er	1.73	1.58	1.56	1.66	0.62	0.49	0.37	0.85
Tm	0.26	0.22	0.22	0.23	0.09	0.06	0.04	0.1
Yb	1.75	1.35	1.43	1.44	0.57	0.35	0.22	0.63
Lu	0.28	0.2	0.22	0.21	0.09	0.05	0.03	0.09
ΣREE	79.59	88.89	80.11	102.46	21.56	25.65	14.95	103.13

From Table 6. it is evident that all water samples showed Medium-REE/MREE enrichment pattern, with value of (MREE/MREE*) NASC more than 1 (ranged from 1.18 to 1.57). 5 samples are also exhibit LREE-enrichment pattern (Sample SW-1, SW-2, SW-4, SW-7 and SW-9), but generally enrichment patterns for all water samples are categorized as MREE-Enrichment.

REE enrichment in overburden samples show more varying result. 15 samples show MREE-enrichment with (MREE/MREE)NASC (Sm/Yb)NASC dan (Sm/La)NASC value more than 1.20, 6 samples show LREE-enrichment pattern and only 3 samples, i.e. S-1; S-5;-S16 show HREE-enrichment.

Table 3 REE Concentration in Overburden Samples (Sample ID S9 – S16).

Sample ID	S9	S10	S11	S12	S13	S14	S15	S16
Mining Site	TAL	TAL	BB	MTB	MTB	TAL	BB	MTB
				REE concentration in mg/kg				
La	7.3	5.82	18.08	7.49	22.35	11.01	8.2	11.69
Ce	18.44	16.05	33.72	15.51	45.37	29.43	26.95	27.77
Pr	2.21	1.94	3.35	1.5	4.52	3.29	3.22	3.01
Nd	9.43	8.37	11.04	4.93	14.78	13.65	13.37	12.1
Sm	2.39	2.19	2.21	0.94	2.83	3.15	3.09	2.7
Eu	0.63	0.56	0.29	0.12	0.26	0.79	0.74	0.72
Gd	2.58	2.32	2.14	0.81	2.5	3.17	2.86	2.98
Tb	0.4	0.36	0.37	0.13	0.41	0.46	0.44	0.48
Dy	2.34	2.1	2.39	0.84	2.53	2.49	2.52	3.08
Ho	0.46	0.41	0.49	0.17	0.52	0.45	0.49	0.67
Er	1.27	1.15	1.49	0.52	1.57	1.19	1.35	2.09
Tm	0.18	0.16	0.23	0.08	0.25	0.15	0.19	0.3
Yb	1.08	0.99	1.52	0.55	1.79	0.92	1.23	1.96
Lu	0.16	0.15	0.23	0.09	0.29	0.13	0.19	0.31
ΣREE	48.87	42.56	77.55	33.68	99.97	70.28	64.83	69.86

Table 4 REE Concentration in Overburden Samples (Sample ID S17 – S24).

Sample ID	S17	S18	S19	S20	S21	S22	S23	S24
Mining Site	MTB	BB	BB	BB	BB	BB	BB	MTB
				REE concentration in mg/kg				
La	18.39	12.15	12.75	8.6	6.72	9.7	7.31	5.85
Ce	45.2	32.42	33.58	23.92	18.18	25.82	20.31	15.76
Pr	5	3.5	3.7	2.77	2.13	3.04	2.28	1.8
Nd	20.05	13.87	14.65	11.31	8.86	12.6	9.33	7.18
Sm	4.4	3.08	3.22	2.7	2.16	3.03	2.18	1.6
Eu	1.07	0.74	0.77	0.7	0.55	0.76	0.53	0.4
Gd	4.09	2.81	2.91	2.67	2.18	2.93	2	1.52
Tb	0.62	0.41	0.43	0.4	0.33	0.43	0.28	0.21
Dy	3.52	2.27	2.24	2.3	1.86	2.44	1.52	1.18
Ho	0.66	0.41	0.39	0.43	0.34	0.44	0.27	0.21
Er	1.82	1.06	0.98	1.15	0.93	1.2	0.7	0.51
Tm	0.26	0.14	0.12	0.15	0.12	0.16	0.09	0.06
Yb	1.64	0.8	0.73	0.91	0.75	1.01	0.54	0.34
Lu	0.24	0.11	0.1	0.13	0.1	0.16	0.08	0.05
ΣREE	106.95	73.75	76.57	58.15	45.22	63.73	47.42	36.67

Table 5 Equation for Enrichment Pattern Parameter of REE.

Enrichment Parameter	Calculation used
LREE enrichment relative to HREE	$=(La/Yb)_{NASC}$
LREE enrichment relative to MREE	$=(La/Sm)_{NASC}$
MREE enrichment relative to LREE	$=(Sm/\mathrm{La})_{NASC}$
MREE enrichment relative to HREE	$=(Sm/Yb)_{NASC}$
HREE enrichment relative to LREE	$=(\mathrm{Yb}/\mathrm{La})_{NASC}$
HREE enrichment relative to MREE	$=(\mathrm{Yb}/\mathrm{Sm})_{NASC}$
MREE Enrichment Relative to LREE and HREE	$(MREE/MREE^{*})_{NASC} = \frac{\overline{MREE_{NASC}}}{\sqrt{\overline{LREE}_{NASC} \times \overline{HREE_{NASC}}}}$

Table 6 Calculation for Enrichment Pattern Parameter of REE in Water and Overburden Samples.

Sample ID	$(La/Yb)_{NASC}$	$(La/Sm)_{NASC}$	$(Sm/Yb)_{NASC}$	$(Sm/La)_{NASC}$	$(Yb/La)_{NASC}$	$(Yb/Sm)_{NASC}$	(MREE/ MREE*)NASC
Water Samples							
SW1	0.74	0.62	1.19	1.61	1.35	0.84	1.53
SW2	2.03	1.41	1.44	0.71	0.49	0.69	1.18
SW3	1.85	1.65	1.12	0.61	0.54	0.89	1.19
SW4	2.12	1.4	1.52	0.72	0.47	0.66	1.32
SW5	0.96	0.76	1.27	1.32	1.04	0.78	1.55
SW6	0.98	0.82	1.19	1.21	1.02	0.84	1.47
SW7	3.32	2.3	1.44	0.43	0.3	0.69	1.36
SW8	1.29	0.98	1.31	1.02	0.77	0.76	1.47
SW9	1.57	1.16	1.35	0.86	0.64	0.74	1.34
SW10	0.61	0.58	1.05	1.72	1.64	0.96	1.57
SW11	1.72	1.44	1.2	0.7	0.58	0.83	1.32
Overburden Samples							
S1	0.98	1.28	0.77	0.78	1.02	1.31	0.86
S2	1.13	0.75	1.50	1.33	0.89	0.67	1.34
S3	1.23	1.26	0.98	0.80	0.82	1.03	0.91
S4	1.23	0.78	1.58	1.28	0.81	0.63	1.34
S5	0.56	0.58	0.97	1.72	1.77	1.03	1.30
S6	1.23	0.65	1.88	1.54	0.82	0.53	1.54
S7	0.68	0.23	2.93	4.29	1.46	0.34	2.98
S8	3.31	1.02	3.24	0.98	0.30	0.31	1.22
S9	0.67	0.55	1.21	1.82	1.50	0.83	1.48
S10	0.58	0.48	1.21	2.09	1.73	0.83	1.50
S11	1.17	1.47	0.80	0.68	0.85	1.25	0.86
S12	1.35	1.44	0.94	0.70	0.74	1.07	0.81
S12	1.35	1.44	0.94	0.70	0.74	1.07	0.81
S13	1.23	1.42	0.87	0.71	0.81	1.15	0.78
S14	1.18	0.63	1.88	1.59	0.85	0.53	1.54
S15	0.66	0.48	1.38	2.09	1.52	0.73	1.40
S16	0.59	0.78	0.76	1.29	1.70	1.32	1.12
S17	1.10	0.75	1.47	1.33	0.91	0.68	1.32
S18	1.49	0.71	2.10	1.41	0.67	0.48	1.44
S19	1.72	0.71	2.42	1.41	0.58	0.41	1.49
S20	0.93	0.57	1.62	1.75	1.08	0.62	1.52
S21	0.88	0.56	1.57	1.79	1.14	0.64	1.55
S22	0.95	0.58	1.64	1.74	1.06	0.61	1.51
S23	1.35	0.60	2.23	1.66	0.74	0.45	1.55
S24	1.71	0.72	2.61	1.52	0.58	0.38	2.64

Discussion

Convex pattern in NASC-normalized REE concentration, which indicated medium-REE/MREE enrichment is one of signature of REE-enrichment in acid mine drainage/AMD (Cao et al. 2019; Zhao et al. 2007), despite other study showed that Light REE/LREE enrichment pattern in acid mine drainage (Bozau et al. 2004) Several studies also showed the same pattern of REE-enrichment from water samples and sediment samples which indicates the possibility of REE enrichment in water from its source (Zhao et al. 2007).

This study results that 15 of 24 samples of overburden samples show MREE enrichment pattern (15 out of 24 samples) and all water samples show MREE enrichment pattern which indicates the possibility of enrichment in water samples is controlled by enrichment of its source.

Conclusions

Similarity between enrichment type of AMD and overburden samples shows that processes controlling REE enrichment in AMD is somewhat relate to the source of REE, in this study the overburden. Further study on the mechanism of REE enrichment from overburden to AMD to determine whether the mechanism is controlled by the source of REE or the geochemical characteristics of AMD is needed to obtain more information of processes of REE enrichment in AMD.

Acknowledgements

The authors thank PT Bukit Asam for assisting during sampling, Dr. Bill Perkins from Aberystwyth University for assisting during laboratory testing and other parties for help and assistance during sampling, testing and analysis.

References

Bozau, E., Leblanc, M., Seidel, J. L., & Stärk, H.-J. (2004). Light Rare Earth Elements enrichment in an acidic mine lake (Lusatia, Germany). *Applied Geochemistry*, 19(3), 261–271. https://doi.org/https://doi.org/10.1016/S0883-2927(03)00150-1

Cao, X., Zhou, S., Xie, F., Rong, R., & Wu, P. (2019). The distribution of rare earth elements and sources in Maoshitou reservoir affected by acid mine drainage, Southwest China. *Journal of Geochemical Exploration*, 202, 92–99. https://doi.org/https://doi.org/10.1016/j.gexplo.2019.03.019

Gautama, R. S. (1994): Acid Water Problem in Bukit Asam Coal Mine, South Sumatra, Indonesia. – Proceedings, 5th International Mine Water Congress, Nottingham, U.K., 2: 533-542, 5 fig., 2 tab.; Nottingham.

Gautama, R.S. & Hartaji, S. (2004). "Improving the Accuracy of Geochemical Rock Modelling for Acid Rock Drainage Prevention in Coal Mine". Mine Water and the Environment. 23,100-104.

Gautama, Rudy Sayoga; Perkins, William; Bird, Graham; Adjie, Wisjnoe; Moore, Oliver; Kusuma, Ginting Jalu; Badhurahman, Abie (2018): Acid Mine Drainage in a Tropical Environment: A Case Study from Bukit Coal Mine Site in South Sumatra, Indonesia. – In: Wolkersdorfer, Ch.; Sartz, L.; Weber, A.; Burgess, J. & Tremblay, G.: Mine Water – Risk to Opportunity (Vol II). – p. 611 – 617; Pretoria, South Africa (Tshwane University of Technology).

McLennan, S. M., Nance, W. B., & Taylor, S. R. (1980). Rare earth element-thorium correlations in sedimentary rocks, and the composition of the continental crust. *Geochimica et Cosmochimica Acta*, 44(11), 1833–1839. https://doi.org/https://doi.org/10.1016/0016-7037(80)90232-X

Zhao, F., Cong, Z., Sun, H., & Ren, D. (2007). The geochemistry of rare earth elements (REE) in acid mine drainage from the Sitai coal mine, Shanxi Province, North China. *International Journal of Coal Geology*, 70(1), 184–192. https://doi.org/https://doi.org/10.1016/j.coal.2006.01.009

Trace Element (As, F, U) Contamination and Hydrogeochemistry in the Vicinity of a Mexican Ore Mine

Andre Banning[1], Desiree Schwertfeger[1], Sócrates Alonso Torres[2], Antonio Cardona Benavides[3]

[1]*Hydrogeology Department, Faculty of Geosciences, Ruhr University Bochum, Universitätsstr. 150, 44801 Bochum, Germany, andre.banning@rub.de*

[2]*Postgraduate Program in Minerals Engineering, Faculty of Engineering, Universidad Autónoma de San Luis Potosí (UASLP), Mexico*

[3]*Earth Sciences Department, Faculty of Engineering, UASLP, Mexico*

Abstract

Dissolved fluoride (F), arsenic (As) and uranium (U) concentrations in ground and surface waters around the San Antonio el Grande Mine in Chihuahua, Mexico, exceed WHO drinking water limits for F and As, and the German guideline value for U in 72.8%, 64.0% and 58.4% of all samples, and thus threaten the most important drinking water source in the region. To address the question of the origin of elevated concentrations and the underlying mobilisation and transport processes, element distributions of 125 water samples were analysed and evaluated. Lithology is dominated by acidic igneous rocks and limestones with numerous mineralisation zones. Solution processes were identified as the main driver for the increased concentrations depending on pH value, temperature and redox potential.

Keywords: Metal ore mining, Mexico, uranium, arsenic, fluoride

Introduction and study area

Groundwater around the San Antonio el Grande Mine in Chihuahua, Mexico, was found to partly contain elevated concentrations of several trace elements of toxicological concern, amongst them arsenic (As), uranium (U) and fluoride (F). Their origin, distribution and mobilization were unknown which gave rise to the present study.

The study area forms part of the eastern edge of the Sierra Madre Occidental (400 km wide and 1500 km long structure in the north-western part of Mexico), is semi-arid (average annual precipitation from 280–420 mm/year) with a mean annual temperature of 17.3–20.1 °C and ephemeral streams. It is located in the North America tectonostratigraphic terrane characterized by Tithonian to Albian basal conglomerate, limestone, fine grained marine siliciclastic rocks, deposited in the Chihuahua Trough (Sedlock et al. 1993). Massive limestone (Lower Cretaceous), light grey micrite and biomicrite with locally abundant biostromes and chert beds, outcrop in the Santo Domingo mountain (Fig. 1). It is overlain by a thin-bedded limestone-arenite and a thin to medium-bedded limestone-mudstone with bioclasts and hematite concretions (Upper Cretaceous). Tertiary rocks (Eocene-Oligocene) unconformably overly the Cretaceous sequence; magmatic rocks in the area include mostly felsic plutonic and volcanic rocks of the upper volcanic complex (pyroclastic and polymictic conglomerate, dacite, rhyolitic porphyry, rhyolitic ignimbrite-tuff, rhyolite and basalt) of McDowell and Keiser (1977). Most of these rocks were erupted from overlapping caldera complexes. Tectonic extension during Miocene to Pleistocene created large-scale N-S oriented horst and graben structures occupied with basin fill sediments.

The Santa Eulalia mining district within the study area consists of calc-silicate skarns and massive sulfide orebodies containing Pb-Zn-Ag deposits. The mineralization is associated to felsite intrusions, ore textures indicate mineralization occurred primarily by limestone replacement (Megaw 1990). At the time of field work, the San Antonio mine was

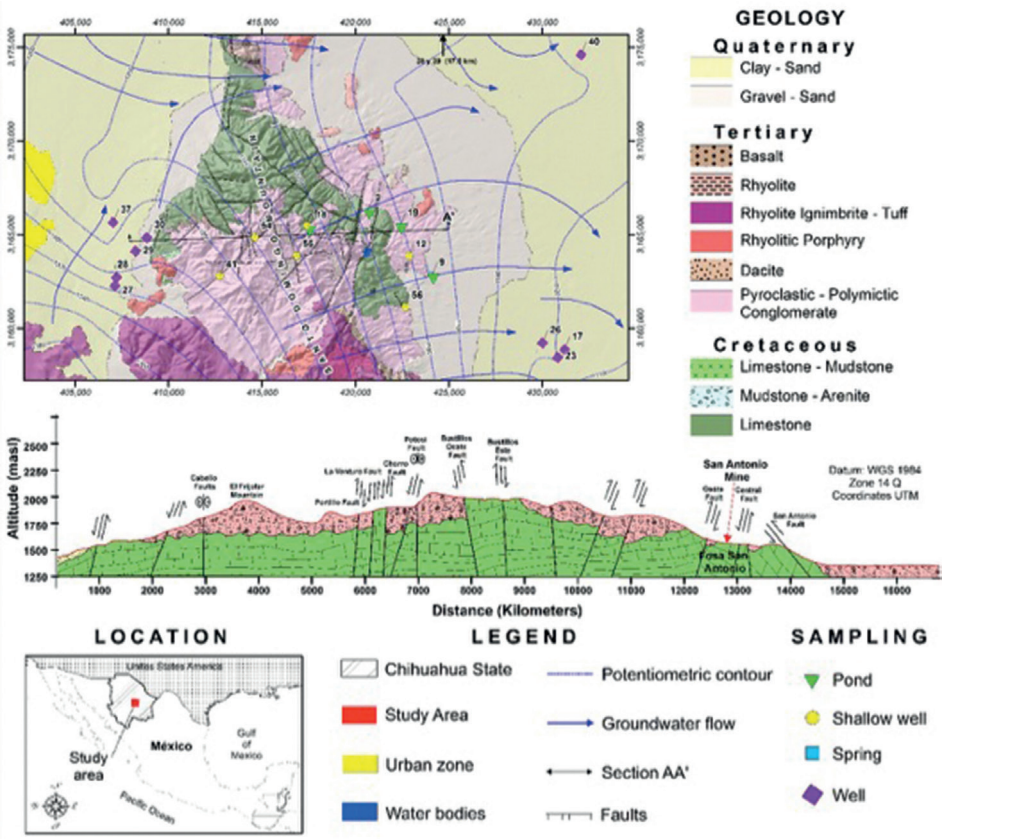

Figure 1 *Geological and piezometric map, and geological cross section through the study area.*

producing Pb-Zn-Ag concentrate, nowadays the mining operation has been terminated after a big flood event inside the mine.

The granulometric distribution and thickness of the basin fill sediments is determined by the graben geometry, gravel and sand sediments are generally associated with alluvial fan deposits, to clay-sand deposits in the playa region. The identified hydrogeological units in the study area include: i) karstic unit (Cretaceous massive limestone), ii) fractured unit (Tertiary volcanic rocks) and iii) granular unit (basin fill and alluvial sediments). Groundwater flow determined from water level measurements in wells and in the mining operation, indicate a south to north direction in the western flank of the Santo Domingo mountain, a northeast flow direction from side to side of the Santo Domingo Mountain flowing through the karstic unit; and groundwater flow from west to east along the basin fill sediments eastern edge of the mountain (Fig. 1).

Methods

The data set consists of 125 water samples – 118 groundwater samples and seven surface water samples – all taken between December 2013 and December 2015. Parameters such as pH, temperature, redox potential, electrical conductivity, dissolved oxygen and alkalinity were determined in the field. In addition, 75 elemental analyses of main and trace elements as well as 74 isotope ratio values for oxygen and hydrogen were determined. The geographical and (hydro)geological situation of the study area was characterized and visualised by evaluation of available information. For the concentrations of the three trace elements, isoline maps were created and related to the geology of the study area. Stability fields of dissolved species were visualized by means of Eh-pH diagrams. Using the knowledge gained from all these perspectives, it was then possible to derive and discuss the origin, mobilisation, transport and accumulation processes of relevant trace elements in the study area.

Results

Median pH of all waters is 7.60, values are generally circumneutral to slightly alkaline (Tab. 1). However, the maximum value of 10.9 indicates that there are also waters with more alkaline pH values. Median temperature is 31.7 °C (Tab. 1). The maximum value of 47.0 °C indicates the presence of thermal water. In total, 20 of the 125 samples have a temperature of more than 35 °C.

The measured F concentration is up to 19.6 mg/L and 2.59 mg/L on average (Tab. 1). The WHO drinking water limit of 1.5 mg/L is exceeded in 72.8% of the samples. The As content of the water reaches up to 1422 µg/L at a mean value of 56.6 µg/L (Tab. 1). The drinking water limit value of 10 µg/L is exceeded in 64% of the samples. U concentration is up to 122 µg/L and 21.5 µg/L on average. The German guideline value of 10 µg/L is exceeded in 58.4% of the samples. (See Table 1)

Figure 2 shows the relation between dissolved U and water temperature. R2 of 0.16 indicates a weak but statistically significant ($p<0.01$) linear relationship between the two parameters. All water samples below 29 °C have U concentrations <50 µg/L, while the 12 samples >50 µg/L U plot in the T range of 29 to 37.5 °C. However, the two samples with highest T (>43 °C) show relatively low U values. In total, Fig. 2 also shows that the majority of the values clearly exceed the drinking water limit value of 10 µg/L.

The 125 water samples were taken at 67 different sites, 43 of them are located closely to the mine (Fig. 3). The interpolated distribution of F concentration (Fig. 3, left) indicates lowest concentrations in the range from <0.1 to 1.5 mg/L are located in the west of the mountain range and increase continuously towards the east in the northern area. In the area of the San Antonio Mine, a more diffuse picture can be seen, which, however, is also caused by the extremely high density of measuring points in this area compared to the rest of the map. Concentrations of around 6 mg/L are reached here. The highest F contents are found in the southeast in Quaternary alluvial sediments with up to 10 mg/L. However, the maximum concentration is found in only one sampling point with only 4 or 2 mg/L in the two directly adjacent measuring points.

Figure 3 (right) shows the distribution of U concentrations in the study area. Values range from <1 to 42 µg/L with the lowest values in the south and the highest values around the mine. Concentration increases from the southwest to the northeast, reaches its peak at the mine and continues to decrease to the northeast until it increases again to 26 µg/L. The U concentration pattern looks quite different from the similar F

Table 1 *Trace elements hydrochemistry and physico-chemical parameters (n=125).*

	pH	T [°C]	F [mg/L]	As [µg/L]	U [µg/L]
mean	7.77	29.3	2.59	56.6	21.5
median	7.60	31.7	2.25	12.1	14.8
maximum	10.9	47.0	19.6	1422	122
minimum	6.68	11.4	<0.1	1.06	0.37
guidelines	6.5-9.5	-	1.50	10.0	10.0
max. factor	1.14	-	13.1	142	12.2
exceedence frequency %	0.8	-	72.8	64.0	58.4

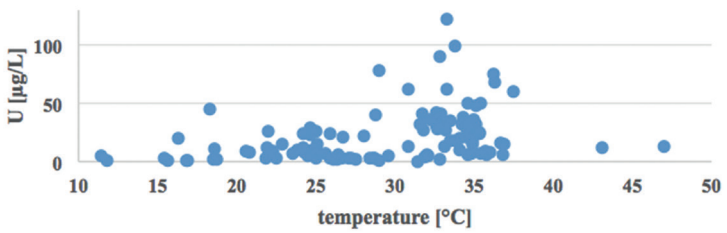

Figure 2 *Correlation of U concentration and temperature, n = 125.*

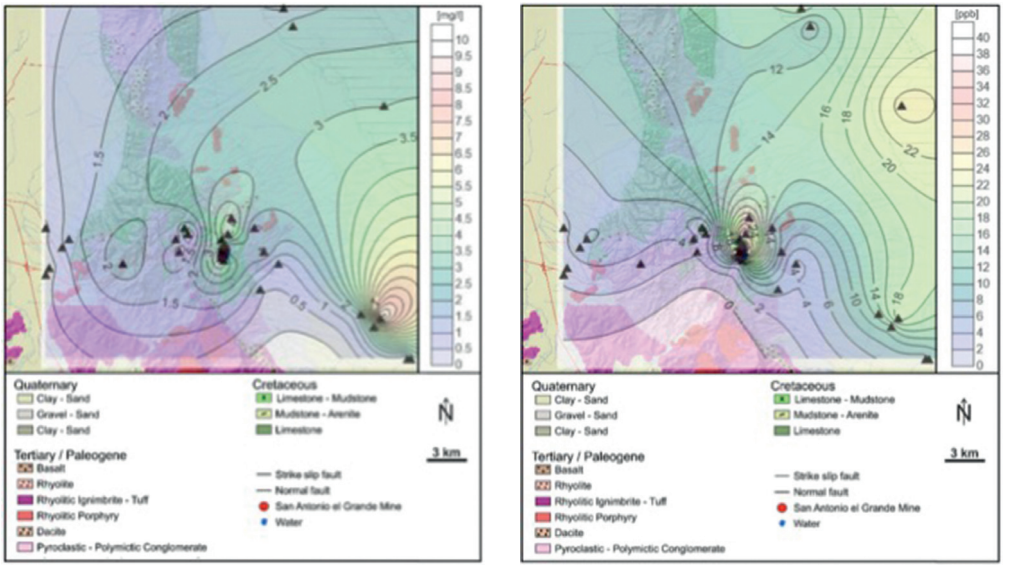

Figure 3 Isolines of F (left) and U (right) concentration in relation to the geological map of the study area.

and As (not shown) distribution patterns, potentially indicating different sources and/or mobilization processes.

Dissolved As and U species are presented in Eh-pH diagrams in Fig. 4. Fluorine species were also investigated, but as expected, only fluoride (F-) was present (diagram not shown). Based on Fig. 4 (left), a clear As species distribution of almost exclusively HAsO42- can be assumed under the given conditions. Only one sample is in the field for H2AsO4-. Both species contain pentavalent As. Figure 4 (right) shows the U species distribution. Here, samples are divided into UO2OH+ and (UO2)3(OH)7-. The proportion of UO2OH+ outweighs that of (UO2)3(OH)7-. Both species contain hexavalent U, arguing for high U mobility. Though not included in Fig. 4 (right), it can be assumed that Ca-U(VI)-CO3 complexes play a major role in U speciation (e.g., Riedel and Kübeck, 2018).

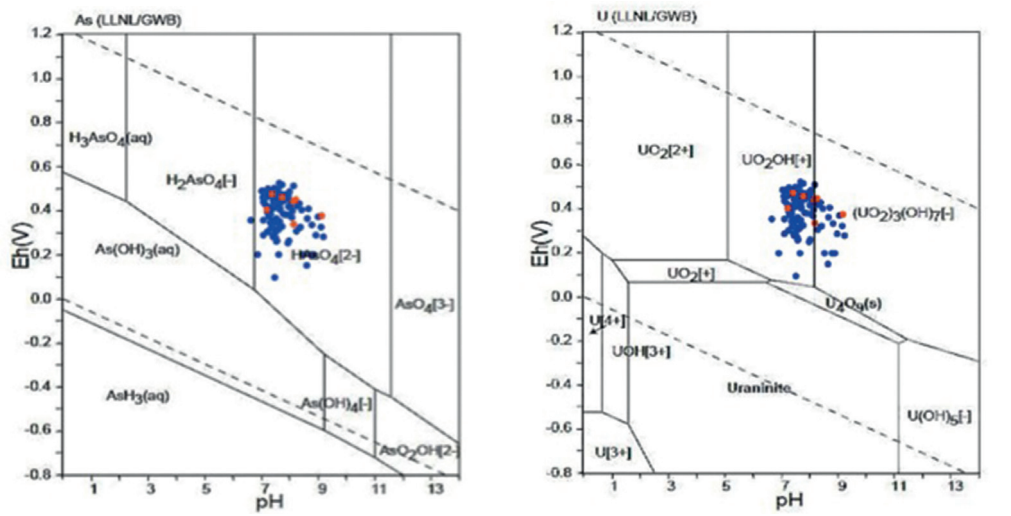

Figure 4 Eh-pH diagrams of As (left) and U (right) (modified after Takeno, 2005; blue dots: groundwater, red dots: surface water).

Figure 5 shows the 74 available data sets for deuterium (3H) versus oxygen (18O). Groundwater and surface water samples are plotted in addition to the global meteoric waterline and the local meteoric waterline for Chihuahua. The four surface water samples show significantly higher levels of deuterium and oxygen than the groundwater samples, as well as greater scattering. The groundwater values are concentrated in a much narrower area.

Discussion

The fact that the drinking water limit values for F, As and U are exceeded in 72.8%, 64.0% and 58.4%, respectively, of all studied samples around the mine is alarming (Table 1). The massive exceedances of the guideline value in the case of As can represent an enormous health risk for the human population and ecosystems. Due to the numerous private wells in the study area, there is often no control authority and contaminated water is thus not detected.

The dissolution capacity of the water for most mineral phases increases with rising temperature. The thermal waters therefore have the greatest potential to dissolve the trace elements from their host phases, probably mainly silicates, sulphides and volcanic glass. Increased solution and mobility of U at elevated temperatures is indicated. Elevated F contents can also be caused by a temperature above 30 °C. Only As mobility does not seem to be controlled by water temperature.

The spatial distribution patterns of the trace elements must be regarded a rough estimate. Observation points are inhomogeneously distributed and concentrate to a large extent on a very small area around the San Antonio Mine. In wide areas in the west and east of the mountain range there are only very few measuring points, which causes the isolines in these areas to be very uncertain. The highest concentrations were often found only once in single measuring points but strongly influence the overall picture of the isolines. On the one hand, for more reliable isoline representations, the spatial distribution of the measuring points should be reconsidered and more homogeneously distributed. It would be helpful to supplement the knowledge gained from this work with recent water samples and measurements of trace element concentrations in previously unconsidered parts of the study area. On the other hand, the diffusely distributed concentration patterns can also indicate fluctuating redox conditions, rapidly changing solution capacities, or small-scale heterogeneities of source rocks. It is noticeable that F and As have very similar distribution patterns, which indicates a common source and simultaneous solution. Uranium, on the other hand, shows a different distribution patterns. Especially in the area of the San Antonio mine, maximum concentrations are measured, whereas in the case of As in the same area, rather low concentrations occur. Arsenic is more mobile under reduced conditions, U under oxidized conditions. The results of the spatial distribution patterns underline this very well. High As and U concentrations are not to be expected simultaneously in the water although they are known to derive from the same source rocks (Banning et al. 2012). Fluoride, on the other hand, is not redox-sensitive and the increased mobility is mostly controlled by the higher pH value. The latter is also valid for As, explaining the similar spatial

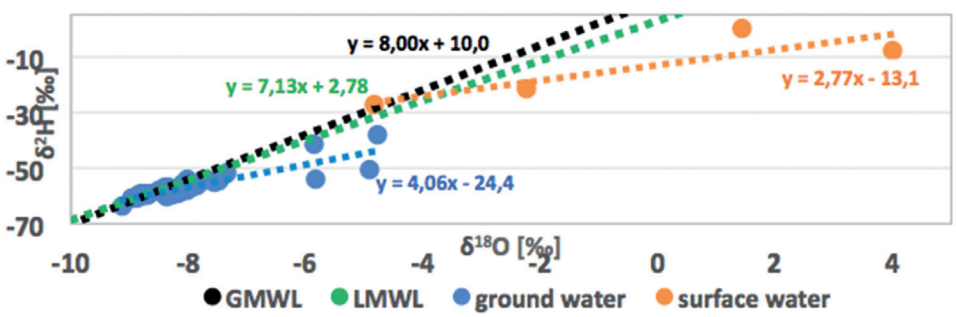

Figure 5 Scatter diagram of isotope values for oxygen and deuterium.

groundwater distribution of both elements.

As seen in the Eh-pH diagrams, As(V) and U(VI) are the dominant redox species. The pentavalent As shows that mostly oxidized conditions prevail (Masscheleyn et al. 1991), where also the hexavalent U is easily soluble. Both trace elements have a high mobility in the study area. From the isotope diagram, clear evaporation tendencies of the surface and ground waters are visible. Due to evaporation, especially in the case of surface waters, the light isotopes pass into the gas phase and heavy isotopes accumulate in the remaining water. From the diagram, it can be concluded that these waters are mainly of meteoric origin, and rather not from a deep source.

The predominantly acidic character of the magmatic rocks in the study area supports the thesis of them being the main source of high trace element concentrations based on the incompatible character of F, As and U and their enrichment in late magmatic lithologies. The carbonates also represent a possible source of U and As (Riedel and Kübeck 2018, Banning et al. 2012). Karst formation and dissolution processes of limestones can cause increased concentrations. In addition to the acidic igneous rocks, the ore enrichments with minerals such as pyrite also represent a source of the trace elements. 50 km northwest of Santa Eulalia in the Sierra Peña Blanca, there is for example the El Nopal Mine, where U ores are mined.

Conclusions

The increased concentrations of F, As and U in ground and surface waters in the area around the San Antonio el Grande Mine in Chihuahua, Mexico, are of geogenic origin. The incompatible elements accumulated in the course of magma differentiation in the predominantly acidic igneous rocks in the study area. In addition, the frequent mineralization zones and limestones are further potential sources. Mobility of F and As seems to be mainly controlled by pH with alkaline values causing higher concentrations. Especially for the mobility of U, water temperature seems to be a decisive factor. However, dissolved F concentration is also increased by elevated temperatures. Fluorite precipitation, on the other hand, does not seem to be a decisive control mechanism. The San Antonio mine likely increases the dissolved trace element concentrations in the waters by creating larger contact areas with the acidic igneous rocks and ore minerals, and new pathways.

The ever decreasing groundwater level will lead to further problems in the future. It is likely that more and more deep water will be pumped, which could further increase the content of the dissolved trace elements. In order to ensure the long-term security of the drinking water supply in the study area and to protect the population from the potentially toxic trace element concentrations, urgent measures to reduce the dissolved contents should be implemented. A possible precipitation of fluoride via the mineral fluorite could be considered. Also, controlling pumped groundwater temperature – as it was suggested for other parts of Mexico (Cardona et al. 2018) – might be a promising approach.

References

Banning A, Cardona A, Rüde TR (2012) Uranium and arsenic dynamics in volcano-sedimentary basins – an exemplary study in north-central Mexico. Appl Geochem 27:2160-2172.

Cardona A, Banning A, Carrillo-Rivera JJ, Aguillón-Robles A, Rüde TR, Aceves de Alba J (2018) Natural controls validation for handling elevated fluoride concentration in extraction activated groundwater flow systems. Environ Earth Sci 77:121-133 .

Masscheleyn P, Delaune R, Patrick W (1991) Effect of redox potential and pH on arsenic speciation and solubility in a contaminated soil. Environ Sci & Technol 25:1414-1419.

McDowell FW, Keizer RP (1977). Timing of mid-Tertiary volcanism in the Sierra Madre Occidental between Durango City and Mazatlan, México. Geol Soc Am Bull 88:1479-1487.

Megaw PK (1990) Geology and geochemistry of the Santa Eulalia mining district, Chihuahua, Mexico. PhD Thesis, The University of Arizona. http://hdl.handle.net/10150/187549.

Riedel T, Kübeck C (2018) Uranium in groundwater – A synopsis based on a large hydrogeochemical data set. Water Res 129:29-38.

Sedlock RL, Ortega-Gutierrez F, Spedd RC (1993) Tectonostratigraphic terranes and tectonic evolution of Mexico. Geological Society of America Special Papers 278.

Takeno N (2005) Atlas of Eh-pH diagrams – Inter-comparison of thermodynamic databases. Geological Survey of Japan Open File Report No. 419.

Catastrophe Vulnerability and Risk Mapping in the Iron Quadrangle, Brazil – Preliminary Results in the Rio das Velhas Watershed

Raphael de Vicq[1], Teresa Albuquerque[2], Rita Fonseca[3], Mariangela Garcia Praça Leite[4]

[1]*Earth Science Institute (ESI), University of Evora, Portugal and Federal University of Ouro Preto, Brazil*

[2]*Earth Science Institute (ESI), University of Evora and Polytechnique Institute of Castelo Branco| CERNAS|QRural, Av. Pedro Álvares Cabral, nº 12, 6000-084 Castelo Branco, Portugal, ORCID-0000-0002-8782-6133, teresal@ipcb.pt*

[3]*Earth Science Institute (ESI), Department of Geosciences, School of Science and Technology, AmbiTerra Laboratory, University of Évora, Portugal*

[4]*Department of Geology, School of Mines, Federal University of Ouro Preto, Brazil*

Abstract

The geochemistry of fluvial deposits is one of the most used proxies for contamination assessment in mined areas. A river sediment survey was carried out in Iron Quadrangle (IQ), Brazil, between 2013 and 2015. Subsequently, in the last four years, two dam failures happened, causing great environmental damage. Geostatistical modelling was used to model Potentially Toxic Elements' spatial patterns and the definition of hot/cold clusters for Arsenic contamination risk concerning catastrophic scenarios, such as dam failure. and so used as a tool for vulnerability and risk assessment. The preliminary results for Arsenic spatial distribution are introduced and discussed.

Keywords: Iron Quadrangle, Potentially Toxic Elements, Geostatistical Modelling

Introduction

Fluvial sediments come from a myriad of sources, diffuse and punctual, whose relative contribution varies over time and space. Their geochemical composition is a response to the availability of materials, whether due to natural causes or human activities, such as mining. Mining industries produce enormous volumes of waste material, mainly tailings, which can be a relevant source of trace element contamination for the environment, especially in the river basins (Krıbek et al. 2014). Worldwide, billions of tonnes of tailings are contained in impoundments behind huge dams (Owen et al. 2020). Several characteristics of these structures make them more susceptible to failures.The enormous volume and characteristics of the material released in the environment with the collapse of the dam, especially in watersheds and river basins, affect the quality of sediments and water (Kossoff et al. 2014).

Mining is still among the most productive activities that support the Brazilian economy (12.5% of total exports and 36.6% of the trade balance – AMN 2019) and Minas Gerais State is responsible for the other 40% of the commercialized mineral production (AMN 2019). The Iron Quadrangle (IQ), southeast of Minas Gerais State, (fig. 1) is one of the most important mining producing provinces in Brazil and one of the World's most important mineral regions, covering an area of approximately 7,000 km^2. Mining activities are focus on iron and gold exploitations, whose wastes are stored in large tailings dams. The IQ yields the headwaters of two major Brazilian River basins: Doce and São Francisco. The last one, fed by Velhas (largest drainage basin in IQ) and Paraopeba rivers. Unfortunately, during the last six years, IQ experience two of the most dramatic accidents involving the dam's tailings failure. Fundão dam (Bento Rodrigues/Mariana), on 5 November 2015, released 4.3×10^7 m^3 of tailings in Doce River basin (Carmo et al. 2017) and Córrego do Feijão dam (Brumadinho), on 25 January 2019, released

1.2×10^7 m^3 of tailings in Paraopeba River basin (Thompson et al. 2020).

A preliminary multivariate study was performed through Principal Component Analysis (PCA) (Shaw 2003) to understand the attributes of preferential association and the reduction of the space of analyses. The analysis begins with p random attributes X1, X2, …, Xp, where no assumption of multivariate normality is required. Considering the ACP outputs, Cr, Zn, Cd, Ni, Cu and Pb were kept for further spatial analysis as they can act as accurate indicators for the pollution characterization.

In the herein survey the results for the As spatial distribution are introduced and discussed as As plays a key role in soil and sediments pollution (Gonzalez-Fernandez et al. 2018). Indeed, among the elements present in iron and gold tailings, Arsenic appears as one of the most dangerous to the environment, including human health (Fewtrell et al. 2005, Zhang et al., 2019). Although the interaction between arsenic and the various environmental compartments (sediment, soil, water) still needs to be better understood, there is no doubt that one of the main sources of arsenic contamination in river basins is mining activity (Deschamps & Matschullat, 2011). Several studies have identified anomalous concentrations of arsenic in IQ waters and sediments (Costa et al. 2015). In the case of sediments, there are reports of levels above 4700 $\mu g.g^{-1}$ (Borba et al. 2000), much higher than the average concentration in the Earth's crust (between 1.0 – 4.8 $\mu g.g^{-1}$, according to Taylor & McLennan, 1995 and Rudnick & Gao, 2003).

Arsenic is defined as a 'Regionalized Variable (Matheron 1971) and consequently additive by construction, since the mean value within given observed support is equal to the arithmetic average of sample values, regardless of the statistical distribution of the values. Geostatistical modelling (Goovaerts 1997, Journel and Huijbregts 1978) was used, throughout conventional variography followed by Sequential Gaussian Simulation algorithm (SGS) and local G clustering, to model Arsenic concentration's spatial patterns and the definition of hot/cold spots for contamination risk. The Standard Deviation map, obtained from the performed one hundred simulations (SGS), allowed the visualization of the correspondent spatial uncertainty and, therefore, acting

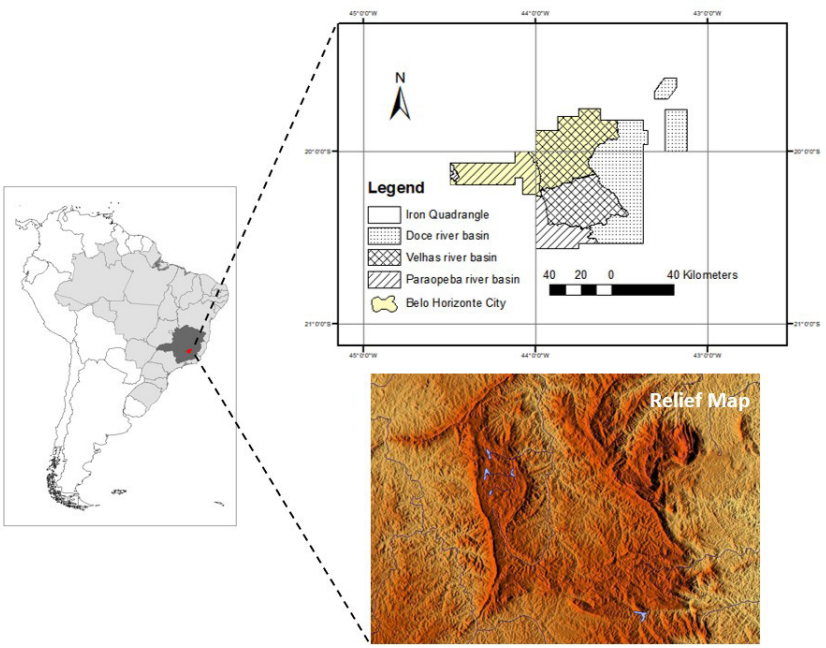

Figure 1 *Study area location.*

as a measurement of the obtained clusters robustness and providing a faster and more intuitive way to verify whether the problematic zones detected previously are true of concern, focusing on the visualization and delineation of potential zones for future monitoring and remediation.

Methods

Five hundred and forty-one (541) stream sediments were sampled throughout the entire IQ (7,000 km^2), providing a sampling density of one sample per 13 km^2. The concentrations of the key PTEs: As; Cd; Co; Cr; Cu; Ni; Pb and Zn and associated metals (Fe, Mn) were obtained through aqua regia digestion followed by ICP-AES (Spectro Ciros CCD) analysis.

A three-stepgeostatistical modelling methodology was used for the construction of the Arsenic spatial distribution maps and the definition of spatial hot-spots, as follows:

1. Selected attributes went through structural analysis and experimental variograms were computed. The variogram is a vector function used to compute the spatial variation structure of regionalized variables (Matheron 1971; Journel and Huijbregts 1978);
2. Sequential Gaussian Simulation (SGS) was used as a stochastic simulation algorithm. SGS starts by defining the univariate distribution of values, performing a normal score transform of the original values to a standard normal distribution. Normal scores at grid node locations were simulated sequentially with simple kriging (SK) using the normal score data and a zero mean (Goovaerts 1997). Once all normal scores had been simulated, they were back-transformed to original grade values (Albuquerque et al., 2017). For the computation, the Space-Stat Software V. 4.0.18, Biomedwere, was used. The outcome of a simulation is a twisted version of an estimation process, which reproduces the statistics of the known data, making a realistic look of the exemplar, but providing a low prediction behaviour. If multiple sequences of simulation is designed, it is possible to obtain more reliable probabilistic maps;
3. Finally, Local G clustering allowed measurement of the degree of association that results from the concentration of weighted points (or region represented by a weighted point) and all other weighted points included within a radius of distance from the original (Getis and Ord 1992).

When predicting the risk of contamination (e.g. months ahead), it is mandatory to stress the relevance of the chances for the future estimated values exceeding maximum admissible values. The delineation of zones of high and low risk requires the interpolation of risk values to the nodes of a regular grid making possible proper risk assessments, and a prediction model working as guidance to a more sustainable environmental management. The three watersheds (Doce, Velhas, and Paraopeba) were processed separately (fig. 2) guarantying that only the samples inside each geographic envelop were

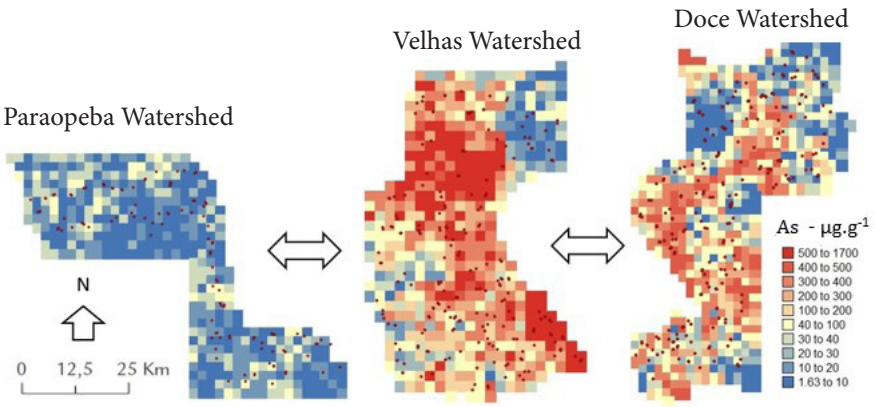

Figure 2 *Arsenic Spatial Distribution – SGS mean image.*

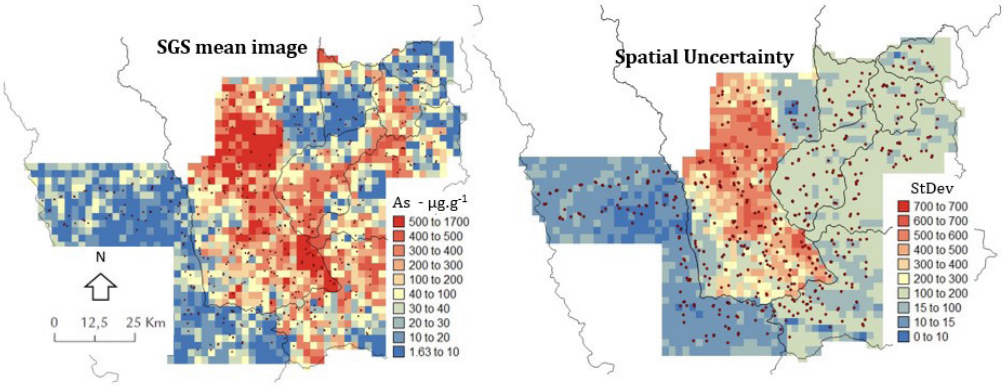

Figure 3 *Arsenic Spatial Distribution – SGS mean image and spatial uncertainty (standard deviation).*

used for the correspondent spatial modelling. Finally, all the representations were projected together for visualization purposes (fig. 3 and fig. 4). Observing the three surveyed units, Velhas, Doce, and Paraopeba watersheds, it is possible to acknowledge, for As spatial distribution, the low risk in the Paraopeba and the high risk observed mostly in the central area of the Velhas basin.

It is also worth notice the high spatial uncertainty associated with the Velhas' basin data, mainly due to the presence of several severe outliers within the studied area (fig. 3). Seventeen percent of As concentration values are higher than the mean (32.33 µg.g^{-1}) and 6,7% higher or equal to 100 µg.g^{1}.

Finally, when observing the G-clusters it is possible to identify high rings (hot spots for As pollution) and low rings (cold spots for As pollution) pointing out to the Velhas and Doce watersheds as the ones in need of close monitoring.

Still, a source of countless debates, the anthropogenic contribution to high concentrations of arsenic in fluvial sediments is not well defined. Even so, establish the natural abundance of an element is essential to support any type of environmental analysis. Concerning sediments, global or regional standards can be used. Arsenic average concentrations calculated for QF (18.17 µg.g^{1}), Velhas river basin (32.33 µg.g^{-1}) and Doce river basin (14.23 µg.g^{-1}) are considerably higher than the highest value

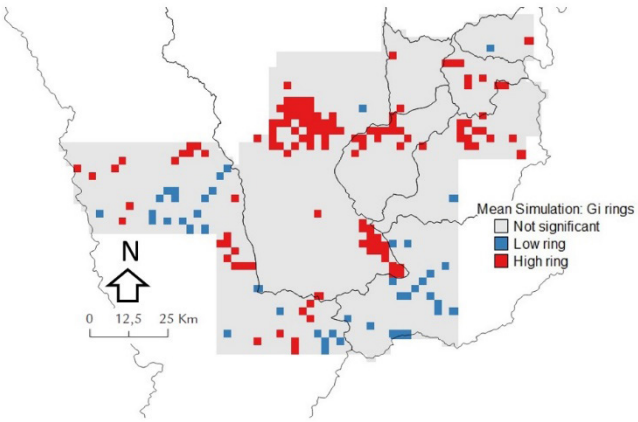

Figure 4 *Arsenic Spatial G-Clusters.*

set for the Earth's crust (4.8 $\mu g.g^{-1}$ – Rudnick & Gao 2003). Only in the Paraopeba river watershed As mean concentration is lower (4.01 $\mu g.g^{-1}$). Besides that, Costa et al. (2015) defined the natural background of As concentration in IQ as 6.1 $\mu g.g^{-1}$ and values >12.8 $\mu g.g^{-1}$ as anomalies. Regardless of the limits considered, Velhas and Doce river basins can be considered areas with anomalous values of As concentrations.

Several studies pointed out that in IQ, arsenic concentrations in water and sediments are related to gold deposits, present in minerals such as arsenopyrite and arseniferous pyrites (Borba et al. 2000). Gold can be found in veins of quartz and carbonates from the Nova Lima Group (base of the Rio das Velhas Supergroup) and base of the Minas Supergroup (Deschamps and Matschullat, 2011). Moreover, gold mine waste (tailings) containing arsenic have been released to the environment or store in tailing dams for the last three centuries (Matschullat et al. 2000, Borba et al. 2000). Although iron ores usually have As concentrations <1 $\mu g.g^{-1}$, sorbed, or coprecipitated in iron (oxy)(hydr) oxides, their tailings can be enriched in As. Indeed, it is possible to identify significant-high rings in the northern and southeast areas of the Velhas River watershed, all famous locations for primary gold deposits and gold mines. Considering the Au/As ratio presented by Costa (2007) for gold ore exploitations in IQ, almost 2,000,000 tons of As are potentially scattered in the basin or stored in waste piles and tailings dams, including abandoned mines, which represents a major concern in catastrophic scenarios identified in this research. Besides that, in Velhas river basin there are, actually, 16 iron tailing dams, five of then with a high risk of failure. It should be noted that in the high ring identified in the north of figure 3, currently, 450,000 inhabitants live, in addition to hosting the main source of water supply for the city of Belo Horizonte, the state capital, with 2,500,000 inhabitants. Three of the five dams with a risk of failure are localized in or upstream this area, and part of the people living downstream from these structures have already been removed.

Conclusions

The stochastic modelling of the arsenic concentrations in the fluvial sediments in the IQ allowed to identify the Velhas River watershed as the most vulnerable area to catastrophic risk given the high concentrations of Arsenic in this basin, with an average of 32.33 $\mu g.g^{-1}$, about 16 times above the upper crustal average, showing that there is a significant amount of this element scattered throughout the watershed.

In this basin there are 18 gold mines, six in operation and 12 paralyzed, (Pinto and Silva, 2014), which extracted approximately 692 tons of gold over the last 40 years (Goldfarb and Groves 2015, Codemge 2017), considering the Au/As ratio presented by Costa (2007), it is estimated that 1,868,400 tons of As, are potentially scattered in the basin or stored in tailings piles, including abandoned mines and waste pile, which represents a major concern in catastrophic scenarios, which are identified in this research.

Although recent dam breaks have occurred in the Doce river basin and the Paraopeba River Basin, the average As concentrations in these areas, when compared with Velhas river basin, are much lower, 4.01 $\mu g.g^{-1}$ (8 times below) in the Paraopeba river and 14.23 $\mu g.g^{-1}$ (2.3 times below) in the Doce River, which points to its higher risk in the event of the failure of one or more tailings dams, as in the other two basins.

Thus, it was observed that in the Rio das Velhas Basin there is a greater catastrophe vulnerability, which confirms the need to apply geostatistical modeling as a tool to identify these areas and spatial patterns of PTEs, supporting government agencies in the prevention of environmental damage and the execution of more accurate monitoring.

Acknowledgments

The authors thank all co-organisers for hosting the IMWA2020 Conference. Amy Kokoska, Hetta Pieterse as well as Glenn MacLeod provided critical comments on earlier versions of this text. The research was supported by (1) CERNAS-IPCB [UIDB/00681/2020 funding by Foundation for Science and Technology (FCT), by (2) ICT, under contract with FCT (the Portuguese

Science and Technology Foundation) through the Projects UIDB/04683/2020 e UIDP/04683/2020 and by (3) FAPEMIG (Research supporting foundation of Minas Gerais State).

References

Albuquerque MTD., Gerassis S, Sierra C, Taboada J, Martín JE., Antunes IMHR, Gallego JR. (2017) Developing a new Bayesian Risk Index for risk evaluation of soil contamination. Sci Total Environ 603–604:, 1167–177, doi: 10.1016/j.scitotenv.2017.06.068

ANM - Agência Nacional de Mineração. (2019) Anuário Mineral Brasileiro Principais Substâncias Metálicas 2019,

http://www.anm.gov.br/dnpm/publicacoes/serie-estatisticas-e-economia-mineral/anuario-mineral/anuario-mineral-brasileiro/amb_2019_ano_base_2018

Borba RP, Figueiredo BR, Rawlins B, Matschullat J (2000) Arsenic in Water and Sediment in the Quadrilátero Ferrífero, State of Minas Gerais, Brazil. Applied Geochemistry, v. 15, n. 2: 181-190

Carmo, FF, Kamino, LHY, Junior, RT, de Campos, IC, do Carmo, FF, Silvino, G, de Castro, KJSX. Mauro, ML, Rodrigues, NUA, Miranda, MPS, Pinto CEF (2017) Fundão tailings dam failures: the environment tragedy of the largest technological disaster of Brazilian mining in global context Perspect. Ecol. Conserv., 15:145-151

CODEMGE - Companhia de Desenvolvimento de Minas Gerais. (2018) Recursos minerais de Minas Gerais. http://recursomineralmg.codemge.com.br/substancias-minerais/ouro/#

Costa AT (2007) Registro histórico de contaminacão por metais pesados, associadas à` exploração aurífera no Alto e Médio curso da Bacia do Ribeirão do Carmo, QF: um estudo de sedimentos de planícies de inundacão e terraços aluviais. Doctoral thesis, UFOP, Ouro Preto.

Costa RVF, Leite MGP, Mendonça FPC, Nalini JHA (2015) Geochemical mapping of arsenic in surface waters and stream sediments of the Quadrilátero Ferrífero, Brazil Geociências, doi: 10.1590/0370-44672015680077

Deschamps E, Matschullat J (eds) (2011) Arsenic: natural and anthropogenic. Arsenic in the Environment 4, p 209. CRC Press, Boca Raton

Fewtrell L., Fuge, R., & Kay, D. (2005). An estimation of the global burden of disease due to skin lesions caused by arsenic in drinking water. Journal of Water and Health, 3(2), 101–107.

Getis A, Ord JK (1992) The analysis of spatial association by use of distance statistics. Geogr. Anal. 24(3): 189–206

Goldfarb R.J. & Groves D.I. (2015). Orogenic gold: common or evolving fluid and metal sources through time. *Lithos*, **233**:2-26. doi: 10.1016/j.lithos.2015.07.011

Gonzalez-Fernandez B, Rodríguez-Valdes E, Boente C., Menendez-Casares E, Fernandez-Braña A, Gallego JR. (2018) Long-term ongoing impact of arsenic contamination on the environmental compartments of a former mining metallurgy area. Sci. Total Environ. 610-611: 820-830. doi: 10.1016/j.scitotenv.2017.08.135

Goovaerts P (1997) Geostatistics for Natural Resources Evaluation. University Press, New York: Oxford

Journel A, Huijbregts CJ (1978) Mining Geostatistics. Academic Press, San Diego

Kossoff D, Dubbin WE, Alfredsson M, Edwards SJ, Macklin MG, Hudson-Edwards, KA (2014) Mine tailings dams: characteristics, failure, environmental impacts, and remediation Appl. Geochem., 51:229-245

Krıbek B, Davies TC, De Vivo B (2014) Mining vs. environment in Africa. J Geochem Explor 144:387–580

Matheron G (1971) The Theory of Regionalized Variables and Its Applications. Edição 5 de Les Cahiers du Centre de morphologie mathématique de Fontainebleau, Centre de morphologie mathématique de Fontainebleau, ISSN 1157-1195

Mattschullat J, Borba RP, Deschamps E, Figueiredo BF, Gabrio T, Schwenk M (2000) Human and environmental contamination in the Quadrilátero Ferrífero, Brazil. Applied Geochemistry, v. 15, p. 181-190. 10.1016/S0883-2927(99)00039-6

Owen JR, Kemp D, Lèbre É, Svobodova, Pérez Murillo, KG (2020) Catastrophic tailings dam failures and disaster risk disclosure. International Journal of Disaster Risk Reduction 42:101361

Pinto CP, Silva MA (2014). *Mapa Geológico do Estado de Minas Gerais, Escala 1:1.000.000.* Companhia de Desenvolvimento Econômico de

Minas Gerais, CODEMIG e Serviço Geológico do Brasil, CPRM.

Robb L (2004) Introduction to Ore-forming Processes. Wiley-Blackwell, Oxford.

Shaw PJA (2003) Multivariate statistics for the Environmental Sciences, Hodder-Arnold. ISBN 0-340-80763-6

Rudnick RL, Gao S (2003) Composition of the continental crust. In The Crust, Treatise on Geochemistry, Vol. 3, (ed. Rudnick, R.L.). Elsevier, 1-64.

Taylor SR, McLennan SM (1995) The geochemical evolution of the continental crust. Rev Geophys; 33: 241-265.

Thompson F, Oliveira BC, Cordeiro MC, Masi BP, Rangel TP, Paz P, Freitas T, Lopes G, Silva BS, Cabral AS, Soares M, Lacerda D, Vergilio CS, Ferreira ML, Lima C, Thompson C, Rezende CE (2020). Severe impacts of the Brumadinho dam failure (Minas Gerais, Brazil) on the water quality of the Paraopeba River. Science of The Total Environment, 705, 1-24. doi.org/10.1016/j.scitotenv.2019.135914.

Zhang Y, Xu B, Guo Z, Han J, Li H, Jim L, Chen F, Xiong Y (2019) Human health risk assessment of groundwater arsenic contamination in Jinghui irrigation district, China. J. Environ. Manag., 237:163-169

Magnetic Coagulation Technology for Coal Gasification Wastewater Treatment

J. L. Gao[1], Y. Liu[1], Y. X. Yan[1], W. H. Wang[2]

[1]*School of Ecology and Environment, Zhengzhou University, Zhengzhou 450001, Henan, China*
[2]*Zhengzhou University Comprehensive Design and Research Institute Co., Ltd.*

Abstract

Coal gasification wastewater is refractory for its high colority, complex water quality components, heavy toxicity and poor biochemical purification ability. This study focused on the wastewater treatment of coal gasification in a coal chemical enterprise by magnetic coagulation technology. Under the optimum condition, the removal rate of COD, turbidity and solube SiO2 were 27.6%, 97.0% and 68.4%, respectively. And the average recovery of magnetic powder was up to 97.38%. This paper provides technical guidance for the engineering application of the magnetic coagulation in coal gasification wastewater.

Keywords: influencing factors, recovery, economic analysis

Introduction

At present, the treatment of polluted wastewater from coal gas production has become an important factor restricting the further development of coal gas industry. Coal gasification wastewater is a kind of typical industrial organic wastewater with high concentration, complex components and strong toxicity, which mainly comes from washing, condensation and fractionation (Lan LL 2019). Magnetic coagulation technology (MCT) is a novel rapid coagulation technology. In the MCT, the magnetic powder is purposely added on the basis of the traditional coagulation technology, and the combination of the flocs with the magnetic powder increases the flocs density and accelerates the solid-liquid separation (Lv M et al. 2019; Luo LQ et al. 2017). Thus, the refractory organic matter which is mostly in suspended and colloidal state in coal gasification wastewater can be removed effectively.

This study focused on the wastewater treatment of coal gasification by MCT. The optimum treatment conditions, the recovery and reuse of the magnetic powder and the technical and economic feasibility were analyzed.

Material and Methods

Material

The raw water was sampled from the primary settling tank of a coal chemical enterprise in Henan Province, which was from the gasifier prior to chemical-conditioning (cationic polyacrylamide). The quality of the wastewater is shown in tab. 1.

Coagulation experiment

The coagulation experiments were undertaken on a TJ6 (Wuhan Hengling Technology Co., Ltd., China) jar tester with six beakers of 1 L. Appropriate PAC and magnetic powder were dosed under a 2 min rapid mix stage at 120 rpm, and then PAM was added with a 10 min flocculation stage at 40 rpm before a 15 min settlement period. The supernatant sample was collected from the beaker 2 cm below the surface for determining the removal of COD, turbidity and SiO2.

Table 1 *Water quality of coal gasification wastewater.*

T °C	pH	COD mg/L	Turbidity NTU	SS mg/L	SiO_2 mg/L	NH_3-N mg/L	T-P mg/L
32-38	8.2-8.8	200-500	92-125	180-230	132-150	45-60	0.27-0.36

Magnetic powder recovery test

The procedure was as follows: removed the supernatant and transferred the magnetic flocs into a 500 mL baker, followed by a 5 min rapid stirring of 200 rpm and a 3 min adsorption stage by magnet block on the bottom of baker, removed the supernatant and washed the magnetic powder with deionized during the adsorption, the same process was repeated until supernatant was clarified, and then weighed the magnetic powder after drying in oven at 50 °C.

Indexes analysis

The COD digestion instrument (5B-1BV8, Lanzhou Lianhua Environmental Protection Technology Co., Ltd., China) was used to determine COD (Yuan MT 2018); the turbidity was measured via a 2100AN turbidimeter (Hach Company, US). The SiO2 was determined by spectrophotometry (National Standard of China, GB/T 12149-2007).

Results and Discussion

Optimization of magnetic coagulation process parameters

Effects of PAC dosage on the treatment efficiency

As shown in fig. 1, the removal efficiency of COD, turbidity, SiO2 increased gradually with the increase of PAC dosage. At 120 mg/L of PAC, the removal efficiency of COD, turbidity and SiO2 achieved 26.6%, 96%, 63.71%, respectively. Further increasing of PAC did not cause the obvious increase of removal efficiency. This may be attributed to that the high dosage of coagulant leaded to the colloidal re-stability by increasing counter-charge polymerized ions (Luo GH et al. 2019a). Therefore, the dosage of PAC was determined to be 120 mg/L.

Effects of PAM dosage on the treatment efficiency

It can be seen that obvious removal appeared when the dosage of PAM was 0.5-1.5 mg/L, and increased slightly as dosage increased continually (fig. 2). PAM is able to increase pollutants removal with adsorption-bridging and sweep-floc formation, but excessive dosage can decrease the settling velocity due to the exclusion of polymer (Luo GH et al. 2019b). Therefore , the 1.5 mg/L PAM dosage was chosen for subsequent experiments.

Effects of magnetic particle on the treatment efficiency

The particle size of magnetic of 200 and 300 mesh removed organic matter effectively as shown in fig. 3. It can be interpreted as the large particle size of magnetic powder weakened the adsorption capacity, and the specific gravity was not conducive to solid-liquid separation (Qiu JX et al. 2018). Small particle size has the problem of low flocs density and poor compression and settling performance. Finally, magnetic powder of 200 mesh was selected due to the removal

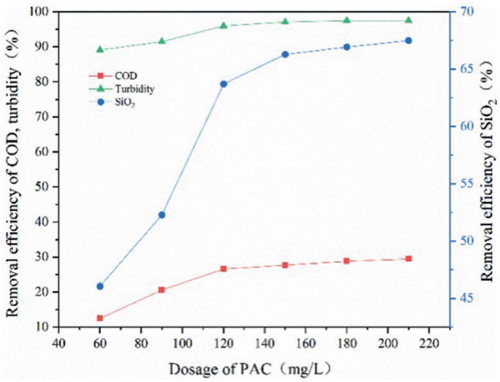

Figure 1 *Effects of PAC dosage on the removal efficiency of coal gasification wastewater (PAM 1.5 mg/L, 200 mesh magnetic powder 200 mg/L, desilicating agent 200 mg/L, pH 8.5).*

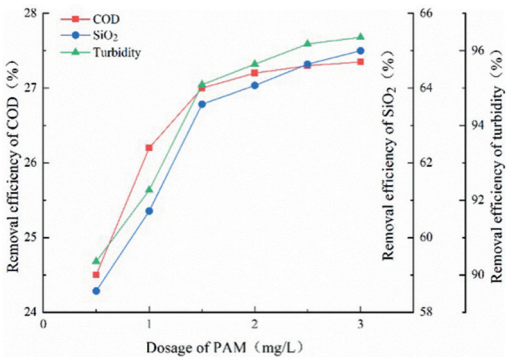

Figure 2 *Effects of PAM dosage on the removal efficiency of coal gasification wastewater (PAC 120 mg/L, 200 mesh magnetic powder 200 mg/L, desilicating agent 200 mg/L, pH 8.5).*

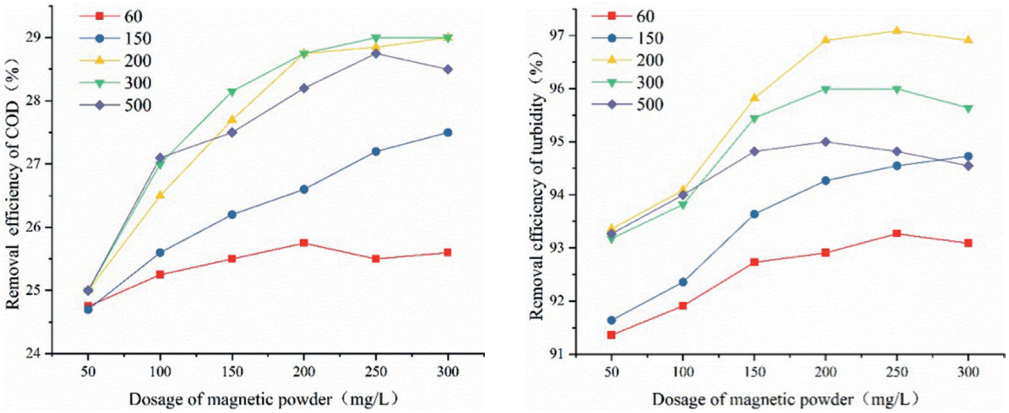

Figure 3 Effects of particle size of magnetic on COD, turbidity of coal gasification wastewater (PAC 120 mg/L, PAM 1.5 mg/L, pH 8.5).

efficiency of turbidity by magnetic powder of 200 mesh was higher than 300 mesh.

Effects of magnetic powder dosage on the treatment efficiency

The results showed that the pollutants removed effectively once the magnetic powder was dosed to the sample water until a stead-state removal was reached (fig. 4). At 200 mg/L of magnetic powder, the removal efficiency of COD, SiO2 and turbidity was 27.75%, 68.36%, 97%, respectively. It has been accepted that increasing the dosage of magnetic powder within a certain range is equivalent to increasing the crystal nucleus, which accelerates reaction by the collision, adsorption and condensation, but the excessive dosage leads to the magnetic powder collides with each other (Chen WS et al. 2004). It was appropriate to choose dosage at 200 mg/L.

Effects of initial pH on the treatment efficiency

The adjustment of pH was an effective method to enhance removal efficiency in coagulation process, in this process, the flocs size and structure can be changed, influencing the solid-liquid separation effect (Cao BC et al. 2011). As shown in fig. 6, a peak shape with a highest removal efficiency (30.75%, 71%, 97.36%) at pH 6.0, in the range of 6 to 8, the removal declined slightly. When pH value up, the removal efficiency became worse, which is due to the compounds dissolve (pH>9-10), producing negative charge that reduce the coagulation effect.

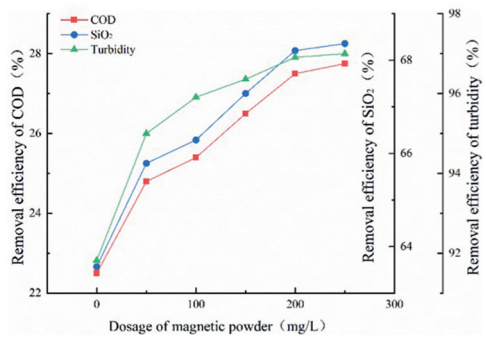

Figure 4 Effects of magnetic powder dosage on the removal efficiency of coal gasification wastewater (PAC 120 mg/L,PAM 1.5 mg/L, desilicating agent 200 mg/L, pH 8.5).

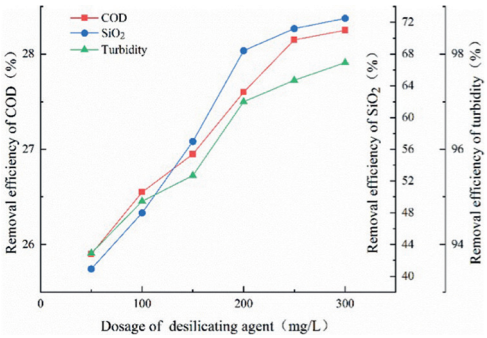

Figure 5 Effects of desilicating agent dosage on the removal efficiency of coal gasification wastewater (PAC 120 mg/L, PAM 1.5 mg/L, 200 mesh magnetic powder 200 mg/L, pH 8.5).

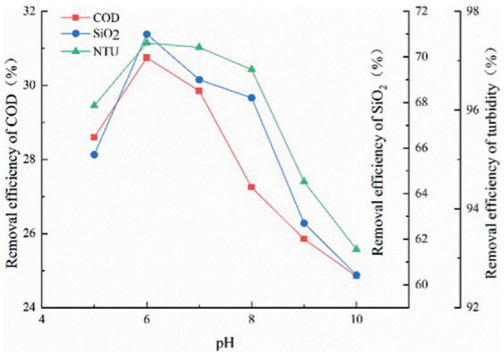

Figure 6 *Effects of pH on the removal efficiency of coal gasification wastewater (PAC 120 mg/L, PAM 1.5 mg/L, 200 mesh magnetic powder 200 mg/L, desilicating agent 200 mg/L).*

Optimization of operation parameters based on orthogonal test

Four important factors and three levels near the optimum point were determined by preliminary single factor experiments: the dosage of PAC (90 mg/L, 120 mg/L, 150 mg/L), the dosage of magnetic powder (150 mg/L, 200 mg/L, 250 mg/L), initial pH (6, 7, 8) and the dosage of desilicating agent (150 mg/L, 200 mg/L, 250 mg/L). Results showed that: PAC of 120 mg/L, PAM of 1.5 mg/L, initial pH value 7.0, magnetic powder (200 mesh) of 200 mg/L, desilicating agent of 200 mg/L were optimal when removal and cost were comprehensively considered.

Recovery and reuse of magnetic powder

The recovery of magnetic powder was determined by three parallel experiments, excellent recovery (97.38% ± 0.46%) may be attributed to a few magnetic powder was lost through flocs residue, hydraulic action and manual operation.

The recovered magnetic powder was used to investigate the influence of the using times on the treatment efficiency, a series of experimental date (27.42% ± 0.24%, 97.13% ± 0.09%, 68.32% ± 0.11%) showed that the magnetic powder was stable and its repeated use had no influence on the treatment of coal gasification wastewater.

Analysis of technical and economic feasibility

Compared with traditional coagulation (fig. 7), the removal of COD, turbidity and SiO2 increased 5.1%, 6.2%, 4.8%, respectively. The sedimentation time was decreased from 30 min to 2 min, and the settlement velocity was 16 times of that traditional coagulation. The formation of dense flocs depends on the particles collision rate, which greatly enhances the settlement velocity and the solid-liquid separation effect in MCT.

On the premise of the same treatment effect, the economic cost of two processes for treating coal gasification wastewater was analyzed (tab. 2). The chemical cost of the MCT was 0.28 yuan/m3, which was 17.6% less than that of conventional treatment process, and the magnetic powder can be recycled for many times after separation. It indicated that magnetic coagulation had cost advantage in treating coal gasification wastewater.

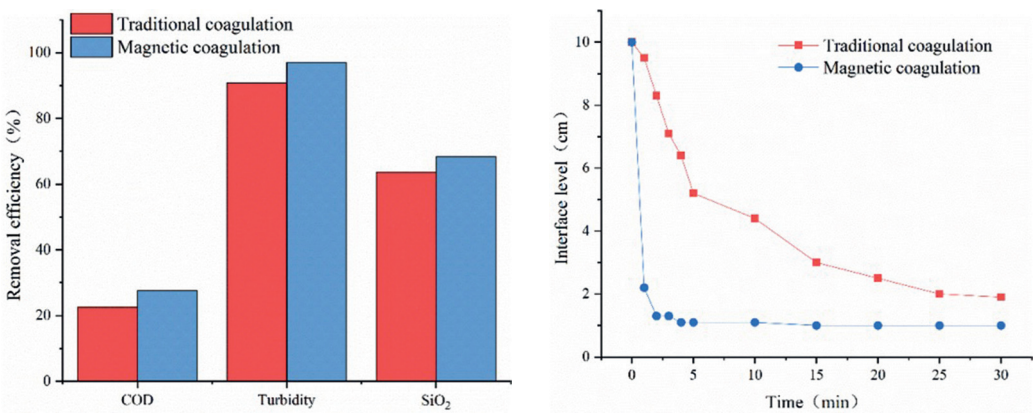

Figure 7 *Treatment efficiency and settlement velocity of traditional coagulation and magnetic coagulation.*

Table 2 Reagent cost comparison.

Items	Traditional coagulation	Magnetic coagulation
PAC (2000 yuan/t)	150 mg/L	120 mg/L
PAM (20000 yuan/t)	2.0 mg/L	1.5 mg/L
Magnetic powder (3000 yuan/t)	/	5 mg/L
Total reagent cost (yuan/m^3)	0.34 yuan/m^3	0.28 yuan/m^3

Conclusions

The results showed that the optimum conditions were as follows: PAC dosage of 120 mg/L, PAM dosage of 1.5 mg/L, initial pH value 7.0, magnetic powder (200 mesh) dosage of 200 mg/L, desilicating agent dosage of 200 mg/L.

The technical feasibility of magnetic coagulation technology was verified. Under the optimum process conditions, the removal efficiency of COD, turbidity and SiO2 was achieved at 27.6%, 97.0%, 68.4%, the concentration decreased to 144.5 mg/L, 3.3 NTU, 44.24 mg/L, respectively.

This study showed that magnetic powder can be recycled and the average recovery of magnetic powder reached 97.38%, the cost of chemical was 17.6% less than that of traditional coagulation. MCT was an effective way to reduce the cost of wastewater treatment in coal chemical enterprises.

Acknowledgements

The authors thanks all comrades of Henan Energy Luoyang Yonglong Energy Chemical Co., Ltd. for providing a convenient laboratory environment for the experiment.

References

Cao BC, Gao BY, Liu X, Wang MM, Wang ZL, Yue QY (2011) The impact of pH on floc structure characteristic of polyferric chloride in a low DOC and high alkalinity surface water treatment. Water Research 45:6181–6188.

Chen WS, Wei CH, Han H (2004) Study on the optimum parameters and mechanism of magnetic flocs formation. Sichuan Environment 23:1-4 [in Chinese]

Lan LL (2019) Research progress and application of coal chemical wastewater treatment technology. Guangzhou Chemical Industry 47:43-45 [in Chinese]

Luo LQ, Anh V. Nguyen (2017) A review of principles and applications of magnetic flocculation to separate ultrafine magnetic particles. Separation and Purification Technology 172:85-99

Luo GH, Zhang C, Zheng LB (2019) Optimization and evaluation of magnetic coagulation process pretreating swine manure biogas slurry. Chinese Journal of Environmental Engineering [in Chinese]

Lv M, Zhang ZH, Zeng JY, Liu JF, Sun MC, Ravi S. Yadav, Feng YJ (2018) Roles of magnetic particles in magnetic seeding coagulation- flocculation process for surface water treatment. Separation and Purification Technology 212:337-343

Qiu JX, Liu J, Huang X (2018) Research progress of magnetic coagulation technology in water treatment. Recylable Resource and Circular Economy 11:40-44 [in Chinese]

Yuan MT (2018) Research on practial application of CODcr determination in water with fast airtight catalysis and digestion method. Modern Chemical Research 01:28-29 [in Chinese]

Quantification of Environmental Risk of U and Th in Witwatersrand Gold-Mine Tailings, South Africa

Robert Hansen

University of the Free State, Department of Geology, 205 Nelson Mandela Drive, Bloemfontein, 9300, South Africa

Abstract

This study explores the most likely mineral hosts and geochemical behaviour of U and Th in Witwatersrand gold tailings facilities with the purpose of quantifying environmental risk. U occurs in the mineral uraninite of which the dissolution is enhanced by the oxidation of pyrite, primarily in the oxidation zone of the tailings facility. U concentrations in tailings pore water may be controlled by secondary U-mineral phases in the tailings zones below the oxidation zone. Th is shown to be insoluble and the phase in which it occurs to be irrelevant in terms of environmental risk of Th leaching.

Keywords: Uranium, Thorium, Acid Mine Drainage, Witwatersrand, Gold Mines

Introduction

The term risk can be defined as the probability of harm or loss and can be considered to be the product of the probability and severity of specific consequences (Watts and Teel 2005). South African law requires the assessment of the environmental risks associated with mineral waste generating mining activities for new as well as existing mining and associated activities. Geochemical modelling is increasingly becoming part of these risk assessments as a powerful tool in quantifying risks, e.g. the formation of acid mine drainage (AMD) conditions and leaching of chemical components from mineral waste material in concentrations that could be deleterious to the surrounding environment. This study focusses specifically on the source terms of the U and Th associated with the Witwatersrand tailings material as well as their geochemical behaviour in these facilities and ultimately the quantification of their environmental risk.

Methods

Material

A total of 13 fresh tailings samples were collected from tailings facilities, six from tailings in the Far West-Rand basin (FWR) and seven from tailings in the Free State (FS) basin (fig. 1). The samples were collected at the point where the tailings from the gold concentrator plants is discharged onto the tailings facilities. The samples were sent to a commercial laboratory for quantitative evaluation of minerals by scanning electron microscopy (QEMSCAN) and concentrated Aqua Regia leach followed by Inductively-Coupled Plasma Mass Spectrometry (ICP-MS) analysis.

Th data of individual uraninite grains from the Witwatersrand gold ore were sourced from literature. This data represents analyses by laser ablation inductively couple mass spectrometry (LA-ICP-MS) (Large et al. 2014, Depiné et al. 2013) and electron microprobe (Hallbauer 1986) data. The dataset used contains 91 analyses on uraninite grains. A Monte Carlo analysis was conducted on the single uraninite grain Th data with the purpose of determining whether the amount of Th in the tailings material can be explained by the Th contained in uraninite, or whether it is more likely that a separate Th-containing phase is required. The Monte Carlo analysis was conducted using the Risk Analysis Collection software plugin for the Microsoft Excel spreadsheet software. The data distribution for the Monte Carlo analysis was determined using the Mathwave Easyfit version 5.6 software.

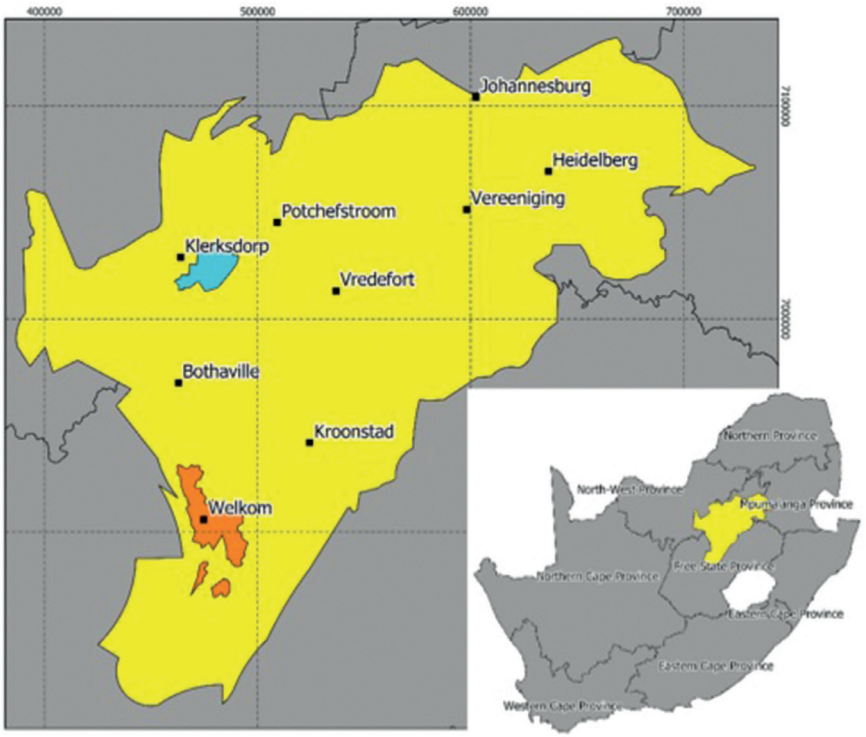

Figure 1 Locality map showing the Witwatersrand Au-mining basin as well as the Far West-Rand basin (turquoise) and the Free State basin (orange).

Conceptual framework

The conceptual framework of the Witwatersrand tailings is discussed in this section and summarised in (fig. 2). In addition to U, the Witwatersrand ore contains pyrite. As soon as pyrite is exposed to the Earth's atmosphere, it starts to oxidise according to the following reaction (Blowes et al. 2014):

Equation 1

$$FeS_{2(s)} + \frac{7}{2}O_2 + H_2O \rightarrow Fe^{2+} + 2SO_4^{2-} + 2H^+$$

Eq. 1 indicates that the oxidation of pyrite by O_2 in the presence of water releases Fe^{2+}, SO_4^{2-} H^+ to the tailings pore water. Natural minerals are very seldom pure and pyrite can contain trace metal(loid)s which have the potential to increase the risk of environmental pollution (Hansen, 2014).

Fe^{2+} is released to the tailings pore water solution and can further be oxidised to Fe^{3+} (Blowes et al. 2014, Stumm and Lee 1961). At pH > ~3, Fe^{3+} will hydrolyse and precipitate in a range of secondary (oxy)hydroxide phases, releasing additional H^+. Ferrihydrite generally serves as a proxy for this process (Blowes et al. 2014):

Equation 2

$$Fe^{3+} + 3H_2O \rightarrow Fe(OH)_{3(s)} + 3H^+$$

At pH values < ~3, ferrihydrite is soluble and the ferric iron ions remain in solution. Under these conditions ferric iron can replace O_2 as the main oxidant according to (Blowes et al., 2014):

Equation 4

$$FeS_{2(s)} + 14Fe^{3+} + 8H_2O \rightarrow 15Fe^{3+} + 2SO_4^{2-} + 16H^+$$

Eq. 4 indicates that for every mole of pyrite oxidised by ferric iron in the presence of water, 16 moles of H+ is produced. The acidity produced by pyrite oxidation can be neutralised by non-Fe-containing carbonates, such as calcite and dolomite according to:

Equation 5

$$CaCO_{3(s)} + H^+ \rightarrow Ca^{2+} + HCO_3^-$$

Equation 6

$$CaMg(CO)_{3(s)} + 2H^+ \rightarrow Ca^{2+} + Mg^{2+} + 2HCO_3^-$$

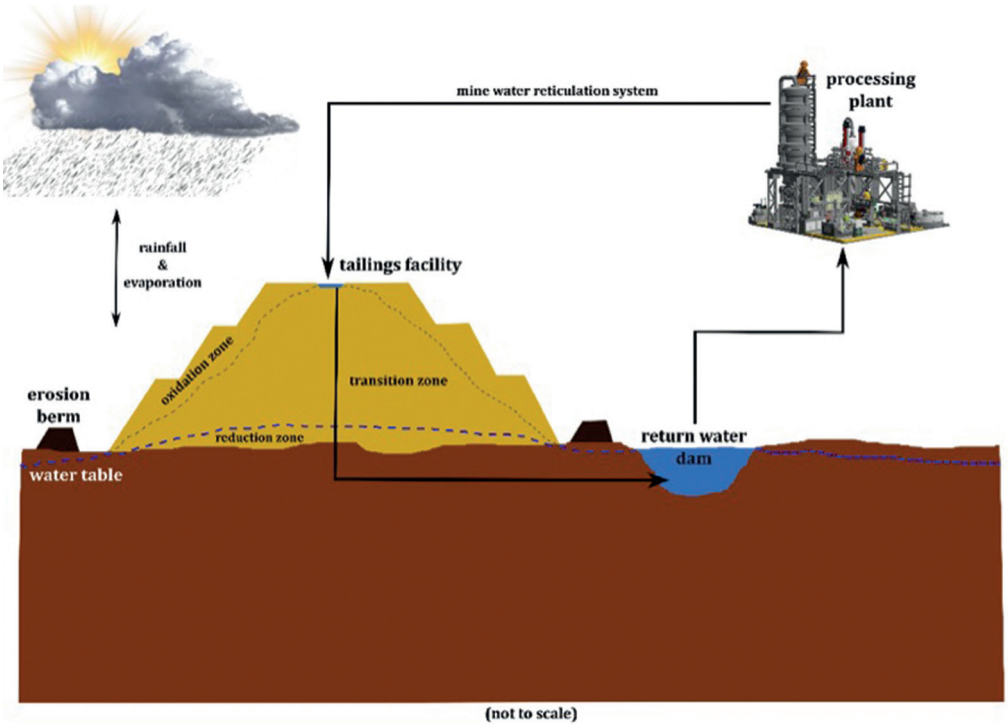

Figure 2 *Conceptual model of the gold tailings facilities in the Witwatersrand gold fields showing the mine-water reticulation flow vectors as well as the geochemical zones.*

The Free State and West Rand gold tailings contain small amounts of carbonates, specifically calcite and dolomite (Hansen 2018). The mass ratio of sulphides to calcite and dolomite are critical in terms of acid buffering in mine waste facilities in general (Jurjovec et al. 2002).

Most Witwatersrand tailings facilities contain the U-bearing phases uraninite and brannerite. Of the two, uraninite is the most abundant in the Witwatersrand (Fuchs et al. 2015, Lottering et al. 2008). Uraninite dissolves in low pH conditions according to:

Equation 7

$$UO_{2(s)} + 4H^{+} \rightarrow U^{4+} + 2H_2O$$

In the presence of O_2, U^{4+} can be further oxidised to U^{6+}, forming the uranyl (UO_2^{2+}) aqueous complex:

Equation 8

$$U^{4+} + \frac{1}{2}O_2 + 2H^{+} \rightarrow UO_2^{2+} + H_2O$$

Eq. 7 and eq. 8 indicates that the dissolution of uraninite in an acidic solution in the presence of oxygen is an acid consuming process.

Thorium is less well studied in the Witwatersrand. Uraninite is a potential source for the Th (Hazen et al. 2009), although thorite has been observed (Smits 1989). However, thorite is often a product of the weathering of thorianite (Smits 1989), making the source mineral of Th in the Witwatersrand uncertain:

Equation 10

$$ThO_{2(s)} + SiO_{2(aq)} \rightarrow ThSiO_{4(s)}$$

Together with uraninite, thorite and thorianite can both weather to add Th to the tailings pore water:

Equation 11

$$ThO_{2(s)} + 4H^{+} \rightarrow Th^{4+} + SiO_{2(aq)} + 2H_2O$$

Equation 12

$$ThSiO_{2(s)} + 4H^{+} \rightarrow Th^{4+} + SiO_{2(aq)} + 2H_2O$$

The solubility of Th in general is very low and typically occurs in solution in the order of µg/L values (Vandenborre et al. 2008, Neck et al. 2002, Langmuir and Herman 1980).

The geochemical processes described above, the hydrological regime of the tailings

facility, and the limitations regarding the depth oxygen can diffuse in the facility, all cause the tailings facility to be stratified into three main geochemical zones (Hansen 2014, Dold and Fontbotè 2001). These three zones from the surface to the base are the oxidation zone (OZ), transition zone (TZ) and reducing zone (RZ) (Dold and Fontbotè, 2001). Recently these zones were modelled geochemically and produced results comparable to water chemistry sites already impacted by tailings material (Hansen 2014).

Numeric modelling

The numeric geochemical model of the Witwatersrand tailings was developed using three main inputs; a gas phase, a liquid phase and a solid phase. The gas phase is initially set to represent the Earth's atmosphere, containing 21% O_2 and 413 ppm CO_2. The fluid phase is set in the OZ model as pure water at pH 7. The output fluid phase at the end of the OZ calculations are used as input to the TZ model. The TZ model fluid output is in turn used as input solution to the RZ model. The output fluid from the RZ model represents the tailings pore water that has percolated through the tailings facility and reaches the substrate as well as the groundwater below the base of the tailings. The OZ and TZ are also in contact with the substrate beneath the tailings, therefore their model fluid outputs also represent tailings pore water from these specific zones, which are in contact with the substrate.

The model solid phase input is the various mineral phases as identified by the QEMSCAN results, of which the main phases are quartz, pyrophyllilte, muscovite and chlorite. Pyrite, uraninite and thorite/thorianite were also added to the model, as these are the main drivers, together with small amounts of calcite and dolomite, of the tailings geochemical system. All the minerals were described kinetically, with the exception of calcite and dolomite. Silicate mineral dissolution was modelled using the default rate equation of the software (Bethke 2008). Pyrite and uraninite reaction rates were modelled using the rate laws of Williamson and Rimstidt (1994) and Torrero et al. (1996) respectively.

There is uncertainty regarding the dominant Th mineral phases, as uraninite, thorianite and thorite are potential candidates. As the mineral phase in which Th resides may have a relevant influence on the release rates of Th and the concentration in the tailings pore waters, it is necessary to either quantify the mineral phase(s) in which Th resides, or to determine whether this quantification is important from an environmental risk assessment perspective.

A Monte Carlo analysis (Purton and Allan 2015, Ulfsbo et al. 2015, USGS 2008, EPA 1997) was conducted to determine whether Th is hosted within uraninite grains, or whether the amount of Th in the Witwatersrand ore material can only be explained by the presence of a separate Th-hosting mineral phase, i.e. in addition to uraninite. The following equation was evaluated in the probabilistic analysis:

Equation 13

$$\frac{(Ur_{\text{whole rock}} \times Th_{\text{Ur grains}})}{Th_{\text{whole rock}}} \times 100$$

In eq. 13, $Ur_{\text{whole rock}}$ represents the amount of uraninite in Witwatersrand gold ore, $Th_{\text{Ur grains}}$ the amount of Th in individual uraninite grains and $Th_{\text{whole rock}}$ represents the total amount of Th in the tailings material.

The simulation results, which are summarised in (tab. 1), indicate that 76% of 10 000 iteration data points lie below the study median of 34, while 24% lie above it. The 95th percentile simulation value is 56%. This indicates that the probability of uraninite accounting for < 56% of the Th in the basin is 95% implying that it is unlikely that uraninite is the only Th-containing phase in the Witwatersrand and that any environmental risk assessment for Th in Witwatesrand tailings needs to take this into account. The other two options are thorianite and thorite, as they are the most likely to occur together with uraninite in the Witwatersand gold ore. Model scenarios were developed for each of these minerals to evaluate their contribution to tailings pore water Th.

The model results (tab. 1) indicate that the pH is acidic in the OZ and increases to 6.02 in the TZ, where it remains relatively constant throughout the rest of the tailings facility. The OZ is oxic, while the TZ become reducing and stays so throughout the RZ.

Table 1 Model output resulst for the three geochemical zones of the tailings facility.

Parameters	Units	Oxidation Zone		Transition Zone		Reduction Zone	
		Thorianite	Thorite	Thorianite	Thorite	Thorianite	Thorite
pH		3.88	3.88	6.02	6.02	6.04	6.04
Eh	V	0.96	0.96	-0.02	-0.02	-0.03	-0.03
TDS	mg/L	4 372	4 372	4 584	4 584	4 552	4 552
U	µg/L	5 060	5 060	202	202	168	168
Th	µg/L	18	23	20	24	20	25

Initially in the OZ, the U concentration is elevated at 5 060 µg/L, but decreases significantly to 202 µg/L in the TZ and to 168 µg/L in the RZ. The Th concentration in the model tailings pore water remains relatively constant in both the thorianite and thorite models at ~20 µg/L.

Discussion

The geochemical models have indicated that U concentrations are likely to decrease in the tailings pore water as it percolates through the material from the OZ though the TZ and RZ to the tailings facility's base. The model has indicated that a number of secondary U mineral phases are over-saturated. They would thus be able to precipitate from the tailings pore water solution. Some of the U minerals over-saturated in the TZ and RZ include uranophane, soddyite, coffinite and uraninite itself. This indicates that the precipitation of secondary U mineral phases in the TZ and RZ may have a significant control on the concentration of U in the Witwatersrand tailings pore water.

Another control on U tailings pore water concentrations may be adsorption. Tab. 2 shows the aqueous species of U in the three geochemical tailings zones. The most important mineral phases in terms of adsorption capacity predicted by the model to be present in the tailings facility are hydrous ferric oxide (HFO) and goethite. However, the point of zero charge (PZC) of HFO is 8.1 and the PZC of goethite is between 6 to 7 (Smith, 1999). Therefore, in the OZ, with a median pH of 3.1, the negatively charged aqueous species are more likely to adsorb (Smith, 1999).

The complex $UO_2(SO_4)_2^{2-}$ occurs in the tailings OZ and can therefore potentially adsorb. The $UO_2(SO_4)_2^{2-}$ complex accounts for 14% of U in the OZ, as well as in the tailings as a whole. Therefore a maximum of 14% U can be expected to adsorb in the absence of competing ligands, which is not the case, as abundant SO42- is present in the tailings pore water, and in the presence of sufficient amounts of HFO and goethite. It is therefore unlikely that adsorption is a dominant geochemical control on the tailings pore water U concentration, although this will need to be quantified in follow-up studies.

Most of the U in the tailings pore water is introduced in the OZ. This implies a causal relationship between pyrite oxidation and uraninite dissociation. eq. 1 to eq. 4 and eq. 7 to eq. 9 indicate that pyrite oxidation introduced H+ into the tailings water, which is then utilised in the uraninite dissolution reaction in the presence of oxygen to produce soluble U(VI) as the UO_2^{2+} species. Thorium can occur in uraninite, but the Monte Carlo analysis has indicated that it is unlikely the major portion of Th in the Witwatersrand is hosted in uraninite grains.

The minerals thorianite and thorite are potential mineral hosts for Th, in addition to uraninite. The geochemical modelling results indicates that from an environmental risk perspective it does not matter in which of the two mineral phases, thorianite and thorite, Th is hosted, as the dissolution of both minerals results in equivalent model tailings pore water Th concentrations. In addition, the Th concentrations in the tailings pore water is low with a maximum of 25 µg/L.

This indicates that either the reaction rate is too slow to introduce environmentally relevant concentrations of Th into the tailings pore water, or that the solubility of the Th minerals are too low.

Table 2 *Model output results of the most important U aqueous species in the various tailings geochemical zones.*

Geochemical Zone	Species	Concentration molality	Concentration U molality	Proportion in tailings zone %	Proportion in whole tailings %
Oxidation Zone	$UO_2(SO_4)_2^{2-}$	$6.59x10^{-6}$	$3.40x10^{-6}$	14.0	14.0
	UO_2^{2+}	$1.08x10^{-5}$	$9.54x10^{-6}$	39.3	39.3
	$UO_2SO_{4(aq)}$	$1.67x10^{-5}$	$1.08x10^{-5}$	44.6	44.6
Transition Zone	$UO_2(CO_3)_2^{2-}$	$1.12x10^{-9}$	$6.83x10^{-10}$	83.0	< 0.1
	$UO_2(CO_3)_3^{4-}$	$1.63x10^{-10}$	$8.64x10^{-11}$	10.5	< 0.1
	$UO_2CO_{3(aq)}$	$6.15x10^{-11}$	$4.44x10^{-11}$	5.4	< 0.1
Reduction Zone	$UO_2(CO_3)_2^{2-}$	$1.14x10^{-10}$	$6.95x10^{-11}$	74.8	< 0.1
	$UO_2(CO_3)_3^{4-}$	$2.61x10^{-11}$	$1.38x10^{-11}$	14.9	< 0.1
	UO_2^{+}	$5.96x10^{-12}$	$5.26x10^{-12}$	5.7	< 0.1
	$UO_2CO_{3(aq)}$	$4.68x10^{-12}$	$3.38x10^{-12}$	3.6	< 0.1

Thorium minerals in general have low solubilities (Neck et al. 2003). Therefore it is likely that the low solubility of the Th mineral host phases is the main important control on tailings Th pore water concentrations.

Conclusions

Although Th does occur in the uraninite mineral structure in the Witwatersrand tailings material, it is not the most important. Most of the Th is hosted by primary Th phases, such as thorianite and thorite. From an environmental risk and geochemical modelling perspective, it does not matter which phase, thorianite or thorite, is chosen to represent Th in the Witwatersrand tailings facilities, as the solubility of both these mineral phases is too low to introduce environmentally relevant concentrations of Th into the tailings pore water.

The most elevated U concentrations in the Witwatersrand tailings facilities occur in the oxidation zone. As the pore water percolates vertically through the tailings facility, the U concentration in the pore water decreases. This is most likely due to the precipitation of secondary U mineral phases. Uranophane, soddyite, coffinite and uraninite were all oversaturated in the model tailings pore water. It is unlikely that adsorption can account for the substantial removal of U from that tailings pore water, as the U generally forms neutral and negatively charged aqueous species in the tailings pore water. This aspect will need to be quantified in follow-up studies.

As most of the U in the tailings pore water is introduced in the oxidation zone, remediation and mitigation efforts for U should be focussed on this zone. These methods can either focus on the pyrite oxidation process or on the secondary impacts, e.g. treatment of groundwater pumped from a borehole adjacent to the oxidation zone down-gradient from the tailings. The challenge with regards to engineering options for operational and post-operational tailings facilities is that funding is much more difficult to source to cover the operational expenditure of many existing technologies. New technologies will have to be developed which provide long-term low operational cost solutions or ideally sustainable passive solution. Bioremediation is a promising field.

References

Cao BC, Gao BY, Liu X, Wang MM, Wang ZL, Yue QY (2011) The impact of pH on floc structure characteristic of polyferric chloride in a low DOC and high alkalinity surface water treatment. Water Research 45:6181–6188.

Chen WS, Wei CH, Han H (2004) Study on the optimum parameters and mechanism of magnetic flocs formation. Sichuan Environment 23:1-4 [in Chinese]

Lan LL (2019) Research progress and application of coal chemical wastewater treatment technology. Guangzhou Chemical Industry 47:43-45 [in Chinese]

Luo LQ, Anh V. Nguyen (2017) A review of principles and applications of magnetic flocculation to separate ultrafine magnetic particles. Separation and Purification Technology 172:85-99

Luo GH, Zhang C, Zheng LB (2019) Optimization and evaluation of magnetic coagulation process

pretreating swine manure biogas slurry. Chinese Journal of Environmental Engineering [in Chinese]

Lv M, Zhang ZH, Zeng JY, Liu JF, Sun MC, Ravi S. Yadav, Feng YJ (2018) Roles of magnetic particles in magnetic seeding coagulation- flocculation process for surface water treatment. Separation and Purification Technology 212:337-343

Qiu JX, Liu J, Huang X (2018) Research progress of magnetic coagulation technology in water treatment. Recylable Resource and Circular Economy 11:40-44 [in Chinese]

Yuan MT (2018) Research on practial application of CODcr determination in water with fast airtight catalysis and digestion method. Modern Chemical Research 01:28-29 [in Chinese]

Effects of Coal Mining on the Lower Zambezi Basin, Tete Province, Mozambique

Vibeke Johansson[1], Estêvão Pondja[2], Kenneth M. Persson[3]

[1]*Division of Water Resource Engineering, Lund University, Lund, Sweden, vibeke.johansson1@gmail.com*

[2]*Chemical Engineering Department, Eduardo Mondlane University, Maputo, Mozambique, tindjombo@gmail.com*

[3]*Division of Water Resource Engineering, Lund University, Lund, Sweden, Kenneth_m.persson@tvrl.lth.se*

Abstract

Recent discoveries of coal in Mozambique have attracted international mining companies to the area. Large amounts of groundwater and surface water are abstracted for coal mining drainage and coal processing. All wastewater is discharged to tributaries of the Zambezi River, which are used for irrigation, domestic purposes, and drinking water supply. A water quality assessment was done of two mines in the Zambezi basin through observations, chemical analysis and measured field parameters. Fieldwork was conducted in April 2019, revealing that both mines lack sufficient treatment of wastewater and one of tailing storage as it is led straight to the tributary.

Keywords: Coal Mining, Mine Drainage, Mine Water, Tete Moatize-Mozambique, Zambezi Basin

Introduction

In the beginning of the 2000's, geological surveys found vast seams of high-value coal in Mozambique which attracted some of the world's largest mining companies to the area. The most affected areas are located in Moatize district in Tete province which has no history of mining. Multinational mining companies such as Vale (Brazil), Jindal (India), ICVL (India), Minas de Moatize (UK) now extract coal there (Pondja E. 2017). It is particularly the high-quality coking coal and metallurgical coal for steel production that is dominating the Mozambican mining sector, where the Permian Karoo formation reserves are estimated to have 23 billion tonnes of exportable coking coal (Resource Sector Mozambique 2018).

The coal mines are extracting large amounts of groundwater and surface water from Zambezi river to meet the needs of the plants. Wastewater is released to tributaries, which downstream are used for irrigation, domestic purposes, and drinking water supply. The aim of this study was to investigate the water quality in the Zambezi basin in Moatize district. It was known that communities around the mines were complaining about deteriorating water quality. By finding out the water components and see what pollution are encountered, prevention and precautions can be developed in a more effective way.

Methodology

The field work was completed the 15th–21st of April, 2019. Field measurements and samples were conducted from five locations: Nhanstanga, Catete, Mbirimbe, Cachoeira and Luenha. The first two are located close to coal mines. Catete is upstream the mines and the last two are in association with small scale gold mining and will not be discussed further in this report. The exact location and number of sampling points were determined when in field. The coordinates for each site were logged in-situ. Photographs and notes were taken during the visits. Collected water samples were sent to a laboratory for analysis. To obtain a better understanding of how the water can affect communities that are using the tributaries for domestic purposes, the results were compared with WHO-drinking water guidelines and the Mozambican standards for water regulations from Ministério Da Saúde (MISAU).

The mines are called Mine A and Mine B on the next page.

Sampling

The sampling process proceeded similarly at each sampling point. A 2L bucket was used to collect water as a grab-samples. Immediately after sampling, the field parameters were measured in the bucket to limit external influences. While collecting water, particles were avoided as much as possible. The measured parameters were pH, electric conductivity, dissolved oxygen, total dissolved solids, salinity, redox-potential and temperature. All measurements were repeated five times. The mean value of the parameters at each point was determined as well as the standard deviation. At each sampling point, two bottles of 100-500 mL with water samples were retrieved. One for analysis of major ions and one for trace elements or metal. All water samples taken for metals analysis were filtered with 0.2 µm filters using a funnel. Four drops of nitric acid per 100 mL sample was then added to the bottles with filtered water to lower pH below 2 and preserve the samples.

Laboratory analysis

Collected samples were kept in cool until sent to a laboratory for analysis. Mbirimbe samples were analysed at Laboratório de Engenharia de Mocambique with an X-ray fluorescence spectroscopic (XRF). The following metals and ions where analysed: Fe, Al, Mn, Zn, Cu, K, Ca, Mg, CL, NH_4^+, SO_4^{2-}, NO_3, CO_3^{2-}, HCO3-. Nhanstanga samples were sent to Instrumental Chemistry at Lund University, where an Inductively Coupled Plasma Optical Emission Spectrometry (ICP-OES) was used for determination of Na^+, K^+, Li^+, Ca^{2+}, Mg^{2+}, Fe, Al, Mn, Zn, Cu, Hg, As, Cd, Pb, and Co. Ion chromatography for analysis of Cl, NO_3^-N and SO_4^{2-} and flow injection analysis (FIA) for analysis of NH4-N.

Water demand

The current size and locations of the mines in Moatize district was found by using google earth satellite images and compared with the conditions 2012, 2015 and 2019. Presently the mines cover an area of approximately 47 km2 altogether. The mines have a lifespan of at least 20 years whereas about 10 has passed. Hence, the mines will continue to grow and cover even larger areas for at least 10 more years.

A rough estimation of the water demand from the mines was made based literature values suggesting an average demand of 250 L of freshwater per tonnes of coal produced (Moon E. 2017) and related to the annual mean flow rate in Zambezi of 3242 m3/s (World Bank 2010). The four main mines have currently a production capacity of extracting almost 40 million tonnes of coal per year or 1.2 tonnes per second (Resource Sector Mozambique 2018), resulting in a water demand of 10 M(m3)/year or 0.32 m3/s. This is equal to 0.1 ‰ of the total average flow in Zambezi River.

Results and discussion

A general picture of the water quality in Tete province was gained, even though conclusions about variations in time and space are rather limited. It has been possible to see some effects on the water quality caused by the mining activities in the area.

Mbirimbe River

Mbirimbe River is a small tributary to Zambezi. It discharges south of Moatize River and Tete City. The water samples were taken a couple of kilometres upstream from the outlet to Zambezi where Mine A has a well-hidden outlet. The community collecting water from the river were complaining about the bitter taste and strange colour that changed over the last two years.

At the first sampling point, left figure 1, the water was brown-red. This could indicate a high content of manganese, iron or aluminium which can give this colour. Degradation of organic matter may also change colour of the water but should not have changed over two years since the mine got operational.

The oily floating layer at sampling point 2, middle photo figure 1, assumingly come from washing the machineries at the mine site with inadequate or no wastewater treatment. An oil-separator could be used to minimize this kind of effluent together with more sufficient waste management.

At sampling point number 3, where the mines wastewater is discharged to the river, the musty smell implied bad water quality as

Figure 1 From left: sampling point 1, 2 and 3 in Mbirimbe River.

Table 1 Measured field parameters in Mbirimbe River.

Mbirimbe	T °C	pH	DO %	DO mg/L	EC µS/cm	TDS mg/L	PSV	Std H2 mV
Point 1	27.7	7.5	109	8.3	8197	5328	4.5	306
Point 2	28.1	7.5	98.5	7.4	7018	4562	3.8	316
Point 3	32.4	7.8	130	9.1	5537	3599	3.0	297

well as the shifting colours and turbidity. It was obvious that the wastewater affected both the water and the biological activity as the type of algae, right picture figure 1, was only found on this spot and in the leakage water.

As in table 1, the high electric conductivity, total dissolved solids and salinity reveal a huge problem with the quality. These parameters all increase downstream in the river from the discharge point. An explanation could be that wastewater coming from the mine dissolve minerals in the rock along the river and thus increasing the metal concentration downstream.

When analysing the water samples several elements were found in large contents, see figure 2 and 3. The high salinity and especially magnesium could explain the bitter taste. The concentrations of Na, Ca, Mg, Cl, SO42-, Fe and Mn all exceeds the drinking water regulations and can cause serious health consequences for the communities that are using the river as a source of water. The community close to Mbirimbe River already noticed problem with agricultural growth and it will probably get worse if no actions are taken.

The reason for the high concentrations is most likely the mining, the use of chemicals in the coal mining process and weathering of rocks. Limestone was observed in the area which might have been neutralizing the acid mine drainage giving the high levels of Ca and Mg. When the limestone is consumed, the pH increases and thereby neutralizing the drainage. SO42-and Fe as well as Al and Mn can all be attributed to acid mine drainage.

Mbirimbe River does not have the capacity, neither flowrate nor quantity

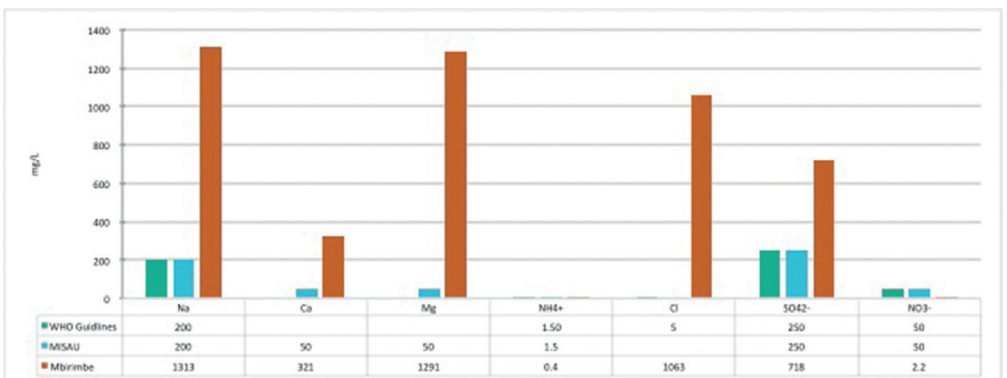

Figure 2 Observed ion concentrations in Mbirimbe River (red) in comparison with WHO-drinking water guidelines (green) and MISAU regulation (blue).

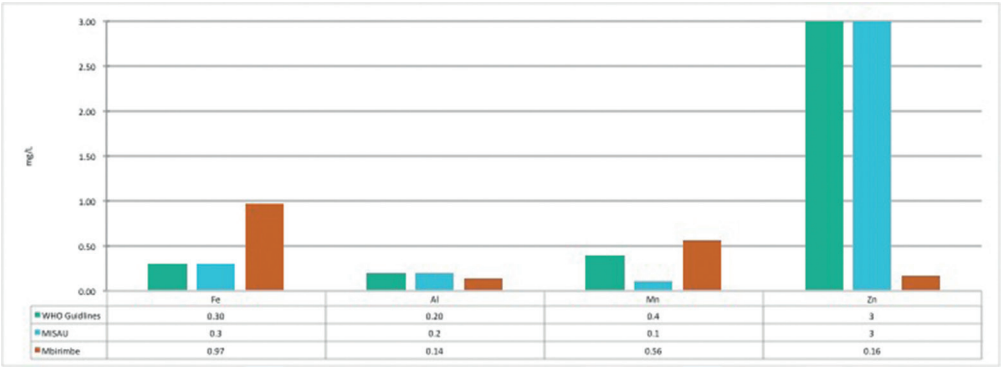

Figure 3 *Observed metal concentrations in Mbirimbe River (red) in comparison with WHO-drinking water guidelines (green) and MISAU regulation (blue).*

to dilute the mine discharge. The mine wastewater needs better treatment and storage for flow equalization.

Nhanstanga River

Nhanstanga River lies in Marara district, north east of Tete City. The river first merge into Chirodzi River, then Sanangua River which flows to the Zambezi River. Mine B discharge wastewater to this tributary and Nhanstanga River has been strongly influenced by the coal mine. What used to be a river that provided whole communities with good drinking water just a couple of years ago is now a black river of tailing from the coal mine. This is not sustainable and directly affects hundreds of people. The depth of coal was about 0.4 m where the river passes the community, left figure 3, about a kilometre from where the mine discharge. Due to low permeability in the coal and recent rain, the surface water found in the river was assumed to be rainwater. At the discharge point, right figure 3, tailing was going straight into the river and will later end up in the Zambezi river.

The borehole measurements in table 2 come from a dug well, 30 m from Nhanstanga river from where the community got their water supply. Another water source in the community was untreated water transported from Zambezi River, referred to as tap water in table 2. Measured field parameters in table 2 shows a significant difference between the discharge water and borehole water compared to the tap water and the water from the river that assumingly was rainwater. In the borehole samples, the water showed similar values to the discharge water with high electrical conductivity and TDS. Water from the river probably infiltrates to the groundwater and thereby affecting the quality of the borehole.

Figure 4 *Left Nhanstanga River, right Mine B discharge point.*

Table 2 Measured field parameters in Nhanstanga River area.

Nhanstanga	T °C	pH	DO %	DO mg/L	EC µS/cm	TDS mg/L	PSV	Std H2 mV
Discharge 1	31.9	8.1	117	8.2	1513	983	0.7	-
Discharge 2	32.4	7.8	120	8.3	1486	966	0.7	294
Discharge 3	32.3	7.7	119	8.2	1468	954	0.7	295
River	32.4	6.9	101	7.0	872	567	0.5	300
Borehole	28.7	6.9	56.7	4.2	1317	848	0.6	333
Tap water	29.3	7.9	112	8.2	143	92.0	0.0	295

The mine effluent at the discharge point contain high levels of Cl, Fe, Al and Hg that exceeds health regulations, figure 6. These are typical elements in mine drainage. While the high contents of Ca and Mg, figure 5, could be a result of weathering rocks, neutralizing acid mine drainage as limestone was observed in the area. Even if the inhabitants in the community did not drink water directly from the river anymore, the cattle still did. Contaminants can be transferred to humans from the cattle through meat and milk or trough crops, if irrigated with unsafe water.

Environmental impact

The timescale it will take for a water quality problem in the tributaries to evolve to Zambezi is difficult to predict. The dilution rate highly depends on the flow which varies between the seasons. The highest concentrations of contaminants will be found in the end of the dry season when the flow is low. Higher

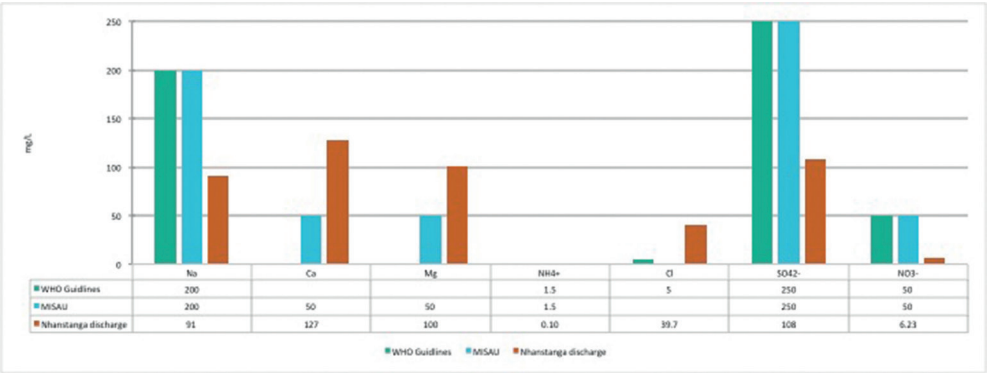

Figure 5 *Detected ion concentrations in Nhanstanga River (red) in comparison with WHO-drinking water guidelines (green) and MISAU regulation (blue).*

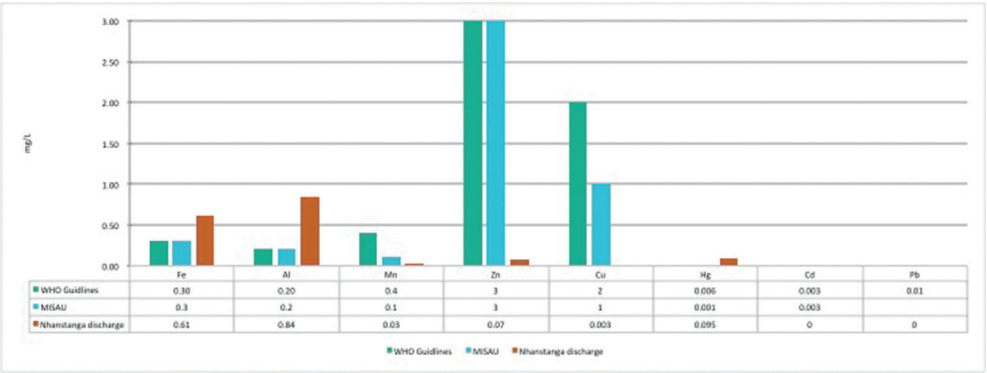

Figure 6 *Detected metal concentrations in Nhanstanga River (red) in comparison with WHO- drinking water guidelines (green) and MISAU regulation (blue).*

flows, on the other hand, gives more dilution and more erosion but less infiltrates and so the contaminates will spread over a larger area. Hence, the time of the field work is very important and effects the results. The field work was carried out in the end of wet season/ beginning of dry season. To fully understand the situation, more measurements are needed over the year, not only in April.

While the mines are growing, more coal is extracted, and larger areas affected, resulting in a higher freshwater use and larger pollution discharge. The composition of the emissions might change as the mining moves through different layers in the ground.

The pH was during both surveys rather neutral and by this the conclusion could be drawn that acid mine drainage has not been and is currently not a problem or that magnesium and calcium carbonates are dissolved by the mine water, thus neutralising it. Elevated sulfate and iron in the drainage indicates a pyrite oxidation process.

Conclusions

The coal mining in Tete province have negative environmental impact. Not only by colouring the ground black and changing the topography, it deteriorates the groundwater and surface water quality. Hundreds of people have already been affected as their drinking water sources are polluted by the mining activity. The local communities noticed that the water changed colour, taste got bitter and crops do not grow as it used to a couple of years ago. The comparison with WHO and MISAU drinking water limits made it clear that the water is not safe for human consumption. The water demand from the mines and areal magnitude has increased over the years. Since not even half of the permitted lifetime has passed yet, the mines will continue to grow with increased water demand and greater emissions. Although, the composition of the emissions might change as the mining moves through different layers in the ground. The large flows within the Zambezi River Basin provide extensive natural dilution but the small tributaries are more vulnerable to pollution. It is of most importance to highlight this problem as the pollution will spread downstream.

Acknowledgements

The authors would like to thank the Swedish International Development Cooperation Agency (SIDA) and S-MultiStor – Unesco-IHE Project for funding this study. A special thanks to the laboratory at Eduardo Mondlane University, Laboratório de Engenharia de Mocambique and Instrumental Chemistry at Lund University which both took part in the laboratory analysis. We are also grateful for the help from ARA Zambeze in Tete during the fieldwork.

References

Johansson V. (2019) A water quality assessment and environmental impact analysis of the local mining along the Zambezi River in Tete, Mozambique, Lund University.

Ministério Da Saúde, MISAU (2004), Regulamento sobre a Qualidade da Agua para 0 Consumo Humano, Boletim Da República- Publicaçã oficial de República de Moçambique, número 37.

Moon E. (2017), Why do coal mines need so much water? https://phys.org/news/2017-04-coal.html, Accessed 7 July 2019.

Pondja, E. (2017). Environmental aspects of coal mine drainage: a regional study of Moatize in Mozambique Lund University.

Resource Sector Mozambique (2018), New markets – New Opportunuties, Club of Mozambique, Deutsche Gesellschaft für Internationale Zusammenarbeit.

The World Bank (2010), The Zambezi River Basin A Multi-Sector Investment Opportunities Analysis Volume 3 State of the Basin, The World Bank, Washington DC.

World Health Organisation (2017), Guidelines for drinking-water quality: fourth edition incorporating the first addendum, Geneva, WHO Library Cataloguing-in-Publication Data 2017 ISBN978-92-4-154995-0.

Characterisation of Secondary Minerals to Minimise Post Rehabilitation Downstream Water Quality Issues at Legacy Mine Sites

David Jones[1], Paul Ferguson[2], Jackie Hartnett[3]

[1]*Principal, DR Jones Environmental Excellence, 7 Edith St, Atherton, Queensland, Australia, 4883, drdrjjones@gmail.com*

[2]*Principal Environmental Geochemist, Robertson Geoconsultants Inc, 580 Hornby St, Vancouver, BC V6C 3B6, Canada, pferguson@rgc.ca*

[3]*Principal Project Manager Rum Jungle Stage 2A, Mines Division, Department of Primary Industry and Resources Northern Territory Government, GPO Box 4550, Darwin, NT, 0801, Australia, jackie.hartnett@nt.gov.au*

Abstract

The remediation of legacy mine sites can be more challenging than operating mines because the waste rock at legacy sites is often substantially oxidised. Oxidised material can contain immediately leachable acidity and metals as well as poorly soluble acidic secondary minerals such as potassium jarosite. The validation of a method to quantify the amount of jarosite, and its implications for the remediation of waste rock at Rum Jungle in Australia is addressed here. Quantifying poorly soluble acidic secondary minerals should be a key component of geochemical characterisation programs and remediation programs for oxidised sulfidic material producing acid mine drainage.

Keywords: acid mine drainage, secondary minerals, jarosite, waste neutralisation, rehabilitation

Introduction

The downstream effects of legacy or abandoned mine sites due to acid and metalliferous drainage (AMD) represent, in the mind of the community, one of the most negative aspects of the mining industry. However, the rehabilitation of these sites to meet contemporary standards can be challenging since, in contrast to operating mine sites that are mining and managing fresh material, sulfidic waste at legacy sites is often broadly distributed across the landscape and already substantially oxidised. This oxidised material can contain immediately leachable acidity and metals as well as poorly soluble acidic secondary minerals such as potassium jarosite - $KFe_3(SO_4)_2(OH)_6$. Thus, achieving protection of the receiving environment from this partly oxidised material can be more complex than for fresh waste rock where protection from oxidation alone can be an effective management strategy.

The former Rum Jungle mine legacy site (Rum Jungle) in Australia's Northern Territory has a long history of adverse effects on downstream water quality and aquatic ecosystem health in the East Branch of the Finniss River (EBFR) and the main Finniss River (Mudd and Patterson 2008). Major rehabilitation works undertaken in the mid-1980s succeeded in reducing (by up to 70%) the loads of acid and metals released from the site, resulting in substantive recovery of the aquatic ecosystems in the EBFR (Jeffree et al. 2001). Despite this extent of improvement, metal concentrations in the EBFR do not meet contemporary water quality standards for ecosystem protection. Additionally, the site is on traditional aboriginal land, with it currently not being in a condition suitable for return to the groups involved.

Since 2009 the Northern Territory and Australian Governments have been working together and engaging with traditional Aboriginal owners, the Kungarakan and Warai peoples, under the framework of a National Partnership Agreement (NPA) to develop a final rehabilitation strategy for the site (fig. 1).

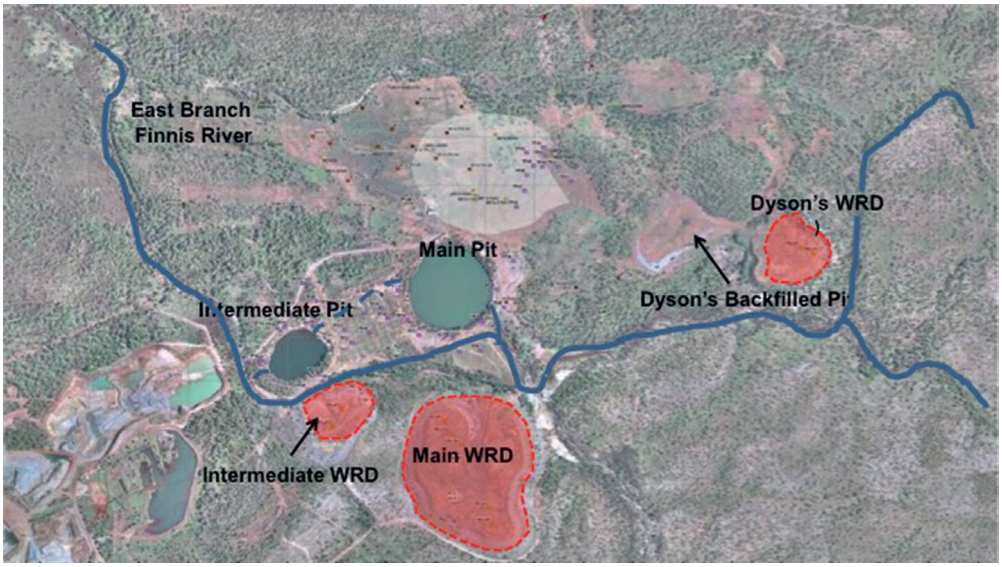

Figure 1 Current configuration of Rum Jungle showing the three covered waste rock dumps (WRD) and the two flooded open pits in close proximity to the east branch of the Finnis River.

Descriptions of the current layout and status of the site, and full details of the proposed rehabilitation strategy, are provided in the recently released Environmental Impact Statement and supporting technical documentation (DPIR 2020). Summaries of the geochemical characterisation program and environmental performance assessment for the proposed works are provided in Jones et. al. (2017) and Ferguson et al. (2017) respectively.

The key objectives of the geochemical characterisation program completed in support of the rehabilitation plan are to:

1. Determine the physical and geochemical properties of Potentially Acid Forming (PAF) and Non-Acid Forming (NAF) waste rock in the existing Waste Rock Dumps (WRDs) and other locations on site; and to
2. Identify PAF waste rock types in the three existing WRDs and surface disseminated material and prioritise for re-location as pit backfill or to a new waste storage facility to minimise future release of existing sulfide oxidation products and ongoing AMD generation from the re-located materials.

Critical to objective 2 is estimating the amount of neutralant required to neutralise existing acidity in re-located PAF materials, so as to reduce as much as practicable the future potential for this existing load to be released to the environment. Existing acidity comprises directly titratable acidity and acidity from poorly soluble secondary minerals. The first of these components can be easily measured by titration. However, quantifying the amounts of secondary minerals present is more challenging. The implementation and validation of a chemical method to quantify the amounts of poorly soluble secondary minerals, and the implications of secondary mineral content for the remediation of waste rock material at Rum Jungle is the focus here.

Methods

Details of the site and the methods of sample collection and preparation and analysis by the standard suite of static tests used for conventional Acid Base Accounting (ABA) to estimate AMD potential (AMIRA 2002, Price 2009, Preventing Acid and Metalliferous Drainage 2016) have been described previously (Jones et al. 2017). The ABA work on material from Rum Jungle was

done by a commercial laboratory (Australian Laboratory Services – ALS, Brisbane).

The mineralogy of a selection of samples was determined by quantitative powder X-Ray diffraction at the Queensland University of Technology, Brisbane. It was identified by this method that the higher PAF category of material contained substantial (up to 5 wt.%) quantities of jarosite, and no detectable alunite or barite. Since the jarosite component comprised a substantial proportion of the existing acidity in these selected samples it was concluded that all of the samples that had been characterised by the conventional ABA approach should also be screened for their jarosite content. A less costly and time-consuming method than X-ray mineralogy was needed to be applied to the large numbers of samples collected for this work. There are three chemical methods that have been evaluated for accuracy in the determination of jarosite:

1. Overnight extraction at room temperature with 4M hydrochloric acid
2. Pyrolysis at 550 °C for 1 h, followed by extraction with 4M HCl for 30 min. (Li et al. 2007).
3. Extraction with boiling sodium carbonate solution (MEND 2009)

In summary, these methods involve the determination of total sulfate in a sample, from which the water-soluble sulfate is subtracted to yield secondary mineral sulfate by difference. Sulfate comprises 38.3% by weight of potassium jarosite.

However, as noted by Price (Price 2009, Chapter 12) the efficacy of chemical methods to quantitate the amount of jarosite often depends on the provenance of this phase. Consequently, it was necessary to validate the recoveries of each of the potential methods against the XRD-determined jarosite contents for material from Rum Jungle, prior to screening the large numbers of samples required (Jones 2015).

Method 1 has been reported to underestimate the amount of sulfate associated with jarosite, although it has been suggested that 16h extraction should be long enough to recover at least 80% (Li et al. 2007). The muffle furnace pre-treatment functions by converting all sulfide sulfur in the sample to volatile sulfur dioxide, which is lost from the furnace. The jarosite is thermally altered to a much more soluble form such that only a sort time (ca. 30min) extraction with the 4M HCl should be sufficient (Li et al. 2007).

Each of the three methods was evaluated for jarosite recovery using a number of samples with different jarosite content, with the XRD-determined values for jarosite used for comparison (Jones 2015). It was found that Method 1 substantially underestimated (by >50%) the jarosite content. Method 2 was found to provide good recovery of jarosite, albeit with somewhat variable results. However, it would be a more difficult and time-consuming method to carry out for a large number of samples given the requirement for the muffle furnace pre-treatment.

Overall, Method 3 was found to provide the most consistent agreement with the jarosite content as determined by XRD (see Results and Discussion). It was also a very easy method to apply for the large number of samples required for the Rum Jungle project. The samples were sent to the ALS laboratory in Vancouver British Columbia Canada, which had a routine implementation of the method (ALS method GRA06).

Results and discussion

The identification of a reliable and robust method for the determination of jarosite in the variably oxidised Rum Jungle waste rock was key to efficiently quantifying the total existing acidity and hence neutralant demand of the material. The process of testing of three candidate methods was summarised above. Final confirmation of the efficacy of the sodium carbonate extraction method (Method 3) was provided by comparing XRD values with Method 3 for 10 samples spanning a wide range of jarosite contents (fig. 2). The correlation is high as demonstrated here in Figure 2.

The two existing acidity components (titratable and jarosite) are summarised below (tab. 1) for the three PAF classes defined for the waste from Rum Jungle (Jones et al. 2017). It can be seen in this summary that jarosite is by far the dominant component of total existing acidity.

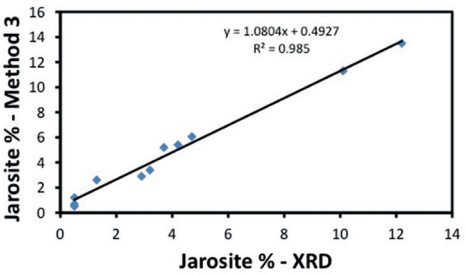

Figure 2 Correlation between jarosite content determined using Method 3 (sodium carbonate extraction and quantitative XRD.

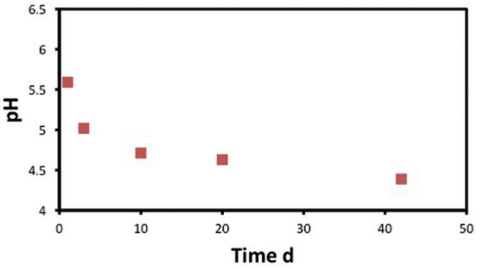

Figure 3 Decline in pH through time if only titratable acidity in waste rock is neutralised.

The data in Table 1 show that for the Rum Jungle site, measuring only readily titratable acidity would have resulted in a gross underestimate of neutralant demand for the waste and hence failure to add sufficient neutralant to stabilise this component of acid (and hence leachable metal) load. In particular, a neutralisation QC program that used short term pH alone as an indicator of success would not have detected that anything was wrong with the remediation work. The consequence of incomplete neutralisation would be that over time the acidity contained in the slowly reacting jarosite would buffer the pH downwards to around pH 3 to 4, resulting in the redissolution of initially precipitated and immobilised metals. This effect is shown (fig. 3) for a sample of waste rock containing 15 kg H_2SO_4/t jarosite acidity and 4 kg H2SO4/t titratable acidity, to which sufficient finely ground $CaCO_3$ was added to account for the titratable acidity only. The starting pH prior to neutralant addition was 3.4.

Finely ground agricultural lime – $CaCO_3$ – was selected as the neutralant of choice for the waste remediation project based on the findings from mixing tests that indicated the bulk of target metals were removed from solution by the pH (ca. 7) that could be achieved with this neutralant (Jones et al. 2017). Excess neutralant will be added according to the conservative dosing regime that has been determined for each of the PAF categories (Jones and Ferguson 2019).

Conclusions

The room temperature hydrochloric (HCl) acid extraction method currently routinely used to determine jarosite content in AMD assessments was found to substantially underestimate the amount of jarosite present in the Rum Jungle waste rock. Of the two methods tested that did yield good recovery, the one using extraction with boiling sodium carbonate is recommended for routine application.

The existing acidity (neutralant demand) of the acidic samples that were tested from Rum Jungle was found to be dominated by jarosite. This is a critical finding since failure to quantify the acidity contributed by jarosite would have resulted in a gross underestimate of the amount of neutralant needed to account for this source of acidity. The findings from this work emphasise the need for a validated method for the measurement of acidic low solubility secondary minerals to be applied for those remediation projects involving oxidised waste rock.

Table 1 80th Percentile Values for PAF Rock Types.

Type	%S	AMD Potential	Jarosite Acidity kg H_2SO_4/t	Titratable Acidity kg H_2SO_4/t	Total Existing Acidity kg H_2SO_4/t
PAF-I	5.1	High	14.8	2.8	17.6
PAF-II	1.5	Medium	13.1	1.5	14.6
PAF-III	0.8	Low	3.2	1.2	4.4

References

AMIRA (2002), ARD Test Handbook – Prediction & Kinetic Control of Acid Mine Drainage, Project P387A, AMIRA International Limited, Melbourne, Australia. https://www.resolutionmineeis.us/documents/amira-2002

DPIR (2020) Draft Environmental Impact Statement for the former Rum Jungle mine site, Department of Primary Industry and Resources, Northern Territory Government, January 2020.

https://ntepa.nt.gov.au/environmental-assessments/register/rum-jungle-former-mine-site/draft-environmental-impact-statement.

Ferguson P, Jones DR and Laurencont T (2017) Rehabilitation Planning at the Former Rum Jungle Mine Site in Northern Australia. Part 2. Environmental Performance Assessment for the Preferred Rehabilitation Strategy. In (Eds. Bell, LC, Edraki, M, Gerbo C (Eds) Ninth Australian Workshop on Acid and Metalliferous Drainage, Burnie, Tasmania, p 280-289.

Jeffree RA, Twining JR, Thomson J (2001) Recovery of fish communities in the Finniss River, Northern Australia, following remediation of the Rum Jungle uranium/copper mine site Environ. Sci. Technol 35: 2932-2941.

Jones DR (2015) Validation of Methods to Determine the Neutralant Demand of Rum Jungle Waste Rock, Report DME001/14, NT Dept of Mines and Energy.

Jones DR and Ferguson P (2019) Rum Jungle mine site. Physical and geochemical characteristics of waste rock and contaminated materials (rev2), REPORT NO. 183008/2 by Robertson Geoconsultants Inc and DR Jones Environmental Excellence for Northern Territory Department of Primary Industry and Resources, November 2019, 379pp. https://dpir.nt.gov.au/mining-and-energy/mine-rehabilitation-projects/rum-jungle-mine/completed-studies.

Jones DR, Ferguson P, Laurencont T (2017) Rehabilitation planning at the former Rum Jungle mine site in Northern Australia Part 1. Geochemical Characteristics of Mine Wastes and Inferred Post Rehabilitation Source Terms. In (Eds. Bell, LC, Edraki, M, Gerbo C (Eds) Ninth Australian Workshop on Acid and Metalliferous Drainage, Burnie, Tasmania, p 271-279 .

Li J, Smart R, Schumann R, Gerson A, Levay G (2007) A simplified method for estimation of jarosite and acid-forming sulfates in acid mine wastes. Science of the Total Environment, 373:391-403.

Mudd GM, Patterson J (2008) The Rum Jungle U-Cu Project: A Critical Evaluation of Environmental Monitoring and Rehabilitation Success. In: Broder JM, Andrea HB (Eds), Uranium Mining and Hydrogeology V, Freiberg, Germany, p 317-327.

Preventing Acid and Metalliferous Drainage (2016) Leading Practice Sustainable Development Program for the Mining Industry, Australian Government Department of Industry Innovation and Science, September 2016, 221pp. www.industry.gov.au/resource/Programs/LPSD/Pages/LPSDhandbooks.aspx#

Price WA (2009) Prediction Manual for Drainage Chemistry from Sulphidic Geologic Materials. MEND Report 1.20.1. CANMET – Mining and Mineral Sciences Laboratories. Smithers, British Columbia. V0J 2N0.

Beneficiation of Salts Crystallized from Lake Katwe Brine

Joseph Ddumba Lwanyaga[1,2], Hillary Kasedde[2], John Baptist Kirabira[2], Alan Shemi[3], Sehliselo Ndlovu[3]

[1]*Department of Mining and Water Resources Engineering, Faculty of Engineering, Busitema University, P.O. Box, 236, Tororo, Uganda.*

[2]*School of Engineering, College of Engineering, Design, Art and Technology, Makerere University, P.O. Box, 7062, Kampala, Uganda.*

[3]*School of Chemical and Metallurgical Engineering, University of Witwatersrand, Private Bag 3, Wits 2050, 1 Jan Smuts Avenue, Johannesburg, South Africa.*

Abstract

A salt extraction process to enhance the quality and quantity of salt produced at Lake Katwe in Uganda is presented. To validate the designed process, laboratory experiments were conducted. The techno-economic analysis of the process flow sheet was modeled and simulated by SuperPro Designer. Halite of purity >98% was obtained by floating burkeite and trona which co-precipitate with it during evaporation. The other feasible products of the process are soda ash and sodium sulfate. With a net present value of US$25,077,817, the proposed process is economically viable.

Keywords: Salt Extraction, Lake Katwe, Sodium Chloride, Soda Ash, Sodium Sulfate, SuperPro Designer

Introduction

In Uganda, Lake Katwe is the major source of brine containing valuable minerals (Kirabira et al. 2013). The reserve contains about 22.5 million tonnes of crystalline salts (UDC 1997). At the deposit, salt mining has been taking place since precolonial times using rudimentary methods. As a result, the mined salt is of low quality (55.8 – 94.8% halite content) (Kasedde et al. 2014) and quantity thus, fetching small prices on the market. Due to this, Uganda imports over 90% of the salt from neighbouring countries (Chopra 2020).

The government of Uganda in the 1970's established a salt processing plant which failed within a few months without posting any results (UDC 1997). The process involved heating brine by steam in a series of evaporators operating at different temperatures. Additionally, cyclones, centrifuges, and filters were employed to separate crystals from the mother liquor. The expected primary product of this process was halite with potassium chloride as the secondary product. The failure of this process could be attributed to lack of the requisite phase chemistry knowledge of the raw material that resulted in severe corrosion of the plant equipment.

Kasedde et al. (2014) characterised the raw material and determined that the brine constituted mainly Na^+, Cl^-, SO_4^{2-}, CO_3^{2-}, HCO_{3-} with lesser amounts of K^+, Mg^{2+}, Ca^{2+}, Br^-, and F^- ions. Several thermodynamic studies followed (Kasedde et al. 2013; Lwanyaga et al. 2018, 2019b,a)with a rich source of mineral salts. The present work aims at evaluating possibilities of future salt extraction from the lake deposit. An isothermal evaporation experiment was conducted on the lake brines. The precipitated salts were characterized by X-ray diffraction (XRD that established the major evaporites as halite, burkeite, trona, and thenardite. These phase equilibrium studies have reported the mineral crystallization sequence as generally sulfate, halides and lastly carbonates. Furthermore, the evaporites co-precipitate with each other (Lwanyaga et al. 2019b,a) 40, 50, 60 and 70 and therefore, cannot be separated by simple techniques. From the above-mentioned studies, it was found that Lake Katwe brine composition is different from sea water and other notable salt lakes (e.g. Magadi, Dead

Sea, and Searles Lake). Therefore, a unique salt extraction process has to be tailored/ customised to suit the brine at hand.

It is upon the knowledge of the aforementioned phase chemistry that the existing single solar pond system at Lake Katwe can be improved. The climate at Katwe is semi-arid with ambient temperatures ranging between 24 – 38 °C, an annual evaporation rate of 2160 mm/yr, and a precipitation of 860 mm annually (Kasedde et al. 2014). The foregoing conditions, coupled with low energy, capital and labour costs, make Lake Katwe a suitable place for solar salt production (Hocking 2005). Thus, the present study aims at developing a conceptual design for a commercial salt extraction process at Lake Katwe for the recovery of common salt and its co-products with solar as the main source of energy. SuperPro Designer v10 (Intelligen Inc 2019), a computer aided process design and simulation tool was used to conduct a techno-economic evaluation of the proposed process.

Process Development and Description

The proposed process employs sequential solar evaporation ponds as crystallizers for the readily processable salts from the brines of Lake Katwe. The evaporation ponds operate at atmospheric pressure and at an average ambient temperature of 30 °C (Kasedde et al. 2015). The brine residence time in a particular pond is determined by the brine density and pH. In the first pond, the brine is concentrated to precipitate calcite and magnesite. The brine is further concentrated in the second pond to precipitate sodium chloride with minimum contamination from burkeite and trona. By employing the flotation technique, the burkeite and trona crystals are separated from the sodium chloride (halite) slurry. The halite slurry is then dried in an open tray to produce common salt. The second pond filtrate is carbonated to precipitate the insoluble sodium bicarbonate, also known as nahcolite, in a NaCl saturated solution. The nahcolite is then calcined to produce sodium carbonate (soda ash). The supernatant from this step is processed first by freezing it in a cooling crystallizer to produce mirabilite also known as Glauber's salt. The mirabilite is further dehydrated in an evaporative crystallizer to produce thenardite, a useful raw material in the glass and paper industries. The rest of the liquid is discarded as waste.

Methods and Materials

Laboratory experiment

A 3 L natural brine sample obtained from the surface of Lake Katwe during the rainy season was used in the experiment. The chemical composition of the brine is shown in Table 1. The brine solution was evaporated sequentially in a thermostatic water bath (Model 207, Lenton Furnaces, South Africa) at a temperature of 85 °C under atmospheric conditions for 12 h until a pH of 9.74 and density of 1.282 g/cm^3 were attained. A high temperature of 85 °C was employed in order to reduce the time needed to concentrate the brine to the desired brine conditions. Upon the start of crystallization, the brine was cooled down to 30 °C, which is the average ambient temperature at Lake Katwe (Kasedde et al. 2015). The subsequent evaporation processes were handled under the same conditions of temperature and pressure.

The precipitates from the first evaporation step were filtered off using a vacuum filter (Model LVS 300 Z, Welch, Germany) and discarded. The filtrate from the first evaporation step was further concentrated to a density of 1.302 g/cm3 and the crystallised solids ground to -35 mesh particle size and later mixed with water at a ratio of 1:2 before loading the mixture on a laboratory froth flotation machine (D12 (VFD-L), Denver, USA). The flotation was done in the presence of octadecylamine surfactant at a concentration of 500g/ton for 30 min. The froth was discarded and the clarified material dried in a desiccator at 70 °C for 3 h. This was followed by evaporating the filtrate from the second evaporation step to dryness. The resulting solids were dissolved and carbonated in a jacketed reactor at 50 °C for 3 h to produce sodium bicarbonate. The sodium bicarbonate was filtered and calcined in a muffle furnace (Model KLS 03/10/M, ThermConcept, Germany) at 200 °C for 1 h to form soda ash. The filtrate from the carbonation process was cooled in a cooling

Table 1 Brine chemical composition.

pH	Brine Temperature (°C)	Density (g/mL)	Major ions (mg/L)								
			Na	K	Mg	Ca	Cl	Br	SO_4	HCO_3	CO_3
10.4	25	1.12	4350	766	3.08	1.44	33600	390	21700	1710	4330

crystallizer at -2 °C for 30 min and later dehydrated in an evaporative crystallizer at 50 °C for 45 min.

Analyses

The mineralogy of the solids was determined using an X-ray diffractometer (Model, Malvern PANalytical Aeris 300W, Netherlands) operated with a PIXcel detector and fixed slits with Fe filtered Co-Kα radiation (λ = 0.1540 nm, operating at 40kV and 7.5 mA). The XRD data was collected from 5 to 80° (2θ) in a continuous scan mode with a scanning step size of 0.02°. The phases were identified using X'Pert Highscore plus software that runs with the ICDD database. The relative phase amounts (weight %) were estimated using the Rietveld method. For the liquid samples, the anion composition of Br^-, Cl^-, SO_4^{2-} CO_3^{2-}, and HCO_3^- in the liquid phase were determined using the ion chromatography method. The cations in the aqueous phase were determined using the ICP-OES technique. The pH was measured by an Ohaus starter 300 pH meter and the density of the liquid samples was determined gravimetrically using a pycnometer and a weighing scale.

Results and Discussion

Process scheme validation

In the first evaporation step, the mineral composition of the precipitates after concentrating raw brine from a density of 1.12 to 1.282 g/cm^3 comprised calcite and magnesite at 30 °C. The brine pH decreased from 10.4 to 9.74. At this stage, according to the thermodynamic calculations performed by PHREEQC (Parkhurst and Appelo 2013) a Pitzer specific-ion-interaction aqueous model, and the SIT (Specific ion Interaction Theory, about 56% of the initial free water had been evaporated. The precipitates from this step were not processed further due to their low quantities and thus low economic importance. The filtrate saturated with sodium chloride from the first evaporation step was concentrated further to a density of 1.302 g/cm^3 in the second evaporation step. To get to this point, 76% of the initial free water was evaporated. This resulted into the precipitation of salts that weighed 273.514 g which comprised mainly halite contaminated by trona and burkeite as seen in Table 2 (sample 1). In the third evaporation step, the filtrate from the second evaporation step was evaporated to dryness producing burkeite with traces of trona, halite and calcite as seen in Table 2 (sample 2). These precipitates weighed 150.771 g. It should be noted that, glaserite was not present as predicted by PHREEQC. The reason for this is that, the PHREEQC model only accounts for thermodynamic aspects yet at the deposit, both the thermodynamics and kinetics aspects affect the mineral crystallization (Lwanyaga et al. 2019a). As a result, some minerals precipitating from the model might not precipitate in the actual setting and vice versa (Lwanyaga et al. 2019a).

The precipitates from the second evaporation step were subjected to a flotation process using octadecylamine as the surfactant to float burkeite and trona thus leaving purer halite. The froth presumably containing burkeite and trona was discarded. The clarified material was dried in an open

Table 2 XRD Quantitative analysis of evaporites from the second and third evaporation steps (wt%)

Sample ID	Trona	Burkeite	Halite	Calcite
1	5.8	2.6	91.6	0
2	10.6	84.8	4.3	0.3

pan and a sample of the solids characterised. The XRD qualitative analysis as shown in Fig. 1 reported halite as the only crystalline material remaining thus confirming the removal of burkeite and trona. It, however, reported a 10.1wt.% composition of amorphous material. This could be due to zan error in the determination of the quantity of the amorphous material which was reported to be about ±15 weight %. Halite was reported to be 89.9wt.% and the amorphous material, 10.wt.%. However, the amorphous content was higher than expected.

A sample of the precipitate from the carbonation process was characterised. The XRD analysis revealed that 81.6% was nahcolite (sodium bicarbonate) contaminated by burkeite and trona with traces of halite. The reported amorphous phase composition of 5.6wt.% is within the margin of error. The crystalline precipitate (majorly sodium bicarbonate) from the carbonation step were calcined at 200 °C for 1 h. This produced crystalline solids constituting mainly natrite (soda ash) contaminated by burkeite and thermonatrite with traces of halite. There is a big composition (38.1wt%) of the amorphous phase in the posted results. This could be due to the presence of some impurities like clay. It is worth noting that all the nahcolite from the carbonation process was converted into soda ash and thermonatrite. However, the burkeite composition remained constant since the calcination process was not intended to decompose it into its constituent compounds.

The supernatant from the carbonation process was frozen at -2 °C for one hour; a white emulsion was observed. The XRD analysis shows that burkeite is the dominant phase followed by nahcolite, trona, natrite, thermonatrite and halite. The purpose of this step was to crystallise out mirabilite and thereafter dehydrate it to produce thenardite. The results posted here deviate from the expected results. This could be attributed to the variation in temperature of the sample during transportation to the storage facility at the XRD lab. The presence of burkeite attests to the presence of sulfate which were the target of the process. The presence of nahcolite and other carbonates of sodium may be due to the incomplete precipitation process during the carbonation process or vacuum filtration inefficiency. In a well controlled environment, the suggested unit procedures are expected to produce thenardite.

Process flow sheet simulation

In this study, a flowsheet based on the laboratory experiment and PHREEQC software was simulated. As seen in Fig. 2, the raw brine (Table 1) is concentrated at 85 °C in the first reactor (R-101)/ Pond 1 for 12 h to precipitate carbonates and sulfate of

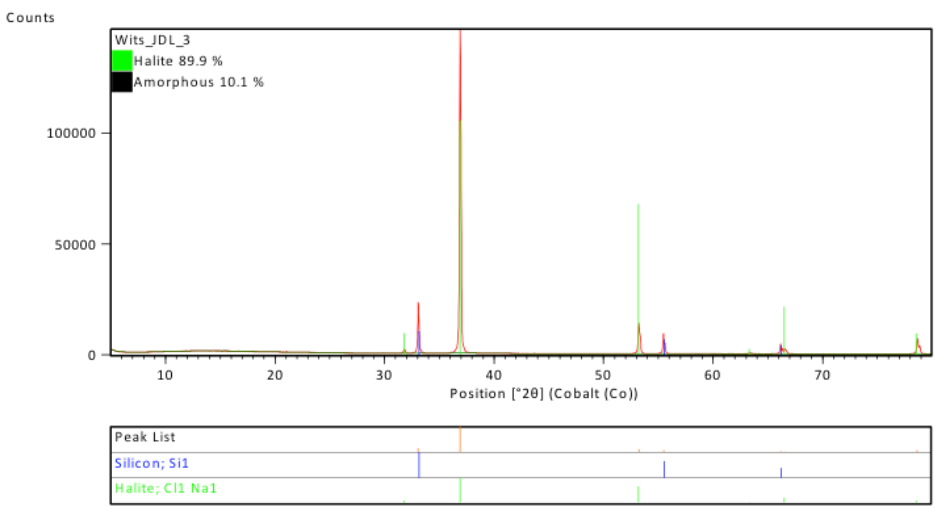

Figure 1 *XRD analysis of purified halite*

calcium and magnesium. These are filtered off (P-2/ PFF-101) and discarded. The solar pond is presumed to behave like a reactor where both evaporation and crystallization take place. The filtrate from the first pond is further concentrated in the second reactor (R-102)/Pond 2 to mainly precipitate halite contaminated by burkeite and trona. The precipitates are filtered off (P-4/ PFF-101) and the cake subjected to flotation (FL-101). The froth presumably constitutes mainly burkeite and trona which are discarded. The halite is the clarified material that is dried at 70 °C in the tray drier (TDR-101)/grainer pan to form common salt of over 99% purity. It was noticed that instead of evaporating the filtrate from pond 2 before carbonation, it was better to carbonate it in order to avoid formation of complex minerals such as burkeite and trona (Garrett et al. 1975). Therefore, the filtrate from Pond 2 was carbonated (R-103) at 50 °C for 4 h to form sodium bicarbonate. The bicarbonate was further calcined (Garrett et al. 1975) (GBX-101) at 200 °C for 45 min to form soda ash. The supernatant from the carbonation process was cooled at -2 °C in a crystallizer (CR-101) to form mirabilite. The formed mirabilite is dehydrated in an evaporative crystallizer (CR-101) at 50 °C to form sodium sulfate (Garrett et al. 1975).

Cost analysis and Economic evaluation

The economic feasibility of the proposed process was modeled using SuperPro Designer. For design purposes, the simulation was set to design mode to automatically size the equipment and the size of the equipment determined its purchase cost. An extra 20% on the equipment budget was factored in for contingencies such as the minor equipment which was not enlisted in the process flow sheet. The costs arising from building, installation and piping were integrated into the total investment cost.

A number of economic evaluation parameters for the entire project were assumed; year of analysis and construction as 2020, and a project lifetime of 20 years. Out of the 365 days in a year, the plant will be operated for a period of 243 days annually because the other 122 days are not suitable for solar salt production due to the rainy season. Therefore, the rainy season will be used for plant maintenance.

A minimum of 500,000 L of raw brine per batch is needed for economic viability of the venture. A total of 41 batches are executed annually requiring 52.47 h per batch. From this, 63,729 kg, 10,499 kg, and 8,239 kg per batch of common salt, soda ash and sodium sulfate respectively are expected to be produced. As

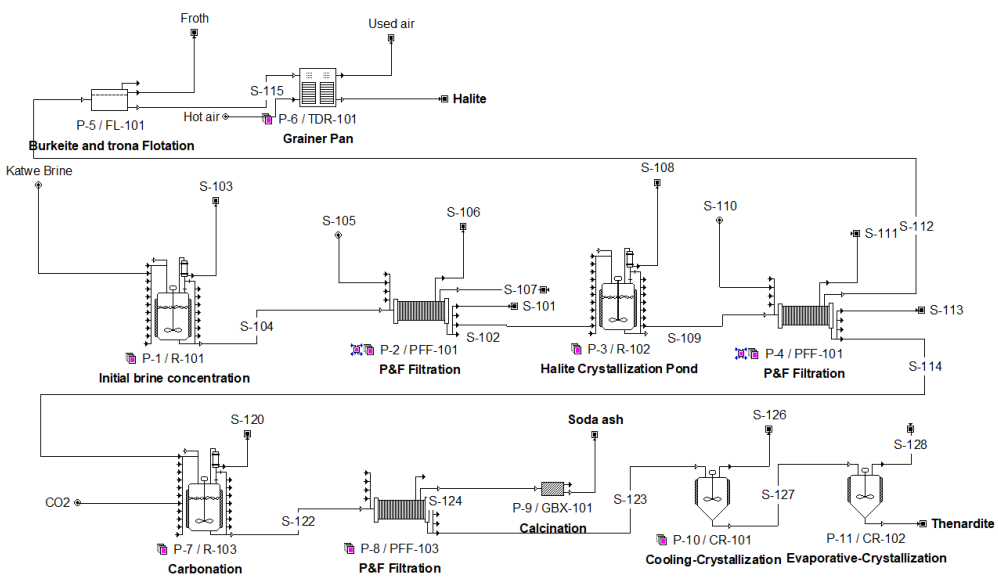

Figure 2 *Process flow sheet for the extraction of halite, soda ash and thenardite from Lake Katwe brine.*

a result, a total investment worth US$7.5m is required to start the project. Between 30% and 40% of the annual operating cost will be spent on maintaining the plant. On average, the annual salt imports in Uganda for the year ended December 2019 was UGX. 94.7 billion shillings (US$25 million) (Chopra 2020). An average cost of capital of 10% was used as per the Uganda Development Bank that can support the financing of the plant (Khisa 2020). All the profitability indices are positive with a payback period of 18 years, Return on Investment of 10.54%, an Internal rate of return of 6.955 and a net present value of US$25,077,817.30 without inflation consideration. Therefore, it is economically feasible to exploit Lake Katwe brine which in turn will reduce Uganda's dependency on imported salt.

Sensitivity Analysis

A differential sensitivity analysis was performed with the aim of studying how changes in the project economic variables would influence the economic viability of the project. Sensitivity margins are computed and summarised in Table 3.

From Table 3, the total annual revenue/salt revenues, has the lowest sensitivity margin (i.e. 0.518) as compared to other parameters. This implies that if the salt sales are decreased below 51.8%, then the process plant will cease to be economically viable. Salt being a domestic necessity, such a fall in revenue isn't expected unless other competitors join the market. The sensitivity results also show that, the project will not be economically viable should the annual operating costs increase beyond 295%. The sensitivity margins in Table 3, suggest a sound process design simulation in Fig. 2. For the plant investment to break even, the cost of capital should not be beyond 16.87%. A headline inflation rate of 2.8% was adopted to adjust the annual revenues while an inflation rate of 6.2% for energy, operating, production and maintenance costs was used (UBOS 2020). Table 4, indicates the effect of change in the inflation rate on payback period and net present value (NPV). A double digit (high-end) inflation rate of 10% still indicates that the designed process is still economically viable with an NPV of US$ 18,872,444.23.

Conclusions

An improved solar salt extraction process is presented as an alternative technique to foster the purity and quantity of salt extracted at Lake Katwe. The method is based on solar evaporation coupled with flotation and drying for the production of common salt of purity >98%. Soda ash is produced by carbonation and calcination after the extraction of halite. Lastly, successive cooling and evaporative crystallization processes lead to the production of sodium sulfate. An economic analysis conducted in SuperPro Designer revealed that the salts can be produced at a cost that is competitive on the market.

Acknowledgements

The authors gratefully acknowledge the financial support from the Swedish

Table 3 *Sensitivity Margins for economic variables.*

Item	Amount US$	PV US$	Sensitivity Margins
Direct Investment cost	6,204,320	(6,204,320.0)	4.042015843
Indirect Investment cost	1,523,826	(1,523,826.0)	16.45723313
Annual operating cost	998,336	(8,499,433.4)	2.950544894
Annual Energy cost	33,267	(283,222.0)	88.5452607
Equipment purchase cost	751,250	(751,250.0)	33.38164357
Annual Direct Production Cost	427,369	(3,638,448.7)	6.892486792
Indirect Production cost	71,228	(606,406.7)	41.35501752
Annual Maintenance Cost	215,679	(1,836,204.7)	13.6574965
Total Annual Revenues/Sales	5,687,271	48,419,150.4	0.517934733
Salvage	12,926	1,920.8	13055.97289

Table 4 Sensitivity analysis of change in inflation rate on economic viability.

	Without Inflation	Single digit inflation	Double digit inflation
Payback period (years)	4.61	5.48	6.01
NPV US$	25,077,817.30	26,914,589.01	18,872,444.23

International Development Cooperation Agency (Sida) and Makerere University. Special thanks go to the Hydrometallurgy Research Group at the School of Chemical and Metallurgical Engineering, University of Witwatersrand, Johannesburg South Africa for hosting and assisting the lead author to run the experimental work.

References

Chopra A (2020) Annual salt import grow to Shs 94.7 billion. Dly. Monit.

Garrett DE, Kallerud MJ, Chemtob EM (1975) Beneficiation of Salts Crystallized for Searles Lake Brine. 6.

Hocking MB (2005) Handbook of Chemical Technology and Pollution Control. Elsevier.

Intelligen Inc (2019) SuperPro Designer, User Guide. Scotch Plains, NJ, USA.

Kasedde H, Bäbler MU, Kirabira JB, et al (2013) Mineral recovery from Lake Katwe brines using isothermal evaporation. In: Brown A, Figueroa L, Wolkersdorfer C (eds) Reliable Mine Water Technolgy. Publication Printers, Denver, Colorado, USA, pp 855–860.

Kasedde H, Kirabira JB, Bäbler MU, et al (2014) Characterization of brines and evaporites of Lake Katwe, Uganda. J African Earth Sci 91:55–65. doi: 10.1016/j.jafrearsci.2013.12.004.

Kasedde H, Lwanyaga JD, Kirabira JB (2015) Optimization of Solar Energy for Salt Extraction from Lake Katwe, Uganda. Glob NEST J 16:1152–1168. doi: 10.30955/gnj.001367.

Khisa I (2020) Uganda Development Bank to cut lending rates. Indep.

Kirabira JB, Kasedde H, Semukuuttu D (2013) Towards The Improvement of Salt Extraction At Lake Katwe. Int J Sci Technol Res 2:76–81.

Lwanyaga JD, Kasedde H, Kirabira JB (2018) Thermodynamic Modeling Of Lake Katwe Brine For Industrial Salt Production. Int J Sci Technol Res 7:31–37.

Lwanyaga JD, Kasedde H, Kirabira JB (2019a) Effect of Temperature on Mineral Precipitation Sequence of Lake Katwe Brine during Evaporation. Curr J Appl Sci Technol 33:1–12. doi: 10.9734/cjast/2019/v33i630104

Lwanyaga JD, Kasedde H, Kirabira JB (2019b) Mineral Precipitation Sequence During Evaporation of Lake Katwe Brine. In: Khayrulina E, Wolkersdorfer C, Polyakova S, Bogush A (eds) IMWA2019 -Mine Water:Technological and Ecological Challenges. International Mine Water Association, Perm, Russia, pp 515–521.

Parkhurst DL, Appelo CAJ (2013) Description of Input and Examples for PHREEQC Version 3 — A Computer Program for Speciation, Batch-Reaction, One-Dimensional Transport, and Inverse Geochemical Calculations. In: U.S. Geological Survey Techniques and Methods, book 6, chapter A43. p 497.

UBOS (2020) Uganda consumer price index: 2009/10=100. Kampala.

UDC (1997) Feasibility study of the rehabilitation of Lake Katwe Salt Project. Kampala.

A Multicomponent Reactive Transport Modelling Toolbox for Prediction of Drainage Quality from Mine Waste Facilities

Muhammad Muniruzzaman[1], Teemu Karlsson[2], Päivi M. Kauppila[2]

[1]*Water Management Solutions, Geological Survey of Finland, Neulaniementie 5, 70211 Kuopio, Finland, md.muniruzzaman@gtk.fi*

[2]*Circular Economy Solutions, Geological Survey of Finland, Neulaniementie 5, 70211 Kuopio, Finland, teemu.karlsson@gtk.fi, paivi.kauppila@gtk.fi*

Abstract

This study presents a new multiphase multicomponent mine-waste simulator, which is capable of capturing variably saturated water flow, multicomponent advective-dispersive transport both in aqueous and gaseous phase, and chemical reactions (solved with PHREEQC, utilizing PhreeqcRM module) including thermodynamic databases. We particularly emphasize on the Nernst-Planck and Maxwell-Stefan based formulations for the aqueous and gaseous transport, respectively, to explicitly resolve the multilevel process coupling, driven by solute/surface charge or gaseous pressure, across and within different phases. This framework radically goes beyond the state-of-the-art of classical mine-waste models, which exclusively rely on Fickian transport and capture only a subset of governing processes.

Keywords: Acid Rock Drainage, Nernst-Planck Equation, Maxwell-Stefan Equation, Reactive Transport Modelling, Lysimeter Experiment

Introduction

Management of mine wastes represents a key challenge in mining industry because uncontrolled disposal of such extractive materials, which typically have no value or even a negative value when they pose a threat to the environment, may result in liability for the operators with the risk of financial consequences and reputational damage (e.g. Blowes et al. 2014, Nordstrom et al. 2015). Of primary concern is the generation of acidity in the pore water, the release and mobilization of toxic metals and metalloids, and the subsequent leaching of contaminated drainage from these waste systems (e.g. Muniruzzaman et al. 2018a,b). Propagation and spreading of such mining-influenced acid rock drainage (ARD) in waterborne environments have the potential to severely contaminate ground- and surface water resources in the proximity of a mine site (e.g. Amos et al. 2015, Battistel et al. 2019). Despite the fact that the individual processes responsible for the generation/propagation of ARD is fairly well-known, the prediction of overall behavior in a mine-waste system is challenging due to nonlinearity and multilevel coupling associated with these physiochemical mechanisms. Reactive transport models proved to be instrumental in describing such systems but most of the published mine-waste simulators mainly focus on the formulation based on Fick's law and consider only a subset of the key processes. In fact, to the best of our knowledge, a simulator rigorously capturing the simultaneous effects of the inherent inter- and intra-phase process coupling is still missing although processes such as gaseous movement due to compositional changes on pressure (e.g. van Berk and Wisotzky 1995) and/or electrostatic interactions induced by ionic charge or charged surfaces (e.g. Appelo and Wersin 2007, Rolle et al. 2013, Muniruzzaman et al. 2014) are extensively explored in the geochemical literature and their relevance on multicomponent transport is increasingly recognized.

In this work, we propose a new three-phase multicomponent reactive transport modeling toolbox taking into account the variably saturated water flow,

multicomponent advective-dispersive transport both in aqueous and gaseous phase, and geochemical reactions including thermodynamic databases. The modeling approach is based on the Nernst-Planck equation for aqueous species' transport, and Maxwell-Stefan formulation for gaseous transport to explicitly capture the species-species coupling due to solute/surface charge or gas phase pressure. The chemical reactions, including mineral dissolution/precipitation, are solved with PHREEQC (Parkhurst and Appelo 2013), utilizing PhreeqcRM (Parkhurst and Wissmeier 2015) module and taking advantage of the capabilities of coupling this geochemical simulator with the flow and transport code (e.g. Muniruzzaman and Rolle 2016, 2019, Sprocati et al. 2019). The proposed tool is applied to interpret a series of datasets collected in pilot-scale lysimeter setups packed with waste rocks from two different mine sites in Finland. These experiments involve extensive monitoring of lysimeter drainage compositions for a period of more than three years.

Modelling Approach

The water flow in partially saturated mine wastes is typically described by the Richards equation:

$$\frac{\partial \theta^w}{\partial t} - \nabla \cdot [\mathbf{K}(h)(\nabla h + \nabla z)] = Q_s \qquad (1)$$

where θw is the water filled porosity, h is the pressure head, **K** is the tensor for unsaturated hydraulic conductivity (which is a function of h and θw), Qs is the source/sink term, and t is time.

The governing equation for multicomponent aqueous and gaseous transport including Coulombic interactions, interphase mass-transfer, and geochemical reactions can be written as:

$$\frac{\partial(\theta^w c_i^w)}{\partial t} + \frac{\partial(\theta^g c_i^g)}{\partial t} + \nabla \cdot (\mathbf{q}^w c_i^w) + \nabla \cdot (\mathbf{q}^g c_i^g) - \nabla \cdot (\theta^w \mathbf{J}_i^w) - \nabla \cdot (\theta^g \mathbf{J}_i^g) = \sum_{r=1}^{N_r} \nu_{ir} R_r \qquad (2)$$

where θg is the gas phase porosity, c_i^w and c_i^g are the aqueous and gaseous concentrations (which are connected via Henry's law: $c_i^g = H_i c_i^w$ with H_i being the dimensionless Henry's law coefficient), $\mathbf{q}^w$ and $\mathbf{q}^g$ are the specific discharge vectors in each phase, $\mathbf{J}_i^w$ and $\mathbf{J}_i^g$ are the vectors for diffusive/dispersive fluxes, R_r is the reactive source/sink term, and υ_{ir} is the stoichiometric coefficient. The most distinctive feature of the proposed modeling approach is associated to the explicit incorporation of intra- and interphase coupling, mainly caused by ionic/surface charge or gaseous pressure, between different aqueous and gaseous solutes. Instead of using Fick's law, which is a common practice in classic mine waste simulations, we adopt the Nernst-Planck equation (e.g. Appelo and Wersin 2007) for the movement of aqueous species, and the Maxwell-Stefan equation (e. g. Krishna and Wesselingh 1997) for the gaseous species' transport (fig. 1):

$$J_i^w = -D_i^w \left(\frac{\partial c_i^w}{\partial z} + c_i^w \frac{\partial \ln \gamma_i^w}{\partial z} + \frac{\zeta_i \mathrm{F}}{\mathrm{RT}} c_i^w \frac{\partial \varphi}{\partial z} \right) \qquad (3)$$

$$- \sum_{j=1, j \neq i}^{N} \frac{\chi_i^g J_j^g - \chi_j^g J_i^g}{\mathfrak{D}_{ij}^g} + \frac{J_i^g}{D_i^K} = -\left(\frac{\partial c_i^g}{\partial z} + \frac{M_i^g c_i^g g}{\mathrm{RT}} \right) \qquad (4)$$

where D_i^w is the hydrodynamic self-dispersion coefficient of species i (i.e. when ion i is electrostatically "liberated" from the other charged solutes in a multicomponent environment), γ_i^w is the activity coefficient, ζ_i is the charge number, F is Faraday's constant, R is ideal gas constant, T is the temperature, φ is the electrical potential (induced by the different mobility of dissolved charged species or by the external electric field), D_{ij}^g and D_i^K denote, accordingly, the binary Maxwell-Stefan and Knudsen diffusion coefficients, g is the gravitational acceleration, χ_i^g is the mole fraction in the gas phase, and M_i^g is the molecular weight. The advection terms in both phases (Eq. 2) are described by the Darcy's law. This formulation certainly provides an improved representation of the multiphase solute transport processes compared to the Fickian based description, and allows capturing the interdependency between different gaseous and aqueous species' fluxes as well as the resultant coupled movement of the multicomponent solutes in the individual phases (e.g. Krishna and Wesselingh 1997, Muniruzzaman and Rolle. 2015, 2017).

We use a cell-centered finite difference method (FD) to numerically solve the water flow (Eq. 1) into variably saturated mine waste systems. In this step, a backward Euler scheme was adopted for the temporal integration,

and the system of equations is solved with the Thomas algorithm in connection with Piccard iteration. In contrast, the multiphase multicomponent reactive transport is solved with the finite volume method (FVM) by adopting a sequential non-iterative operator splitting scheme to decouple the transport and reaction calculations. The latter is handled with the geochemical solver PHREEQC as a reaction engine (e.g. Rolle et al. 2018, Muniruzzaman and Rolle 2019). The coupled system of equations describing the advective-dispersive transport within aqueous and gaseous phases (Eq. 2 to 4) is solved with the direct matrix solver UMFPACK and by utilizing a Piccard iterative scheme. After the computation of flow and transport in a time step, the concentrations are passed to PHREEQC, utilizing PhreeqcRM module, to perform all the geochemical calculations including mineral dissolution/precipitation (e.g. Sprocati et al. 2019, Muniruzzaman et al. 2020). A series of averaging approaches at the numerical cell interfaces, flux computation methods (upwind, central and TVD), time integration schemes (implicit Euler and Crank-Nicolson), and time varying boundary conditions are employed to provide enhanced flexibility and numerical rigor. The entire toolbox is implemented in MATLAB, and further details regarding the implementation steps, numerical solution strategies, and the benchmarking of the different features are presented in a recent study (Muniruzzaman et al. 2020).

Lysimeter Experiments

To demonstrate the capability of the modeling toolbox, we simulate two datasets collected within pilot-scale lysimeter experiments involving different types of waste rocks. The experimental setup is equipped with two cubic lysimeters with dimensions of 1 m × 1 m × 1 m (fig. 2). The lysimeters were installed, by following the guidelines of MEND, at the premises of Geological Survey of Finland (Kuopio, Finland), and were subjected to outdoor atmospheric conditions. The first lysimeter was packed with the mica schist waste rock samples from the Hitura nickel mine site (northern Ostrobothnia, Finland), whereas the second setup was packed with the olivine pyroxenite containing waste rocks from the Kevitsa nickel-copper mine site (Sondankylä, Finnish Lapland). These waste rocks have distinct properties with a relatively higher sulfide content (2.3%: with 0.86% pyrrhotite, 0.5% pyrite, 0.1% pentlandite and 0.1% chalcopyrite) and no observable carbonate minerals for the Hitura materials but a considerably lower sulfide content (<0.29%: 0.09% pyrrhotite, 0.02% pentlandite, 0.03% pyrite and 0.01% chalcopyrite) and a minor fraction of carbonate minerals (1.3%: with 0.23% calcite, 1.01% dolomite and 0.05% magnesite) for the Kevitsa materials.

The experiments were initiated as the rainwater flushed through the waste rocks within the lysimeters. The drainage samples were periodically collected at the bottom of the setup for a duration of more than three

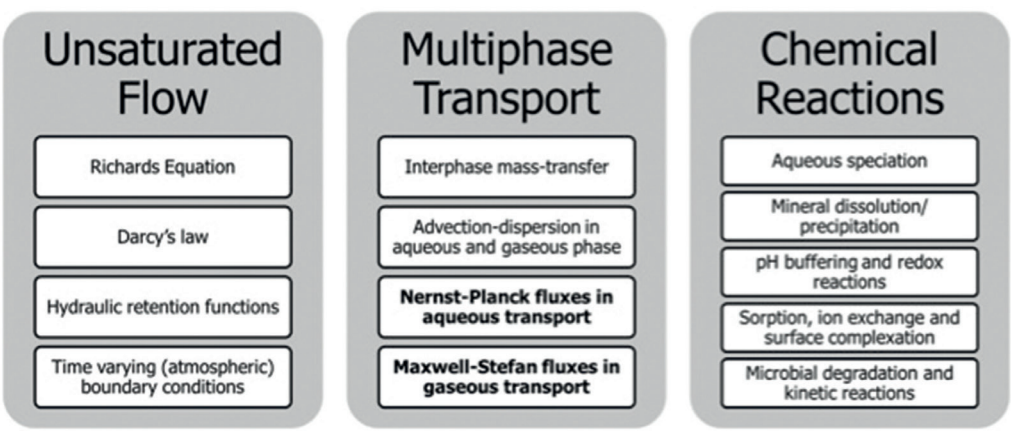

Figure 1 *Schematic of the multiphase multicomponent reactive transport modeling toolbox.*

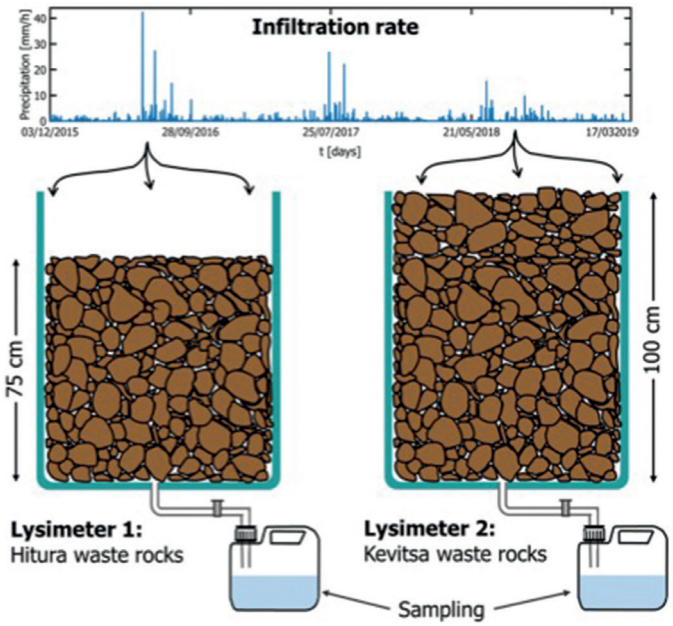

Figure 2 *Schematic diagram of the lysimeter experiments.*

years (fig. 2). The composition of the effluent samples was measured with ICP-MS, ICP-OES, and ion chromatography (Labtium Oy, Kuopio), whereas the waste rocks' mineralogy was measured with a field emission electron microscope (FE-SEM, JEOL JSM 7100F Schottky with EDS X-Max 80 mm2). As both lysimeters were located at the outdoor environment, we mimic the natural conditions in the simulations by employing a temporally variable water infiltration rate proportional to the observed hourly precipitation rates (Finnish Meteorological Institute, fig. 2, top panel) at the top boundary and a free drainage boundary at the bottom.

Results and Discussion

This section summarizes the results obtained from the lysimeter experiments along with the reactive transport simulations performed with the proposed approach. Fig. 3 shows a comparison between the measured (markers) and simulated (lines) drainage concentration profiles for both lysimeters. The simulations include advection-dispersion in the water phase, coupled diffusion of gaseous species (O_2, N_2 and CO_2), kinetic dissolution of sulfide, carbonate and a range of silicate minerals (biotite and tremolite in the first lysimeter; and talc, chlorite and serpentinite in the second one), and precipitation of the secondary minerals ($Fe(OH)_3$, gypsum, jarosite and gibbsite). It is evident that the waste rocks from Hitura mine site lead to a characteristic composition of acid rock drainage as reflected in the low pH (about 4.3) and elevated sulfate concentrations (up to 3000 mg/L) in the effluent (fig. 3a-b). Such behavior is certainly driven by the lower carbon to sulfur ratio (=0.22) of the material,

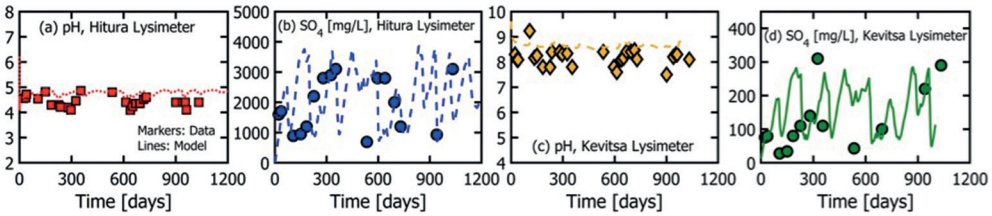

Figure 3 *Evolution of the drainage chemistry as a function of time in different experiments.*

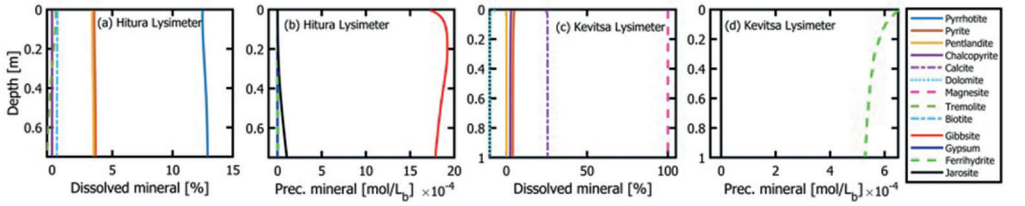

Figure 4 *Dissolved/precipitated mineral contents after 1200 days of simulation in different lysimeters.*

and indicates ongoing oxidation of the sulfide minerals (fig. 4).

The situation is different in the second lysimeter, where the effluents show basic pH values (>8) due to the presence of the considerable extent of carbonate minerals (C/S=1.29) and the subsequent buffering of the acidity. The released sulfate concentrations are also more than an order of magnitude lower compared to the observed values in the first lysimeter (fig. 3b,d). Due to the variation in the atmospheric infiltration rates and the subsequent complex sequence of weathering within waste rocks, a very dynamic pattern is evident in all breakthrough curves shown in fig. 3. However, the model could reproduce very well most of these complex dynamic trends and the concentration ranges in the different breakthrough curves.

The observed behavior in the effluent breakthrough curves is also supported by the acid base accounting (ABA) test, which showed a neutralization potential ratio (NPR) of 0.2 (indicative of potentially acid generating material) for the Hitura waste rocks and 7.4 (indicative of non-acid generating material) for the Kevitsa waste rocks. Dissolution of silicates and the precipitation of secondary minerals can also exert further controls on the buffering of pore water pH and the release and attenuation of the major ions (Ca, Mg and K, results not shown). In fact, the drainage from the Hitura waste rocks show a characteristic pH range (4.3), which is known to be controlled by gibbsite buffering reactions (Dold 2017). The smaller depletion of different minerals at the end of the experiments indicates a rather long lifecycle for the weathering processes in these wastes.

Conclusions

In this study, we have presented a new multiphase multicomponent reactive transport modeling toolbox specifically tailored for mine waste simulations and capable of taking into account the coupled water-gas movement and a wide range of geochemical reactions in homogeneous and heterogeneous unsaturated porous media. The most unique feature of the proposed approach includes the Nernst-Planck and Maxwell-Stefan based description of the multicomponent solute fluxes, which allows capturing the species-species interactions due to ionic/surface charge and/or gas phase pressure. To demonstrate the capability of the modeling toolbox, we have also presented a series of long-term pilot-scale lysimeter experiments involving mine waste rocks from two different mine sites in Finland. In these experiments, the dynamic evolution of the lysimeter drainage composition was monitored for more than three years in all setups and the potential for a particular waste rock to generate acidic drainage was evaluated. The simulation results reveal that the proposed approach allows us to accurately describe the complex behavior within waste rock systems and to reproduce the experimental observations along with the dynamic trends. Such outcomes verify that the presented toolbox can be effectively used in mine waste applications such as drainage quality prediction from waste dumps (waste rocks or tailings), robust risk analysis in environmental impact assessment, interpretation of lysimeter tests, humidity cell tests or column studies, long-term prediction in a decommissioned pile, early predictions in proposed piles, evaluation of effective remediation options, and design of cover structures. The current formulation provides particular advantages over the classic mine waste or subsurface codes when the specific objective is to capture the involved mechanisms from a process-based

approach. Besides the application examples presented in this study, the proposed tool is also applicable to other complex mine waste settings (e.g. real field-scale piles or sophisticated laboratory experiments) or even generic vadose zone studies (e.g. landfills, biocovers or multiphase transport). Further developments are also envisioned to incorporate non-isothermal heat transport processes, freeze-thaw cycle, coupling between porous media flow and atmospheric free flow, and electrokinetic transport mechanisms, which have implications both in the ARD simulations in Nordic conditions or in engineered remediation.

Acknowledgments

The authors the support from the European Regional Development Fund (KaiHaMe and Kaivasu projects) and the internal funding from the Geological Survey of Finland (TUMMELI project).

References

Amos RT, Blowes DW, Bailey BL, Sego DC, Smith L, Ritchie AIM (2015) Waste-rock hydrogeology and geochemistry. Appl Geochem. 57:140-156

Appelo CAJ, Wersin P (2007) Multicomponent Diffusion Modeling in Clay Systems with Application to the Diffusion of Tritium, Iodide, and Sodium in Opalinus Clay. Environ Sci Technol. 41:5002–5007

Battistel M, Muniruzzaman M, Onses F, Lee JH, Rolle M (2019) Reactive fronts in chemically heterogeneous porous media: Experimental and modeling investigation of pyrite oxidation. Appl Geochem 100:77-89.

Blowes DW, Ptacek CJ, Jambor JL, Weisener CG, Paktunc D, Gould WD, Johnson DB (2014) 11.5 - The Geochemistry of Acid Mine Drainage, In: Holland HD, Turekian, KK (Eds), Treatise on Geochemistry (Second Edition). Elsevier, Oxford, p 131–190

Dold B (2017) Acid rock drainage prediction: A critical review. J Geochem Explor 172: 120–132

Krishna R, Wesselingh JA (1997) The Maxwell-Stefan approach to mass transfer. Chem Eng Sci 52: 861–911.

Muniruzzaman M, Haberer CM, Grathwohl P, Rolle M (2014) Multicomponent ionic dispersion during transport of electrolytes in heterogeneous porous media: Experiments and model-based interpretation. Geochim Cosmochim Acta 141: 656–669

Muniruzzaman M, Karlsson T, Ahmadi N, Rolle M (2020) Multiphase and multicomponent simulation of acid mine drainage in unsaturated mine waste: Modeling approach, benchmarks and application examples, Appl Geochem, doi: 10.1016/j.apgeochem.2020.104677

Muniruzzaman M, Karlsson T, Kauppila PM (2018a) Modelling tools for the prediction of drainage quality from mine wastes. Geological Survey of Finland, Bulletin 408:27-42

Muniruzzaman M, Kauppila PM, Karlsson T (2018b) Water quality prediction of mining waste facilities based on predictive models. Geological Survey of Finland, Open File Research Report 16/2018.

Muniruzzaman M, Rolle M (2019) Multicomponent Ionic Transport Modeling in Physically and Electrostatically Heterogeneous Porous Media With PhreeqcRM Coupling for Geochemical Reactions. Water Resour Res 55:11121–11143

Muniruzzaman M, Rolle M (2017) Experimental investigation of the impact of compound-specific dispersion and electrostatic interactions on transient transport and solute breakthrough. Water Resour Res 53:1189–1209

Muniruzzaman M, Rolle M (2016) Modeling multicomponent ionic transport in groundwater with IPhreeqc coupling: Electrostatic interactions and geochemical reactions in homogeneous and heterogeneous domains. Adv Water Resour 98:1–15

Muniruzzaman M, Rolle M (2015) Impact of multicomponent ionic transport on pH fronts propagation in saturated porous media. Water Resour Res 51: 6739–6755

Nordstrom DK, Blowes DW, Ptacek CJ (2015) Hydrogeochemistry and microbiology of mine drainage: An update. Appl Geochem 57: 3–16

Parkhurst DL, Appelo CAJ (2013) Description of input and examples for PHREEQC version 3 – a computer program for speciation, batch-reaction, one dimensional transport, and inverse geochemical calculations. U.S. Geological Survey Techniques and Methods 6-A43:497

Parkhurst DL, Wissmeier L (2015) PhreeqcRM: A reaction module for transport simulators based on the geochemical model PHREEQC. Adv Water Resour 83: 176–189.

Rolle M, Muniruzzaman M, Haberer CM, Grathwohl P (2013) Coulombic effects in advection-dominated transport of electrolytes in porous media: Multicomponent ionic dispersion. Geochim Cosmochim Acta 120: 195–205

Rolle M, Sprocati R, Masi M, Jin B, Muniruzzaman M (2018) Nernst-Planck-based Description of Transport, Coulombic Interactions, and Geochemical Reactions in Porous Media: Modeling Approach and Benchmark Experiments. Water Resour Res 54:3176–3195

Sprocati R, Masi M, Muniruzzaman M, Rolle M (2019) Modeling electrokinetic transport and biogeochemical reactions in porous media: A multidimensional Nernst–Planck–Poisson approach with PHREEQC coupling. Adv Water Resour 127: 134–147

van Berk W, Wisotzky F (1995) Sulfide oxidation in brown coal overburden and chemical modeling of reactions in aquifers influenced by sulfide oxidation. Geo 26, 192–196

Williamson MA, Rimstidt JD (1994) The kinetics and electrochemical rate-determining step of aqueous pyrite oxidation. Geochim Cosmochim Acta 58:5443–5454

Effect of Mining to Water Quality in Chua and Revué Rivers, Mozambique

Clemêncio Nhantumbo[1], Estêvão Pondja[1], Dinis Juízo[1], António Cumbane[1], Nelson Matsinhe[1], Bruno Paqueleque[1], Miguel Uamusse[1], Gretchen Gettel[2], Mário J. Franca[2,3], Paolo Paron[2]

[1]*Eduardo Mondlane University, Faculty of Engineering, Av. de Moçambique km 1.5, C. Postal 257, Maputo, Mozambique, Clemencio.nhantumbo@uem.mz*

[2]*IHE-Delft Institute for Water Education, 2611 AX Delft, Delft, The Netherlands, m.franca@un-ihe.org*

[3]*Delft University of Technology, Department of Hydraulic Engineering, Stevinweg 1, 2628 CN Delft, The Netherlands, M.J.Franca@tudelft.nl*

Abstract

Anthropogenic activities, particularly artisanal and industrial gold mining, have been affecting water resources in Manica Province, in Mozambique. Evaluation of water pollution in Révue and Chua rivers due to gold mining was done through field observations and laboratory analysis. This investigation revealed that water quality is being affected by activities developed in the river basin. Turbidity (200-5600 NTU) and concentration of sulfate (25-56 mg/L) are the most affected parameters. pH values measured were below 6.5 in two monitoring points. Although, agriculture is also present in the studied area, gold mining is likely to be the main source of water pollution.

Keywords: goal mining, river, water quality, environmental impact

Introduction

Water is an important resource, since it is widely used for Human consumption, agricultural activities, recreational and industrial purposes. Currently, anthropogenic activities have been affecting seriously the water quality. Organic, inorganic and biological pollutants, as well as extremely toxic metals are usually released to the water resources (Asare Donkor et al. 2018). Toxic metals in water represents a serious threat to the health of animals, particularly Humans and aquatic animals, due to their persistence and bioaccumulation in the food chain (Asare Donkor et al. 2018). In Southeast Asia including Bangladesh, India and the Bengal region, were recorded cases of skin, kidney, bladder and lung cancer associated with the consumption of arsenic-loaded water in rice food crops (Keita et al. 2018).

Mining activity is developing fast in most developing countries and when regulated, it brings revenue to government. However, mining is also linked to severe impacts to the environment and water resources on a global scale (Nhantumbo et al. 2015). Mining is linked to the increase of turbidity, acid mine drainage, sediment transport and is the main source of toxic metals released to water (Ochieng et al. 2010). Mining is contributing to the degradation of the environment with negative environmental impacts that outweigh socioeconomic benefits, such as, the pollution of air, water and soil degradation (Ncube-Phiri et al. 2018).

In most cases, artisanal and industrial gold mining is carried out in developing countries where the regulation is limited and it is not well implemented, thus, with higher potential impact on the environment. The release of pollutants to the environment affects the entire ecosystem and biodiversity, and it contributes to deforestation (Keita et al. 2018; Mamodu et al. 2018).

In Mozambique, the artisanal and industrial gold mining occurs mostly in Manica province. There were about 13,000 workers working in six legal mines until 2009 and it is known that more illegal mines are operating in private properties, rivers, or remote, uninhabited land (Drace et al. 2012). These mines are operated preferable near the

rivers, because the water of the rivers is used for washing the gold, and there are several reports of water quality being affected by gold mining in Manica (Drace et al. 2012; Muacanhia et al. 2012). However, limited data on water quality in the rivers affected by gold mining is available, thus limiting selection of measures to prevent and mitigate the negative effects to water resources. This paper intends to evaluate the level of pollution of the Révue and Chua rivers due to gold mining in Manica district, through field observations and laboratory analysis.

Description of study area

Manica district is located in Manica province in the central part of Mozambique, Figure 2. Manica district is bordered in north by the Barué district through the Pungue River, in south by the district of Sussundenga through the Zónue and Révue Rivers, in east by the Vandúzi district and in west by Zimbabwe (Castigo et al. 2017). The district has about 4400 km2 and the population density is approximately 59 habitants/Km^2 (MAE 2014). The present study will be restricted to Révue and Chua Sub Basins.

Gold deposits are common in Manica District, and they can be classified as primary deposits or alluvial. Primary deposits are in ferrous quartzite. The gold is associated with sulfides, pyrite (FeS_2) pyrrhotite (FeS), aresnopyrite (FeAsS), chalcopyrite ($CuFeS_2$) which is about (10-35%) of the ferrous quartzite (Maculuve, 2001). The alluvial gold can be found in the river banks and it is distributed irregularly (Maculuve 2001; Marrumbe 2012).

Due to high concentration of deposits, gold mining is common in the Manica District and it can be classified as industrial and artisanal. Artisanal mining is more common than industrial mining. There are 23 mining areas identified in the Révue River and its tributaries, in which, 8 are industrial and the remaining 15 are artisanal, Figure 2 (Marrumbe 2012). Artisanal gold mining is done using instruments such as shovels, picks, baskets and industrial mining is done using open pits or galleries (Manhique 2011).

Artisanal mining in Manica District is not organized due to limited legislation and its weak implementation. The rivers are highly affected due to inappropriate techniques during extraction and processing of gold. Gold is processed and washed in the rivers and it leads to high turbidity, and concentration of solids and metals, Figure 1. Additionally, mercury is used for artisanal gold processing in artisanal gold mining and it also contaminates the water of the rivers. Some industrial gold mining companies are mobile and do not have environmental management plans that makes environmental monitoring and protection inefficient (Castigo & Fopenze 2017).

Figure 1 *Revué River (right) Chua River (left) (image: Bruno Paqueleque).*

Table 1 Location of Monitoring points.

Monitoring Points	Location	Latitude	Longitude	Altitude
1	Révue River	78o99'04.4"	13o41'04"	793
2	Messambúzi River	78o95'71.6"	14o59'53"	706
3	Révue River	79o00'29.6"	14o56'73"	744
4	Confluence of Chua and Révue River	79 o00'56.9"	14o71'33"	727
5	Upstream Révue River	79o03'43.2"	15o80'51"	716
6	Chua River	79o02'75.9"	15o16'89"	724
7	Upstream Chua River	78o98'39.0"	15o41'30"	713

Methods

Seven monitoring points were chosen along the rivers, Figure 2. The points were selected in order to get information on water quality upstream and downstream the mining area. The samples were collected using 500 ml polyethylene containers previously washed and identified. Sampling was carried out using a rope in the opposite direction of the stream flow, and at the depth of approximately 10 centimetres. Analysis of the following physical parameters, pH, conductivity and TDS were done using the HQ40D Multi-Meter Portable. Turbidity was measured using the 2100Q Portable Turbidimeter using the USEPA 180 method. Determination of the alkalinity was done using the volumetric method with potentiometric detection and the titration was done until the set pH of 4.8. pH, electric conductivity, TDS and turbidity were measured in the field while other parameters were measured in the laboratory.

Analysis of the chemical parameters, sulfate, sulfite and metals (arsenic, copper, iron, manganese, chromium and zinc) were made using the DR 1900-Portable Spectrophotometer. The samples were diluted before the measurement and the determination of the initial concentration was done by the USEPA Bicinchoninate-Powder Pillows method. The concentration of iron, manganese, zinc, sulfate (SO_4^{2-}), (S^{2-}) and arsenic were determined FerroZine-Reactant Solution Pillows Method; USEPA Periodate Oxidation-Powder Method Pillows, USEPA Zincon-Powder Pillows, USEPA SulfaVer 4, and USEPA Methylene Blue and Arsenic Test, respectively.

Results and Discussion

Results of chemical analysis in Figure 3 and Table 2, show that the water quality of Chua and Revué Rivers is affected by mining. Considering the monitored parameters, before the mining area the water quality is good, monitoring points, P7 and P5. Most analysed parameters were affected negatively when the rivers streams passed through the mining area, turbidity, (200-5600 NTU), concentration of arsenic (0.01-15 mg/L), copper (1.6 mg/l), iron (0.73-6 mg/L), manganese (8-165mg/L), chromium (0.11-4.95 mg/L), zinc (4.8-24.2 mg/L), sulfate (25-56 mg/L) and and pH (values below 6.5). Worst water quality results were obtained from analysis of water in the monitoring points P6, P4 and P3. P6 is a monitoring point along Chua River within the mining area, P4 is the monitoring point at the confluence of Chua and Révue River, and P3, is immediately downstream the confluence of Chua and Révue River. Most mining sites are located upstream monitoring points P4 and P3, Figure 2. As the water moves downstream the mining sites, the water quality recover its quality, Figure 3.

Water quality of the river was also compared to water quality standards obtained from Mozambican Legislation, "Diploma Ministerial no. 180/2004 de 15 de Setembro". It has been observed that, most of monitored parameters satisfy the water quality standards before the mining area, except concentration of copper (Cu) and chromium (Cr+6), monitoring points P7 and P5. However, once the river enters the mining area, the pH drops to values below the standard value, (pH=6.5) in monitoring points P6 and P3, and the turbidity, concentration of arsenic, iron, manganese, zinc and sulfate, become higher that the standards, Table 2.

Beside of mining, agriculture is also common in the studied area (MAE 2014). Relative contribution of agriculture and mining to changes of water quality of the

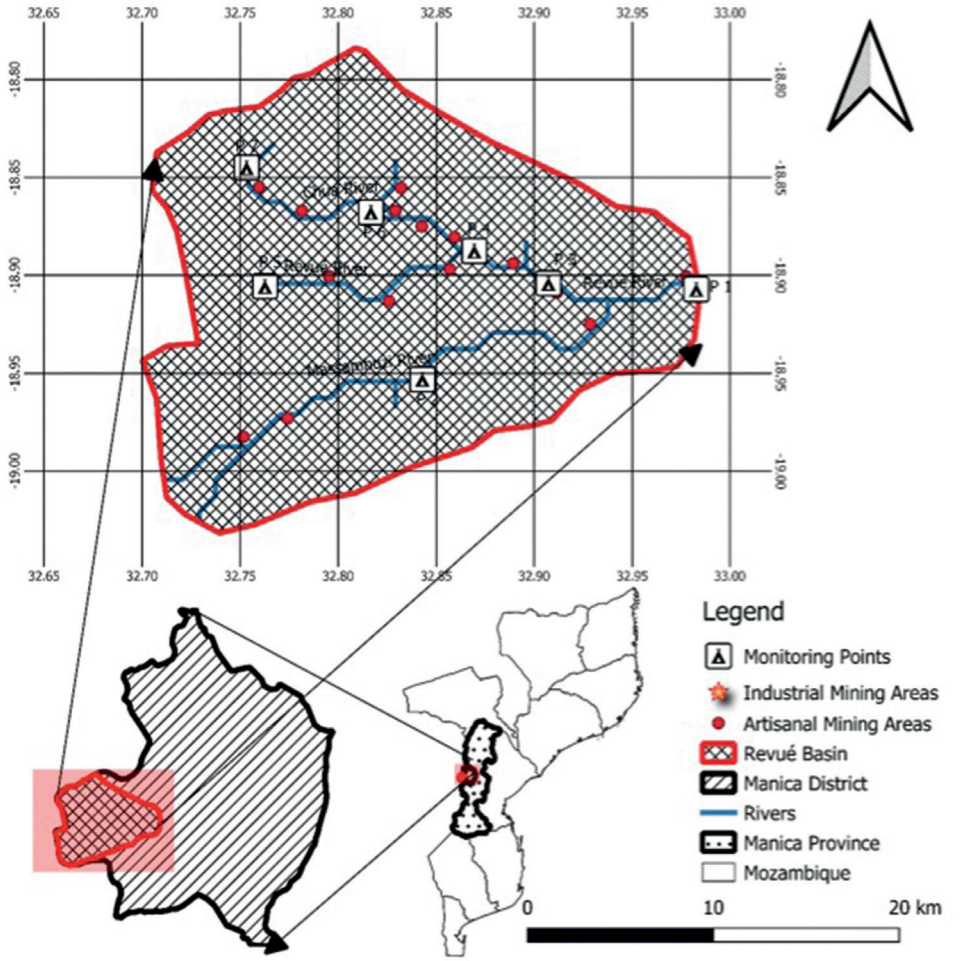

Figure 2 Mining areas and monitoring points in the Chua and Révue River Basin.

rivers is not known. It was also observed that mercury is used for artisanal gold processing. No measurement of mercury concentration in the water of the rivers and its bioaccumulation to the food chain was done, while mercury is known on its negative impact to environment and Human health. Results of this study showing that the Chua and Revué River water quality is being affected, opens an opportunity for further investigation on the relationship between sources of pollution and water quality of rivers, on human health and biodiversity, and using statistical tools and mapped using drone with multispectral camera.

Conclusions

Twenty-three mining sites where identified in the studied area, among them, fifteen are artisanal and eight are industrial. Water quality of Chua River and Revué River is being affected by activities developed in the river basin. Most analysed parameters were affected negatively when the rivers streams passed through the mining area, for example turbidity, (200-5600 NTU), concentration of arsenic (0.01-15 mg/L), chromium (0.11-4.95 mg/L), sulfate (25-56 mg/L) and pH (<6.5). Monitored parameters, exhibit recover after the mining area. Although, agriculture is notable in the studied area, mining is likely to be explaining the water quality changes.

Acknowledgments

We thank the support and assistance of National Water Directorate of Mozambique Manica and *Sustainable Hydropower and*

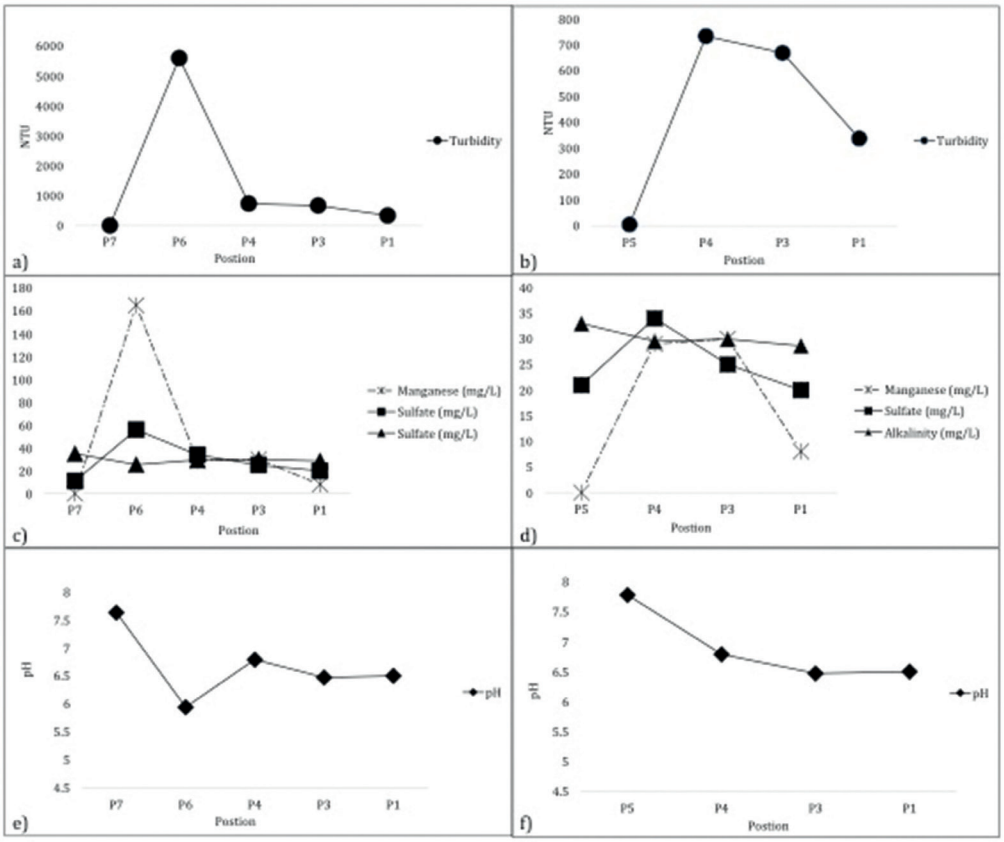

Figure 3 *Change of turbidity, alkalinity, pH and concentration of manganese and sulfate along Chua River [a), c) and e)] and Revué River [b), d) and f)]. P1, P3, P4, P5, P6 and P7 are the monitoring points indicated in Figure 2.*

Table 2 *Results of chemical analysis in Chua and Revué rivers, and standard values. P1, P2, P3, P4, P5, P6 and P7 are monitoring points indicated in Figure 2.*

		Monitoring points							
Parameter	Units	P7	P6	P5	P4	P3	P2	P1	Standard*
pH	-	7.63	5.94	7.78	6.79	6.47	6.91	6.50	6.5 - 8.5
EC	µ.S/cm	896	659.3	941	760.3	749	148.6	837	50 – 2000
TDS	mg/L	423	378	545	362	358	705	407	1000
Alkalinity	mg/L	35	25.4	33	29.51	29.96	-	28.63	-
Turbidity	NTU	6	5600	5.27	734	669	197	338	5
As	mg/L	0	15	0	1.5	0.5	0	0.01	0.01
Cu	mg/L	0.001	1.6	0.006	0.9	0.3	0	0.27	1.0
Fe	mg/L	1.46	6	1.52	3.68	1.28	2.23	0.73	0.3
Mn	mg/L	0.003	165	0.03	29	30	18	8	0.1
Cr^{6+}	mg/L	0.15	4.95	0.11	1.27	0.96	0.69	0.83	0.05
Zn	mg/L	2.9	24.2	4.8	10.6	8	7.2	4.9	3.0
SO_4^{2-}	mg/L	11.0	56.0	21.0	34.0	25.0	22.0	20.0	25.0
S^{2-}	mg/L	0.21	4.18	0.11	1.50	1.16		0.73	-

Values that exceed the standard

Values that do not exceed the standards

* Mozambican Legislation, extracted from "Diploma Ministerial no. 180/2004 de 15 de Setembro"

Multipurpose Storage to meet Water, Food, and Energy Development Goals: A Program for Collaborative Research and Innovation (S-MultiStor 106472).

References

Asare Donkor, N. K., Ofosu, J. O., & Adimado, A. A. (2018). Hydrochemical characteristics of surface water and ecological risk assessment of sediments from settlements within the Birim River basin in Ghana. *Environmental Systems Reseaarch*, 2. doi:10.1186/s40068-018-0113-1

Castigo, P., & Fopenze, R. L. (2017). *Os percursos e desafiso da mineração de ouro no distrito de Manica: Estudo de caso da sub-bacia do Rio Révue.* Chimoio: AQUA.

Drace, K., Kiefer, A. M., Veigac, M. M., Williams, M. K., Ascaria, B., Knapper, K. A.,… Cizdziel, J. V. (2012). Mercury-free, small-scale artisanal gold mining in Mozambique: utilization of magnets to isolate gold at clean tech mine. *Journal of Cleaner Production*, 88-95.

Keita, M. M., Ogendi, G. M., Owuor, G., & Nyamao, W. N. (2018). Impacts of Artisanal Gold Mining on Water Quality: A Case Study of Tangandougou Commune in Sikasso Region, Mali. *Journal of Environmental Health and Sustainable Development*, 9. doi:10.18502/jehsd.v3i4.228

Maculuve, I. E. (2001). *Trabalho de Licenciatura - O Garimpo de Ouro e a Problematica da Erosão em Manica*. Maputo: UEM- Faculdade de Ciências, Departamento de Geologia.

MAE. (2014). *PERFIL DO DISTRITO DE MANICA*. Maputo: MINISTÉRIO DA ADMINISTRAÇÃO ESTATAL.

Mamodu, A., Ojonimi, I. T., Apollos, S. S., Jacinta, O.-C. N., Salome, W. H., & Enesi, A. A. (2018). Analyzing the environmental impacts and potential health challenges resulting from artisanal gold mining in Shango area of Minna, North-Central, Nigeria. *JOURNAL OF DEGRADED ANDMINING LANDSMANAGEMENT*, 9. doi:10.15243/jdmlm.2018.052.1055

Manhique, H. A. (2011). *Projecto Cientifico - Contribuição para a Caracterização das Alterações Fisicas do Ambiente devido a Mineração Artesanal no Distrito de Manica*. Maputo: Departamento de Geologia - Universidade Eduardo Mondlane.

Marrumbe, P. N. (2012). *Projecto Cientifico-Avaliação das Tecnicas de Recuperação de Ouro com o Recurso a Analise das Concentrações de Mercurio resultantes da Mineração Artesanal na provincia de Manica - Caso de Munhena,Tsetsera e Clean Tech*. Maputo: Departamento de Geologia - Universidade Eduardo Mondlane.

Muacanhia, T., Manuel, I., Magaia, L. L., Deniasse, O., & Bene, B. (2012). *The Problems of Artisanal Gold Mining in Manica Province*. Maputo: UniZambeze & Mining Development Fund .

Ncube-Phiri, S., Ncube, A., Mucherera, B., & Ncube, M. (2018). Artisanal small-scale mining: Potential ecological disaster in Mzingwane District, Zimbabwe. *Jàmbá: Journal of Disaster Risk Studies*, 11. doi:10.4102/jamba.v7i1.158

Nhantumbo, C., Larsson, R., Juizo, D., & Magnus, L. (2015). Key issues for water quality monitoring in the Zambezi River Basin in Mozambique in the context of mining development. *Journal of Water Resources and Protection.*

Ochieng, G. M., Seanego, E. S., & Nkwonta, O. I. (2010). Impacts of mining on water resources in South Africa: A review. *Scientific Research and Essays*, 3351-3357.

Assessment of the Environmental Risk of a Floodplain Contaminated by Metals Based on Different Indices and Environmental Classification Factors, Minas Gerais, Brazil

Catarina Pinho[1,2], Rita Fonseca[1,2], Júlio Carneiro[1], António Araújo[1]

[1]*University of Évora, School of Sciences and Technologies, Department of Geosciences, Institute of Earth Sciences, Évora Pole, Portugal*

[2]*AmbiTerra Laboratory - Rua da Barba Rala, nº 1, Industrial and Technological Park, 7005-345 Évora, Portugal*

Abstract

The geochemical characterization, of an industrial area in Minas Gerais State, Brazil, revealed presence of high levels of potentially toxic metals, higher than the values admitted. The use of three environmental classification indices enabled the comparison of data with the adopted classifications for each index, having identified cadmium, lead and zinc as the main contaminants. The construction of interpolation maps allowed the visualization of the e contaminants evolution throughout the area. It was possible to identify places where natural mitigation processes can be used end produce a comprehensive remediation proposal in places identified as requiring a more complex intervention.

Keywords: geochemical characterization, potentially toxic metals, environmental classification indices, interpolation maps, environmental remediation

Introduction

Metals contamination in soils is very common, and is mostly associated with the deposition of contaminated toxic compounds from anthropic activities (Raymond 2011). Knowledge of metals mobility in the environment is essential for a rigorous assessment of the potential geochemical risks associated with these elements and, it consists of an important tool to control and monitor environmental pollution. The study of the chemical forms and the occurrence of a chemical element allows it to estimate its mobility, bioavailability and ecotoxicity in the environment (Lu 2003, Davidson 2004, Cappuyns 2007). The *Aqua Regia* digestion method for solid samples is a simple approach to determinate mobile phases, based on bi-acid dissolution of the fractions with greater facility to be transferred to the environment and resulting, as residual fraction, silicate minerals geologically stable and therefore neither influencing the chemical conditions of the environment nor the assimilation by biota (Pinho 2013, Pinho 2018). The study area is highly contaminated by toxic metals, including zinc (Zn), nickel (Ni), cadmium (Cd), copper (Co), chromium (Cr), and lead (Pb) and arsenic (As). This contamination is mainly associated to the presence and operation of a local industrial unit. One of the objectives of this work is the elaboration of an environmental remediation proposal, while considering the results obtained from the geochemical characterization and the evaluation of those elements contents according to three environmental classification indices. The investigation and identification of alternative techniques for the remediation and/or recovery of contaminated areas, at low cost and with viable execution times, are currently of high importance (USEPA 2008, Pinho 2018). In this study the proposed solution for the recovery of this area should be applied taking into account the intrinsic and unique chemical and climatic conditions. As a good example of remediation technologies, we can mention the use of innovative reactive materials to fill permeable reactive barriers (PRB's) or bioremediation techniques (Carvalho 2008, Pinho 2018). The success or failure of a technology depends on

the contaminations control on the source, and its applicability depends not only on the nature of the contaminants, but also on the intrinsic characteristics of the geological materials (Pinho 2018).

Overview of the Study Area

The study area, with an area of approximately 3 km^2, is located in the Brazilian State of Minas Gerais, in the municipality of Três Marias. It is embedded in the hydrographic basin of São Francisco River, limited at North and South by two small water ways, the Consciência and the Barreiro Grande creek, geographically located next to the river's bank (Fig. 1) (Pinho 2018, Pinho 2019). Geologically, this area is part of the Três Marias Formation, belonging to the Bambuí Group, which is as lithostratigraphic unit belonging to the São Francisco Group and constitutes a Neoproterozoic sedimentary cover of the São Francisco Craton. This formation is mainly composed of detrital sedimentary rocks consisting of micaceous and clayey siltstones with calcareous matrix, arkoses, ferruginous shales and metamorphosed limestones (Alkimim 2001) in Ribeiro (2010).

Methodology

The study area was divided into three areas (A1, A2 and A3) where samples were collected, trying to guarantee the representativeness of the sedimentary materials. Sampling also took place in an area located upstream and outside of the influence of the industrial activity (A0), representing the geochemical background (Pinho 2018). In the alluvial plain and in the margins of Consciência creek, samples were collected with a manual auger mainly at three depths (0 to 20 cm, 20 to 40 cm and 40 to 60 cm), aiming to have an in-depth knowledge of the levels of contaminants and also the chemical forms in which elements occur. In the stream bed of the waterway samples were collected with a manual Shipeck dredge and for deeper sampling (60 to 80 cm and 80 to 100 cm) a Kajak drilling corer was used and samples were divided into 20cm-thick layers. Sampling was followed by immediate readings of Eh and pH values, using a portable multi-parameter Consort, C5020 model probe (SP10T model for pH, SP50X model for redox potential) and samples were preserved at about 4 °C (from the time of collection) until the transportation to the laboratory. In the laboratory, previously grounder samples through an agate mill, the contamination degree was determined by the *Aqua Regia* digestion with subsequent quantification by ICP-OES (Perkin-Elmer, Optima 8300) following USEPA 2007. Data was compared with the legislated accepted values, that consider two levels of danger: Level 1, which corresponds to the threshold below which no harmful effects are expected on aquatic life

Figure 1 *Overview of the study area.*

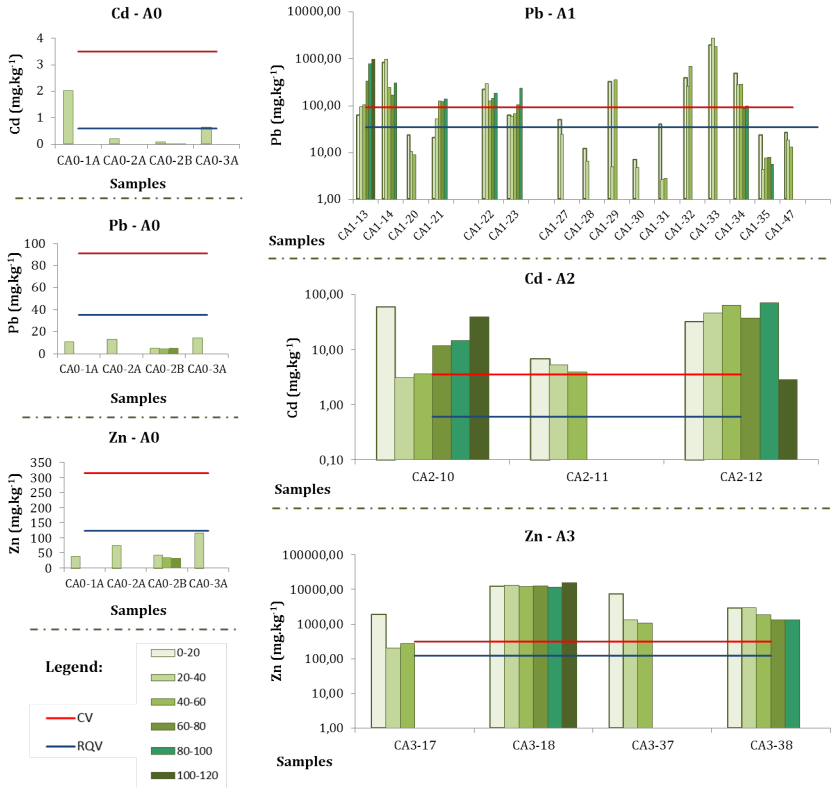

Figure 2 *Content obtained by aqua regia in depth.*

(equivalent to the Reference Quality Values – RQV) and Level 2, which corresponds to the threshold above which harmful effects to biota are expected (equivalent to the Critical Value – CV) (CONAMA 2012). From this comparative study, three environmental classification indices were calculated in order to identify the extent of local contamination: (1) the Enrichment Factor (EF), according to the definition proposed by Lee (1997) (in Nude 2011, Pinho 2013, Martins 2014, Pinho 2018), compares the contents of each element in the samples of the contaminated areas to the corresponding contents in the background area (area A0). (2) the Index of Geochemical Load (IGL) allows the calculation, based on a local reference, of the enrichment for a given element in a given sample (Pendias, 2001, Nude 2011, Trindade 2012, Martins 2014, Pinho 2018), (3) the Contamination Factor (CF), determines the pollution index of a given element from its comparison with the content obtained in area A0, taken as a reference value (Nude 2011, Martins 2014).

Results and Discussion

The geochemical characterization of the samples identified Cd, Pb and Zn as the contaminants with greater expressiveness in the area. The comparison between these levels and the legislated accepted values for RQV and CV, according to CONAMA 2012 (CV in mg.kg^{-1} Cd: 3.5; Pb 91.3; Zn: 315 and RQV in mg.kg^{-1} Cd: 0.6; Pb: 35; Zn: 123), allowed to evaluate their dangerousness in the environment for each area (A1, A2, A3). In the background area A0, as expected, non-compliances under the admitted legal levels were found for most elements. However occasional records of Cd levels above RQV were observed, which may be due to natural enrichment or generated from the wind transport of particles from adjacent areas (Figure 2). Bothe areas A1 and A2 have very high levels for all of these elements, above the RQV and CV, graphically represented by Pb and by Cd, respectively for A1 and A2 (Figure 2). In area Ae Cd has high levels

throughout the sampling profile, with higher levels in the intermediate depth layers (20-40, 40-60 and 60-80 cm) (Figure 2). Concerning area A3, Zn, depicted as an example in the graph of Figure 2, also has levels higher than RQV and CV in all the analysed samples, there is an increase in depth, of the levels of all elements in all the samples collected in the three areas, mainly in the rainy season.

In general, in the sediments of the alluvial plains (areas A2 and A3) and in those deposited on the creek margins (area A1), mostly above water level throughout the year, metal distribution in depth is seasonal, with preferred accumulation on the surface during the dry period, and on deeper layers after the rainy season. This pattern may be due to an increase of the stream flow, with consequent increase of interstitial water circulating through the sediments, dragging the most runoff, but rather as variably soluble salts in surficial porewater and groundwater.

The Enrichment Factors (EF) was calculated using Fe as the standard element, since it did not represent a contaminant fin the area because it is very abundant in the local geology. The results were classified according to the adapted classification of Nude (2011) (in Pinho 2013, Martins 2014, Pinho 2018), which assumes five classes: (1) Min. Enr – Minimum Enrichment; (2) Mod. Enr. – Moderate Enrichment; (3) SE – Significant Enrichment; (4) VHE – Very High Enrichment; (5) EHE – Extremely High Enrichment. The elements Cd, Pb and Zn were identified as those that presented factors of VHE and EHE in all the areas. In relation to As, SE is verified for areas A1 and A3, highlighting in area A2 the classification from SE to EHE. For Cu and Mn, Mod. Enr. to SE in areas A1 and A3, and VHE in area A2, may be related to occasional contamination and to the regional geology rich in Fe-Mn oxides. The Figure 3a) gives an overview of the identified enrichments, where the occurrence of VHE to EHE is verified in all the areas, especially in areas A1 and A2 whose most samples belong to these more enriched classes mainly for Cd, Pb and Zn. The lowest enrichments (Min. Enr., Mod. Enr., SE) of the remaining elements (As, Co, Cr, Cu, Mn and Ni) mostly occur in samples belonging to areas A1 and A3. The Index of Geochemical Load (IGL) was classified according to seven categories, taking into account the concentrations obtained in $mg.kg^{-1}$: (1) Uncontaminated (UN): <0; (2) Uncontaminated to Moderately Contaminated (UN-MC): 0–1; (3) Moderately Contaminated (MC): 1–2; (4) Moderately Contaminated to Highly Contaminated (MC-HC): 2–3; (5) Highly Contaminated (HC): 3–4; (6) Highly to Extremely Contaminated (HC-EC): 4–5; (7) Extremely Contaminated (EC): >5 (Nude 2011, Trindade 2012, Martins 2014, Pinho 2018). Similar to the results obtained for EF, there were also high IGL values for the main contaminants in the area (Cd, Pb and Zn). For these three more problematic metals, IGL was classified as MC-HC, HC, HC-EC and EC for all the areas. In less contaminated classes (UN-MC and MC) and in a few samples in UN, Pb was classified in the areas A1 and A2 (Figure 3b). IGL values for Fe and Mn

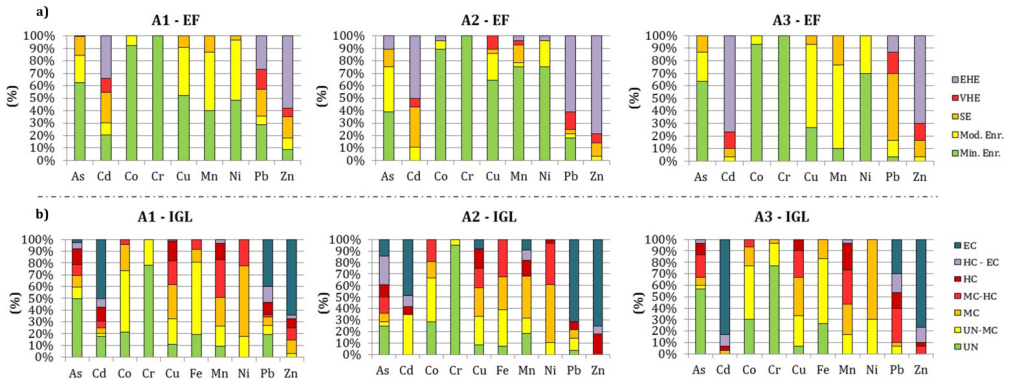

Figure 3 *Classification the levels obtained through the EF and IGL indices.*

range between UN and HC in the three areas with area A2 presenting classifications of EC and HC-EC only for Mn. According to this indices classification, lower contamination was found in Co, Cr, Cu and Ni, ranging, in all the areas, between UN and MC-HC. Only in the A2 area only for Cu, IGL was classified as HC and EC. Thus, the occurrence of IGL with elements in the classes belonging to the most contaminated levels is verified for all the areas, with less representation in areas A1. The Contamination Factor (CF) classifies metals abundances into four categories in $mg.kg^{-1}$: (1) Low level of contamination (LLC): <1; (2) Moderate level of contamination (MLC): 1–3; (3) Considerable level of contamination (CLC): 3–6; (4) High level of contamination (HLC): >6 (Nude 2011, Martins 2014, Pinho 2018). CF, like EF and IGL, identified Cd, Pb and Zn as the most contaminating elements with most samples classified with high levels of contamination (HLC). Only for As in area A1, and for Mn in all the areas sediments have considerable level of contamination (CLC). The remaining elements, with significantly lower levels compared to the critical levels (Cu, Co, Fe and Ni) area classified as MLC.

Spatial distribution maps of the concentrations of acid-extractable fractions of metals have been constructed in order of obtaining an over view of the dispersion of the most relevant elements throughout the area and in depth. The classes used have been adapted according to the limits considered for each element by CONAMA (2012). The software, based on the kriging method, was SURFER12. Figure 4 shows the maps built for Zn. This element has a heterogeneous distribution in either for sediments collected closer to the waterway or at those located further away, but always with values higher than the critical ones (CV; CONAMA 2012). Although concentrations are mostly above the CVs, there is a decrease in sediments accumulated at the margins of Consciência creek and near the mouth with São Francisco River, visible at 40-60 cm in depth. This decrease may be due a result of the natural attenuation caused by the diluting effect the rainwater, the stream and the river.

Conclusion

The geochemical characterization of sediments deposited in a floodplain on a in the margins and bed of a narrow waterway near an industrial unit identified Cd, Pb and Zn as elements with higher environmental hazard, as their contents are much higher than the CV proposed by current environmental standards. The quality parameters attained from the application of three selected indices proved to be very similar to each other, also indicating these three metals as the main contaminants. However, making a comparison between the three, EF and IGL show as greater agreement. CF is the index that allows the simplest identification of the main contaminants in the area, although it also depends directly on the reference values. The use of any of these indices and

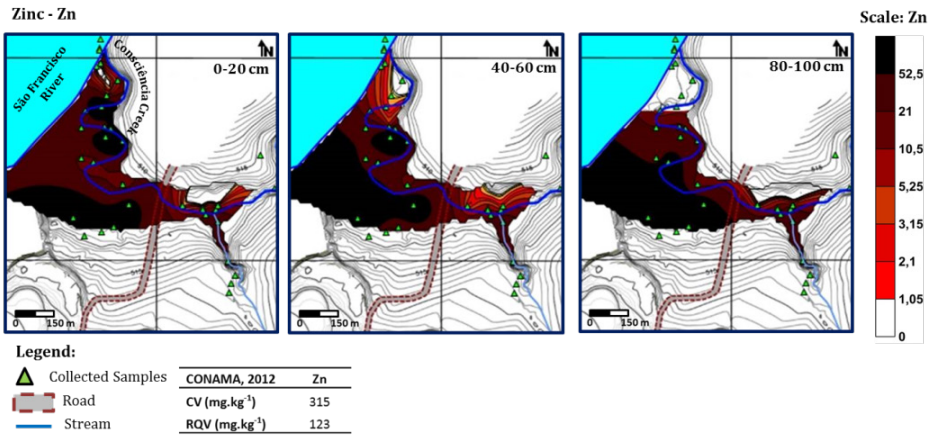

Figure 4 Spatial distribution of the levels obtained for Zn in the study area.

the analysis of their results was carried out bearing in mind all the interferences to which they are subject, without any disadvantages for anyone, which is why they were used together in order to allow a more reliable characterization. The spatial and depth distribution of the contents of these elements allowed a visualization of the contaminants evolution throughout the whole area, with the subsequent identification of zones of possible natural attenuation. The proposal of an appropriate remediation methodology for this area will have to be based on in situ techniques, with preferential application in the dry season, in order to minimize the effects of dispersion of contaminants by dissolution, In the alluvial area, the capping technique to increase its infiltration capacity, followed by the construction of a Permeable Reactive Barrier with a "funnel and gate" configuration and impermeable lateral areas, is suggested as the most appropriate in order to guarantee its greater effectiveness.

Acknowledgements

The authors would like to thank Votorantim Metais S.A., for financing the project "Proposed strategy for the remediation of the area of the Consciência and Barreiro Grande creek - Phase 2." The research was also supported by ICT, under contract with FCT (The Portuguese Science and Technology Foundation) through the Projects UIDB/04683/2020 e UIDP/04683/2020.

References

Cappuyns, V, Swennen, R. Nicolaes, M. (2007) Application of the BCR sequential extraction scheme to dredged pond sediments contaminated by Pb-Zn mining: A combined geochemical and mineralogical approach. Journal of Geochemical Exploration. 93:78-90.

Carvalho, G, (2008) Preliminary determination of constructive parameters of permeable reactive barriers using columns for the remediation of chromium with zerovalent iron. Master's Dissertation in Geotechnical and Geoenvironmental Engineering, Superior Engineering Institute of Porto, Portugal, p. 189.

CONAMA 2012 Resolutions in force published between September 1984 and January 2012. Ministério do Meio Ambiente, Brasília, Brazil, p. 1125

Davidson, CM, Hursthouse, AS, Tognarelli, DM, Ure, AM, Urquhart, GJ, (2004) Should acid ammonium oxalate replace hydroxylammonium chloride in step 2 of the revised BCR sequential extraction protocol for soil and sediment. Analytica Chimica Acta. 508 (2):193–199.

Lu, A., Zhang, S., Shan, X., Wang, S., Wang Z. (2003) Application of microwave extraction for the evaluation of bioavailability of rare earth elements in soils. Chemosphere. 53:1067-1075.

Martins, L, (2014): Geochemical evaluation of the impact of dredging sediments from a waterline with high concentrations of heavy metals, in a dry tropical climate. Master Thesis in Earth, Atmosphere and Space Sciences and Technologies. University of Évora, Portugal, p. 434.

Nude, PM, Foli, G, Yidana, SM (2011) Geochemical Assessment of Impact of Mine Spoils on the Quality of Stream Sediments within the Obuasi Mines Environment, Ghana. International Journal of Geosciences, (2):259-266.

Pendias, KA, (2001) Trace elements in soils and plants. CRC press, 3ªed.

Pinho, C, (2013) Geochemical assessment of environments contaminated by mining in two distinct geological and climatic regions. Master's Thesis in Geological Engineering, University of Évora, Portugal, p. 230.

Pinho, C, (2018) Characterization of the Environmental Risks of Contaminated Materials in the Aluvionar of a Metallurgical Unit in the State of Minas Gerais (Brazil)." PhD Thesis on Earth Sciences and Space, University of Évora, Portugal, p. 645.

Pinho C, Fonseca R, Carneiro J (2018) Environmental Characterization of an Alluvial Plain and Proposal for its Remediation. Congress of Geochemistry of the Portuguese-speaking countries - XIX Geochemistry Week.

Pinho C, Fonseca R, Carneiro J (2019) Environmental Risk Assessment of Contaminated Materials in the Alluvial Plain of a Metallurgical Unit. Magazine of the Portuguese Association of Geologists, Geonovas 32 (1):43-56.

Raymond AW, & Felix EO, (2011) HeavyMetals in Contaminated Soils: A Review of Sources, Chemistry, Risks and Best Available Strategies

for Remediation. International Scholarly Research Network, ISRN Ecology Article ID 402647, p. 20, Doi:10.5402/2011/402647

Ribeiro, EV, (2010) Water quality assessment of the São Francisco River in the segment between Três Marias and Pirapora-MG: Heavy metals and anthropogenic activities. Master's Dissertation in Geography, Federal University of Minas Gerais, Belo Horizonte, Brazil p. 196.

Trindade, WM, Horn, AH, Ribeiro, EV (2012) Heavy metal concentrations in São Francisco River sediments between Três-Marias and Pirapora - MG: Geochemistry and Environmental Risk Classification. Geonomos, 20 (1):64-75.

USEPA (2007) Method 3051A: Microwave Assisted Acid Digestion of Sediments, Sludges and Soils. In: http://www.epa.gov/osw/hazard/testmethods/sw846/pdfs/3051a.pdf (consulted 15/11/2013).

USEPA (2008) Nanotechnology for Site Remediation Fact Sheet. United States Environmental Protection Agency, Solid Waste and Emergency Response, p. 17.

Application of Multivariate Statistical Analysis in Mine Water Hydrogeochemical Studies of the Outcropped Upper Carboniferous, Ruhr Area, Germany

Tuan Quang Tran[1, 2], Andre Banning[1], Stefan Wohnlich[1]

[1]*Hydrogeology Department, Faculty of Geosciences, Ruhr University Bochum, Universitätsstr. 150, 44801 Bochum, Germany, quang.tran@rub.de or tranquangtuan@humg.edu.vn*

[2]*Hydrogeology Department, Faculty of Geosciences and Geoengineering, Hanoi University of Mining and Geology, Hanoi, Vietnam*

Abstract

This study aimed to identify the processes controlling the geochemical characteristics of adit mine waters using correlation analysis and multivariate statistical techniques. The Hierarchical cluster analysis (HCA) classified water samples into 5 geochemically distinct clusters of similar characteristics. HCO_3^- and Ca^{2+} were the dominant ions in the mine water (clusters C1, C2, C3, and C4), indicating the processes of carbonate dissolution, while Na^+ was the most abundant of the cations in cluster C5, suggesting processes of rock weathering. Samples of C2, C4, and C5 were of Ca-Na-HCO_3-SO_4, Ca-Mg-Na-HCO_3-SO_4-Cl, and Na-Ca-HCO_3-SO_4 types, respectively, while those from C1 and C3 were of Ca-Mg-HCO_3-SO_4 type. A total of three principal component analysis (PCA) components accounted for 82.95% of the total variance. PCA 1 accounted for a variance of 58.18%, characterized by high positive loadings for HCO_3^-, SO_4^{2-}, Ca^{2+}, Mg^{2+}, Na^+, K^+, TDS, and EC, suggesting carbonate dissolution, rock weathering, and water salinity. The other components may be related to more local and geological effects. This study demonstrated the usefulness of multivariate statistical analysis in hydrogeochemistry.

Keywords: multivariate statistics, cluster analysis, principal component analysis, mine water

Introduction

The last remaining German active hard coal mine was closed in December 2018. However, after mining, the mine water quality is still one of the concern issues nowadays. The study area is a part of the Ruhr coalfield, where the coal-bearing Upper Carboniferous strata crop out directly on the surface of the Ruhr river valley or underneath very thin overlying sediments of Quaternary age (Frankenhoff et al. 2017; Zieger et al. 2018), with about 50 km in East-West length and 15 km North-South width (Drozdzewski et al. 2008). It covers an area of about 754 km2 (Fig. 1), spreading over the cities Hattingen, Sprockhövel, Witten, Wetter and Schwerte, and including parts of the cities Essen, Bochum, Dortmund, Holzwickede and Herdecke. The topography of the study area is generally shallow hills and undulating terrain, the elevation ranges between 20 and 333 m above sea level. The highest elevations are in Sprockhövel (about 330 m in Holthausen). The annual average precipitation in the area is 891 mm (DWD 2019). The geology is characterized by Upper Carboniferous cyclothems: sandstone, silt-, mud-, and claystone layers, interspersed with hard coal seams. The layers contain clay minerals and mica (kaolinite, chlorite, biotite), feldspar (albite, anorthite), siderite, dolomite, calcite, quartz, and pyrite (Strehlau 1990; Wisotzky 2017).

It is not easy to identify the processes controlling the geochemical characteristics of mine water, especially in abandoned coal mines, through complex hydrogeochemical data. To protect water resources, it is important to understand processes controlling geochemical variability in such post-mining systems.

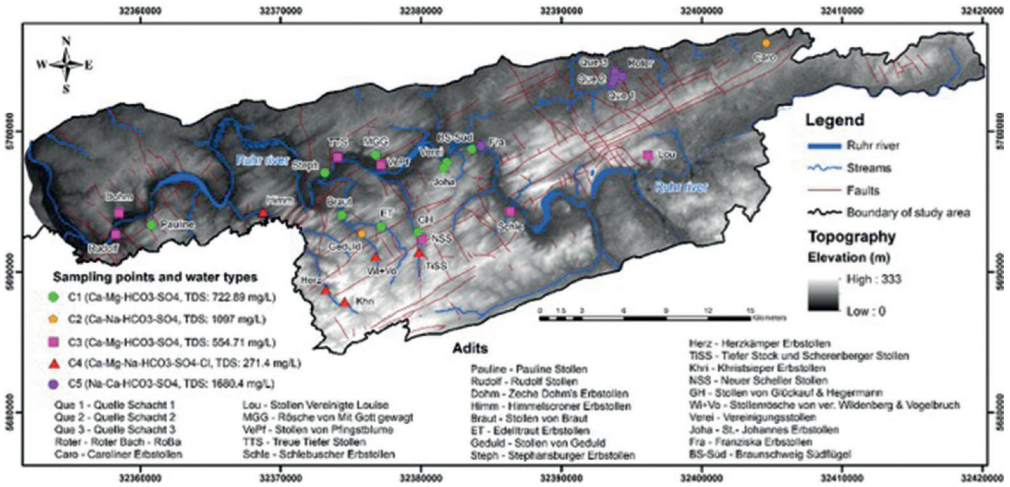

Figure 1 *Map of the study area, including sampling points and spatial distribution of the mine water types.*

For decades, besides hydrogeochemical and isotopic methods, multivariate analysis techniques have also been used widely in mine water studies (e.g. Li et al. 2018). These methods are performed as useful tools to reduce and organize a large hydrogeochemical data set into a small number of factors, grouping samples with similar characteristics (Reghunath et al. 2002). Multivariate techniques also were used to study the environmental impacts of medieval mining (Horák and Hejcman 2016) or have been extensively applied to groundwater quality data (Khelif and Boudoukha 2018). Moreover, multivariate analysis has been applied to hydrogeochemical data by many researchers to analyze hydrogeochemical parameters to classify groundwater of varied geochemical features and to identify primary processes controlling groundwater chemical components (e.g. Qian et al. 2016).

The purpose of this study was to characterize the chemistry of mine water and to develop hypotheses about processes controlling mine water composition and the origin of the chemical constituents present in mine water of abandoned coal mines in the outcropped Upper Carboniferous of the Ruhr area, Germany. The present study also contributed and demonstrated the usefulness of multivariate statistical analysis in mine water assessment and established a better understanding of hydrogeochemical characteristics of mine water in the study area.

Sample collection and methods

Sampling and analysis

Water samples were collected from the 28 different drainage sites of abandoned coal mines in the study area from January to March 2018. The sampling locations are given in Fig. 1. Physicochemical parameters of water (pH, EC) were measured in situ using portable meters (WTW, Weilheim, Germany). These probes were calibrated using standard solutions, and bottles were washed and rinsed thoroughly with sample water. Samples for cation analysis were acidified using concentrated HNO_3. Samples were stored in the refrigerator at 4 °C until completed analyses. HCO_3^- concentrations were measured using HCl titration. Major anions (SO_4^{2-}, Cl^-, NO_3^-, F^-) were measured using the DIONEX Ion Chromatography System model ICS-1000, with an AD20 Absorbance Detector system. Major cations (Ca^{2+}, Mg^{2+}, Na^+, and K^+) were analyzed by CD25 Conductivity Detector, IP 20 Isocratic Pump DIONEX.

Multivariate statistical techniques

The correlation matrix, Hierarchical cluster analysis (HCA), and Principal component analysis (PCA) methods were used to evaluate the physicochemical parameters of water samples. Spearman correlation was used to evaluate correlations between different variables, using the statistical software SPSS

23, combined with the XL-Stat software to check and compare results. These methods were applied to a subgroup of the dataset to evaluate their usefulness for classifying water samples and identifying relevant geochemical processes. The dataset consisted of 28 hydrogeochemical analyses.

The Q-mode HCA technique was performed on the water chemistry data to classify samples into distinct hydrogeochemical groups using values for 12 physicochemical parameters (HCO_3^-, SO_4^{2-}, Cl^-, NO^{3-}, F^-, Ca^{2+}, Mg^{2+}, Na^+, K^+, pH, EC, and TDS). The Ward's linkage method with Euclidean distance was used for the measurement of similarity between the water quality variables. The results were represented in a dendrogram. PCA was used to identify major factors governing mine water geochemistry. The varimax rotated factor analyses were carried out for 12 parameters and factor loading was calculated using eigenvalue greater than 1 and sorted by the results having values greater than 0.3. Most mine water physicochemical parameters in this study are non-normally distributed, the Spearman method and Kaiser-Meyer-Olkin (KMO) test were used to indicate the proportion of common variance

Results and discussion

General hydrogeochemical characteristics

The pH values ranged from 6.39 to 7.65, indicating circum-neutral mine water conditions. EC values were in the range of 202 to 1713 µS cm^{-1} and TDS values ranged between 157 and 1806 mg L^{-1}, which indicates that mine water of several adits is highly mineralized, implying fresh and brackish waters. A Durov diagram (Durov 1948) was plotted for 28 water samples to examine the hydrogeochemical types of mine waters (Fig. 2).

This diagram shows the chemical composition of water in the study area that was formed by the main types: Ca-Mg-HCO3-SO4, followed by Na-Ca-HCO_3-SO_4, Ca-Mg-Na-HCO_3-SO_4, and Na-Ca-Mg-HCO_3-SO_4 water types. The average ion concentrations followed the order: HCO_3^- > SO_4^{2-} > Cl- > NO_3^- > F- and Ca^{2+} > Mg^{2+} > Na^+ > K+ (% meq L^{-1}). The mine water samples showed the dominance of weak acids (HCO_3^-) over strong acids (SO_4^{2-} + Cl^-), and

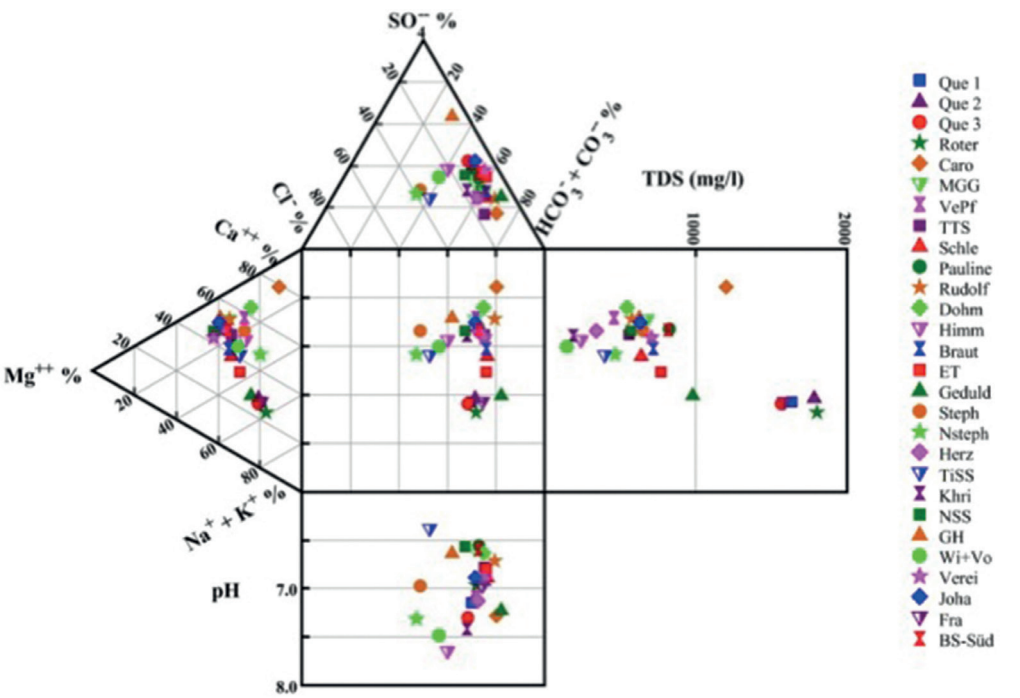

Figure 2 *Durov diagram of mine water hydrogeochemistry in the study area.*

alkaline earths (Ca^{2+} + Mg^{2+}) over the alkalies (Na^{+} + K^{+}).

Multivariate Statistical Analysis

Correlation matrix

The Spearman correlation coefficients were calculated, the results of the correlation matrix for 12 variables are given in Table 1. The interpretation of the correlation matrix showed that the pH values are not correlated with ions.

TDS values are strongly correlated (r > 0.8) with most of the ions in the water samples, such as TDS - HCO_3^- (r = 0.936) and TDS - SO_4^{2-} (r = 0.847), mostly statistically significant at the 0.01 level (p < 0.01), while TDS values show a weaker correlation with Cl- (r = 0.44), significant at the 0.05 level (p < 0.05).

Na^{+} and K^{+} in water samples are correlated positively with Cl^- (r = 0.659, p < 0.01) and (r = 0.476, p < 0.05), respectively. This may indicate halite/sylvine dissolution influencing mine water chemistry. Ca^{2+} and Mg^{2+} concentrations are correlated with HCO_3^- with r = 0.738 (p < 0.01). This suggests calcite and dolomite dissolution. Ca^{2+} is also correlated significantly with SO_4^{2-} (r = 0.796, (p < 0.01)), suggesting possible gypsum dissolution.

Ca^{2+} and Na^{+} ions have an average correlation (r = 0.536, p < 0.01), indicating that Ca/Na ion exchange also increases the Ca^{2+} concentration in the mine water. EC showed strong to moderate positive and negative correlations with HCO_3^-, SO_4^{2-}, Ca^{2+}, Mg^{2+}, Na^{+}, K^{+}, Cl^- and NO_3^-. It reflects the participation of these elements in the brackish mine water environment in the study area.

Hierarchical Cluster Analysis (HCA)

The main result of the HCA performed on the 28 mine water samples is the Dendrogram (Fig. 3). The Q-mode factor analysis, sampling sites with larger similarities are first grouped. Next, groups of samples are joined with a linkage rule and the steps are repeated until all observations have been classified. Based on the desired level of resolution for interpretation and the potential of the data considered, the number of groups is chosen (Ribeiro and Macedo 1995). Ward's method was more successful to form clusters, with the phenomena line of 2.5. Results showed that the HCA classified mine water samples into 5 geochemically distinct clusters (C1-C5) of similar characteristics, represented in Dendrogram to categorize different levels, which the Stiff diagrams show for each group (Fig. 3).

Samples of C2, C4, and C5 are of Ca-Na-HCO_3-SO_4, Ca-Mg-Na-HCO_3-SO_4-Cl, and Na-Ca-HCO_3-SO_4 types, respectively, while those from C1 and C3 are of Ca-Mg-HCO_3-SO_4 type. The C4 cluster accounts for 17.9% of the total samples, including 5 samples, with the average EC and TDS values of 301.6 µS cm^{-1} and 271.4 mg L^{-1}, respectively, mostly distributed in the southern part (the highest elevation). C3 consists of 7 samples located at a lower elevation, accounts for 25% of the total samples (average EC: 579.71 µS cm^{-1} and mean TDS: 554.71 mg L^{-1}). The common feature of these water types is low

Table 1 *Spearman correlation matrix of major physicochemical parameters.*

	HCO_3^-	SO_4^{2-}	Cl^-	NO_3^-	F^-	Ca^{2+}	Mg^{2+}	Na^{+}	K^{+}	pH	EC	TDS
HCO_3^-	1.000	**0.758**	0.436	**-0.728**	0.210	**0.738**	**0.738**	**0.751**	**0.827**	-0.036	**0.877**	**0.936**
SO_4^{2-}		1.000	0.433	**-0.595**	0.319	**0.796**	**0.928**	**0.675**	**0.759**	-0.140	**0.898**	**0.847**
Cl^-			1.000	-0.172	0.114	**0.639**	0.417	**0.659**	0.476	0.014	**0.573**	0.440
NO_3^-				1.000	-0.332	-0.376	**-0.668**	**-0.557**	**-0.677**	0.170	**-0.537**	**-0.602**
F^-					1.000	-0.014	0.231	0.477	0.380	0.185	0.268	0.299
Ca^{2+}						1.000	**0.718**	**0.536**	**0.646**	-0.063	**0.865**	**0.767**
Mg^{2+}							1.000	**0.630**	**0.733**	-0.268	**0.794**	**0.773**
Na^{+}								1.000	**0.837**	0.099	**0.804**	**0.773**
K^{+}									1.000	0.029	**0.870**	**0.851**
pH										1.000	0.038	-0.075
EC											1.000	**0.933**
TDS												1.000

Bold indicates correlation is significant at the 0.01 level (2-tailed),

Underlined indicates correlation is significant at the 0.05 level (2-tailed).

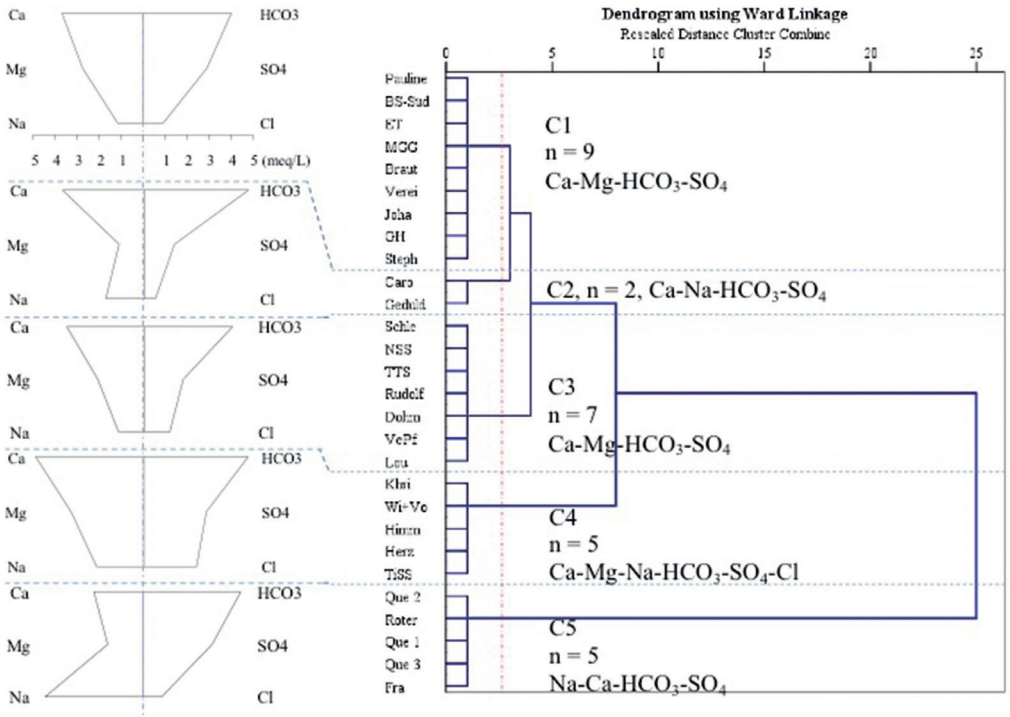

Figure 3 *Dendrogram of the major ions in mine water and corresponding Stiff diagrams.*

salinity. C1 is composed of 9 samples and represents 32.1% of the total samples. This water type is relatively fresh, with an average EC of 746.89 µS cm^{-1} (mean TDS = 722.89 mg L^{-1}), mostly distributed in the central study area (Fig. 1). C2 included by two water samples (mean EC and TDS values of 897.5 µS cm^{-1} and 1097 mg L^{-1}, respectively), characteristic for mixed water. C5 is represented by 5 samples, with an average EC of 1609.8 µS cm^{-1} (mean TDS = 1680.4 mg L^{-1}), interpreting the character of blended water and characterized by high salinity, mostly distributed in the east-northern part (Fig. 1). HCO_3- and Ca^{2+} were the dominant ions in the mine water of the study area (clusters C1, C2, C3, and C4), while Na^+ was the most abundant of the cations (cluster C5). The Que 2, Roter, Que 1, Que 3 and Fra water samples presented the highest average values of HCO_3-, Ca^{2+}, SO_4^{2-} and Na^+ ions.

Principal Component Analysis (PCA)

The PCA was used to identify major factors governing groundwater geochemistry by many researchers (e.g. Qian et al. 2016). The value of the KMO test is 0.752 > 0.5, indicating the total number of significant factors. The loadings of different elements, including the total eigenvalues of different factors, the percentage of variances, and the percentage of cumulative variances are summarized in Table 2. A system of orthogonal axes is created, which helped to visualize the projections of the data matrix elements in a plan diagram (Fig. 4).

From the hydrogeochemical data, a total of three PCAs were extracted with total eigenvalues higher than 1 which account for 82.95% of the total variance (Table 2). Three components reflect the major effective factors controlling the mine water chemistry.

The PCA 1 contributed 58.18% of the total variance and is characterized by high positive loadings on HCO_3-, SO_4^{2-}, Ca^{2+}, and Mg^{2+} (Table 2, Fig. 4). High scores of this component indicate high mineralization of mine water. This suggested that PCA 1 represented the dissolution or precipitation processes of carbonate, such as calcite and dolomite and sulfate minerals (Qian et al. 2016). However, PCA 1 had also high positive loadings for Na^+, K^+, TDS, EC, and Cl^- (Table 2, Fig. 4), suggested that it represented rock weathering

Table 2 Loadings of different parameters for the three PCAs following varimax rotation.

Parameters	Principal Components		
	PCA 1	PCA 2	PCA 3
HCO_3-	**0.913**	-0.163	0.184
SO_4^{2-}	**0.873**	-0.192	0.249
Cl-	**0.650**	0.354	-0.230
NO_3-	-0.275	**0.839**	-0.277
F^-	0.206	0.014	**0.843**
Ca^{2+}	**0.802**	-0.018	-0.397
Mg^{2+}	**0.738**	-0.559	0.097
Na^+	**0.852**	0.035	**0.419**
K^+	**0.785**	-0.240	0.197
pH	0.059	**0.801**	0.360
EC	**0.974**	-0.082	0.184
TDS	**0.944**	-0.118	0.193
Total eigenvalue	6.981	1.702	1.271
% of variance	58.18	14.18	10.59
% of cumulative variance	58.18	72.36	82.95

High loading values are highlighted in **bold**

and water salinity. It is addressed as the highly mineralized factor, because of exhibited high loadings on TDS (0.944), EC (0.974), SO_4^{2-} (0.873), Cl^- (0.65) and Na^+ (0.852). Therefore, mine water is not only contributed by Ca^{2+} and Mg^{2+} but also contributed by Na^+. It implied that it might be represented the ion exchange. The PCA 2 was 14.18% of the total variance in mine water dataset, with mainly consisted of NO_3- and pH (Table 2, Fig. 4), implied that it might be the consequence of agricultural activities in the study area. The PCA 3 explained 10.59% of the total variation of the matrix data and mainly consisted of F^- (Table 2, Fig. 4), suggested that it was contributed from the primary geological environment (Teng et al. 2018). Moreover, in Table 2, the PCA 3 had also a low positive loading on Na^+ (0.419) and a negative one for Ca^{2+} (-0.397), implied that ion exchange processes may occur in the mine water environment, as mentioned above.

Conclusions

Multivariate statistical methods were used to characterize the origin of the chemical constituents present in mine water of abandoned coal mines in the study area. The correlation of ions in mine water was assessed. The dissolution of carbonate, sulfate, silicate, and chloride minerals are the primary processes controlling mine water chemical composition. The HCA in Q-mode showed 5 statistical groups based on the major distinguishing factors of EC and TDS values. The PCA identified three principal components, which explained 82.95% of the total variance. The first PCA accounted for 58.18% of the total variance and is related to rock weathering, such as dissolution or precipitation of carbonate and sulfate minerals, ion exchange processes, and water salinity, while the other components are controlled primarily by agricultural activities and local geological environment (14.18% and 10.59%, respectively). The results of this study illustrated the usefulness of multivariate statistical analysis in hydrogeochemical studies.

Acknowledgements

This study is financially supported by the 911 Scholarship of the Vietnamese Government and the German Academic Exchange Service (DAAD). Thanks to M.Sc. Sarah Burscheid who helped with sampling in the field, as well as the helping of Mr. N. Richard and Mr. O. Schübbe (Hydrochemistry Laboratory, Institute of Geology, Mineralogy and Geophysics, Ruhr University of Bochum) for the analyzing assistance the mine water hydrogeochemical samples. Last but not least, the hosts who allowed to access their property.

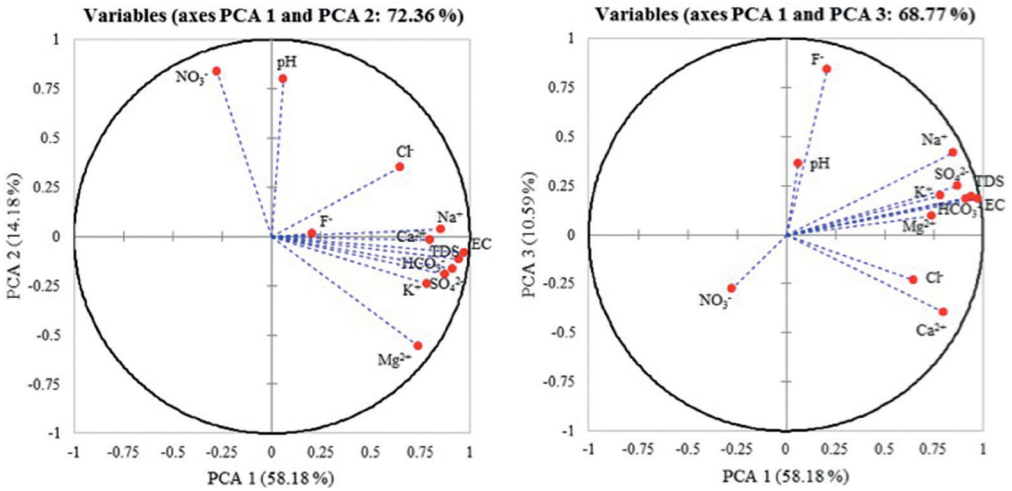

Figure 4 Representation of the parameters in the factorial plan PCA 1-PCA 2 and PCA 1-PCA 3.

References

Drozdzewski G, Schäfer A, Brix MR (2008) Excursion Guidebook, 26th Regional meeting of the International Association of Sedimentologists

Durov SA (1948) Classification of natural waters and graphic presentation of their composition. Dokl Akad Nauk SSSR 59(1):87-90

DWD (2019) Weather and Climate-German Weather Service (Deutscher Wetterdienst). Online source, https://www.dwd.de/DE/klimaumwelt/cdc/cdc_node.html. Accessed 2019

Frankenhoff H, Balzer I, Witthaus H (2017) Mine water concept in detail - A case study of closing a German coal mine at Ruhr district. pp 175-182

Horák J, Hejcman M (2016) 800 years of mining and smelting in Kutná Hora region (the Czech Republic)-spatial and multivariate meta-analysis of contamination studies. J Soils Sediments 16:1584-1598

Khelif S, Boudoukha A (2018) Multivariate statistical characterization of groundwater quality in Fesdis, East of Algeria. J Water L Dev 37:65-74

Li P, Tian R, Liu R (2018) Solute geochemistry and multivariate analysis of water quality in the Guohua phosphorite mine, Guizhou province, China. Expo Heal 11:81-94

Qian J, Wang L, Ma L, et al (2016) Multivariate statistical analysis of water chemistry in evaluating groundwater geochemical evolution and aquifer connectivity near a large coal mine, Anhui, China. Environ Earth Sci 75:1-10

Reghunath R, Murthy TRS, Raghavan BR (2002) The utility of multivariate statistical techniques in hydrogeochemical studies: an example from Karnataka, India. Water Res 36(10):2437-2442

Ribeiro L, Macedo ME (1995) Application of multivariate statistics, trend- and cluster analysis to groundwater quality in the Tejo and Sado aquifer. In: Groundwater Quality: Remediation and Protection. Proc. conference, Prague. pp 39-47

Strehlau K (1990) Facies and genesis of Carboniferous coal seams of Northwest Germany. Int J Coal Geol 15:245-292

Teng Y, Hu B, Zheng J, et al (2018) Water quality responses to the interaction between surface water and groundwater along the Songhua River, NE China. Hydrogeol J 26:1591-1607

Wisotzky F (2017) Water chemistry of the "Erbstollen" waters in the southern Ruhr area. In: Korrespondenz Wasserwirtschaft (KW), p 10 (in German)

Zieger L, Littke R, Schwarzbauer J (2018) Chemical and structural changes in vitrinites and megaspores from Carboniferous coals during maturation. Int J Coal Geol 185:91-102

Geochemical and Mineralogical Study of Lithologies and Tailings from the Whabouchi Lithium Mine Site, Québec, Canada

Tomy Roy[1], Benoît Plante[1], Mostafa Benzaazoua[1], Isabelle Demers[1], Isabelle Petit[2]

[1]*University of Québec in Abitibi-Témiscamingue, 445 boulevard de l'Université, Rouyn-Noranda (QC) J9X 5E4, Canada, Tomy.Roy@uqat.ca, Benoit.Plante@uqat.ca, Mostafa.Benzaazoua@uqat.ca, Isabelle.Demers@uqat.ca*

[2]*Nemaska Lithium, 101 avenue Chahoon, Shawinigan (QC) G9T 7J1, Canada, isabelle.petit@nemaskalithium.com*

Abstract

From growth in demand for lithium, especially for electric batteries, arises renewed interest in lithium mining from hard-rock deposits such as spodumene pegmatites. However, water quality from lithium mine tailings remains a poorly studied subject. Six samples of rock lithologies and tailings coming from various ore beneficiation steps at the Whabouchi spodumene mine site were studied in laboratory and on-site. Results show that pegmatite tailings produce neutral leachates, with spodumene responsible for Li leaching up to a few milligrams per liter. Laboratory and field results were consistent and, overall, similar.

Keywords: lithium, pegmatite, water quality prediction, geochemistry, mineralogy

Introduction

In the past few years, worldwide demand for lithium (Li) increased continuously, driven by the growing market of batteries for electric vehicles (Eftekhari et al. 2019). Although brine deposits in South America account for roughly two-thirds of all known Li resources, other types of deposits are also attracting renewed interest (Grosjean et al. 2012). Spodumene (LiAlSi2O6), a pyroxene mineral, was in 2019 the main source of Li (U.S. Geological Survey 2019) and remains a prime exploration target due notably to its presence on all continents and its century-long history of production and processing (Grosjean et al. 2012). It is found in rare-metal pegmatites and can be accompanied by a wide range of minerals with economic relevance, e.g. beryl and tantalite.

Despite a decades-long mining history, only a few studies have been conducted specifically about the environmental challenges associated with spodumene extraction from pegmatites, and thus the geochemical behavior of Li-pegmatite mine wastes is still poorly understood to date (Bradley et al. 2017). Karavaiko et al. (1979) reported concentrations between 4 and 8 mg/L Li2O (1.9 to 3.8 mg/L Li) in the pit lake and along rock walls of an open pit spodumene mine. No more details were given about mine water geochemistry in this context. Similarly, Rahn et al. (1996) reported circumneutral (8-9) pH and low (10-130 µS/cm) electric conductivity for pit water of abandoned spodumene mines in the Black Hills (U.S.A.), but without giving any more details. Li concentrations up to 15 mg/L have also been reported from "tailings dams of lithium mineral beneficiation plants" (Aral and Vecchio-Sadus 2011). Substantial amounts of unrecovered spodumene in tailings have been observed at different historic Li mining operations such as Foote Minerals' Kings Mountain, U.S.A. (0,44% Li2O) (Browning et al. 1964) and Transbaikal Mining-and-Processing Integrated Works, Russia (0.26% Li_2O) (Yusupov et al. 2015), for example. Besides challenges associated with industrial extraction of Li from spodumene, this mineral has been known for a long time to readily alter under meteoric conditions, losing primarily its Li content (Ginzburg 1959; Singh and Gilkes 1993).

Although it is not the only process that can occur in pegmatitic mine tailings

exposed to meteoric conditions, Li release from residual (unrecovered) spodumene is the main focus of this paper. It is part of a broader research project aimed at better understanding the geochemistry of tailings and wastes produced at a spodumene mining site. Results of laboratory and field tests (the latter conducted over a 2-year time period) are presented, along with some mineralogical characterizations, in order to compare how different materials produced throughout Li ore processing behave geochemically at different scales.

Materials and Methods

Site Description and Sampling

Nemaska Lithium's Whabouchi lithium mine is currently being developed approximately 30 km southeast of the Cree community of Nemaska, northern Québec, Canada. A total of 36.7 Mt ore with an average grade of 1.30% Li2O will be extracted during the mine's life (Nemaska Lithium, 2020). The site has a subarctic climate, with a snow-free period ranging from June to October. Geologically, the orebody consists of a poorly zoned albite-spodumene pegmatite being approximately 1.3 km long, 60 to 330 m wide and more than 500 m deep. Simpler spodumene-depleted ("barren") pegmatites are also encountered in association with the orebody. Enclosing rocks consist of metamorphised amphibolites, but they are not the subject of this paper.

A spodumene concentrate will be produced on-site. Ore processing begins with crushing and screening at a 850 µm grain size. Coarser (grain size > 850 µm) particles undergo a 2-step dense media separation (DMS), where the lesser dense particles (density < 2.7) are discarded. Coarser particles with a density over 2.96 are considered as spodumene concentrate. Coarser particles with an intermediate density (between 2.7 and 2.96) are milled to a grain size under 850 µm and, along with the screened < 850 µm ore, undergo chemical conditioning (including an attrition step done at pH = 12 by adding caustic soda) prior to spodumene hydroflotation. Fig. 1 summarizes the ore processing to be done at the Whabouchi site and highlights the origin of some of the materials studied.

Sampling of rock lithologies (spodumene pegmatite and barren pegmatite) was achieved by selecting halves of drilling cores in order to have "fresh" samples spatially distributed over all the projected mine pit. Samples from each lithology were then crushed (<2 cm) and homogenised.

Samples of sieved ore, DMS tailings and flotation tailings were randomly collected from materials produced during pilot processing tests (fig. 1). A mix of flotation tailings and screened ore (half-half by weight) was also produced to simulate a "worst case" scenario where spodumene recovery would be low and also to obtain enough material to fill the field test cells (see below).

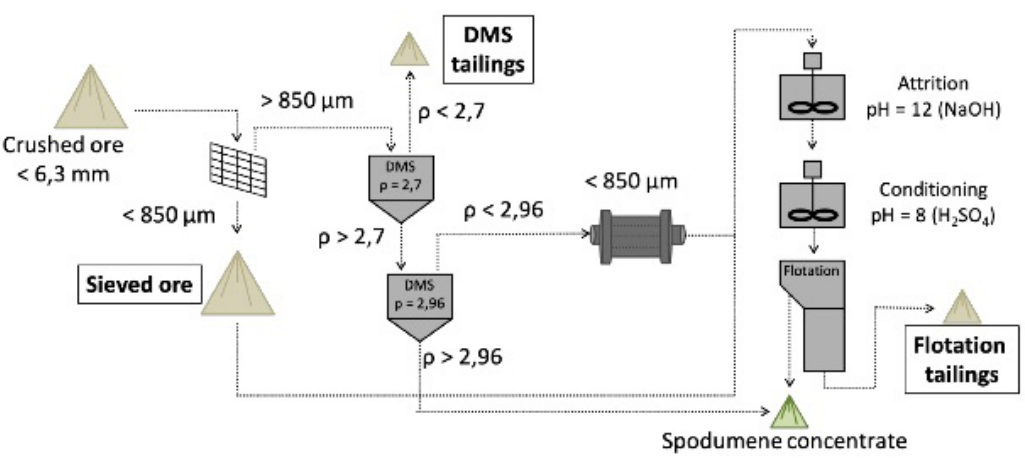

Figure 1 *Simplified flowsheet of the ore beneficiation process at the Whabouchi mine site highlighting studied materials. Note: ρ is in g/cm³; DMS = Dense Media Separation.*

Mineralogical Characterizations

For each rock lithology, a subsample was further crushed to <2 mm to render more statistically representative results by mass unit and mounted on 2 epoxy polished sections. Mineralogical composition was investigated by scanning electron microscope (SEM) with TIMA (Tescan Integrated Mineral Analyser). Li contents in spodumene and in other possible carrying minerals (chiefly muscovite) were quantified by laser ablation coupled with inductively coupled plasma - mass spectrometry (LA ICP-MS). Mineralogical characterizations for other materials are currently being performed and are not presented in this paper. Nevertheless, as they are all derived from the ore (spodumene-pegmatite), their composition should be related to that of the ore. Sulfur and carbon contents of the 6 materials were determined with an induction furnace (ELTRA CS-2000) coupled with an infrared analyzer.

Column Laboratory Kinetic Tests

Six plastic columns with a 14 cm-inner diameter were set up (one for each material tested) and kept at room temperature (18-25 °C). Each column was filled with approximately 25 kg of material. Once every two weeks (for crushed drill cores) or once every month (for tailings and screened ore), 2 L of deionized water is added to the top of the column and left to percolate during 4 h while the column's bottom valve is closed. Then, the valve is opened and columns are allowed to drain by gravity until leachates stop flowing (but not more than 24 h for drill core columns and 48 h for tailings and screened ore columns to ensure freshness of the leachates). Leachates are then collected and immediately analyzed. Rinse cycles were repeated for 10 to 14 months, until stabilization of the geochemical response.

Field Test Cells

Experimental field cells were built on the Whabouchi property in late 2017 (fig. 2) as part of a broader research program. Two of them were filled with the mix of screened ore and flotation tailings, but with different configurations. One cell (called Nem-PT for "Nemaska - Pyramidal Tailings") was built with a truncated pyramidal shape using 40 m3 of material and its footprint is impermeabilized with a geomembrane. A bigger cell (called Nem-CD for "Nemaska - Co-Disposal) was built with a flat top using 80 m3 of material, with a 3 m2 impermeabilized lysimeter under its center (see fig. 2). Natural precipitations are allowed to freely drain by gravity. Leachates are collected once every two or three weeks from May to October and

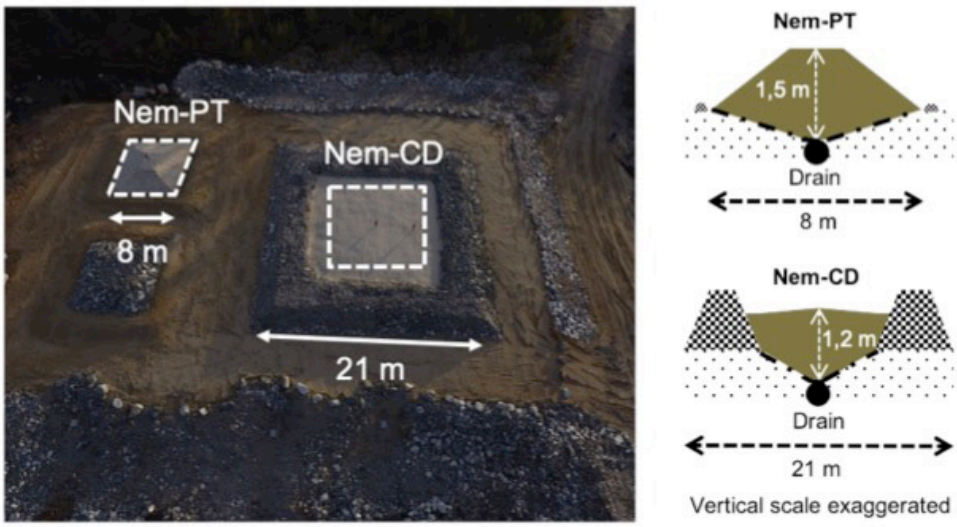

Figure 2 *Aerial view of the field cells built at the Whabouchi site, left (credit: Nemaska Lithium) and schematic cross-sections, right. Note: the lysimeters' surface projections are highlighted by dotted lines.*

immediately sent to a laboratory where they are analysed on the same day.

Leachates Analyses

Leachates are analysed for many physico-chemical parameters, but this paper will focus only on pH, electrical conductivity, sodium (Na) and Li. Cations (including Na and Li) were determined by inductively coupled plasma-atomic emission spectroscopy (ICP-AES) using a Perkin-Elmer Optima 3100. Samples were previously filtered (0.45 µm) using nylon filters and acidified with environmental-grade nitric acid.

Results and discussion

Mineralogical Characterizations

TIMA mineralogical composition of the rock lithologies (parent material) is presented in table 1. In spodumene-pegmatite, the average Li content in spodumene is 3.82% (w/w), which is slightly higher than the theoretical stoichiometric value (3.73%). It indicates that the spodumene is "fresh" and has not been submitted to prior substantial alteration. Muscovite has an average Li content of 0.14%, corresponding to a negligible part of the sample's total Li content. Quartz and feldspars both make up to 90% of the barren pegmatite and more than three-quarters of the spodumene-pegmatite. In plagioclase feldspars, the sodic end-member (albite) is predominant. Major minerals (quartz, feldspars, spodumene and even muscovite) appear as often pluricentimetric well-shaped crystals that are consequently fairly well liberated when crushed to finer grain sizes as it is the case for tailings.

Carbon and sulfur contents determined by induction furnace were under the detection limits (0.05 and 0.009 wt% respectively for C and S) for all 6 materials. In addition to results shown above, preliminary mineralogical characterizations (not shown) suggest a sometimes elevated (about 5% or more) residual spodumene content in flotation tailings.

Water Quality

The pH of the leachates (fig. 3) remained circumneutral (6.5-8.5) for all tested materials in all settings. The pH of the leachates from field cells showed slightly greater variability, which can be explained by variability of precipitation and temperature under a natural climate. ORP values (not shown) exhibited no clear trend, but remained in the range 200-700 mV for all materials, indicating oxic conditions.

Electrical conductivity measurements are also presented in figure 3. This parameter is affected by the leachates ionic strenght and can be, at least qualitatively, a proxy for overall reactivity of the materials. In laboratory columns, electrical conductivity quickly settled around a near-constant value after a few rinse cycles. It exhibited few if any variation from the start for DMS tailings, stabilizing around a low value of 50 µS/cm. In field cells, even if it shows some variation that could be attributed to climate (and mostly precipitation) fluctuations, electrical conductivity seems to be on an overall decreasing trend which will be validated with coming seasons. For Nem-CD, the first sample of 2019, which shows unusually low values for many parameters, was heavily diluted due to ongoing snow melting. Also, the effect of the cells' geometry on water infiltration will have to be closely looked upon.

Li concentrations (fig. 3) from the field cells, as well as those obtained during early laboratory rinse cycles, are similar to those reported in the literature for Li mines (2-15 mg/L). In laboratory, Li values tend to settle near or under 1 mg/L. It will be interesting,

Table 1 *TIMA mineralogical composition of the rock lithologies (in wt%).*

Mineral	Chemical Formula	Barren Pegmatite	Spodumene Pegmatite
Quartz	SiO_2	32.7	23.2
Plagioclase	$(Na,Ca)(Si,Al)_4O_8$	49.3	39.6
K-Feldspar	$KAlSi_3O_8$	10.2	14.2
Spodumene	$LiAlSi_2O_6$	3.1	20.6
Muscovite	$KAl2(AlSi_3O_{10})(OH,F)_2$	2.5	1.6
Other*	-	2.2	0.8

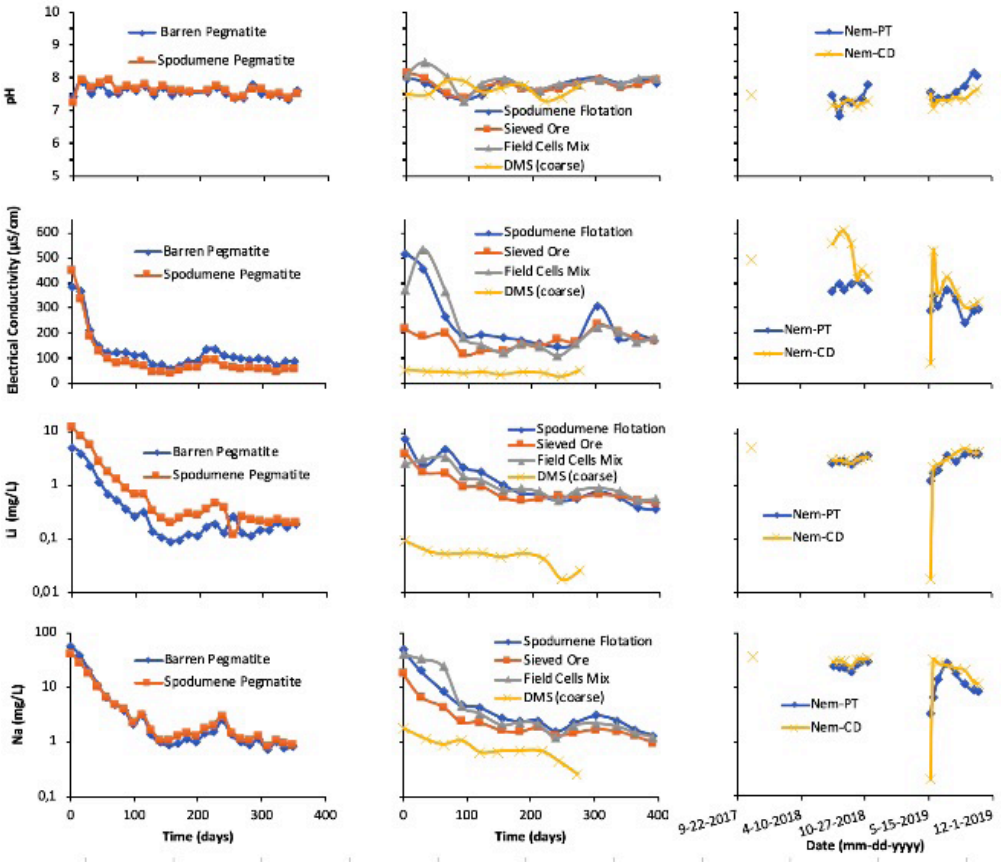

Figure 3 Water quality results (selected parameters) for rock lithologies columns (left), tailings columns (center) and field cells (right).

in the upcoming years of the research project, to see if this is the case as well for field cells, which currently vary around 2-5 mg/L. Na (fig. 3), which is assumed to come mostly from plagioclase dissolution, follows similar patterns as Li in laboratory. On-site, it shows slightly greater variation, with a somewhat decreasing trend in 2019 compared to the previous year.

Flotation tailings are the only tested material to have been exposed to chemical conditioning prior of being submitted to laboratory and field testing. Further physical and mineralogical characterizations will allow to assess potential effects of processing on the materials reactivity, especially in regard to mineral liberation and physical weakening of the particles.

In Québec as in many other jurisdictions, Li is not a regulated parameter (there is no numerical criterion for Li in mining effluents), nor is it regarded as a potential threat for the environment. However, as virtually almost every compound, it is indirectly regulated by toxicity standards (in Québec specifically, for *Daphnia magna* and *Oncorhyncus mykiss*). Thus, a detailed knowledge of the release mechanisms of a metal in water, its mineralogical origin and its typical concentrations under relevant settings can prove valuable to help minimize harmful effects on the receiving environment.

Conclusions

This paper presented water quality results from 6 samples coming from various beneficiation steps of a hard-rock lithium ore. These samples were submitted to laboratory kinetic tests as well as field-scale tests under a natural subarctic climate. Results showed that all these samples produce circumneutral leachates. Spodumene's signature in

drainage waters was also evidenced, with Li concentrations up to a dozen mg/L during early testing. In general, laboratory results were very consistent with field results. This research highlights the interdependency between mineralogy, ore processing, tailings storage and water quality. More detailed mineralogical characterization will allow a better understanding of the influence of various parameters (e.g. mineral liberation, associations and textures) on water quality. Furthermore, it will also make possible to assess if minor minerals, which are numerous in spodumene pegmatites and are sometimes very specific to these rocks, play an important role in these materials' geochemical behavior.

Acknowledgements

The authors gratefully thank Simon Thibault, Nathalie Tremblay and Pierre Mercier for their implication during the project's initial years and field logistics. Many thanks to Yvan Poirier, Pierre-Alain Jacques, Joël Beauregard, Joseph Tsopnang, Marc Paquin and Mélinda Gervais for their help with field and laboratory work. TIMA and LA ICP-MS analyses were performed by PMC Process Mineralogical Consulting Ltd. (Maple Ridge, BC, Canada). All other laboratory work was performed at UQAT's *Unité de recherche et de service en technologie minérale* (URSTM). This research is funded by a Collaborative Research and Development Grant from the Natural Sciences and Engineering Research Council of Canada.

References

Aral H, Vecchio-Sadus A (2011) Lithium: Environmental Pollution and Health Effects. In: Nriagu JO (ed) Encyclopedia of Environmental Health. Elsevier, p 499-508

Bradley DC, McCauley AD, Stillings LL (2017) Mineral-deposit model for lithium-cesium-tantalum pegmatites. U.S. Geological Survey Scientific Investigations Report 2010–5070–O, doi:10.3133/sir20105070O

Browning J, McVay T, Bennett P (1964) Continuous flotation of beryl from spodumene mill tailings, Foote Mineral Company, Kings Mountain, NC. US Bureau of Mines Report of Investigations 6466:24

Eftekhari A (2019) Lithium Batteries for Electric Vehicles: From Economy to Research Strategy. ACS Sustain Chem Eng 7:5602-5613, doi:10.1021/acssuschemeng.8b01494

Ginzburg AI (1959) Spodumene and its alteration processes. Works of the Mineralogical museum of the Academy of Sciences of the USSR [trudy mineralogicheskogo muzeya] 9:19-52

Grosjean C, Miranda PH, Perrin M, Poggi P (2012) Assessment of world lithium resources and consequences of their geographic distribution on the expected development of the electric vehicle industry. Renew Sustain Energy Rev 16:1735-1744, doi:10.1016/j.rser.2011.11.023

Karavaiko G, Avakyan Z, Krutsko V et al. (1979) Microbiological investigations on a spodumene deposit. Microbiol 48:393-398

Nemaska Lithium (2020). Lithium Resources & Reserves, available at: https://www.nemaskalithium.com/en/whabouchi/lithium-resources-reserves/ [accessed 23 March 2020].

Rahn P, Davis A, Webb C, Nichols A (1996) Water quality impacts from mining in the Black Hills, South Dakota, USA. Environ Geol 27:38-53

Singh B, Gilkes R (1993) Weathering of spodumene to smectite in a lateritic environment. Clays and Clay Min 41:624-630

U.S. Geological Survey (2019) Mineral commodity summaries 2019. U.S. Geological Survey, https://doi.org/10.3133/70202434

Yusupov TS, Isupov VP, Vladimirov AG et al. (2015) Analysis of material composition and dissociation potential of minerals in mine waste to assess productivity of lithium concentrates. J Min Sci 51:1242-1247

Efficacies of Pervious Concrete and Zero-Valent Iron as Reactive Media for Treating Acid Mine Drainage

Ayanda Shabalala

School of Biology and Environmental Sciences, University of Mpumalanga, Private bag x 11283, Mbombela, South Africa, Shabalala203@gmail.com, ORCID 0000-0002-3539-2943

Abstract

Batch reactor tests using pervious concrete (PervC) made at 0.27 water/cement ratio by mixing granite aggregate and Portland cement CEM I 52.5 R were performed to compare the use of PervC versus zero-valent iron (ZVI) for treatment of Acid Mine Drainage (AMD). The removal rates for Ca, Mg, Al, Fe, Mn, SO_4 and Cu were greater for AMD samples that were treated with PervC reactive media relative to those treated with ZVI. The pH-driven metal precipitation and adsorption of precipitates onto the surface of PervC and gypsum by-product are the main mechanisms of removal of metals from AMD.

Keywords: removal mechanisms, pervious concrete, acid mine drainage, batch reactor test, zero-valent iron

Introduction

Recent researches have shown pervious concrete to be a promising reactive material for effectively treating acid mine drainage (AMD) using the permeable reactive barrier (PRB) system. Pervious concrete is made by mixing a single-size coarse aggregate with cement to form a binder matrix of a highly porous network. During AMD treatment, the polluted water is percolated through pervious concrete at a sufficiently low controlled rate, to allow chemical interaction between the AMD and concrete. It has been shown that pervious concrete may be a more effective adsorbent than most other established reactive materials used in PRBs for treating AMD, such as zero-valent iron (ZVI) and zeolites (Ekolu and Bitandi 2018; Shabalala and Ekolu 2019; Solpuker et al. 2014; Majersky 2009).

The reactions resulting from the treatment of AMD using pervious concrete PRB, leads to an increase in the pH of AMD, causing most metals including Al, Zn, Fe, Cu, and Pb present in the polluted water to precipitate out of solution in form of metal hydroxides (Seneviratne 2007). Furthermore, the dissolved sulfate in the AMD react with $Ca(OH)_2$ in concrete to form gypsum. The formation of gypsum in already hardened concrete is expansive, leading to cracking and disintegration of the concrete (Ekolu et al. 2014). However, concrete deterioration due to gypsum formation can be controlled or mitigated by incorporating supplementary cementitious materials such as fly ash into pervious concrete mixtures (Shabalala et al. 2017).

Recent studies have shown pervious concrete to be an effective reactive material for treating AMD. However, there are presently few or no published literatures available on the mechanisms responsible for concrete's efficacy in removing metals from AMD. As such, the present study focussed on this research subject. The investigation involved a batch reactor test done using pervious concrete comprising Portland cement CEM I 52.5R with or without fly ash. Microanalytical studies were done using X-ray powder diffraction (XRD), Fourier transform infrared spectrometry (FTIR), and scanning electron microscopy (SEM) equipped with energy dispersive spectroscopy (EDS).

Methods

Mine water, pervious concrete and zero-valent iron

The AMD samples used in the present study were obtained from two sources comprising an abandoned coal mine (TDB) and an underground gold mine (WZ). The batch test

was conducted for both WZ and TDB using pervious concrete. The materials used to prepare previous concrete, comprising CEM I and 6.7 mm granite aggregate, were both supplied by Afrisam Cement (pty) Ltd. The FA used was obtained from Ash Resources (pty) Ltd. To prepare ZVI substrates, standard 100 mm cube moulds were filled with equal proportions of fine silica sand of size range 0.4 – 0.85 mm, coarse silica sand of size range 0.8 to 1.8 mm, fine ZVI grade GH 80 of size range 0.18 to 0.42 mm and coarse ZVI grade GH 18 of size range 1.0 to 1.4 mm. The ZVI material was supplied by BV Boksburg (Pty) Ltd. Each mixture was placed in an 8 L plastic container and filled with 3 L of WZ or TDB.

Batch tests

Six plastic containers, each of dimensions 130 mm by 215 mm were set up for the batch tests. In each container was placed a cube of CEM1, cube of 30% FA or ZVI-sand mixture of $1cm^3$. Three litres of WZ or TDB were added to each container. Vadapalli et al. (2008) observed that the active treatment and neutralization of AMD to circumneutral or alkaline pH was optimized when the ratio of AMD to reactive media was 3:1. Accordingly, a ratio of one concrete cube of 1 L by volume to 3 L of AMD was used in this study. Containers were tightly closed to ensure no evaporation took place. During the first 10 days, aqueous samples were collected once a day. Thereafter sampling frequency was decreased to once a week. The experiment was conducted continuously for a period of 43 days.

Analytical studies and microanalyses

Measurement of pH, conducted using MP-103 microprocessor-based pH/mV/Temp tester, was done immediately after collection of aqueous samples from batch tests. The pH electrode was calibrated using standard NIST-traceable pH 2.0, 4.0, 7.0 and 10.0 buffers. Collected samples were used for determination of the following cations: Al, Fe, Mn, Na, Mg, K, Ca, Mn, Fe, Co, Ni and Cu analysed using the PerkinElmer SCIEX (Concord, Ontario, Canada) ELAN® 6000 inductively coupled plasma-mass spectrometry system. SO4 was determined by ion chromatography (Dionex QIC-IC). Residues of the reacted adsorbents were taken from the batch reactors and used for XRD, SEM and FTIR microanalyses. Samples of the residues were oven-dried at 50 °C then used to prepare powder specimens for XRD analysis done using the Pan Analytical X-ray X'pert PRO PW3830 diffractometer. SEM examination of the residues was done using the TESCAN VEGA3SEM with AZtec EDS. Functional groups were determined using BX-II PerkinElmer FTIR equipped with the Universal Attenuated Total Reflectance (ATR) diamond crystal.

Results and Discussion

In the batch experiments, pH of raw AMD increased from initial values of 4.15 – 5.79 to pH = 6 to 8 for ZVI and pH = 9 to 12 for PervC. For both reactive media, a rapid increase of the pH was observed within the first 24 h of the experiment. The high pH values observed in the PervC-treated AMD is related to dissolution of portlandite from cementitious matrix which adds alkalinity into the system (Chandrappa and Biligiri 2016). The low final pH values attained for acidic water samples that were treated with ZVI as compared to those that were treated with PervC may be attributed to additional source of acidity provided by hydrolysis of Fe^{3+} in the ZVI samples, which lowers the pH.

The metal removal efficiency and changes in anion/cation concentrations were calculated as summarised in Table 1 and Fig. 1 for the PervC and ZVI reactive media. Average concentrations of elements over the period 10 to 43 days, were calculated for each element and then used to determine proportional decrease or increase from original AMD feed. Al, Fe, Ni, Co, Pb and Zn were successfully removed by both PervC and ZVI reactive media. The removal efficiency levels for Al, Mn, Mg and Cu were greater when AMD was treated with PervC as compared to treatment with ZVI. The lowest removal efficiency was observed in Mn and Mg concentrations when ZVI was used as a reactive media. After treatments using PervC or ZVI, the final concentration of SO_4 in treated effluent was always higher than that in the initial AMD feed.

Table 1 Contaminant removal efficiency levels of pervious concrete and ZVI reactive media.

AMD Type	Reactive Media	Al (%)	Fe (%)	Mn (%)	SO4 (%)	Mg (%)	Ni (%)	Co (%)	Cu (%)	Pb (%)	Zn (%)
WZ	CEM1	98	100	100	- 24	96	97	95	96	99	100
	30%FA	99	100	100	-32	91	96	93	96	99	100
	ZVI	82	96	44	-51	12	95	95	59	99	94
TDB	CEM1	99	100	100	-75	99	98	99	76	99	100
	30%FA	99	100	99	-46	100	97	98	81	99	98
	ZVI	97	100	58	-95	16	96	98	80	99	100

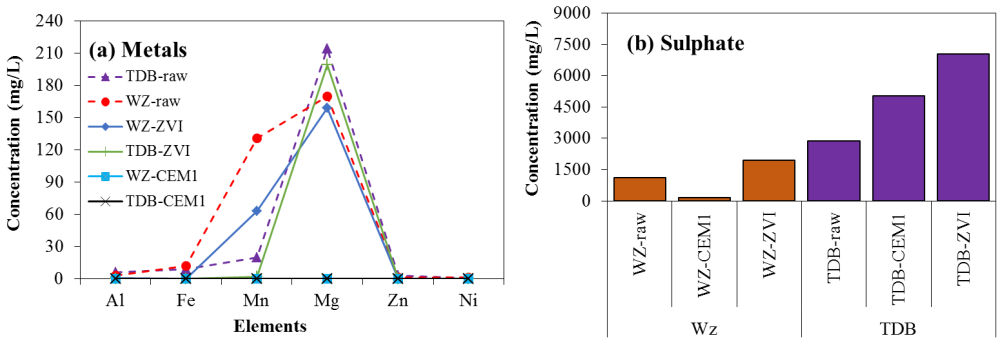

***Figure 1** Contaminant removal and concentration changes after 43 days of pervious concrete or ZVI treatment.*

Residues of reacted pervious concrete were taken from the batch reactors and examined by XRD. Figures 2 gives the XRD analyses done on residues of the reacted CEM I and 30%FA pervious concretes. Evidently, the most abundant product phase in all the mixtures is gypsum. The XRD spectra for TDB-CEM1 and TDB-30%FA also indicate the presence of thernadite (Na_2SO_4) as a minor mineral phase in both concrete mixtures. The WZ-30%FA residues gave a similar XRD pattern as TDB-30%FA of Figure 2a, generally showing an intermixture of metal precipitate complexes including calcium, strontium, aluminium, silica ($CaSrAl_2SiO_7$). The calcite observed in Figure 2a is likely to have formed due to exposure of the solid samples to the atmosphere, during sample preparation. The functional groups formed in the reacted pervious concrete following its exposure to AMD, are shown in Figure 2b. The FTIR spectra indicate the presence of vibrating carbonate stretches of calcite at a wavenumber 2349 cm^{-1}. Stretches at the wavenumber 1000 cm^{-1} are attributed to gypsum (Prasad et al. 2006). These findings provide evidence for the formation of gypsum and calcite - bearing precipitates, and are consistent with the observations from XRD analyses (Figure 2a). Geothite (FeOOH) was identified as the mineral phase formed in both WZ-ZVI and TDB-ZVI, as seen in Fig.3. At higher value of pH, the ferric hydroxides (FeOOH, FeOH3) may be created on the surface of ZVI, on which metals in cationic form may be sorbed. The iron corrosion products appear as a result of Fe0 oxidation to Fe^{2+} and then to Fe^{3+} (Suponik and Blanco 2014).

Concrete's mechanisms for removal of metals

Findings from the present study show that concrete's removal of metals from AMD occurs through two simultaneous processes. The initial removal step is the precipitation of metal (oxy)hydroxides owing to rise in the pH of AMD as driven by $Ca(OH)_2$, a cement hydrate which is massively present in concrete. Simultaneous to metal precipitation, is the formation of gypsum as a by-product upon

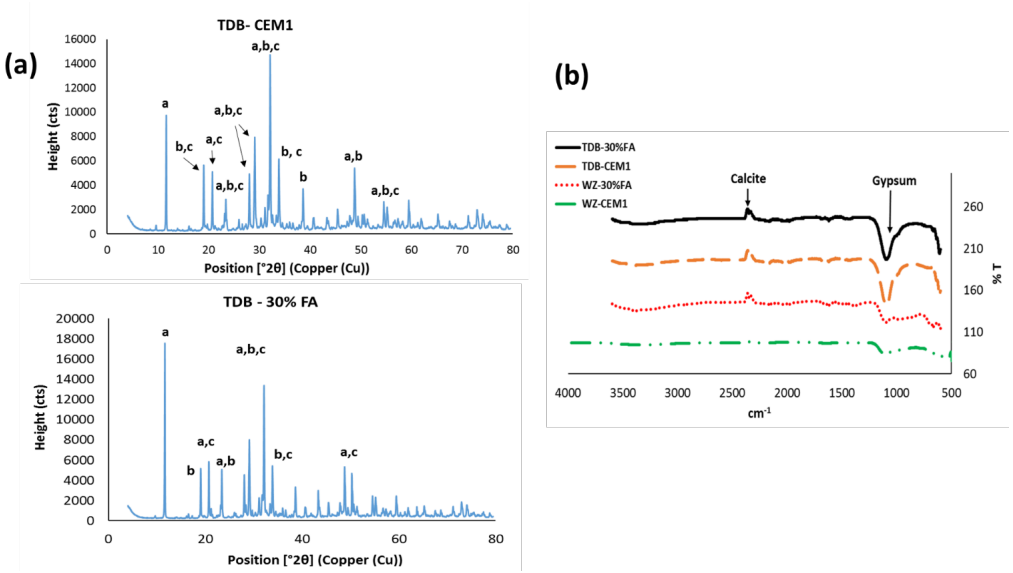

Figure 2 (a): XRD analysis on residues of TDB-CEM1 and TDB-30%FA concrete mixtures: a - gypsum (CaSO4·2H2O); b- Calcium strontium aluminium silicate (CaSrAl2SiO7); c – Calcite (CaCO3). (b) FTIR patterns of TDB-30%FA, TDB-CEM1, WZ-30%FA and WZ-CEM1 residues of pervious concrete.

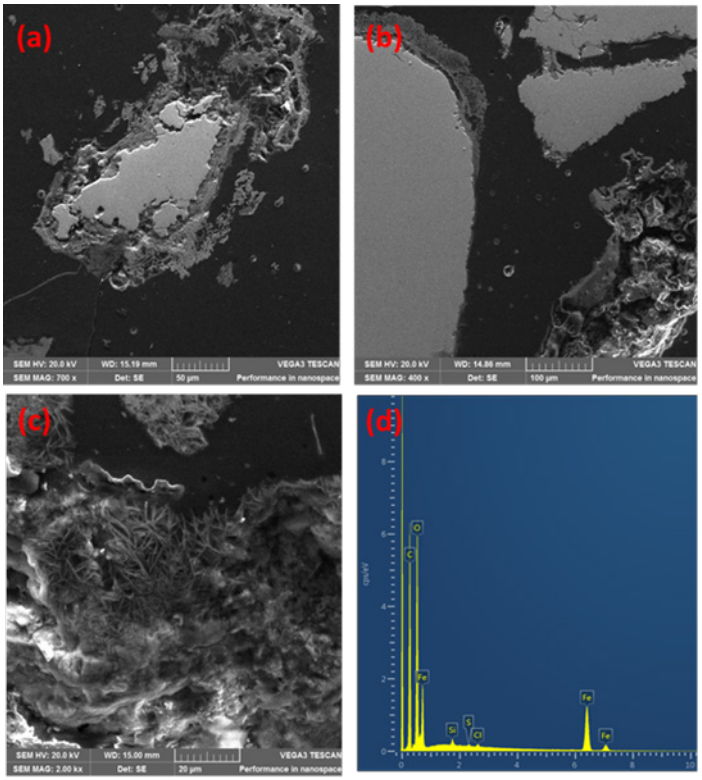

Figure 3 SEM examination of surface coating for ZVI: (a) reacted WZ-ZVI residues, (b) reacted TDB- ZVI residues, (c) close up of ZVI showing needle-like/acicular shaped crystals typical of goethite (FeOOH), (d) EDS spectra with high intensities of Fe and O which supports the presence of FeOOH.

the reaction of $Ca(OH)_2$, with sulfuric acid from pyrite oxidation and with the sulfate in AMD. The gypsum by-product formed, in turn adsorbs the metal precipitate complexes through physical adsorption processes.

Conclusions

A batch reactor test was done to compare the effectiveness of using pervious concrete for treating acid mine drainage relative to use of the conventional zero-valent iron system. The calcium hydroxide hydrate in pervious concrete reacts with AMD, increasing its pH to a high alkaline level, in turn leading to precipitation of metals out of solution. The removal rates for Al, Fe, Mn, Mg, Ca, and Cu were 95 to 100% when acid mine drainage was treated using pervious concrete as compared to 12 to 99% for zero-valent iron treatment. Gypsum is formed as a by-product upon the reaction of calcium hydroxide with sulfuric acid from pyrite oxidation and with the sulfate in AMD. The gypsum formed, adsorbs the metal oxy(hydroxide) precipitates through physical adsorption processes. Accordingly, the mechanisms of pervious concrete's removal of metals from AMD comprise the pH-driven metal precipitation occurring simultaneously with physical adsorption of the precipitates onto the surface of PervC and gypsum by-product formed.

Acknowledgements

The research presented in this paper is part of the PhD study of Ayanda N. Shabalala. This research was partly supported by the National Research Foundation (NRF) of South Africa, IPRR Grant Nos. 96800 and 116811. The author is grateful for the NRF's financial support.

References

Chandrappa AK, Biligiri KP (2016) Pervious concrete as a sustainable pavement material – Research

findings and future prospects: A state-of-the-art review. Constr Build Mater 111: 262–274, doi: 10.1016/j.conbuildmat.2016.02.054.

Ekolu SO, Bitandi L (2018) Prediction of longevities of ZVI and pervious concrete reactive barriers using the transport simulation model. J. Environ. Eng 144(9): 04018074, doi:10.1061/(ASCE)EE.1943-7870.0001402

Ekolu SO, Azene FZ, Diop S (2014) A concrete reactive barrier for acid mine drainage treatment, Proc. Inst. Civil Eng. Water Management 167(7): 373–380, doi:10.1680/wama.13.00035

Majersky G (2009) Metals recovery from acid mine drainage using pervious concrete. VDM Publishing House, Germany, ISBN 978-3-639-02618-4, paperback, 69p.

Prasad PSR, Prasad KS, Chaitanya VK, Babu EV, Sreedha B, Murthy SR (2006) In situ FTIR study on the dehydration of natural goethite. J Asian Earth Sci 27(4): 503-511, doi: 10.1016/j.jseaes.2005.05.005

Seneviratne M (2007) A practical approach to water conservation for commercial and industrial facilities, Queensland Water Commission, Elsevier Ltd, ISBN 978-1-85-617489-3, 372p.

Shabalala AN, Ekolu SO (2019) Quality of water recovered by treating acid mine drainage using pervious concrete adsorbent. Water SA, 45 (4): 638-647, doi: 10.17159/wsa/2019.v45.i4.7545.

Shabalala AN, Ekolu SO, Diop S, Solomon F (2017) Pervious concrete reactive barrier for removal of heavy metals from acid mine drainage - column study. J Hazard Mater 323: 641–653, doi: 10.1016/j.jhazmat.2016.10.027

Solpuker U, Sheets J, Kim Y, Schwartz FW (2014) Leaching potential of pervious concrete and immobilization of Cu, Pb and Zn using pervious concrete. J Contam Hydrol 161: 35–48. doi: 10.1016/j.jconhyd.2014.03.002.

Suponik T, Blanco M (2014) Removal of heavy metals from groundwater affected by acid mine drainage.

Physico Chem Probl MI 50: 359-372, doi: 10.5277/PPMP140130.

Vadapalli, VKR, Klink, MJ, Etchebers O, Petrik LF, Gitari W, White RA, Key D, Iwuoha E (2008)

Neutralization of acid mine drainage using fly ash, and strength development of the resulting solid residues, S Afr j sci 104:317-322, ISSN 1996-7489.

Tailings Facility Management: Modelling Tools for Life of Mine

Roald Strand[1], Muhammad Parker[2], Jaco Grobler[2], Nigel Moon[2]

[1]*Golder, Australia, University of Queensland, rstrand@golder.com*

[2]*Golder, Australia; mparker@golder.com; jgrobler@golder.com, nmoon@golder.com*

Abstract

Tailings facility water balance models have been used historically to simulate major hydrologic drivers on tailings facilities (Strand and Usher 2014). Recently, we have addressed growing regulatory oversight by providing tools to improve understanding of tailings storage facility (TSF) in context of environmental compliance (Moon et al. 2018).

To address our clients concerns with environmental compliance for TSF's, we have developed an integrated approach to service a growing field with customised simulation tools. Specifically, GoldSim has been outfitted with integrated climatic drivers and geochemical drivers to account for unplanned variance in expected responses (Strand et al. 2017). Major considerations include climate change, climatic influences such as evaporation and dilution, geochemical stability of tailings and consideration of such human influences as pump failure or dosing pond dredging.

End users and operators have used simulation systems to manage tailings facilities with higher resiliency to climatic effects, plan water storage and use, plan water treatment capacity, meet water quality compliance at mine lease boundaries, assess environmental impacts of specific projects such as mine waste placement strategies and plan closure (Strand et al. 2010, Usher et al. 2010, Strand and Usher 2014, Moon et al. 2018).

We explore four different examples and highlight how the models aided in solving complex questions, and added value or avoided unnecessary expenditure.

Keywords: Tailings Facility Modelling, Water Balance Modelling, Modelling, Water Quality Modelling

Introduction

Water balance models are required for a variety of regulatory purposes in Australia (DEHP 2012, DAWE 2020, DNRM 2018) and are regularly employed to predict the response of a system either in preparation of the wet season or during the wet season. Water quality models are frequently employed to produce conservative estimates of mass fluxes in association with water balances.

In Australia, with elevated evaporation rates and rainfall occurring predominantly during the wet season, there are other factors to consider, such as solubility constraints.

The authors have developed models to capture critical drivers on system stability and instability while accounting for nuance in operational strategy for TSF systems in Australia and the Americas. The examples indicate that TSF modelling may help operators understand and plan for the seasonal variance – whether that occurs via rainfall, water storage or salinity in mill feeds. We have provided standard water-balances and upgraded water quality models for tailings facilities to enhance understanding of constraints and operational response to human and environmental drivers in context of water and water quality.

Example 1

Location: Western Australia
Mine name: (confidential)
Facility: Tailings facility
Associated infrastructure: Mill, reticulation, pumps required for river abstraction

Description:

A TSF water balance model was built for a Goldmine in Western Australia. The client was concerned about the influences of large tailings beach on the TSF water balance; so,

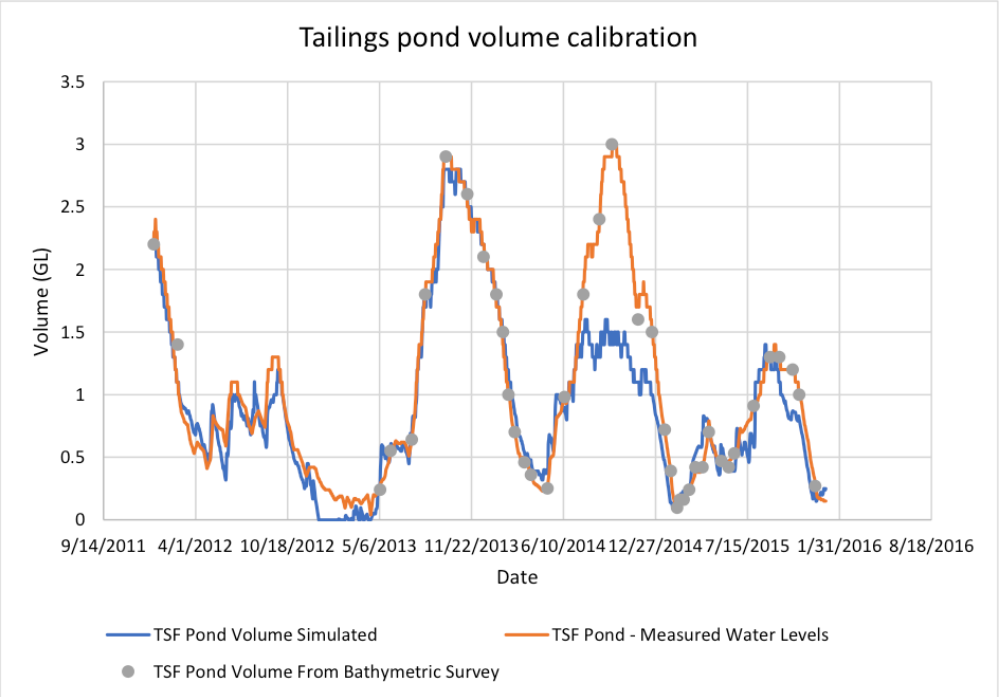

Figure 1 *Comparison of Observed and Modelled Storage Volumes for TSF.*

the model was outfitted with algorithms to predict runoff response based on tailings (beach) moisture and deposition (above the water surface).

Water volume in the TSF was calculated using measured water level elevation data and storage and bed elevations based on the bathymetric surveys. These are shown in Figure 1. These two sets of data were together utilised to derive storage volumes between the bathymetric survey dates.

The calibration of the TSF water balance was achieved by adjusting runoff coefficients associated with the estimated moisture in the tailings beach. The results of this calibration are shown in Figure 1.

Based on a comparison of the simulated and historic storage volumes (Figure 1) the model is able to simulate the general trends and changes in the TSF storage volume over time.

The problem which was solved was a water deficit. After calibration, the model was used to identify potential options to increase water holdings; TSF return water volumes for varying climate conditions including climate change to assess the river abstraction volumes and pumping rates (O'Hara et al. 2012). TSF pond water storage within the extent of the TSF liner has been maintained with the aid of the model.

Example 2

Location: Western Australia
Mine name: (confidential)
Facility: TSF

Description:

The Tailings pond (TSF) model was built to operate at a daily time step and is used to predict the water storage volume of the tailings pond (and its occurrence) driven by probabilistically generated rainfall, evaporation and tailings slurry properties.

The conceptual water balance for the TSF pond is shown schematically in Figure 2. The volume of the tailings pond and associated water fluxes into and out of the pond are dependent on changing dynamics of the TSF top surface landform due to ongoing tailings deposition.

The sources of uncertainty of future TSF pond water volume relates to future rainfall

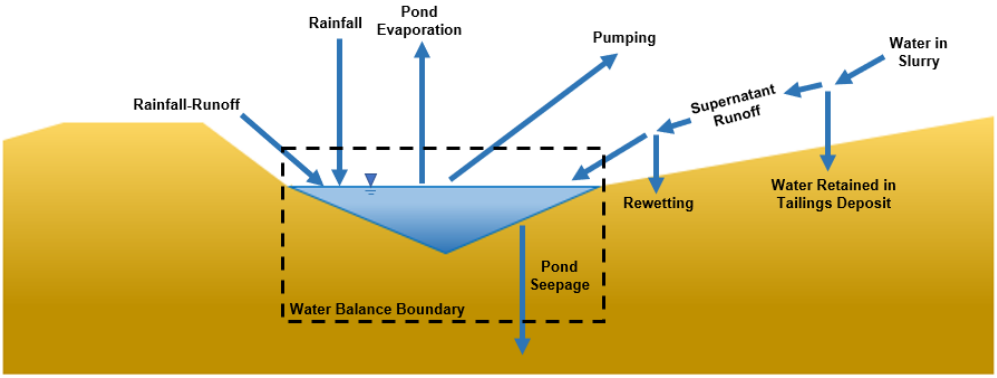

Figure 2 *Conceptual TSF pond water balance model.*

and evaporation. Probabilistically generated rainfall (and other input parameters) allows estimation of the water volume of the TSF pond and through Monte Carlo simulations, quantifies uncertainty associated with climatic effects.

Historic rainfall and evaporation data have been used to calibrate stochastic rainfall and evaporation generators based on the stochastic rainfall generator developed by the Catchment Research Centre (CRC) for Catchment Hydrology (Boughton 1999). These stochastic climate generators provide alternative estimates of rainfall and evaporation sequences with comparable probabilities of occurrence to each other and to the historic sequence.

The generators use transitional probability matrices to provide a representation of the historic probability of rainfall and evaporation rates occurring within defined ranges over the likely magnitude of extreme daily rainfall. This approach also takes into consideration the magnitude of the preceding day's rainfall and therefore preserves the historic daily rainfall patterns, as well as the frequency and magnitude of the daily rainfalls including the more extreme values. The generated rainfall and evaporation sequences also have comparable monthly, seasonal, and annual statistics to the historic period but with alternative, equally likely, daily patterns.

Simulating the water balance using many stochastic climate sequences (typically a minimum of 100) provides alternative, yet equally possible model outputs to provide an indication of the range and variability in likely fluxes and stores of the water balance. Running a larger number of model realisations will increase the likelihood of occurrence of more extreme climate patterns and events, such as prolonged periods of high or low rainfall years.

The client used the TSF water balance to provide an estimation of the return water pumping requirements to manage the pond size and avoid an inadvertent spill from the facility based on confidence limits which were calculated based on the Monte Carlo modelling approach.

Example 3

Location: Central Mexico
Mine name: (confidential)
Facility: Tailings Management Facility (TMF)

Description:

A mine in Central Mexico required modelling of the Tailings Management Facility (TMF) and water management structures as associated infrastructure.

The prefeasibility design for the TMF includes an unlined ring dike constructed of non-potentially acid generating (Non-PAG) waste rock with granular upstream filters and underdrains with central discharge of thickened tailings, alternated with placement of layers of potentially acid generating (PAG) waste rock. The design specifications include thickened tailings being pumped to the TMF.

A water balance model (WBM) was developed for the TMF. The objective of the modelling was to inform estimates of water fluxes and storage requirements over the construction and operations phase of the TMF.

The WBM operates at a daily time step and predicts volumes of the water and flow fluxes, and the associated variation and probabilities of occurrence driven by probabilistically generated rainfall adjusted to include various climate change parameters.

The TMF was separated into two zones to better simulate water fluxes during water balance modelling of:

- deposited tailings; defined as the area within the TMF containing tailings
- TMF dam and internal berms

Each modelled zone includes inflows and outflows; specific inflows and outflows can interact with both zones. For example, outflows from one zone may be inflows to the other. A schematic of the water fluxes within the TMF is shown in Figure 3. A list and a description of the water fluxes are provided below.

This model informed estimates of drainage from the TMF that would be available for re-use, accounting for climate change impacts. Runoff is very sensitive to variation in rainfall and evaporation and because runoff is the difference between precipitation and evaporation over the long term, the relative rate of change of each of these processes is critical in assessing whether water availability, and therefore water resources, will increase or decrease under various climate change scenarios.

Example 4

Location: Peruvian Andes
Mine name: (confidential)
Facility: tailings storage facility (TSF) and
Associated infrastructure: Mill, reticulation systems, seepage collection ponds

The tailings facility at this mine is a receptor for many flows from various parts of the mine. The mine was concerned the TSF was gaining water and wanted to investigate various mitigation options. Incidentally, a mill upgrade was also planned for around the same time as the base mitigation actions would be commissioned. Water balance modelling showed that the single most important water sink was the loss to pore space – a consideration that was not adequately accounted for in planning. As a result, a substantial reduction in water level was achieved in subsequent years – to the point that some mitigation measures were rolled back (Figure 4).

Original predictions for the throughput scale up were undertaken in 2013–2014, and the client had reservations about the

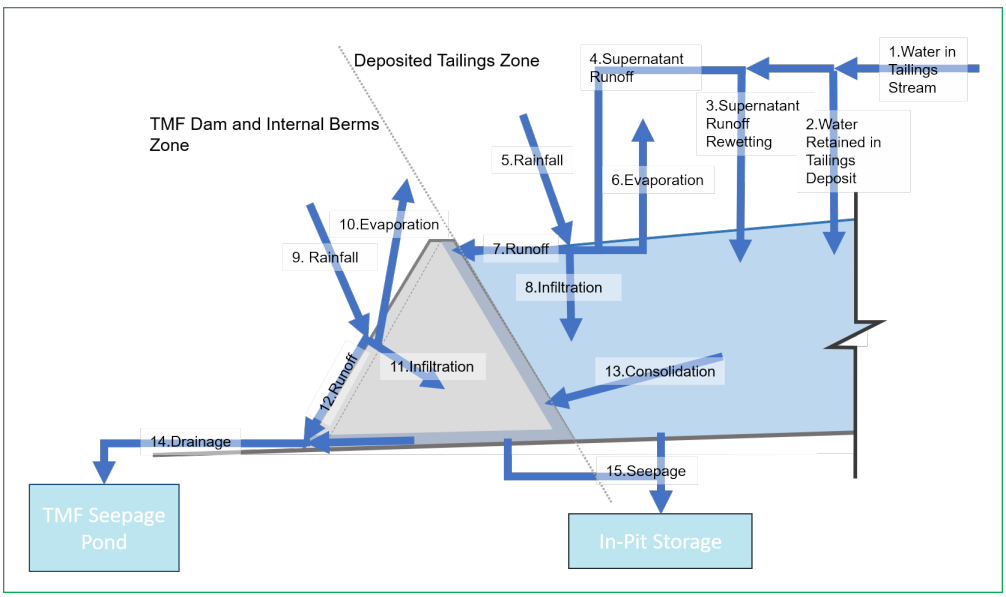

***Figure 3 Conceptual** TMF Flow Diagram.*

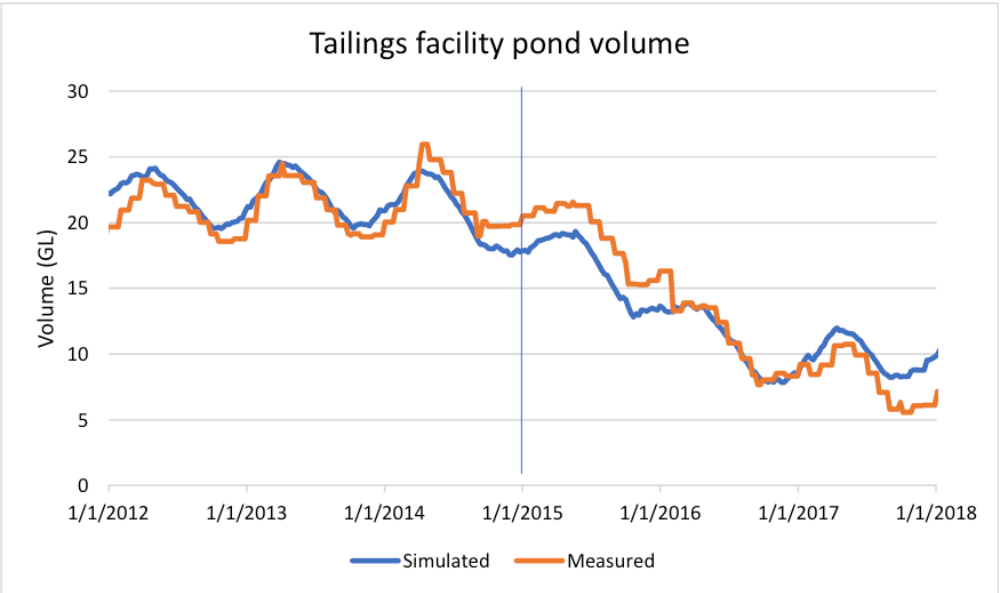

Figure 4 Water volume response for throughput scale up (blue vertical line indicates commissioning date of increased throughput).

predicted response. Other water balances were also employed which did not show this response.

The client invested further into this model, which was outfitted with water quality modelling and geochemical components to aid planning for reactive waste storage, water planning and seasonal discharge planning. Through systemic employment, the client was able to refine planning for reactive waste which reduced water quality influences upstream of compliance points and helped provide economic and environmental valuations for specific projects.

Conclusions

Water balance models are a useful and sometimes required investment. Calibrated models may yield benefits such as avoidance of overflows, effective management of seasonal flows or extreme events, effective management of climate change related factors, reduction of infrastructure expansion (and deferment of capital expenditures) or maintaining compliance with greater certainty.

Examples shown in this publication do not contain significant detail, but endeavour to show how various levels of detail may be used to obtain a relevant result. Various adaptations to water balances such as mass balances and even water quality equilibration systems may further increase utility and return on investment but may require specialist skillsets to build and employ.

Acknowledgements

The authors thank all co-organisers for compiling and reviewing submissions for the IMWA proceedings.

References

DEHP 2012, Queensland Government, Department of Environment and Heritage Protection, July 2012, 'Preparation of Water Management Plans for Mining Activities'.

DNRM 2019, Queensland Government, Department of Natural Resources, Mines and Energy, November 2019, 'Quantifying the volume of associated water taken under a mining lease or mineral development license'.

Moon N, Parker M, Boshoff HJJ, Clohan D. Advances in non-Newtonian dam break studies, in AJC Paterson, AB Fourie & D Reid (eds), Proceedings of the 22nd International Conference on Paste, Thickened and Filtered Tailings, 2018, Australian Centre for Geomechanics, Perth, pp. 165-172.

O'Hara, Conor, Jaco Grobler, Greg Hookey and Jan Vermaak. The Impact of Climate Change on a Mine Water Source, 2012, International Mine Water Association Symposium, Bunbury, Australia.

Strand R, Usher B. Integrated Site Water Balances and Water Quality Models for Decision Making over Life-of-Mine, 2014, AusIMM Life-of-Mine, Brisbane, Australia.

Strand R, Tuff J, Usher B, Strachotta C, Jackson J. Integrated water balance and water quality modelling for mine closure planning at Antamina, 2010, Mine Closure, Vina del Mar, Chile.

Strand R, Tuff J, Usher B. Non-iterative modelling of mine site hydrogeochemistry, 2017, AMD Workshop, Burnie Australia.

Tuff J, Harrison B, Yi Choy S, Strand R, Usher B. Assessing the Robustness of Antamina's Site Wide Water Balance/Water Quality Model over 5 Years of Implementation, 2015, IMWA 10th ICARD, Santiago, Chile.

Usher B, Strand R, Strachotta C, Jackson J. Linking fundamental geochemistry and empirical observations for water quality predictions using GoldSim, 2010 IMWA, Cape Breton, Canada

Simulation of Column Leach Tests using Reactive Transport Modelling

Yuan Tian[1], Johan Fourie[2], Brent Usher[2]

[1]*Golder Associates Pty Ltd, Level 3, 1 Havelock Street, West Perth, WA 6005, Australia, ytian@golder.com.au, iamseanty@gmail.com*

[2]*Klohn Crippen Berger Pty Ltd, Level 1, 154 Melbourne Street, South Brisbane QLD 4101, Australia*

Abstract

Reactive transport modelling, which accounts for geochemical reactions and transport of reaction products, has become an increasingly powerful tool to assist the mining industry for assessing the long-term geochemical behaviour of mine waste materials during operation and post-closure periods.

The reactive transport models were developed in this study to model the key geochemical processes that control sulfide oxidation and subsequent chemical reactions (e.g. dissolution/precipitation) for lab scale column leach tests. The models were refined to allow calibration of kinetic rates of several of the waste rock minerals based on leachate data. The reactive transport models form the basis of the predictive model of drainage water quality for full-scale mine waste facilities.

Keywords: reactive transport modelling, mine waste, column leach test, kinetic rates

Introduction

With the development of modelling codes in the past decades, reactive transport modelling has become increasingly powerful tool to assist the mining industry for assessing the long-term geochemical behaviour of mine waste materials over the course of LOM and mine closure.

By utilising a subset of the column leach tests currently underway to understand the geochemical evolution of the sulfidic waste rock at the mine, several reactive transport models were developed to represent the AMD and/or NMD processes for potentially acid generating and non-acid generating waste. With regular monitoring and chemical analysis of the leachate in column leach tests and field surface water and groundwater samples, these valuable datasets have provided a realistic 'selection-criteria' to assess the effectiveness and reliability of the reactive transport model by comparison to modelled results.

The reactive transport models were developed to model the key geochemical processes that control sulfide oxidation and subsequent chemical reactions (e.g. dissolution, precipitation and sorption) under the laboratory testing conditions. The reactive transport models form the basis of the predictive model of drainage water quality for larger scale field barrel and full-scale mine waste facilities.

Methods

The reactive transport model for lab-scale kinetic column test is schematically visualised in Figure 1 as a 1-D vertical drain system. The modelling domain had the same size as the actual sample material in the column, with its length calculated from sample weight, bulk density and the column internal diameter. The modelling domain was discretized to ten nodal blocks in the direction of drainage flow. The lixiviant (deionised water) recharge rate to the modelling domain was calculated from the average weekly leachate volume and was assumed to be constant in the model. Given the small scale of the column, both the lixiviant and the modelling domain were assumed to be in equilibrium with atmosphere, so temperature and the fugacity of CO_2 and O_2 were fixed throughout the simulation for all columns.

For the assigned column material, the mineralogical composition of column materials

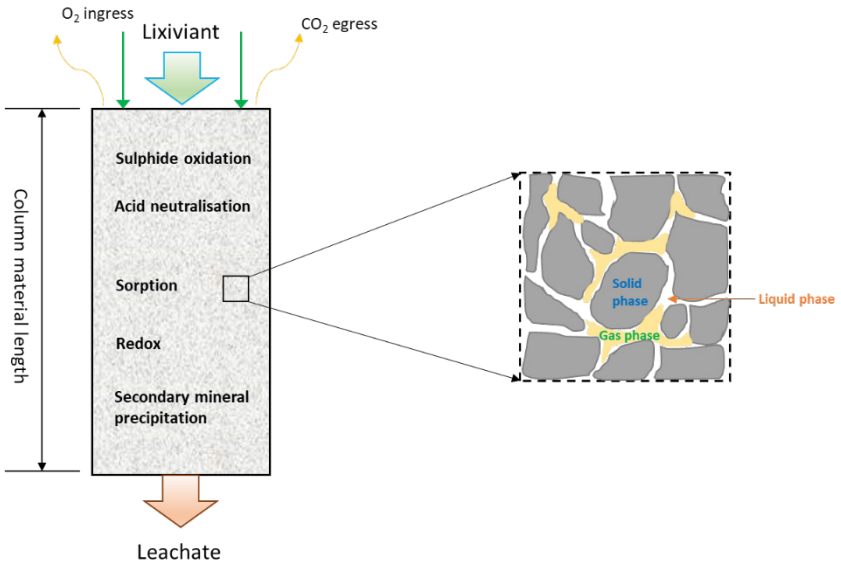

Figure 1 *Schematics of kinetic column leach test.*

was derived from quantitative XRD mineralogical tests. The physical properties of porous medium, including diffusion coefficient, bulk density, porosity, thermal conductivity, and heat capacity, were either derived from field measurements or the default setting of the GWB X2t program where data was unavailable. Due to the small scale of model, both longitudinal and transverse dispersivity were assumed to be zero. The permeability of the porous medium was calculated by GWB program from the porosity based on an empirical correlation (Bethke et al. 2019).

Two kinetic columns were selected for the reactive transport modelling as selected column samples were representative for all ABA and NAG parameters and classified as NAF (HC) and PAF (R), representing the most common types of waste materials.

The extended Lawrence Livermore National Laboratory database in GWB format was used for the reactive transport modelling. A two-layer model type sorption surface based on the dataset of Dzombak and Morel (1990) was used to account for sorption mechanism that is mainly induced by surface functional groups of iron-hydroxide, iron-oxide and iron-oxyhydroxide minerals to form a variety of surface complexes when in contact with aqueous species in water.

In the model, the dissolution rates of primary minerals were controlled by the kinetic rate law as defined by the following equation:

$$r = A_s * k * (1 - \frac{Q}{K})$$

Where r is the reaction rate in mol/s, A_S is the bulk reactive surface area in cm^2/mol; k is the rate constant in mol/cm^2/s, and Q and K are activity product and equilibrium constant for the dissolution reaction. The reduction of mineral reactive surface area was taken into account according to the shrinking core model when the chemical reaction is in progress. To account for the effect of temperature on kinetic rate, an activation energy and pre-exponential factor for the Arrhenius equation was implemented for the rate constant:

$$k = A * e^{-E_a/RT} * \prod_i a_{(i)}{}^{P(i)}$$

Where A is the pre-exponential factor, E_a is the activation energy in KJ/mol; R is gas constant; T is the absolute temperature in kelvin; $a(i)$ is the activity of promoting or prohibiting species i; $P(i)$ is the power of dependence respect to species i used in rate law. The parameters used in the kinetic rate law for various minerals are presented in Table 1.

Table 1 Kinetic rate parameters for sulfides, sulfates and silicates in this study.

Mineral	Formula	Pre-exp	Ea	P(H^+)	P(O_2)	P(Fe^{3+})	Reference
		mol/cm²/sec	KJ/mol				
Pyrite	FeS_2	6.004E-03	56.9	-0.11	0.5		Williamson & Rimstidt, 1994
Arsenopyrite	FeAsS	6.777E-09	18.5	-0.12	0.76		Asta et al, 2010
Sphalerite	ZnS	1.467E-03	41.75	0.2659		0.154	Pan et al, 2013
Galena	PbS	3.162E-13	15	-0.78	0.3		Acero et al, 2007
Gypsum	$CaSO_4.2H_2O$	1.622E-07	0				Palandri & Kharaka, 2004
Kaolinite	$Al_2Si_2O_5(OH)_4$	5.120E-14	22.2				Same as above
K-feldspar	$KAlSi_3O_8$	1.767E-10	38				Same as above
Albite	$NaAlSi_3O_8$	4.661E-05	69.8				Same as above
Quartz	SiO_2	3.350E-02	90.9				Same as above
Muscovite	$KAl_3Si_3O_{10}(OH)_2$	2.015E-14	22				Same as above
Chlorite	$Fe_2Al_2SiO_5(OH)_4$	7.887E-02	88				Same as above

* ***Parameters*** *for epsomite are estimated only as epsomite is readily soluble and there is no available data from literatures.*

Compared to the minerals listed in Table 2, the dissolution of dolomite and calcite is more complicated as their rate constants are subject to three promoting species: H^+, $H_2CO_{3(aq)}$ and H_2O with each species assigned with its own pre-exponential factor, activation energy and power of dependence. The rate constant k of calcite and dolomite is expressed as the equation below:

These three promoting species represent three pathways controlled by acidic, carbonate and neutral mechanisms, which was proposed and defined by Plummer (1978) for calcite dissolution and Busenberg and Plummer (1982) for dolomite dissolution. The kinetic parameters used in this study (Table 2) were fitted by Declercq and Oelkers (2014) based on a summary of several independent studies

$$k = A_{(H^+)} * e^{-\frac{E_{a(H^+)}}{RT}} * a_{(H^+)}{}^{P_{(H^+)}} + A_{(H_2CO_3)} * e^{-\frac{E_{a(H_2CO_3)}}{RT}} * a_{(H_2CO_3)}{}^{P_{(H_2CO_3)}} + A_{(H_2O)} * e^{-E_{a(H_2O)}/RT} * a_{(H_2O)}{}^{P_{(H_2O)}}$$

Table 2 Kinetic rate parameters for calcite and dolomite.

Parameter	Unit	Calcite	Dolomite
Pre-exp (H^+)	mol/cm²/sec	2.13E-02	1.49E-02
Ea (H^+)	KJ/mol	16	29
P (H^+)	unitless	0.33	0.75
Pre-exp (H_2CO_3)	mol/cm²/sec	3.47E-03	1.00E-02
Ea (H_2CO_3)	KJ/mol	46	34.8
P (H_2CO_3)	unitless	0.33	0.75
Pre-exp (H_2O)	mol/cm²/sec	1.17E-02	2.20E-07
Ea (H_2O)	KJ/mol	46	52.2
P (H_2O)	unitless	0.33	0.75

related to calcite and dolomite dissolution under a range of pH, temperature, and chemical conditions.

Model Results

The modelled leachate water quality is compared with experimental results in the following figures. The experimental pH varied in the circum-neutral pH range, and modelled pH values were in broad agreement with experimental results in Figure 2, although some discrepancies can be observed in several leaching events. Figure 3 presents modelled and experimental sulfate concentrations for the NAF (HC) and PAF (R) column leachates. Concentrations of sulfate showed a rapid decline within the first 1-2 weeks, followed by a gradual decrease, and progressively stabilized from around the 100th day. The modelled sulfate concentrations typically captured the early peaks and demonstrated similar decreasing trendline and consistent concentrations that were stabilised in the recent 300 days.

Comparison of modelled and experimental data was made for calcium and magnesium in Figure 4 and Figure 5, respectively. Similar to sulfate, the trend and intensity of calcium and magnesium concentrations were largely reproduced by the model. The rapid decline of sulfate, calcium, and magnesium in the early leach events indicated the dissolution and depletion of secondary sulfate-rich minerals (e.g. gypsum and epsomite). These secondary minerals were present in the samples prior to the kinetic test and are generally readily soluble in response to flush or leach events.

To demonstrate the importance of sorption mechanism, the models simulated the leachate chemistry with and without the two-layer sorption surface. For example, modelled concentrations of arsenic and lead (Figure 6 and Figure 7) without the implementation of sorption surface were typically 2-3 orders of magnitude higher than those with the application sorption surface. And the latter overall showed good agreement with experimental results.

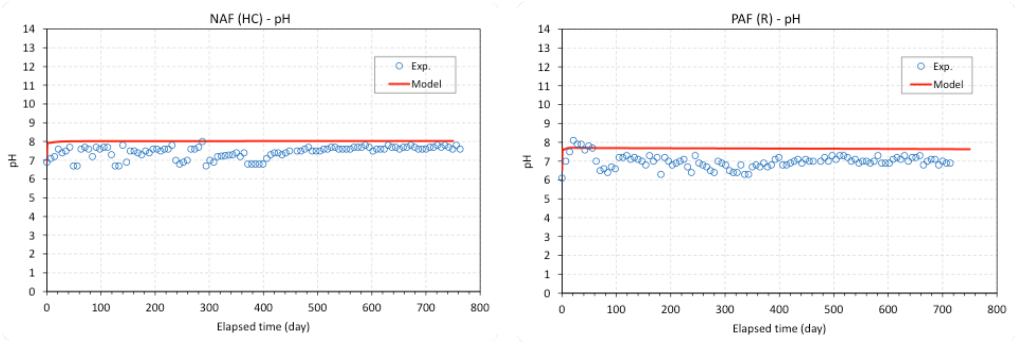

Figure 2 Modelled and experimental pH in column leachates.

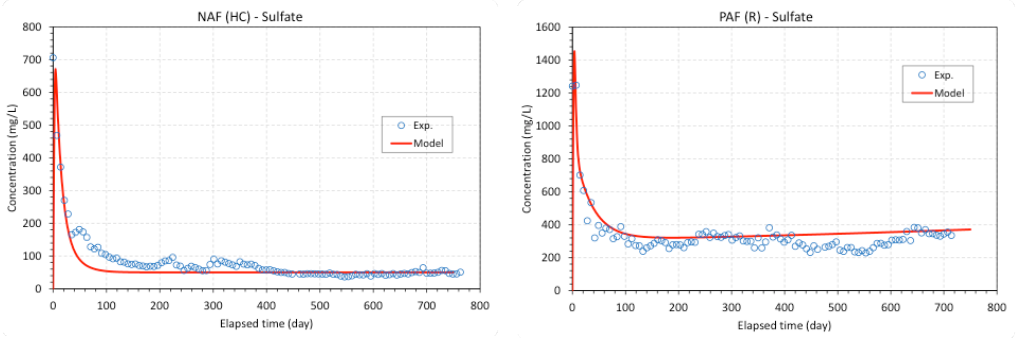

Figure 3 Modelled and experimental Sulfate concentrations in column leachates.

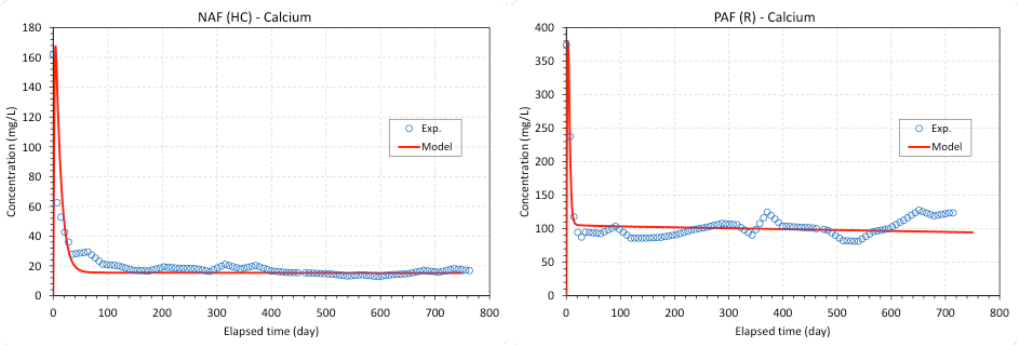

Figure 4 Modelled and experimental Calcium concentrations in column leachates.

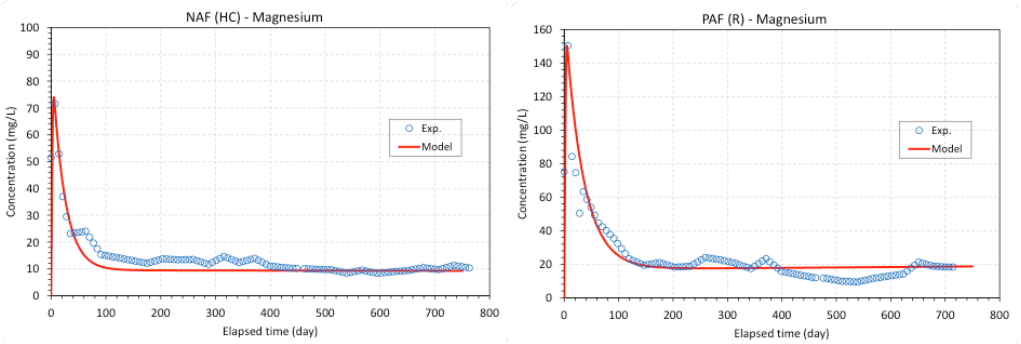

Figure 5 Modelled and experimental Magnesium concentrations in column leachates.

In contrast, the application of sorption mechanism makes negligible influence on the water quality of major cations/anions although related surface complexes were included in the sorption surface dataset of Dzombak and Morel (1990). This is a strong indication of the competition for surface complexation when metallic ions are being adsorbed to the ferrihydrite surfaces. It also demonstrates that sorption mechanism may play a critical role in the leachate water quality and the process may be 'element-selective', depending on the stability of surface complexes.

Conclusion

The reactive transport models developed in this study provided an example to predict drainage water quality for laboratory scale column leach tests. With the calibration to experimental data, the kinetic rates of the key mineral phases in the column samples were refined and the reactive transport model can be validated.

The reactive transport model can be up scaled by integrating site specific conditions (e.g. hydrogeological/meteorological condition) and the physical/chemical property of mine wastes. The model can be benefited from inputs derived from external simulation or measurements such as fluid flow, pore gas composition, mass and heat transport for a full-scale study.

Overall, reactive transport model has the potential to model the key geochemical processes that control sulfide oxidation and subsequent geochemical reactions to predict long-term evolution of mine waste materials and the seepage water quality from a variety of mine waste storage facilities under the mining influenced environment.

References

Acero, P., Cama, J., Ayora, C. (2007). Rate law for galena dissolution in acidic environment. Chemical Geology 245, 219–229

Asta, M.P., Cama, J., Ayora, C., Acero, P., De Giudici, G. (2010). Arsenopyrite dissolution

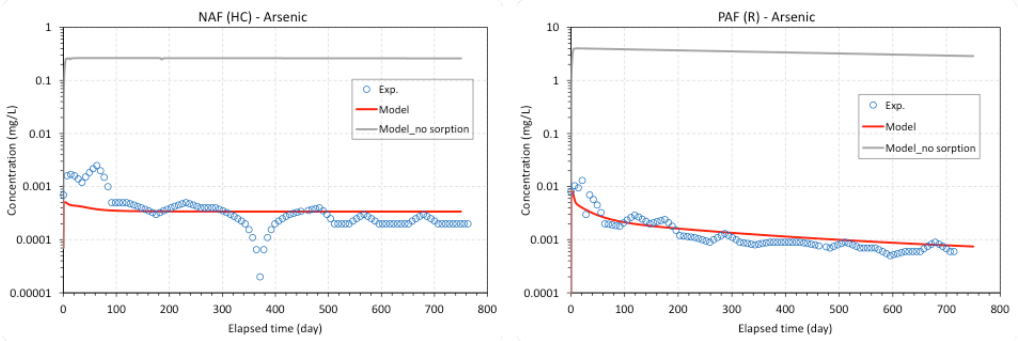

Figure 6 *Modelled and experimental Arsenic concentrations in column leachates.*

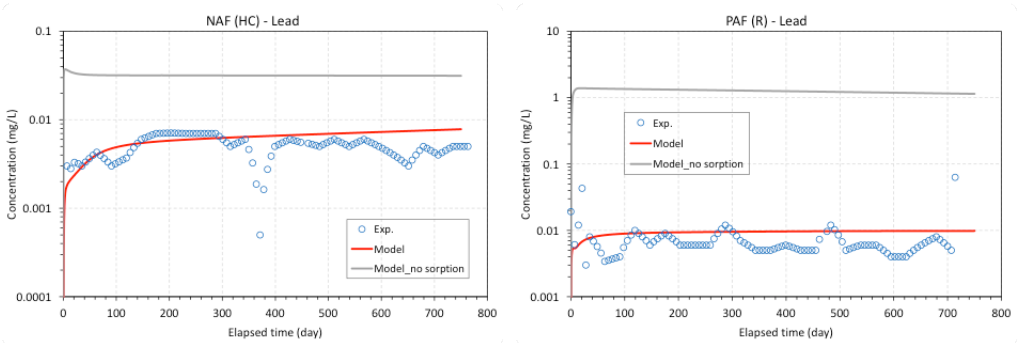

Figure 7 *Modelled and experimental Lead concentrations in column leachates.*

rates in O2-bearing solutions. Chemical Geology 273, 272–285.

Bethke, C.M., Farrell, B., Sharifi, M., and Yeakel. S. (2019). GWB Reactive Transport Modeling Guide, Release 12.

Busenberg, E., Plummer, L.N. (1982). The kinetics of dissolution of dolomite in CO2–H2O systems at 1.5 to 65 °C and 0 to 1 atm pCO2. Am. J. Sci. 282, 45–78.

Chirita, P. & Rimstidt, J.D. (2014). Pyrrhotite dissolution in acidic media. Appl. Geochem. 41, 1–10.

Declercq, J. & Oelkers, E.H. (2014). CarbFix Report 4 PHREEQC mineral dissolution kinetics database. CarbFix Project no. 281348. Geoscience Environement Toulouse, Belin, Toulouse. https://www.or.is/sites/or.is/files/kinetic_database.pdf

Dzombak, D. A. & Morel, F. M. M. (1990). Surface complexation modelling – Hydrous ferric oxide. New York:John Wiley. 393 p.

Palandri, J.L., & Kharaka, Y.K. (2004). A compilation of rate parameters of water-mineral interaction kinetics for application to geochemical modeling: USGS Open File Report 2004-1068, Menlo Park, California, National Energy Technology Laboratory – United States Department of Energy.

Pan Z.P. et al. (2012). A simulation experimental study on oxidative kinetics of sphalerite under hypergene condition. Chinese Journal of Geochemistry, 31(4), pp. 457-464.

Williamson, M. A. & Rimstidt, J. D. (1994). The kinetics and electrochemical rate-determining step of aqueous pyrite oxidation. Geochimica et Cosmochimica Acta 58, 5443–5454.

Abbreviation

AMD – Acid and Metalliferous Drainage
NMD – Neutral Mine Drainage
XRD – X-Ray Diffraction
GWB – Geochemist's workbench
ABA – Acid Base Accounting
NAG – Net Acid Generation
PAF (R) – Potentially Acid Forming (reactive)
NAF (HC) – Non-Acid Forming
(high capacity)

A Model of the Behaviour of Cyanide in a Witwatersrand Sulfidic Au-tailings Environment

Megan Welman-Purchase

Department of Geology, University of the Free State, Bloemfontein, 9301, South Africa, purchasemd@ufs.ac.za

Abstract

Cyanide is one of the main chemicals used in the extraction of Au in mining. It is vital that the cyanide behaviour in tailings dam environments is understood as the speciation controls the release of and persistence in the natural environment. This study has direct consequences for the evaluation of environmental risk when planning new Au-mining operations. In addition, this investigation delves into a possible scenario for the behaviour of cyanide, namely Prussian/Turnbull's blue, which are believed to be stable compounds, which is also reiterated in the modelling produced in this study and may be a solution to environmental contamination.

Keywords: Cyanide speciation, Acid mine drainage, Geochemical modelling

Introduction

Cyanide in the environment can be of either natural or anthropogenic sources (Anning et al. 2019). Natural sources include plants in the form of cyanogenic glycoside (for example almonds) and large quantities from anthropogenic sources include mining, electroplating, vehicle exhaust fumes, sewage, fires (Jaszczak et al. 2017). In the mining environment, cyanide (as NaCN/KCN) is the main compound used in the extraction of Au, which, according to Johnson (2015), is preferred in >90% of mines worldwide. The reaction that occurs in the cyanidation process is known as the Elsner process (Kyle 1997):

$$4Au+8NaCN+O_2+H_2O \rightarrow 4[NaAu(CN)]_2+NaOH \quad (1)$$

$$4Au+8KCN+O_2+H_2O \rightarrow 4[KAu(CN)]_2+KOH \quad (2)$$

The Au compounds produced in equation (1) and (2) are then further processed in the Carbon In Leach (CIL) and Merrill Crowe methods (Acheampong et al. 2010). Even though cyanide is used in low concentrations, as little as 0.5 $g.L^{-1}$ (Rademan and Groot 2012) and the "Best Practice" restriction of cyanide in tailings dams is 0.5 $mg.L^{-1}$ (Bakatula and Tutu 2016), there is a potential for cyanide to leach into the natural environment. Anning et al. (2019) reiterates this by stating that a large percentage of cyanide used in the Au extraction process remains in solution in slurries after the completion of this cyanidation process.

Cyanide can be lethal, especially to aquatic life, yet this is all dependent on the chemical species in which the cyanide occurs. These different species are divided into the following categories: free cyanide (HCN), soluble cyanide (KCN, NaCN), CN_{WAD} (weak acid dissociable cyanide – containing Ni, Zn, Cd, and Cu) and CN_{SAD} (strong acid dissociable cyanide – containing Fe, Co, Ag, and Au) (Zagury et al. 2004). Free cyanide is the most lethal and occurs as a volatile substance, where CN_{WAD} and CN_{SAD} may possibly form free cyanide as they dissociate, where CN_{WAD} dissociates at pH of neutral to slightly acid conditions and CN_{SAD} only dissociates in low pH environments (Zagury et al. 2004).

When cyanide reacts with Fe, stable octahedral aqueous complexes (hexacyanoferrates) form and this includes ferrocyanide $[Fe^{2+}(CN)_6]^{4-}$ and ferri-cyanide $[Fe^{3+}(CN)_6]^{3-}$ (Jambor et al. 2009). When these two compounds further react with Fe^{2+} and Fe^{3+} cations the following compounds may form: Prussian blue $Fe_4[Fe(CN)_6]_3$, Turnbull's blue $Fe_3[Fe(CN)_6]_2$, Prussian brown/green $Fe_2(CN)_6$ and Berlin white $Fe_3(CN)_6$ (Ghosh et

al. 1999). Berlin white is only stable in anoxic environments and converts to Prussian blue in oxic environments (Ghosh et al. 1999). Fe-CN compounds are CN_{SAD} compounds and are considered to be among the most stable (Kyle 1997).

This investigation uses PHREEQC, a geochemical modelling software package developed by the USGS, modelling to investigate the possible chemical behaviour and compound formation of cyanide in a gold mine tailings environment, with special reference to Fe-CN compounds, specifically Prussian and Turnbull's blue.

Geological setting

The Witwatersrand was discovered in 1886 in South Africa by George Harrison, who discovered the Au in quartz-pebble conglomerates that outcropped for 45 km (McCarthy 2006). Between 1886 and the 1940s, using drilling and geophysical methods, the Central Rand, East Rand, West Rand, Carletonville and Welkom/Free State goldfields were discovered and developed (McCarthy 2006). These can be viewed in figure 1. This study investigates the tailings of the Free State gold mines where, according to Tucker et al. (2016), the Dreyerskuil, EA, Beatrix, VS5, Basal, Steyn, and Beisa reefs of the Central Rand group are mostly mined. The Beisa reef consists a conglomerate layer that varies from 5 to 150 cm in thickness, the Basal and Steyn are two separate conglomerate layers differing in clast assemblage, the Beatrix is a conglomerate on a disconformity and the VS5 is a conglomerate layer that is sporadically mineralized (McCarthy 2006).

There are currently 5 Au producing mines (Department of Mineral Resources, 2017) of the total of ≈ 17 gold mines (McCarthy 2006) in the Free State goldfields. According to McCarthy (2006) the mines of the Free State goldfields have produced over 7900 t of gold. For arguments sake, if the gold grade of the rocks that were mined for this mentioned gold was 5 $g.t^{-1}$, then 1580 Mt of waste is produces and discarded of on tailing dams.

Methodology

The modelling in the project used PHREEQC which is a United States Geological Survey project developed by Parkhurst and Appelo (2013). The thermodynamic data of Prussian

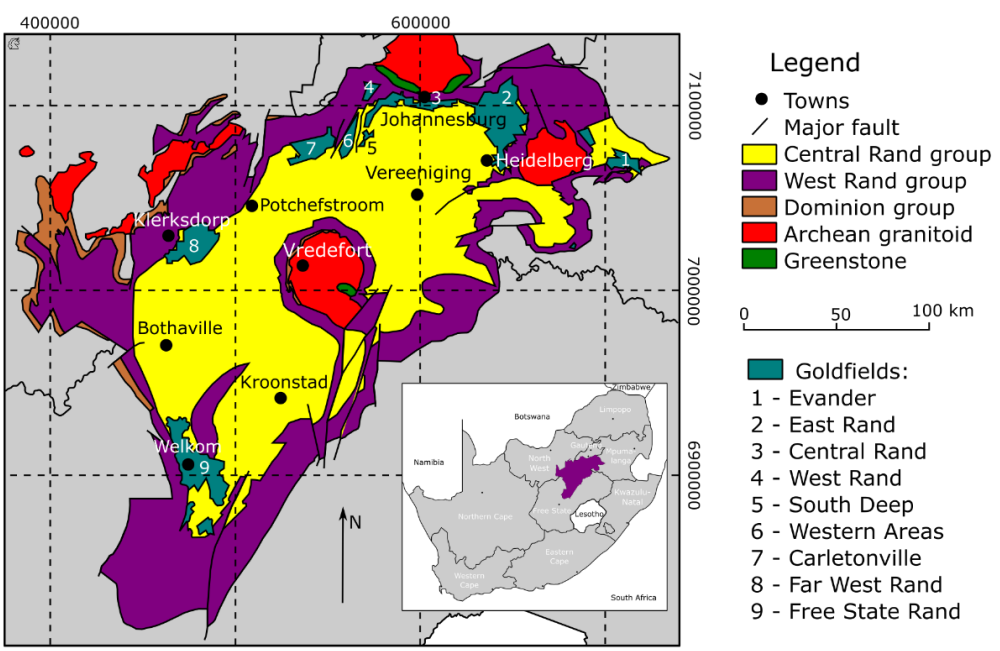

Figure 1 Map of the Witwatersrand basin displaying the position of the current goldfields in South Africa (Modified after Hansen, 2018 and Frimmel et al., 2005).

Table 1 *QEMSCAN data of a tailings dam in the Free State goldfields (FS01) and a near monomineralic pyrite commercial sample.*

Mineral	FS01	Pyrite
	wt%	*wt%*
Quartz	78,61	7,23
Pyrophyllite	7,24	
Mica	6,97	30,19
Chlorite	1,21	
Plagioclase	0,84	
Chloritoid	1,07	
Amphibole	0,21	
Pyroxene/ Olivine	0,43	
Zircon	0,10	
Other silicates	0,19	3,61
Pyrite	2,18	58,97
Other sulfides	0,03	
Fe-oxides	0,26	
Rutile/ Ilmenite	0,19	
Other oxides	0,01	
Dolomite	0,02	
Calcite	0,25	
Ankerite	0,00	
Apatite	0,02	
Alunite	0,05	
Gypsum	0,12	
Total	**100,0**	**100,00**

blue, Prussian brown/green and Turnbull's blue was added to the database of PHREEQC and the values were taken from Wagman et al. (1982). Berlin white was not investigated as it is out of the scope of this study.

The mineralogy used for the speciation model, is Quantitative Evaluation of Minerals by Scanning Electron Microscope (QEMSCAN) data of a tailing sample from one of the dumps of the Free State goldfields, see table 1. The second speciation model was completed using the mineralogy (semi-quantitative results) obtained using X-Ray Diffractometry (XRD) of a natural pyrite sample. The XRD is a Panalytical–Empyrean with a copper side window tube and an X Celerator detector. The geometry of the XRD is Bragg-Brentano and samples are scanned between 3.5° and 70° 2θ at tube settings of 45 kV and 40 mA. The concentration of cyanide added to the speciation models is 0.5 g.L1 after Rademan and Groot (2012). The parameters used for the pH vs pe modelling are as such: cyanide concentration of 0.6 mM was and the Fe content of 0.2327 mM, not in excess, was taken from Ghosh et al. (1999). K (0.4 mM) and NaCl (0.06 mM) are added according to Ghosh et al. (1999) as charge balances.

Results

Prussian/Turnbull's blue did not initially precipitate in the speciation models for both the tailings sample and a pyrite sample at surface conditions. Although a blue substance formed in empirical results (which will be report on in further studies). This led to the investigation into the log K values of Prussian and Turnbull's blue. On altering the log K values, the species formed can be seen in table 2 below, which includes Prussian and Turnbull's blue.

The same log K values were then used to create a pH vs pe diagram, displayed in figure 2 (A). This then led to the investigation of the oxygen fugacity and the effects that O^2 has on the production of ferric and ferrous iron and this effect on the compounds formed. The model can be seen in figure 2 (B).

Discussion

The Fe cation of the hexacyanoferrates determines if the Fe-CN compound is Prussian or Turnbull's blue followed by the Fe cation within this crystallographic structure. Thus, the formation of either of the compounds is dependent on the availability of Fe^{2+} or Fe^{3+} cations in solutions. The FS01 sample mostly consists of silicate minerals and forms Prussian blue and not Turnbull's blue. Contrarily the pyrite sample produces both Fe-CN compounds in the model. A possibility for this is the presence of goethite, hematite and jarosite potentially forming in the model of FS01, which establishes an Fe^{3+} deficient environment. These minerals do not appear in the model of the pyrite sample.

The pH vs pe diagram is similar to the diagram found in Ghosh et al. (1999)

Table 2 *The results of the species models of the tailings dam sample – FS01 and the pyrite sample.*

Minerals	Minerals Chemistry	FS01	Pyrite
Alunite	$KAl_3(OH)_6(SO_4)_2$		x
Anatase	TiO_2	x	
Boehmite	AlO(OH)		x
$CaZrO_3$	$CaZrO_3$	x	
CO_2 (g)	CO_2 (g)	x	
Diaspore	AlO(OH)		x
Goethite	$Fe^{3+}O(OH)$	x	
Hematite	Fe_2O_3	x	
Jarosite	$KFe_3(SO_4)_2(OH)_6$	x	
Jarosite – Na	$NaFe_3(SO_4)_2(OH)_6$	x	
Kaolinite	$Al_2Si_2O_5(OH)_4$		x
Melanterite	$FeSO_4.7H_2O$		x
Nontronite - Ca	$Ca_{0.165}Fe_2Al_{0.33}Si_{3.67}O_{10}(OH)_2.nH_2O$	x	
Nontronite – H	$H_{0.33}Fe_2Al_{0.33}Si_{3.67}O_{10}(OH)_2.nH_2O$	x	
Nontronite – K	$K_{0.33}Fe_2Al_{0.33}Si_{3.67}O_{10}(OH)_2.nH_2O$	x	
Nontronite - Mg	$Mg_{0.165}Fe_2Al_{0.33}Si_{3.67}O_{10}(OH)_2.nH_2O$	x	
Nontronite - Na	$Na_{0.33}Fe_2Al_{0.33}Si_{3.67}O_{10}(OH)_2.nH_2O$	x	
Prussian blue	$Fe_4[Fe(CN)_6]_3$	x	x
Rutile	TiO_2	x	
Turnbull's blue	$Fe_3[Fe(CN)_6]_2$		x

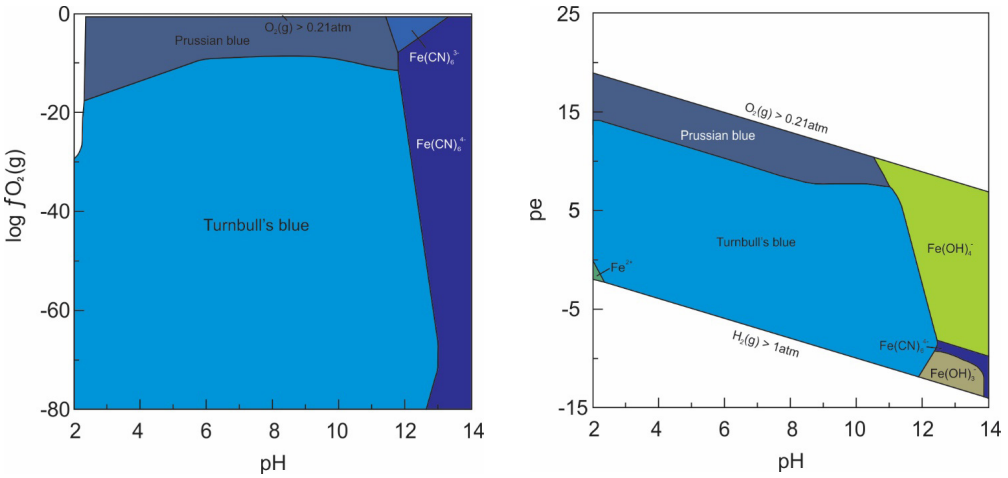

Figure 2 *(A) pH vs pe diagram using the following parameters: cyanide concentration – 0.6 mM, Fe content – 0.2327 mM, K – 0.4 mM and NaCl – 0.06 mM. (B) A pH vs oxygen fugacity diagram of Prussian and Turnbull's blue.*

which was completed using MINEQL+. The diagram in Ghosh et al. (1999) differs in the compounds outside of Prussian and Turnbull's blue compared to figure 2 (A). According to figure 2 (A), Prussian blue is stable between pH ≈ 2 – 11 and pe ≈ 7 – 19. Turnbull's blue is stable (fig. 2A) at pH ≈ 2 – 12.5 and pe ≈ -12 – 15. This is reiterated by Zagury et al. (2004), who suggests that the CNSAD compounds dissociate at low pH levels. In Au mine practices, acid mine drainage is a universal issue and thus should be accounted for and rehabilitated increasing the pH of the tailings dams and thus preserving the stability of the Prussian and/or Turnbull's blue that may form.

During the oxygen fugacity investigation, it was determined that Prussian blue is produced in more oxidizing environments and Turnbull's blue is produced in more reducing conditions. This may be due to the formation of goethite in oxidizing environments.

Conclusions

Cyanide still remains the chemical used to extract Au, even though other options are available. Possibly due to cost effectiveness and the small quantities required for Au extraction. Which reiterates a requirement for studies into the geochemistry and behaviour of cyanide species in the tailings dam environment. This study shows that it is possible for Prussian blue to form and, with an increase in pyrite, Turnbull's blue will form additionally. The stability of these two compounds is a pH from ≈ 2 – 12.5, where dissolution occurs below this and iron-hydroxides form above this area. They also form in both oxidizing and reducing conditions. According to these models, these compounds seems to be great candidates to prevent the release of cyanide into the natural environment. Although further studies are needed, including the altering of cyanide concentration in the modelling and the dissociation of Prussian and Turnbull's blue under UV radiation.

Acknowledgements

The author would like to thank Dr. Robert Hansen for his time, efforts and constant support and Ipakade for their financial support.

References

Acheampong MA, Meulepas RJW, Lens PNL (2010) Removal of heavy-metals and cyanide from gold mine wastewater. J. Chem. Technol. Biotechnol. 85:590–613

Anning C, Wang J, Chen P, Batmunkh I, Lyu X (2019) Determination and detoxification of

cyanide in gold mine tailings: A review, Waste Manag. Res. SAGE 37(11):1117-1126.

Bakatula EN, Tutu H (2016) Characterization and speciation modelling of cyanide in effluent from an active slime dam. S. Afr. J. Chem. 69:140-147

Department of Mineral Resources, South Africa (2017) http://www.dmr.gov.za/mineral-policy-promotion/operating-mines/free-state?search=gold – accessed 06 July 2020

Frimmel HE, Groves DI, Kirk J, Ruiz J, Chelsey J, Minter WEL (2005) The Formation and Preservation of the Witwatersrand Goldfields, the World's Largest Gold Province. Econ. Geol. 100th Anniv. Vol. 769–797

Ghosh RS, Dzombak DA, Luthy RG (1999) Equilibrium precipitation and dissolution of iron cyanide solids in water. Environ. Eng. Sci. 16(4):293-313

Hansen RN (2018) Inter-comparison geochemical modelling approaches and implications for environmental risk assessments: A Witwatersrand gold tailings source term characterisation study. Appl. Geochem. Elsevier 95:71-84

Jambor JL, Martin AJ, Gerits (2009) The post-depositional accumulation of metal-rich cyanide phases in submerged tailings deposits. Appl. Geochem. 24:2256-2265

Jaszczak E, Polkowska Z, Narkowicz S, Namieśnik J (2017) Cyanide in the environment – analysis – problems and challenges. Environ. Sci. Pollut. Res. Springer 24:15929-15948

Johnson CA (2015) The fate of cyanide in leach wastes at gold mines: An environmental perspective. Appl. Geochem. Elsevier. 57: 194-205

Kyle JH (1997) Stability of metal-cyanide and hydroxide complexes. World Gold '97 Conference 163-169

McCarthy TS (2006) The Witwatersrand supergroup. In: Johnson MG, Anhaeusser CR and Thomas RJ (Eds.), The Geology of South Africa. Geol. Soc. S. Afr. Johannesburg/Counc. Geosci. PTA. pp 155-186

Parkhurst DL, Appelo CAJ (2013) Description of Input Examples for PHREEQC Version 3 – a Computer Program for Speciation, Batch-reaction, One-dimensional Transport, and Inverse Geochemical Calculations. book 6, chapter A43. US Geological Survey Techniques and Methods 497. available only at. http://pubs.usgs.goc/tm/06/a43/

Rademan L, Groot DR (2012) Cyanidation of reef and surface gold ores. J. S. Afr. Inst. Min. Metall. 112:295-300

Tucker RF, Viljoen RP, Viljoen MJ (2016) A review of the Witwatersrand basin -the world's greatest goldfield. Epis. 39(2):105–133

Wagman DD, Evans WH, Parker VB, Schumm RH, Halow I, Bailey SM, Churney KL, Nuttall RL (1982) The NBS Tables of Chemical Thermodynamic Properties. J. Phys. Chem. Ref. Data, v.11, Suppl. 2

Zagury GJ, Oudjehani K, Deschênes L (2004) Characterization and availability of cyanide in solid mine tailings from gold extraction plants. Sci. Total. Environ. Elsevier 320:211-224

Full-scale Demonstration Tests of Passive Treatment System by JOGMEC in Japan

Kentaro Hayashi[1], Tsubasa Washio[1], Yusei Masaki[1], Takaya Hamai[2], Takeshi Sakata[1], Masatoshi Sakoda[2], Mikio Kobayashi[2], Nobuyuki Masuda[2], Naoki Sato[2]

[1]*Metals Technology Center, Japan Oil, Gas and Metals National Corporation, Furudate 9-3, Kosaka-kouzan, Kosaka, Akita, Japan, hayashi-kentaro@jogmec.go.jp*

[2]*Metals Environment Management Department, Japan Oil, Gas and Metals National Corporation, Toranomon 2-10-1, Minato-ku, Tokyo, Japan*

Abstract

Full-scale demonstration tests (flow rate: 100 L/min) of biological passive treatment system, which is environmentally-friendly and energy saving, was started at an abandoned mine site in Japan. AMD containing iron and zinc was treated in two vertical-flow bioreactors, aerobic reactor and anaerobic reactor utilizing iron oxidizing bacteria and sulfate reducing bacteria (SRB), respectively. In the aerobic reactor, AMD containing 35 mg/L of Fe was treated to below the wastewater standards by using a water transfer method such as a cascade. In the anaerobic process, applicability of a process using ethanol or rice bran as organic resources of SRB was studied.

Keywords: AMD, Passive Treatment, Sulfate Reducing Bacteria, Iron Oxidizing Bacteria

Introduction

In Japan and many other countries, level areas available for mine drainage treatment are limited due to geographic conditions. Therefore, it is necessary to introduce a compact passive treatment system with a short hydraulic retention time (HRT). Japan Oil, Gas and Metals National Corporation (JOGMEC) investigates compact biological passive treatment system with a vertical flow aerobic and anaerobic process. Iron oxidizing bacteria were utilised in the aerobic process for iron oxidation and removal to treat high iron content in the AMD. The anaerobic process was subsequently set utilizing sulfate reducing bacteria (SRB) with agricultural wastes, rice husk and rice bran as the organic resource for SRB. Pilot-scale test of this compact process has been carried out at an abandoned mine site in Japan since 2016. In this test, continuous removal of metal ions over a year was confirmed with hydraulic retention time (HRT) of 25 hours even at the ambient temperatures dropped to around -15°C in winter. As a next step, the full-scale demonstration tests for AMD containing iron, zinc, copper, and cadmium ions were started since November 2019.

Methods

The full-scale demonstration test was carried out at an abandoned mine site in Japan. In these tests, the AMD (Table 1 shows the concentrations of each metal ion) was treated with two-step passive treatment systems (Fig.1).

The first step was the iron oxidation process (reactor size of 36 m^2) in order to oxidize ferrous ions in the AMD to ferric ions utilizing the function of iron oxidizing bacteria and to remove as schwertmannite. This reactor was filled with crushed stone (d = 20 to 40 mm) which is for (1) a carrier of

Table 1 *Mine Water Quality.*

pH [-]	T-Fe [mg/L]	Zn [mg/L]	Cu [mg/L]	Cd [mg/L]	SO_4^{2-} [mg/L]
3.5 ~ 3.8	35 ~ 40	15 ~ 20	1 ~ 10	0.03 ~ 0.08	250 ~ 350

Figure 1 Full-scale demonstration test.

bacteria, (2) reaction field of Fe precipitation and (3) its capturing. The layer thickness of crushed stone was 0.5 m, a sampling pipe was vertically set to collect a water sample at a depth of 0.25 m. AMD was introduced into this reactor at a flow rate of 100 L/min, and the HRT was 1.2 hours.

The second step was anaerobic process. In these reactors, various metal ions were targeted to immobilize as sulfides resulting from the reaction with hydrosulfide ion generated by SRB. Two reactors were placed in parallel, and output water from iron oxidation reactor was introduced to each reactor with a flow rate of 50 L/min (25 hours of HRT). These reactors (W 5 m × D 16 m × H 3.5 m) made of concrete were buried in the semi-underground. At the bottom of reactors, water collection pipes were installed and limestone was filled to protect the pipes from clogging. Two series of rice husk mixture were filled over the limestone layer: The lower layer (1.0 m) consists of 9 ton of rice husk and 36 ton of limestone, and the upper (0.5 m) consists of 3.5 tons of rice husk and 28 ton of limestone.

One of the reactors is for tests using rice bran as an organic matter source for SRB. In this reactor, a layer of rice bran was placed on top of the rice husk layer. The other reactor is for tests adding ethanol as an organic source for SRB, as a semi-passive process.

The AMD before and after treatment were periodically sampled and analyzed. Items for monitoring were temperature, pH, Oxidation-Reduction Potential (ORP), concentrations of metals (iron, copper, zinc, cadmium, etc.) and sulfate ion, and chemical oxygen demand (COD). Total sulfide ion concentration was analyzed with a spectrophotometric method using methylene blue.

Results and Discussion

(1) Iron oxidation reactor

The iron oxidation reactor was tested since April 2019. At the beginning of the test, ferrous ion (Fe^{2+}) concentration decreased to approximately 6 mg/L and total iron (T-Fe) concentration decreased to 15 mg/L, which exceeds the wastewater standards (T-Fe: 10 mg/L) in Japan. In the pilot scale test, T-Fe concentration decreased to below 10 mg/L, when DO at the surface layer increased over 6 mg/L. On the other hand, DO in the full-scale test was around 5 mg/L. Therefore, a small box was put at the inflow point of raw water for water introduction like a cascade, and the test was restarted at July 2019, resulting that DO in the surface layer increased to 6 mg/L. Fig.2 shows comparison of iron concentration before and after changing the water introduction method.

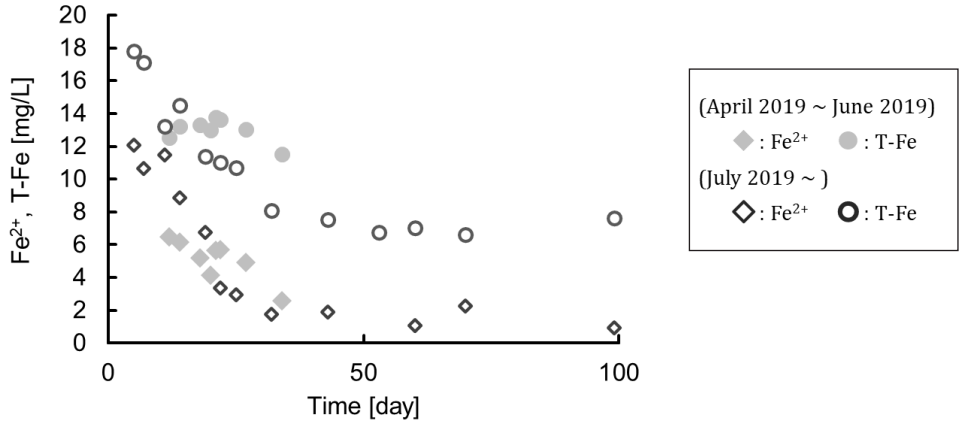

Figure 2 *Changes in iron concentration of treated water.*

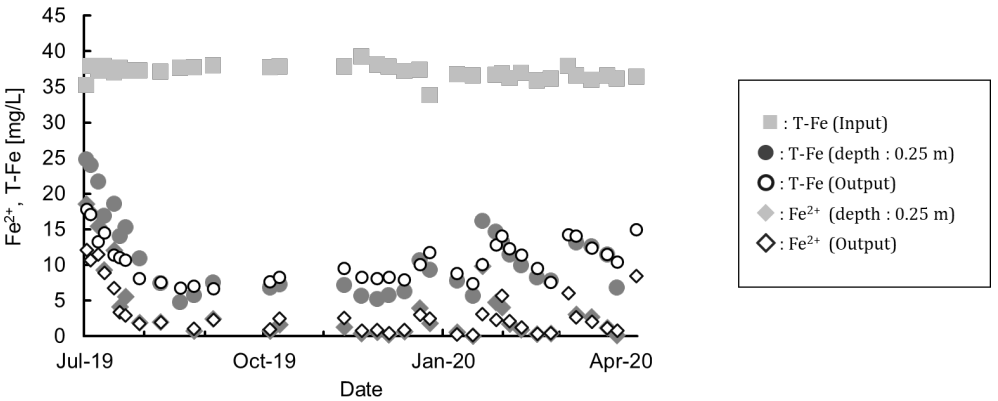

Figure 3 *Annual processing performance of iron oxidation.*

Fe^{2+} concentration of output decreased to 2- 3 mg/L, indicating that relatively high activity of iron oxidizing bacteria. In addition, T-Fe concentration was less than 10 mg/L, and met the wastewater standards.

Fig.3 shows the treatment performance of the iron oxidation reactor after changing inflow method to like cascade. A month after the test restarted, T-Fe concentration decreased to below 10 mg/L, and the treatment performance was maintained till January 2020. After that, the precipitated iron frequently caused clogging in the reactor, and the water level often rose. As a result, the aeration efficiency often decreased, and the treatment performance decreased with T-Fe concentration of 10 to 20 mg/L.

Further, since the iron concentration at the output and the water depth of 0.25 m were almost the same, it is speculated that Fe^{2+} ion oxidation reaction and Fe^{3+} ion precipitation reaction occurred in the upper half area of the reactor.

(2) Anaerobic reactor

Since June 2020, the semi-passive process adding ethanol was started in one of the anaerobic reactors. In many cases, the reactor is shaped like a pond covered with a waterproof sheet, but in this test, it was a rectangular parallelepiped reactor made of concrete, as a result of designing and estimating the construction cost for some shapes. Since the set flow rate and HRT for each series of anaerobic reactor were fixed, the required reactor volume can be calculated. As a result of designing based on the volume of this reactor, as shown in Fig. 4,

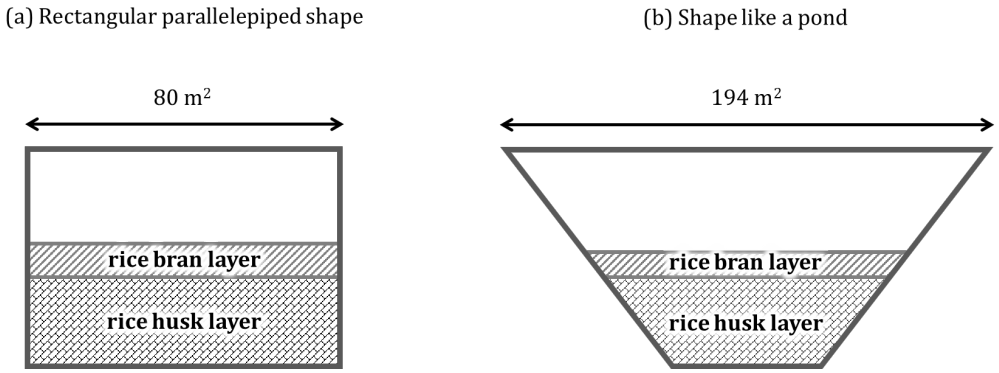

Figure 4 *Anaerobic reactor design results in two shapes.*

when the reactor was made into a rectangular parallelepiped (a), the area required for reactor installation was less than half that in the case where it is shaped like a pond (b). In this design, the reason for the empty space above the rice bran layer was that the drainage level of the previous process (iron oxidation reactor) was lower than the ground surface. Moreover, when the construction cost at this time was estimated, the case of the reactor made of concrete (a) was almost the same as the case of reactor with a waterproof sheet by digging (b). Therefore, a rectangular parallelepiped shape that requires a smaller area was adopted and an anaerobic reactor was placed in this test.

Conclusions

A full-scale passive verification test was started at the closed mine site in Japan since 2019. In this test, the treatment process consists of an aerobic iron oxidation process and an anaerobic process, with a flow rate of 100 L/min.

In the iron oxidation process, surface DO was maintained at around 6 mg/L, owing to the unique water introduction method, resulted in high microbial activity of the iron oxidizing bacteria. T-Fe concentrations was effectively treated (< 10 mg/L), and it was maintained for approximately six months, including the winter season when the microbial activity was lowered. On the other hand, clogging occurred in the reactor due to the precipitates of removed Fe. The precipitation was mainly observed in the upper half of the reactor, and clogging was temporarily solved by stirring the surface. However, since the maintenance interval was gradually shortened, the process improvement to reduce clogging is important.

Regarding the anaerobic treatment process, we designed two cases, a concrete rectangular parallelepiped reactor and a pond-shaped reactor using waterproof sheet. Althought their construction costs were the same level, the former requires small area. Therefore, we chosed and cnstructed a concrete rectangular parallelepiped reactor for the anaerobic process, and its test using ethanol and rice bran as an organic resource is ongoing.

References

Furuya et al. (2012) Research on the applicability of anaerobic passive bioreactor for mine water treatment in Japan. IMWA2012 proceedings, Bunbury

Hamai et al. (2013) Research on the applicability of anaerobic passive bioreactor to acid mine drainage treatment in Japan. IMWA2013 proceedings, Colorado

Hamai et al. (2015) The sequential experiments of passive treatment system using bioreactor for acid mine drainage in Japan. ICARD2015 proceedings, Santiago

Spectral Monitoring Techniques for Optically Deep Mine Waters

Brandon K. Holzbauer-Schweitzer[1], Robert W. Nairn[2]

[1]*Graduate Research Assistant, University of Oklahoma, 202 West Boyd Street, Norman, Oklahoma, 73019, Bholzbauersch10@ou.edu*

[2]*Professor, University of Oklahoma, 202 West Boyd Street Room 334, Norman, Oklahoma, 73019, Nairn@ou.edu, ORCID 0000-0003-1400-6289*

Abstract

Remote estimation of water quality is of increasing interest to monitoring professionals. Unfortunately, environmental and technical limitations inhibit widespread application. The purpose of this study was to demonstrate spectral monitoring techniques utilizing data from two different platforms. Results describe strong linear relationships between remotely collected multispectral reflectance and in-situ metal concentrations. Spatial regression techniques produced a model capable of predicting particulate iron concentrations with moderate confidence (R^2_{adj} = 0.83) and reasonable error (SSR = 69.80). Overall, remote environmental monitoring represents a novel tool to advance and improve the effectiveness of traditional monitoring efforts.

Keywords: Geographically weighted regression, optical depth, water quality, unmanned aerial system

Introduction

As electromagnetic energy reaches an object several interactions will occur (e.g. reflection, transmission, absorption, and scattering) between photons and particles within the media (e.g. optically active constituents (OACs)) until either photons are reemitted (e.g. reflected), or all energy is consumed (e.g. absorbed). In cases where the water column is transparent (e.g. low concentrations of OACs), photons interact with the bottom substrate altering the expected energy signal (e.g. optically shallow water (OSW)). Conversely, if OACs are present in elevated concentrations, even within physically shallow surface waters, and the bottom substrate is not visible, observable energy will decay at an exponential rate and interactions with the substrate will be minimal (e.g. optically deep water (ODW)) (Zeng et al. 2017). Traditional determinations of optical depth (OD) utilize the Beer-Lambert Law and require the measurement or calculation of the spectral intensity of incoming solar radiance (I), the spectral intensity of emitted (e.g. reflected or scattered) solar radiance (I_O), absorption coefficient (κ) of the object, density (ρ) of the object, and the solar zenith angle (Θ) of I. Application of this methodology has been based primarily in meteorological sciences, typically to estimate the OD of water vapor and other aerosols in Earth's atmosphere (Filonchyk et al. 2019).

Small Unmanned Aerial Systems (sUAS) have demonstrated effectiveness in performing remote sensing of traditional OACs (e.g. chlorophyll-a) in ODWs (e.g. Su 2017). Literature gaps exist in the application of these technologies in OSWs and their use for the examination of mine drainage. Therefore, the purpose of this study was two-fold: to examine the feasibility of utilizing sUAS-derived multispectral (MS) imagery (e.g. tens of spectral measurements) to estimate in-situ metal concentrations in ODWs and to investigate in-situ OD utilizing spectroradiometer-derived hyperspectral (HS) data (e.g. thousands of spectral measurements) to discern the effect that remotely sensing substrate has on sUAS-derived MS imagery.

Methods

Study Site Description

Spectral data were collected from the surface of an oxidative process unit (Cell one (C1)),

a part of the larger Mayer Ranch Passive Treatment System (MRPTS) in May, June, and July of 2019. MRPTS is located within the Tar Creek watershed and Tar Creek Superfund Site, and the Oklahoma portion of the Tri-State Mining District (TSMD) (fig. 1). This ten-cell PTS, operated with two parallel treatment trains, was designed to promote various natural biogeochemical processes in specific process units. Overall, the PTS has effectively treated artesian net-alkaline ferruginous lead-zinc mine drainage since late 2008 (Nairn et al. 2009).

Spectral Instrument Calibration and Operation

Before data collection, each instrument was calibrated correctly. The Analytical Spectral Devices (ASD) FieldSpec3 was optimized and standardized with a white calibrated reflectance panel (CFP) designed to reflect 95 – 99% of electromagnetic energy. During this process, the instrument measured reflected electromagnetic energy from the CFP to establish a baseline reference of approximately 100%. To calibrate the MicaSense RedEdge sensor on the sUAS, an image of the same CFP was taken pre- and post-flight. The image processing software (Pix4DMapper) used the two calibration images to account for changes in solar conditions throughout the flight and to transform the uncompressed 16-bit, 1,280 by 960-pixel, digital number values into spectral reflectance values.

In May, the ASD FieldSpec3 was used to collect HS (e.g. 350 – 2500 nm) profiles from a pair of catwalks located in C1. Measurements were collected nadir to the water surface, approximately one m above the surface at one m horizontal increments starting at the water's edge (0 m) to the end of the catwalks (4 and 6 m for the northeast and southeast catwalks, respectively). At each location, the spectral profile measured was an average of five sets of ten measurements, taken in 0.1 s increments. Raw data files were post-processed to spectral reflectance with the ASD ViewSpec Pro software.

In June and July, the Aerial Technology International (ATI) AgBot equipped with

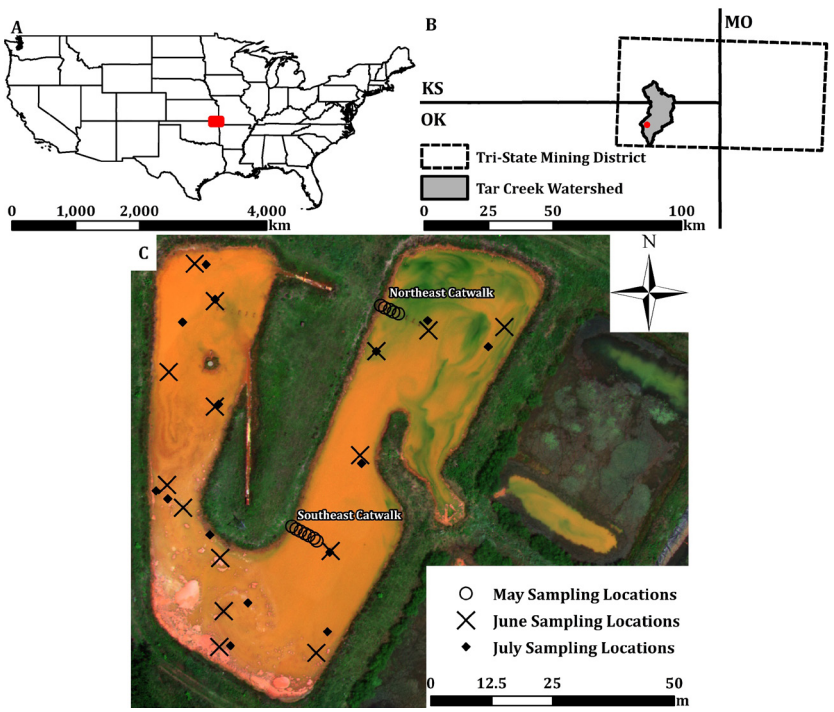

Figure 1 *Location of (A) TSMD in the central United States, (B) Tar Creek watershed in Oklahoma and Kansas, and (C) C1 within MRPTS with May catwalk and June and July in-pond sampling locations identified.*

the RedEdge sensor was used to collect MS reflectance imagery within ±2 h of local solar noon. This vertical take-off and landing (VTOL) quadcopter sUAS measures MS reflectance in five discrete spectral bands (e.g. blue, green, red, red edge (RE), and near-infrared (NIR)) simultaneously with center points at 475, 560, 668, 717, and 840 nm, respectively. Each sUAS flight was completed autonomously, with missions developed in Mission Planner software V.1.3.37. Missions covered approximately 81,000 m^2, at speeds of 6 m s^{-1}, an altitude of 50 m above ground level, with 75% image side and overlap to ensure accurate georeferencing, mosaicking, and high-quality data. Using these mission parameters produced a spatial resolution of roughly 6.82 cm $pixel^{-1}$.

In-situ Surface Water Quality Sampling

Fifteen in-situ surface water grab samples were geo-located and collected from C1 within a one h window of each sUAS flight completion. To adequately address the spatial distribution of surface water quality, ten sampling locations were established around the water's edge of C1. An additional five samples were collected throughout the center of C1 via canoe (fig. 1). Water's edge samples were collected from C1 with a fully extended swing-arm sampling pole (approximately 3.6 m in length). All samples were collected approximately 0.5 m below the water surface, or at the point the 1-L HDPE sample bottle was no longer visible. Samples for analyses of total and dissolved (0.45-mm) metal concentrations were collected at each location following EPA approved methods.

Assessing the Effects of Optical Depth

After the collection of HS data, Secchi disk depth (SDD) and actual physical depth (AD) were measured at the same one m horizontal increments. To minimize the resuspension of substrate and modification to the water column's optical properties, SDD was measured first. Then AD was measured by lowering a weighted line into the water column until it contacted the surface of the substrate. With the assumption that SDD ~ OD, and when the ratio between SDD and AD was equal to one, interferences from the substrate were expected. To characterize this phenomenon in terms of sUAS-derived MS imagery, an exponential relationship was developed. This relationship used HS reflectance data extracted with respect to the red band (668 nm) of the RedEdge sensor and the SDD AD ratio. Visualization of the extent of interference from OSWs (e.g. SDD:AD > 1) was completed utilizing the Raster Calculator, the statistically derived exponential relationship, and the sUAS-measured red band reflectance in ArcMap 10.6.1.

Results and Discussion

Estimating In-situ Surface Water Quality

In pond metal concentrations were typical of net alkaline metal-rich mine waters (tab. 1). Although MS interferences from wind action (e.g. glint) and cloud cover were minimal, interferences occurred from surface scum (e.g. amorphous iron-oxyhydroxide) and algae (e.g. chlorophyll-a), particularly in the southwestern and northeastern portions of C1, respectively. If these conditions affected either dataset, outliers were identified and removed utilizing the inter-quartile range.

In-situ water quality and MS reflectance were defined as the dependent and independent variables, respectively. In reality, OACs (e.g. metals) are independent of and effect the MS signals measured. To that end, Ca, Co, K, Li, Mg, Mn, Na, Ni, Pb, S, Si, and Zn exhibited strong collinearity ($R > 0.90$) and except for Si and Zn exhibited moderately strong inverse relationships ($R < -0.65$) with the untransformed green band (tab. 1). Furthermore, Cd and Fe also displayed collinearity ($R = 0.84$) and exhibited the most robust relationships ($R > 0.80$) with the log-transformed and untransformed red band, respectively. Surprisingly, Zn was not correlated with Cd ($R = 0.23$), and the strongest relationship observed was with the green and RE ratio ($R = -0.68$). Al and Cu were not collinearly related with any other metal and required log transformations to develop any meaningful relationship ($R = -0.50$ and -0.75, respectively). Overall, the optical fraction (e.g. total and particulate) of metal concentrations were more strongly correlated then the non-optical fraction (e.g. dissolved).

For some metals (e.g. Cd, Pb, and Zn), the

prominence and adsorption capabilities of iron-oxyhydroxides were likely contributing to the observed relationships. Additionally, the inverse relationships with the green band were the result of fundamental electromagnetic interactions. Locations with higher metal (e.g. Fe) concentrations reflected more red energy and absorbed more green energy. Conversely, as concentrations of the predominant OAC (e.g. Fe) decreased, the amount of red energy reflected also decreased, while reflected green energy increased.

A series of surface water quality maps were generated in ArcMap 10.6.1 (fig. 2) using these data. The red band was the input to a geographically weighted regression (GWR) model, and local polynomial interpolation (LPI) was used to extrapolate particulate Fe concentrations across C1 (fig. 2A). These maps have a spatial resolution (approximately 30 cm pixel^{-1}) more representative of in-situ water quality than traditional monitoring efforts (e.g. single concentration applied to an entire water body), including a spatial component to the regression model substantially improved performance. Overall, the GWR model produced a sum of squared residuals (SSR), sigma, Akaike information criterion (AICc), and an adjusted R^2 of 69.80, 2.11, 112.09, and 0.83, respectively (fig. 2B). The relatively high SSR is due to an absence of sampling locations in the northern portion of C1 (fig. 2C). At this location (e.g. *hot spot*), there were not sufficient neighbours to develop meaningful statistical relationships, resulting in arbitrarily high residuals to be interpolated.

Table 1 *Summary statistics (n = 23) for sUAS-derived MS reflectance (decimal percent) and in-situ total metal concentration data (mg L^{-1} unless otherwise noted) with the strongest relationship (R), MS band (X), any transformations (Trans.), and the metals fraction (D = dissolved, P = particulate, T = total) exhibiting R; * = $\mu g\ L^{-1}$.*

Parameter	Mean	Maximum	Minimum	R	X	Trans.	Fraction
MS Reflectance							
Blue	0.04 ± 0.01	0.08	0.03	-	-	-	-
Green	0.11 ± 0.01	0.13	0.08	-	-	-	-
Red	0.20 ± 0.03	0.26	0.18	-	-	-	-
NIR	0.13 ± 0.05	0.30	0.08	-	-	-	-
RE	0.20 ± 0.04	0.32	0.15	-	-	-	-
[Total Metals]							
Al	0.06 ± 0.05	0.28	0.02	-0.50	Green	Log10	P
Ca	681.43 ± 59.93	753.96	616.68	-0.68	Green	-	T
Cd*	1.87 ± 0.68	3.00	1.00	0.83	Red	Log10	P
Co	0.04 ± 0.004	0.05	0.04	-0.68	Green	-	T
Cu*	4.13 ± 1.30	8.00	2.00	-0.75	Blue	Log10	P
Fe	11.14 ± 5.90	29.15	5.20	0.88	Red	-	P
K	22.41 ± 2.41	25.08	19.72	-0.71	Green	-	T
Li	0.26 ± 0.03	0.29	0.23	-0.70	Green	-	T
Mg	154.46 ± 14.29	171.36	139.12	-0.69	Green	-	T
Mn	1.17 ± 0.10	1.29	1.05	-0.65	Green	-	T
Na	99.02 ± 9.22	109.45	88.82	-0.71	Green	-	T
Ni	0.66 ± 0.06	0.74	0.58	-0.67	Green	-	T
Pb	0.30 ± 0.03	0.33	0.26	-0.75	Green	-	T
S	746.29 ± 73.42	831.56	660.99	-0.69	Green	-	T
Si	6.84 ± 0.60	7.60	6.04	0.75	Red	-	P
Zn	4.11 ± 0.37	4.58	3.56	-0.68	Green:RE	-	T

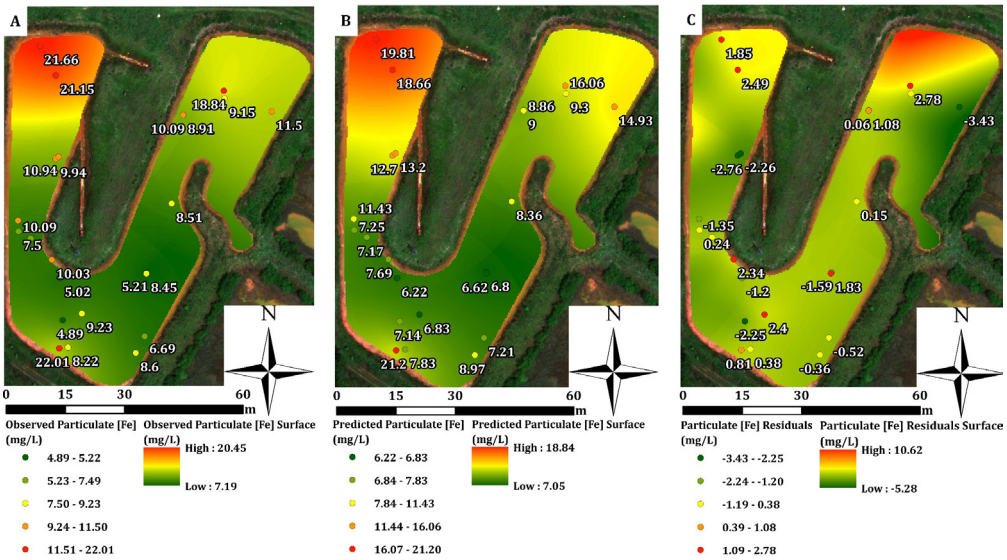

Figure 2 Observed (A) and GWR predicted (B) spatial water quality maps with resulting residuals (C); point values are labeled and were extrapolated with LPI.

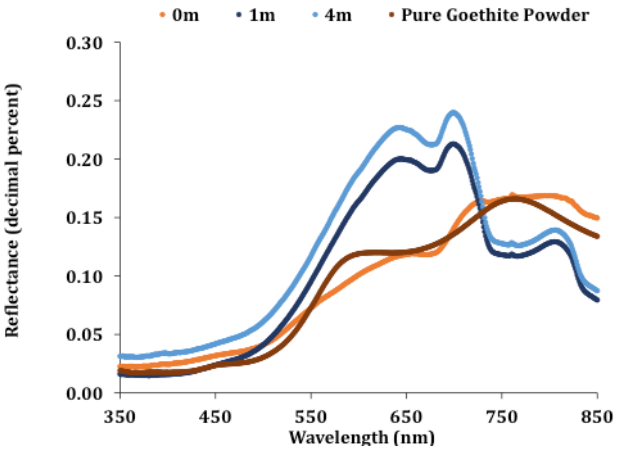

Figure 3 HS profiles collected at the northeastern catwalk in May 2019 (Goethite data: Kokaly et al. 2017).

Determination of Optical Depth Influence

The assumption that SDD ~ OD was verified by examining the shape and magnitude of spectral profiles collected when the substrate was and was not visible through the water column at increasing distances and depths from the water's edge (0 m) (fig. 3). Remotely sensing bottom substrates not only decreased the overall energy reflected (by approximately 20%) but modified the shape of the spectra (e.g. changes to peak reflectance wavelengths) (fig. 3). Furthermore, when the substrate was visible through the water column, a moderately strong negative exponential relationship existed that was representative of the exponential decay of spectral energy in water (R = 0.75). A spatial map identifying the extent of interference caused by OSW (e.g. SDD:AD > 1) within C1 was developed (fig. 4). Based on these results, it would be expected to measure interference from the substrate in the northeast portion of C1. Unfortunately, this identification of OSW was caused by remotely sensed algae (fig. 1), rather than the substrate, resulting in lower red, relative to green, MS reflectance. Overall,

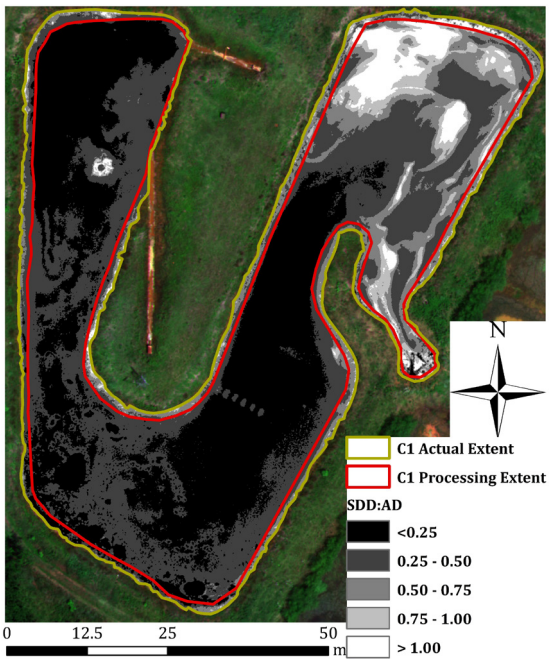

Figure 4 *Extent of expected OD interferences (e.g. SDD:AD > 1) within C1.*

these results represent a valid method of identifying the extent of OD interference to evaluate the feasibility of performing remote surface water quality monitoring in optically complex surface waters.

Conclusions and Future Work

Although the developed spatial water quality model exhibits relatively low residuals, these results have not been validated. It is also likely the results are site and mine drainage (e.g. net alkaline ferruginous lead-zinc waters) specific. Furthermore, the *success* of the model was primarily driven by the dominant optical properties of C1 (e.g. substantial presence of iron-oxyhydroxides) and is untested in the transparent artesian source waters. Rapid identification and estimation of OD in any type of water can address the feasibility of utilizing sUAS technologies for environmental monitoring. Results of the OD analysis support decreasing processing extents (e.g. excluding edge effects) to minimize interferences from OSWs and verified much of the studied water body (e.g. C1) were ODWs, suggesting the presented spatial water quality model was valid and representative of in-situ surface water conditions. Future efforts should include continued training and validation of the developed models in mine waters characteristic of the TSMD. Additional training and validation must occur outside the TSMD in waters affected by other sources of mine drainage (e.g. net acidic coal mine drainage) to address site-specificity. As sUAS technologies and spatial water quality models improve remote monitoring, they can contribute substantial quantities of environmental data (e.g. identify *hot spots* to focus traditional monitoring efforts), decrease field and laboratory costs, and increase spatial and temporal resolutions of traditional monitoring efforts.

Acknowledgments

This work was supported by the Grand River Dam Authority (Agreements GRDA 060910 and GRDA 08272015). The authors thank members of the Center for Restoration of Ecosystems and Watersheds (CREW), Earth Observation and Modeling Facility (EOMF), and private landowners for assistance in data collection, providing additional spectral instrumentation, and access to private lands, respectively.

References

Davis JA, Leckie JO (1978) Surface ionization and complexation at the oxide/water interface II. Surface properties of amorphous iron oxyhydroxide and adsorption of metal ions. J Colloid and Interface Science 67:90-107, doi:10.1016/0021-9797(78)90217-5.

Filonchyk M, Yan H, Zhang Z, Yang S, Li W, Li Y (2019) Combined use of satellite and surface observations to study aerosol optical depth in different regions of China. J Sci Rep 9:6174, doi:10.1038/s41598-019-42466-6.

Kokaly RF, Clark RN, Swayze GA, Livo KE, Hoefen TM, Pearson NC, Wise RA, Benzel WM, Lowers HA, Driscoll RL, Klein AJ (2017) USGS spectral library version 7. USGS Data Series 1035:61, doi:10.3133/ds1035.

Nairn RW, Beisel T, Thomas RC, LaBar JA, Strevett KA, Fuller D, Strosnider WH, Andrews WJ, Bays J, Knox RC (2009) Challenges in design and construction of a large multi-cell passive treatment system for ferruginous lead-zinc mine waters. J American Society of Mining and Reclamation 871-892, doi:10.21000/JASMR09010871.

Su TC (2017) A study of matching pixel by pixel (MPP) algorithm to establish an empirical model of water quality mapping, as based on unmanned aerial vehicle (UAV) images. Int. J Applied Earth Observation and Geoinformation 58:213-224, doi:10.1016/j.jag.2017.02.011.

Zeng C, Richardson M, King D (2017) The impacts of environmental variables on water reflectance measured using lightweight unmanned aerial vehicle (UAV)-based spectrometer system. J Photogrammetry and Remote Sensing 130:217-230, doi:10.1016/j.isprsjprs.2017.06.004.

The Use of Industrial Alkaline Wastes to Neutralise Acid Drain Water from Waste Rock Piles

Nikolay Maksimovich[1], Vadim Khmurchik[1],
Olga Meshcheriakova[1], Artem Demenev[1], Olga Berezina[1]

[1]*Natural Science Institute of Perm State University, Genkel Street 4, Perm, Russian Federation, khmurchik.vadim@mail.ru*

Abstract

Coal mining always results the formation of large volumes of rock wastes, which can be stacked in piles. Around 100 piles of various sizes are located in the Kizel coal basin, Western Urals, Russian Federation; some of these piles are burned nowadays. Rock piles drainage water have pH – 1,8-6,3, Fe – 0,2-28050 mg L^{-1}, Al – 0,5-3550 mg L^{-1}, Mn – 0,13-88 mg L^{-1} and total mineralization up to 50000 mg L^{-1}. A lot of metals and metalloids are transported with drain water from waste piles to soil, groundwater and the nearest river systems and pollute them.

We studied the capability of industrial alkaline wastes, covered waste rock piles, to neutralise drain water, formed during rainfalls. Preliminary laboratory experiments showed high efficiency of acid mine water treatment with lime-containing metallurgical slag, alkaline soda plant's waste and limestone mining waste. The last two substances were used as reagents in the burned and unburned waste rock piles treatment experiment. Two solutions were separately used as leaching agents – distilled water to mimic rainfalls, and solution of organic substances (glucose and sodium acetate, 0.5 g L-1 each) to mimic rainfalls, drained plant vegetation.

The most effective alkaline reagent for drain water neutralization was soda plant's waste. The investigation revealed that organic substances addition increased the efficiency of waste rock piles treatment with alkaline wastes used. Mathematical calculations showed that covering of waste pile with 0.3 m thick layer of soda plant's waste could be enough for long term neutralization of drain water, being formed during rainfalls.

The using of alkaline industrial byproducts and wastes to cover waste rock piles could be economically appropriated treatment method in the Kizel coal basin because such wastes are located in transport accessibility with the basin. The efficiency of alkaline reagents using could be improved by organic matter addition.

Keywords: waste rock pile, acid rock drainage, industrial alkaline wastes, column leaching experiment

Introduction

Mining industry is associated with the production of large quantities of waste, which potentially may cause environmental problems over very long periods of time. The primary process that causes problems is the oxidation of the sulfide minerals in the waste, which are deposited as waste piles or tailings.

Mining in the Kizel coal basin had been carried out for more than 200 years. Mines were closured in the 1990s. Over 35 million m3 of waste rocks had been accumulated in more than 100 piles, composed of fragments of argillite, sandstone, and limestone with inclusions of coal; the content of pyrite in piles reaches 4%. Processes of physical weathering, oxidation, hydrolysis, hydration, and metasomatism occur within piles. The oxidation of pyrite releases sulfur acid and is accompanied with heat production. So, self-ignition and burning of piles, roasting and melting of their rocks, and fumarole processes within piles were detected. Rainfalls, drained piles, are enriched in soluble compounds and pollute soils, groundwaters and rivers (Khayrulina et al. 2016).

To prevent the pollution and acidification of natural waters from mining waste leachates, it is necessary to minimize sulfide oxidation and/or water infiltration in the waste deposit. The installation of unpermeable or semi-permeable covers, the growth of vegetation, the addition of acid-buffering materials are used to prevent formation of acid rock drainage. As the pH of the leachate is of critical importance for the discharge of contaminants, because the solubility and mobility of metals and semi-metals critically depend on their speciation, the use of carbonate minerals and carbonate-containing waste as the cover to waste pile could be an appropriate measure to prevent environment pollution.

The aim of this study is to investigate the capability of carbonate-containing wastes to neutralize the leachate of waste rock piles in small-scale column experiment.

Materials and Methods

Site Description and Sampling

The Kizel coal basin (the Western Urals, Russia) occupies area of 200 km^2 and is located within West Urals folding zone adjacent to the pre-Ural boundary deflection. Rocks of Palaeozoic (Middle Devonian – Late Permian) age are developed in the area and represented by sandstones, mudstones, siltstones, shales, limestones, dolomites, marls, coals, and others. Carbonate rocks are intensely karsted, especially in the upper part of geologic column. Quaternary deposits are mainly represented by sands, loams, and clays and have often a high content of gravel and pebbles (Khayrulina et al. 2016). Coal of the basin exhibits elevated content of sulfur (mainly as a pyrite) – 5.8% (Kler 1988). Annual average regional precipitation is 800-900 mm/a, and the annual average of air temperature is 0-2 °C, with 160-170 days with an average air temperature below 0 °C (Maksimovich, Pyankov 2018).

Samples of burned and unburned waste rocks were taken from the partially burned pile of "Severnaya" mine. About 10 kg of rocks were separately sampled at burned and unburned parts of the pile from the depth of 0.5 m below pile surface. The moisture content of burned waste rock was 18%, pH of water suspension was 3.8. The moisture content of unburned waste rock was 14%, pH of water suspension was 2.8. Samples were sieved and the fraction of less than 1 mm in dimensions was used in column leaching experiment.

Alkaline Wastes

Carbonate-containing wastes of two industrial enterprises, soda plant in Berezniki town and limestone mining quarry at Chusovoy town, were used as alkaline reagents in experiment. These enterprises are located in the transport accessibility with the Kizel coal basin – 20 km for limestone quarry, and 120 km for soda plant.

Soda plant's waste was sampled from the tailing dump. It comprised the water suspension of various minerals with liquid:solid ratio of 85:15 and pH 9.5. Total mineralization of liquid phase was about 180 g L^{-1} (Maksimovich, Pyankov 2018). To determine the water content, the subsample was weighted before and after drying for 2 days at 60 °C. Water content of soda plant's waste was 88%. Mineral composition of the solid phase is presented in tab. 1.

Sample of crushing waste was taken from limestone mining quarry and sieved. The fraction of less than 1 mm in dimensions was used in column leaching experiment. To determine the water content, the subsample was weighted before and after drying for 2 days at 60 °C. Bulk density of the sample was 1.53 kg m-3, water content 2%. Mineral composition of the sample is presented in tab. 1.

Column Leaching Experiment

Inverted bottom-cutted 0.5 L bottles made of high density polyethylene (HDPE) were used as cylindrical columns with tapered lower part. The dimensions of cylindrical part were 0.09 m in height and 0.06 m in diameter. The

Table 1 *Mineral characteristics of alkaline wastes, %.*

Mineral	Soda plant's waste	Limestone mining waste
Calcite	90.6	88.7
Dolomite	0.6	2.4
Quartz	0	8.9
Cristobalite	0.4	0
Gypsum	4.3	0
Halite	4.1	0
Total	100	100

height of conical part was 0.12 m, diameters of conical part were 0.06 and 0.025 m. The lower end of inverted bottle (bottle neck) was sealed with the cap with glued rubber tube (0.2 m in length, 0.005 m inner diameter). HDPE grid (average pore size of 0,5 mm) and filter paper were placed inside the cap to hold sample and prevent finer sample particles escaping from column. Assembled columns were acid washed, triple rinsed with deionised water, and air-dried before use.

250-270 g of waste rock sample was placed into the column and covered evenly with an alkaline reagent, then 50-70 ml of a leaching solution was carefully added to the top of the column to avoid the erosion of cover layer. After percolation of the solution through the column, formed leachate was collected in glass jars and its pH was estimated. The addition of the solution was once a day, the channeling and preferential routs were not observed in the columns during experiment. Columns leaching experiment was performed at room temperature (22.5 ± 2.5°C), the evolution of the leachate's pH was examined.

Different amounts of alkaline reagents were used to cover waste rock samples, 1 and 5% wet weight of waste rock wet weight. Control columns did not contain alkaline reagents.

Two solutions were separately used as leaching agents – distilled water to mimic rainfalls, and solution of organic substances (glucose and sodium acetate, 0.5 g L-1 each) to mimic rainfalls, drained plant vegetation. The matter is, the most of piles are covered with vegetation, so percolating rainfalls are enriched in organic matter originated from root exudates and decomposed plant residues. As a removal of vegetation before the alkaline treatment of piles could be costly and technically difficult, it was the reason to use the solution of organic substances in the experiment. The experiment's scheme is presented in tab. 2.

Results and Discussion

Results of the column experiment with different leaching solutions are presented in fig. 1. Initial pH of water suspensions of burned and unburned waste rock samples were 3.8 and 2.8, correspondingly. pH of distilled water, percolated through the columns, had a tendency to rise gradually and reached 4.4 and 3.5 at 84th day of the experiment. This effect could be attributed to the presence of such alkaline-generating minerals in waste rock piles, as limestone. The presence of this mineral in waste rock piles was observed (Khayrulina et al. 2016).

Addition of organic substances to water, percolated through the columns, induced more substantial rise of pH: *approx*. 5.1 to both burned and unburned waste rock samples at 44th day of the experiment, and *approx*. 6.1 and 5.4 at 84th day, correspondingly. These organic substances, glucose and sodium acetate, are readily used by bacteria, inhabiting pile's rocks and producing CO_2 as an end-product in metabolic processes. We supposed, the implementation of plants vegetation on the pile's surface could to some extent be an acid drainage prevention measure due to enhanced water transpiration by plants, decreasing the amount of drained water, and addition of organic substances, originating from living and dead plants and inducing both bacterial metabolism and formation of CO_2 in piles.

The covering of waste rock samples with alkaline reagents rose pH of leaching solutions. The effect of soda plant's waste addition did not substantially differ from limestone mining waste addition, as it can be seen in fig. 1. However, the water content was 88% in soda plant's waste, whereas it was 2% only in limestone mining waste. So, soda plant's waste was the most effective alkaline reagent in the experiment, based on dry weight calculation.

Table 2 *The numeration of columns in the leaching experiment.*

Alkaline reagent	Soda plant's waste			Limestone mining waste			No reagents	
Amount of alkaline reagent, %	1	5		1	5			
Leaching solution a	W	W	S	W	W	S	W	S
Burned waste rock pile	2, 3	5, 6	4	8, 9	11, 12	10	7	1
Unburned waste rock pile	14, 15	17, 18	16	20, 21	23, 24	22	19	13

The highest pH values were observed in columns covered with alkaline reagent and drained with solution of organic substances.

Mathematical calculations showed that covering of waste pile with 0.3 m thick layer of soda plant's waste could be enough for long term neutralization of drain water, being formed during rainfalls.

Conclusions

The using of alkaline industrial byproducts and wastes to cover waste rock piles could be economically appropriated treatment method in the Kizel coal basin because such wastes are located in transport accessibility with the basin. The efficiency of alkaline reagents using could be improved by organic matter addition.

Acknowledgements

The reported study was funded by RFBR, project number 19-05-50073.

References

Khayrulina EA, Khmurchik VT, Maksimovich NG (2016) The Kizel coal basin (The Western Urals, Russia): Environmental problems and solutions. In: Drebenstedt C, Paul M (eds) Proc, IMWA 2016 Ann Conf. Freiberg/Germany (TU Bergakademie Freiberg), p. 766–771

Kler VR (1988) Metallogeny and geochemistry of coal-bearing and slate series in USSR, Nauka (in Russian)

Maksimovich NG, Pyankov SV (2018) The Kizel Coal Basin: Environmental Problems and Answers. Perm State University, Perm. 288 p. (in Russian)

Appendix

a)

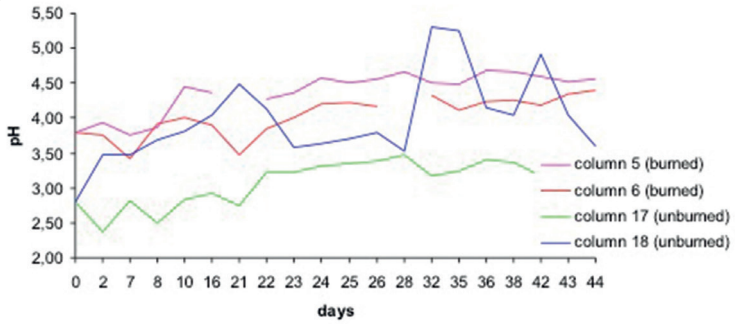

b)

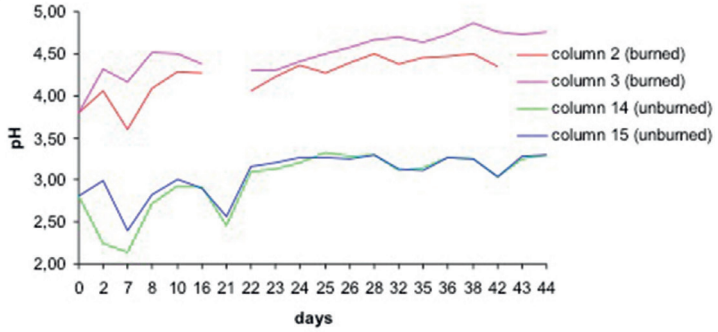

c)

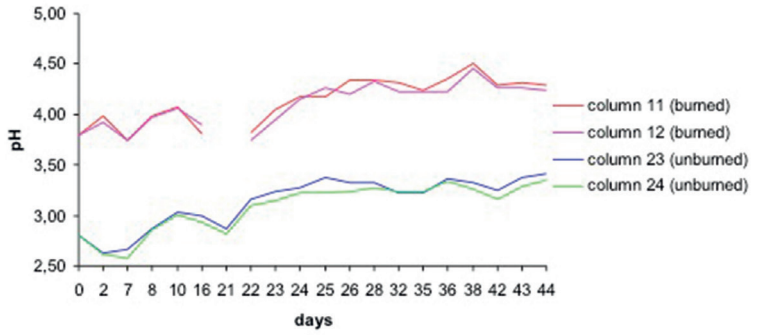

d)

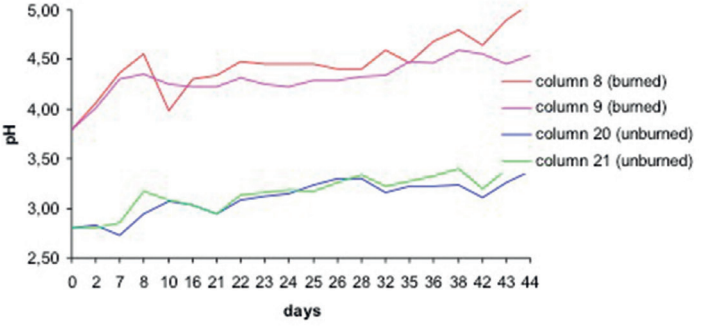

e)

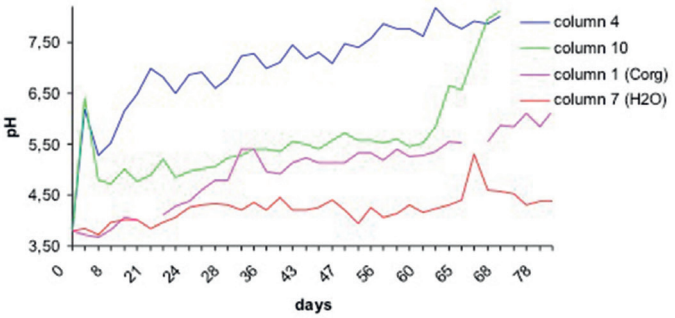

f)

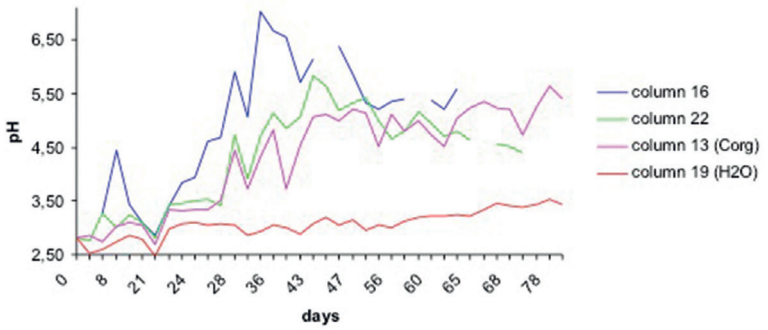

Figure 1 *The evolution of the leachate's pH during experiment.*

a) burned and unburned waste rock + soda plant's waste, 5% + water;
b) burned and unburned waste rock + soda plant's waste, 1% + water;
c) burned and unburned waste rock + limestone mining waste, 5% + water;
d) burned and unburned waste rock + limestone mining waste, 1% + water;
e) burned waste rock: column 4: + soda plant's waste, 5% + Corg solution; column 10: + limestone mining waste, 5% + Corg solution; column 1: + Corg solution; column 7: + water;
f) unburned waste rock: column 16: + soda plant's waste, 5% + Corg solution; column 22: + limestone mining waste, 5% + Corg solution; column 13: + Corg solution; column 19: + water.

Toward Sustainability of Passive Treatment in Legacy Mining Watersheds: Operational Performance and System Maintenance

Robert W. Nairn[1], Julie A. LaBar[2], Leah R. Oxenford[3], Nicholas L. Shepherd[1], Brandon K. Holzbauer-Schweitzer[1], Juan G. Arango[1], Zepei Tang[1], Dayton M. Dorman[1], Carlton A. Folz[1], Justine I. McCann[1], JD Ingendorf[1], Harper T. Stanfield[1], Robert C. Knox[1]

[1]*Center for Restoration of Ecosystems and Watersheds, University of Oklahoma, 202 West Boyd Street, Room 334, Norman, OK, 73019 USA, nairn@ou.edu*

[2]*Centenary University, Science Department, 400 Jefferson Street, Hackettstown, NJ 07840 USA*

[3]*Battelle Memorial Institute, Pueblo Chemical Agent-Destruction Pilot Plant, Pueblo, CO 81001 USA*

Abstract

For 40 years, passive treatment systems (PTS) have been preferred options at many abandoned sites, in part due to presumptions of continuous water quality improvement performance and limited operation and maintenance commitments. However, documentation to support these presumptions is typically lacking. Long-term regular performance evaluation (12 years) was conducted for a large, multi-process unit PTS receiving artesian-flowing lead-zinc mine waters (≈1000 m^3/day) at the Tar Creek Superfund Site, Tri-State Mining District, USA. Since 2008, the Mayer Ranch PTS has consistently retained >95% of targeted metal mass. Regular, periodic, and rehabilitative maintenance commitments were also documented.

Keywords: passive treatment, oxidation ponds, vertical flow bioreactors, operation and maintenance

Introduction

Metals-contaminated waters from derelict mining operations may degrade surface waters for decades to centuries (e.g. Younger et al. 2002). For almost 40 years, passive treatment systems (PTS) have been preferred options at many abandoned sites, in part due to presumptions of continuous water quality improvement performance with limited operation and maintenance commitments. Since initial evaluations of water quality improvement in natural wetland ecosystems in the late 1970s and early 1980s (Huntsman et al. 1978, Weider and Lang 1982), hundreds of PTS have been constructed worldwide to address coal and metal mining influenced waters (e.g. Rose 2010, Skousen et al. 2017). These ecologically engineered ecosystems rely on the managed promotion of naturally occurring geochemical, microbiological, and ecological mechanisms in designed process units, including ponds, wetlands, bioreactors, geochemical reactors and similar systems (Hedin et al. 1994, Younger et al. 2002, Watzlaf et al. 2004, Nairn et al. 2010). Compared to active treatment systems, which typically rely on non-renewable energy inputs, regular additions of alkaline chemicals, and substantial labor and maintenance efforts for effective treatment, PTS rely on hydraulic head differences, extended hydrologic residence times, and provision of appropriate biogeochemical conditions in specific process units. In some cases, solar and wind power may be used to operate compressors or blowers for effective aeration.

In one of the first comprehensive analyses of PTS, Hedin et al. (1994) examined the water quality improvement performance of 13 systems built between 1987 and 1992 in the northern Appalachian coal fields of the eastern United States. These authors developed what have now become widely accepted empirically derived area-adjusted mass removal rates to aid in PTS design. Hedin et al. (1994) found that the net alkaline or net acidic nature of source water quality is the primary driver of passive treatment process unit selection. In terms of long-term performance, the authors suggested the lifetime of aerobic systems receiving net alkaline mine water, which accumulate passively precipitated iron oxide

sludges, is limited by available freeboard. For organic substrate-based systems receiving net acidic mine waters, lifetime is controlled by relationships between available CaCO3 content and rates of bacterial sulfate reduction in the substrate. For designs current at that time, aerobic system lifetimes were estimated at 25-50 years, and organic substrate-based system lifetimes were estimated at 11 years. Furthermore, evolution of source waters through time (e.g., decreasing contaminant concentrations as reactive surfaces are exhausted, passivated, or otherwise rendered non-contributing) made these estimated lifetimes technically feasible and economically reasonable. Also noted by Hedin et al. (1994) were operation and maintenance concerns, including dike stability and pest infestations.

Skousen et al. (2017) provided a recent review of PTS, with an emphasis on systems in the Appalachian coal fields. Based on experience with hundreds of systems constructed during a period of more than 30 years, Skousen et al. (2017) discussed operation and performance of predominantly biological (e.g. aerobic and anaerobic wetlands, bioreactors) and geochemical (e.g. anoxic limestone drains, leach beds) systems. They noted similar design criteria as Hedin et al. (1994) and recognized proper process unit selection and sizing as critical to water quality improvement success. Although these authors failed to provide detailed insight into long-term performance, they emphasized the need for maintenance in all PTS.

However, despite decades of operation, detailed documentation to support continuous long-term water quality improvement performance and to examine operation and maintenance commitments is lacking for most systems. In this study, long-term regular performance evaluation (4 to 12 times per year for 12 years) was conducted for a large, multi-process unit, PTS receiving artesian-flowing lead-zinc mine waters (design flow of ≈ 1000 m3/day) at the Tar Creek Superfund Site, part of the historic and now abandoned Tri-State Mining District, USA. In addition, periodic maintenance activities were documented, including regular (marginally labor-intensive, quarterly to annually), periodic (requiring greater labor efforts, every two to three years) and rehabilitative (requiring substantial labor and equipment commitments, once per decade) maintenance.

Methods

The Mayer Ranch PTS (MRPTS, Figure 1) consists of 10 process units: an initial oxidation pond (OP), followed by parallel trains of surface flow wetlands (SFW), vertical flow bioreactors (VFBR), re-aeration ponds (ReAP), and horizontal flow limestone beds (HFLB), and a single polishing pond/wetland (PPW). The system receives three artesian borehole discharges (SA, SB, and SD) of net alkaline, metals-contaminated mine water from flooded underground workings that have been flowing unabated since 1979.

The University of Oklahoma (OU) Center for Restoration of Ecosystems and Watersheds (CREW) began periodic water quality and quantity data collection in 1998, with regular monthly sampling from 2004 to 2010, and quarterly (four times per year) sampling since 2010. MRPTS has been in effectively continuous operation since November 2008. Details on design, construction, and initial water quality improvement performance may be found in Nairn et al. (2010); details on specific process unit biogeochemical performance may be found in Oxenford and Nairn (2010), LaBar and Nairn (2018), and Nairn et al. (2018).

Regular data collection efforts included volumetric flow rates, physical parameters (pH, dissolved oxygen, temperature, specific conductance, oxidation-reduction potential, alkalinity, turbidity), sulfate, and a full suite of total and dissolved (<0.45 μm) metals (Ag, Al, As, Ba, Ca, Cd, Co, Cr, Cu, Fe, K, Li, Mg, Mn, Na, Ni, Pb, Si, and Zn). OU CREW standard operating procedures follow US Environmental Protection Agency (USEPA) or US Geological Survey (USGS) methods for all analyses and include approved quality assurance/quality control protocols. During each field visit, any operation and maintenance activities were documented.

Results

Since regular monitoring began in 2004, source water concentrations of metals of concern have demonstrated steady and regular decreases. Figure 2 illustrates statistically significant ($p<0.05$) decreases for total Zn concentrations for the three artesian discharges. Fe and Cd concentrations demonstrated similar changes, but Pb concentrations showed a recent anomalous increase in source waters, from 68±1.38 µg/L (2004 – 2017) to 235±18 µg/L (2018 – 2020). As previously hypothesized by Hedin et al. (1994), the evolution of source mine water chemical composition over time, coupled with decades-long design lifetimes, make PTS especially applicable to abandoned mine waters. Assuming no change in the slope of the decreases, MRPTS source zinc concentrations are predicted to be <0.01 mg/L at some point between 2028 and 2036.

Table 1 summarizes MRPTS influent and effluent water quality data from 2008 to 2020. The system consistently increased pH and decreased concentrations of total and dissolved (dissolved data not presented) Fe, Zn, Ni, Pb, Cd, As and SO42-. Concentrations of conservative base cations (e.g. Na) remained effectively unchanged with flow through MRPTS, indicating minimal effects of dilution or evapotranspiration but considerable influences of designed biogeochemical mechanisms.

Figure 3 plots selected constituents for the system influents and effluents of each process unit as the ratio of measured value divided by maximum value (C/Cmax). Iron was effectively retained via oxidation,

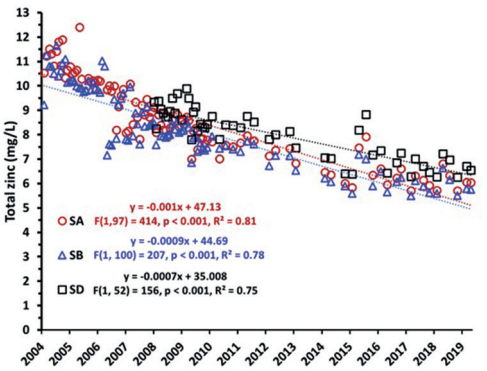

Figure 2 *Total zinc concentrations versus time in three abandoned borehole artesian discharges that flow into MRPTS showing statistically significant decreases ($p < 0.001$) over time. Sample sizes (n) are 99, 102 and 54 for discharges SA, SB, and SD, respectively.*

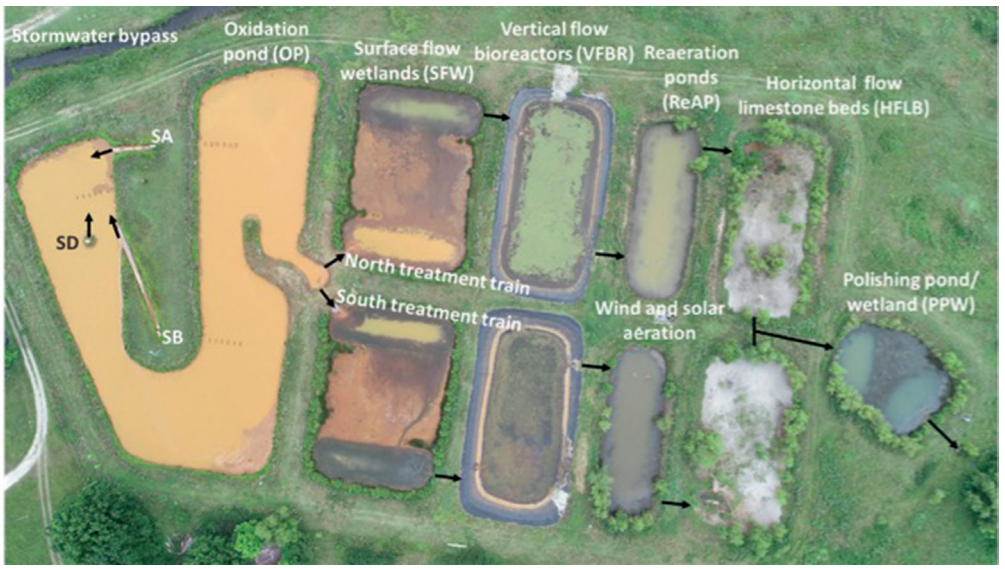

Figure 1 *Aerial image of the Mayer Ranch passive treatment system in June 2018 showing three artesian discharges, ten distinct process units, and water flow paths (black arrows). Image obtained via small Unmanned Aerial System after rehabilitative maintenance operations had been completed.*

Table 1 *Selected water quality data (median ± standard error) for MRPTS, representing 102 influent and 51 effluent sampling events. Effluent lead and cadmium concentrations exceeded practical quantitation limits (PQLs) for only 10 and 6 events, respectively.*

	Influent	Effluent
pH	5.95±0.01	7.03±0.03
Alkalinity (mg/L)	393±3.66	177±6.55
Fe (mg/L)	182±2.03	0.33±0.06
Zn (mg/L)	7.95±0.16	0.14±0.12
Ni (mg/L)	0.91±0.01	0.08±0.03
Pb (µg/L)	69±4.73	30±3.26
Cd (µg/L)	16±0.61	1.01±0.19
As (µg/L)	62±1.14	<PQL
Co (µg/L)	60±2.93	5.13±2.44
Sulfate (mg/L)	2182±35	2096±73
Na (mg/L)	95±1.08	97±2.41

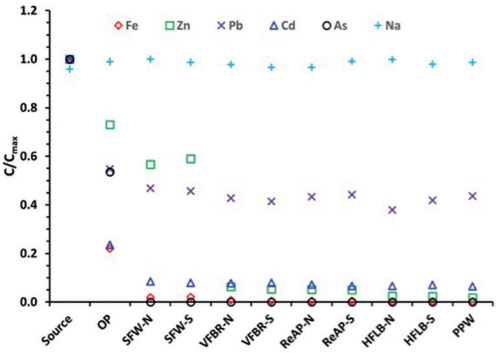

Figure 3 *Selected metal concentrations with flow through MRPTS process units, plotted as median value for each location divided by system maximum median value. Plotted Pb concentrations for all locations other than Source (n=98) and OP (n=38) represent only the <3% of 459 location-date pairs where [Pb]>PQL.*

hydrolysis, precipitation and settling in the OP and SFW. Iron mass removal rates in the OP were 21±2.8 g Fe m-2 day-1, mirroring the 20 g m-2 day-1 design criteria for net alkaline waters from Hedin et al. (1994). In 2014, in situ estimates of wet iron sludge depths ranged from 41 to 116 cm in the OP (design depth ≈ 152 cm) and from 7 to 45 cm in the SFW (design depth ≈ 60 cm). Percent crystallinity increased with depth, with amorphous ferrihydrite in surface samples and evidence of goethite crystallization in deeper samples. Arsenic and other trace metals were also retained through sorptive processes in the oxidative units.

Concentrations of Zn, Cd, Pb, and other trace metals were decreased due to oxidative, reductive and sorptive processes in multiple process units. Sequential extractions of VFBR organic substrates indicated that most of the Cd, Co, Fe, Ni, Pb, and Zn were retained in the refractory organic/sulfide fraction (LaBar and Nairn 2018). These results were confirmed for Cd, Fe, Pb, and Zn through subsequent acid volatile sulfide/simultaneously extracted metals (AVS/SEM) analyses. Framboidal pyrite and zinc sulfide colloidal aggregates were identified in these substrates via scanning electron microscopy.

Since 2008, MRPTS has consistently retained >95% of targeted metal mass, including approximately 37000 kg Fe, 1700 kg Zn, 185 kg Ni, 96 kg Mn, 15 kg Pb, 13 kg As, 11 kg Cot, and 3 kg Cd on an annual basis, with mass differences of calcium, magnesium, sodium and potassium of <5%. Effluent waters met receiving stream ambient water quality criteria and have led to reestablishment of viable and diverse fish communities and aquatic mammal populations without any active in-stream restoration.

Regular (quarterly to annually) system maintenance included monitoring of process unit water surface elevations, removal of debris (typically aquatic vegetation) from flow structures, and exclusion of aquatic mammals (e.g. muskrats, Ondatra zibethica and beavers, Castor canadensis). Water surface elevations were determined continuously by a network of pressure transducers and were critically important in determining maintenance needs (Figure 4). Periodic maintenance (every 2 – 3 years) included removal of woody vegetation (e.g. willows, Salix nigra and cottonwoods, Populis deltoides) and monitoring of solids accumulations. It is estimated that regular and periodic maintenance required approximately 300 person-hours per year.

Rehabilitative maintenance efforts were conducted twice in the first decade of operational life. By early 2017, both VFBRs exhibited evidence of hydrologic and hydraulic failure. Water throughput rates decreased dramatically, resulting in water surface elevation increases and subsequent effects on upstream process units and breaching of protective dikes (Figure 4).

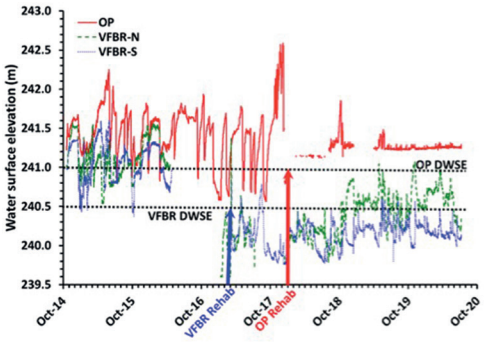

Figure 4 *Water surface elevations for MRPTS OP and VFBR process units for six years. DWSE refers to design water surface elevations. Rehabilitative maintenance events indicated by vertical arrows.*

Table 2 *VFBR hydraulic conductivity (K) values pre-construction, after eight years of continuous operation and after rehabilitative efforts (which have been maintained for more than three years).*

Year	Hydraulic conductivity measurement	Vertical K (m/day) VFBR-N	VFBR-S
2008*	Laboratory falling head	4.77	4.77
2016	Laboratory falling head	0.51	0.43
2016	Field falling head	0.13	0.19
2017	Field falling head (post-rehabilitation)	4.50	4.50

*Pre-construction

These process units were dewatered and the existing organic substrate (45% spent mushroom substrate, 45% wood chips and 10% manufactured sand) was mixed with a small excavator. Despite areas with considerably degraded substrate, the original hydraulic conductivity was restored (Table 2) through these efforts.

In addition, the original buried piping structure between the OP and parallel SFW periodically exhibited substantial water throughput issues over several years. Although calculated head losses were approximately 5 cm in the piping system, measured water level differences in these units were as much as 70 cm (Figure 4), likely due to decreases in cross-sectional areas of the pipes. Repeated attempts to clean the pipes via a flexible auger (plumbers snake) and water jet flushing proved ineffective. It was hypothesized that an air lock periodically formed in the piping system. Therefore, the outflow structure of the OP was replaced with a 3-m wide open water outlet channel feeding two inlet weir structures that connected to the parallel SFW (Figure 1). The existing piping system remained in place to provide maintenance redundancy. Each rehabilitative maintenance effort required approximately two weeks of system down time and rental of small earth moving equipment.

All maintenance work was completed by OU CREW personnel. Other than removal of woody vegetation every 2-3 years, no vegetation harvesting has been required. After 12 years of continuous operation, no iron oxyhydroxide sludge removal from the OP or replacement of organic media in the VFBRs has been necessary, although accumulations and changes are regularly tracked. Notably, all rehabilitative maintenance efforts were driven by hydraulic failures and not by biogeochemical, microbiological, or ecological concerns.

Conclusions

Properly designed and sized PTS may provide water quality improvement performance for many years if adequate maintenance is completed. Design lifetimes are typically estimated at 20 years but may be extended if proper monitoring and maintenance are conducted. In this study, a 12-year old PTS receiving iron-rich lead-zinc mine waters was evaluated. Consistent long-term water quality improvement and ecological recovery of the receiving stream were documented. Maintenance efforts, including vegetation removal, nuisance aquatic mammal control, and two substantial rehabilitative efforts, were documented. VFBR organic substrates were stirred and buried piping systems were replaced. Properly designed, constructed, and maintained passive treatment systems are viable technologies for addressing legacy watershed pollution.

Acknowledgments

The authors thank many previous CREW members who contributed to research at this site and private landowners who provided

site access. Major funding provided by U.S. Environmental Protection Agency (104(b)(3)X7-97682001), U. S. Geological Survey (04HQAG 0131), Oklahoma Department of Environmental Quality (PO2929019163) and Grand River Dam Authority (100052 and A15-240) agreements.

References

Hedin RS, Nairn RW, Kleinmann RL (1994) Passive treatment of coal mine drainage. US Department of the Interior, Bureau of Mines IC 9389

Huntsman BE, Solch JG, Porter MD (1978) Utilization of *Sphagnum* species dominated bog for coal acid mine drainage abatement. In: Abstracts, 91st Meeting Geologic Society America, Ottawa, Ontario, Canada

LaBar JA, Nairn RW (2018) Characterization of trace metal removal products in vertical flow bioreactor substrates at the Mayer Ranch Passive Treatment System in the Tar Creek Superfund Site. Chemosphere 199: 107-113

Nairn, R.W. J.A. LaBar, K.A. Strevett, W.H. Strosnider, D. Morris, C.A. Neely, A. Garrido, B. Santamaria, L. Oxenford, K. Kauk, S. Carter, B. Furneaux. 2010. A Large, Multi-Cell, Ecologically Engineered Passive Treatment System for Ferruginous Lead-Zinc Mine Waters. Proc IMWA Sydney, Nova Scotia, Canada, pp. 255-258.

Nairn RW, Shepherd NL, Danehy T, Neely C (2018) Aeration via renewable energies improves passive treatment system performance. Proc ICARD/IMWA/WISA Pretoria South Africa, 151-156

Oxenford LR, Nairn RW (2010) Progressive iron removal within the initial oxidation cell of a passive treatment system. In: Proc. ASMR, Pittsburgh, Pennsylvania, USA, p 767-779

Rose AW (2010) Advances in passive treatment of coal mine drainage 1998–2009. In: Proc. ASMR, Pittsburgh, Pennsylvania, USA, p 847-887

Skousen J, Zipper CE, Rose A, Ziemkiewicz PF, Nairn R, McDonald LM, Kleinmann RL (2017) Review of passive systems for acid mine drainage treatment. Mine Water Environ 36(1): 133-153

Watzlaf GR, Schroeder KT, Kleinmann RL, Kairies CL, Nairn RW (2004) The passive treatment of coal mine drainage. US Department of Energy, National Energy Technology Laboratory Internal Publication

Weider RK, Lang GE (1982) Modification of acid mine drainage in a freshwater wetland. Symp. on Wetlands of the Unglaciated Appalachian Region, West Virginia Univ, p 43-53

Younger PL, Banwart SA, Hedin RS (2002) Mine water: hydrology, pollution, remediation Vol. 5. Springer Science and Business Media

Integrated Closure Planning for a High Altitude Pit Lake in the Peruvian Andes

Cherie D. McCullough[1], Anibal Diaz[2]

[1]*Mine Lakes Consulting, PO Box 744, Joondalup DC, Australia, cmccullough@minelakes.com*

[2]*ERM, Amador Merino Reyna – 6th Floor, Lima, Peru, Anibal.Diaz@erm.com*

Abstract

A conceptual closure plan was developed for a high altitude copper mine in the Peruvian Andes where pit highwalls extended up to 450 m above equilibrium water level. These highwalls presented a surge wave risk due to regional seismic activity. A key aspect of the conceptual design was the novel use of a waste rock dump to provide surge wave protection to the communities located on the river below the mine site. By incorporating mine waste landforms in the valley downstream of the pit lake we sought to attenuate the risk of these flood events.

Keywords: Peru, Pit Lake, Mine Closure, Seismic Activity, Waves

Introduction

Mine pit lakes are a common feature of open cut mine closures that extend below the local groundwater levels (Castendyk and Eary 2009). With large water volumes which often contain waters degraded by contact with enriched geologies, pit lakes can represent a relevant risk at mine closure.

However, due to the relatively steep lake bottom profiles compared to natural lakes, shoreline stability may also be a substantial limitation to the rehabilitation and sustainable closure of pit lakes (Lund and McCullough 2011). Globally, metal mines tend to have steeper sided lakes and coal mines relatively shallower lakes (Schultze et al. 2016). This steepness may potentially influence upon highwall geotechnical stability, revegetation success, water quality and proposed end uses including wildlife habitat, aesthetics and recreation (McCullough et al. 2020).

Pit lakes can represent the highest environmental risk closure landform for many mines (Doupé and Lymbery 2005). Despite the issues relating to long-term pit lake closure planning and management, there is currently very little information available on pit lakeshore erosion, including potential erosion rates and extent (Vandenberg and McCullough 2017). Although water quality is typically the focus, recent work has highlighted pit lake wave action on sensitive surrounding receptors as a key knowledge gap to many closure plans proposing pit lakes as final landforms (McCullough et al. 2019).

Waves and shoreline erosion

The strength of pit wall materials may change during filling because of reduced normal stress on the materials near the pit walls or as a result of water flow along fractures or geologic structures. Rising lake water levels may then cause erosion of softer deposits, leading to undercutting and overhanging zones to form. These small pit slope failures are therefore not unusual during the pit filling process and may also occur once the final lake level has been established (Read and Stacey 2009).

The shoreline morphometry of a pit lake is determined by the original void shape and modified by any backfilling and shaping. The hydrodynamics of wind-forced waves are well understood and models are readily able to estimate wave characteristics for deep, open water and continuous shorelines (McCullough et al. 2019).

However, even decades-old pit lakes, frequently show very high rates of shoreline erosion (Vandenberg and McCullough 2017), often as sudden catastrophic highwall failures (Castendyk et al. 2020). Steep, eroding pit lake shorelines reduce end use opportunities and values (McCullough et al. 2018) and can

present a relevant risk to health and safety of visitors and local communities (Ross and McCullough 2011). In particular, surge waves have been identified as a potential risk for some pit lakes with potential for large mass failures (landslides) of highwalls in pit lake surface waters (Gammons 2009).

Study site

The Project is located in the Peruvian Andes in the Province of Pallasca in the northern part of the country. Project area altitude ranges from 3,900 to 4,700 m above sea level (masl). The ore deposit is located in a glacial valley with steep valley walls (fig. 1). The top of the projected final pit nearly reaches the 4,600 m elevation above sea level (masl), while the bottom of the pit is at 3,800 masl. This results in a highwall on the north side of the pit that is nearly 800 m high and slightly less on the south side of the pit. The pit above 4,200 masl does not extend the full circumference of the pit. High elevation ore only occurs on the south side of the pit and is below 4,280 masl. Most of the material above 4,200 masl is limestone, none of which is ore grade.

Following dewatering ceasing, hydrogeological modelling indicates that a pit lake will form in the pit void. The open pit will infill predominantly with groundwater over approximately 15 years and then discharge into the valley below. It is expected that rainfall, infiltration and surface drains will maintain a largely stable pit lake water level.

On November 10th, 1946, an earthquake of M7.3 caused 1,400 deaths in the region and nearly all buildings were destroyed or heavily damaged in the Sihuas-Quiches-Conchucos strip (along an active fault close to the Project). Many landslides occurred; one buried the village of Acobamba and another dammed the Pelagatos River, around 10 km north of the Project site (USGS 2020). The downstream village was also flooded by obstruction of the local creek. Consequently, the planned pit lake remains a concern for the inhabitants.

Issues

Previous planning

A previous conceptual mine closure plan (CMCP) proposed a closure design for landforms of the project area. The open pit void was designed as a deep pit lake. A smaller lake in the valley immediately below it was proposed by damming the valley with a large waste rock dump (WRD). A further waste dump was located in the north of the project valley and a wet tailings storage facility (TSF) in the south below the valley WRD.

Following public dissemination of the CMCP, the following points were deemed issues specific to the pit lake that still needed to be resolved to obtain government approval (Hurst and Pacey 2004).

1. The ESIA (containing the CMCP) was initially rejected by the regulators without sufficient community stakeholder engagement and after receiving community feedback.
2. No risk assessment was performed.
3. The large open pit proposed at closure presented a largely unconsidered risk of a

Figure 1 *Site location geography.*

constructed lake upstream and near to the community.
4. There was no proposed rehabilitation and end use development identified for impacted areas.

The pit void presented a highwall fall risk to visitors and local community. The risk of seismic activity and rockfalls presented a risk of surge waves forming within the pit following pit wall collapse; discharging down the project valley. Based upon low likelihood but high consequence, this risk was assessed as moderate. Consequently, the previous operator's mine closure plan was rejected by nearby community stakeholders, primarily because it presented an unacceptable risk of surge waves.

Closure Conceptual Design

The closure plan's objectives aimed to meet both Peruvian mine closure regulatory requirements as well as the expectations of key stakeholders including the concerned villagers downstream of the mine. Following Peruvian mine closure requirements (República del Perú 2008) and international leading practice (e.g. ICMM 2008) the primary aim of the pit void closure concepts is to mitigate risk and to maximise benefit to local and regional communities and environments after mine closure. Given the interaction of the pit void with other closure landforms and the need for mine closure planning to be holistic across the project area and greater region, we also considered other landforms such as the Valley WRD in our design and assessment.

In order to provide a conceptual closure strategy to design, cost and further develop a development of the revised closure and rehabilitation plan was based on the following objectives:

- geotechnical stability of post-mining landforms and safety to the local communities accessing the site;
- geomorphic stability of the reclaimed landscape (i.e., minimize through near-natural rates of erosion and sediment transport);
- consultation with the mining company and other contractors designing the operational site layout to ensure compatibility and minimize earth movements for closure works; and
- provision of a post-mining land use values equal to, or better than, pre-mine land uses.

Backfill

Complete backfill is typically recommended to avoid pit lake water quality and high slope safety and stability problems (Puhalovich and Coghill 2011). However, placing fractured and unweathered rock in a pit void that has filled with water may cause groundwater pollution if the pit lake is a through-flow system (McCullough et al. 2013). Because mine waste contained skarn and porphyry, a plume of highly geochemically enriched groundwater may extend away from the lake system in the direction of groundwater flow. Consequently, pit void backfill was not considered good environmental practice as a surge wave engineering solution.

Pit lake

An holistic conceptual closure design will reduce pit lake risks to health and safety of villagers to acceptable levels as follows. A drainage channel will reduce lake volume from previous designs and also increase the lake freeboard, preventing and mitigating many surges (fig 2, top left). A 10 m high security berm will be constructed from waste rock to attenuate any potential flood waves in the event of a slope failure of the open pit. A 2 m high security berm will be constructed near the outlet to the project's valley. A safety berm will also be constructed around the open pit to prevent access of stock and people to any remaining highwalls. The security berm has been used in other regions of Perú (Letient et al. 2006) and will provide wave protection from small to medium-scale wave events. Beach areas will be constructed where practicable to provide safe entry for stock watering access and also lake edge habitat for wildlife likely including a rainbow trout fishery (*Onchyrynchus mykiss*) used by local communities. The beach areas will also reduce wave erosion potential along their gradient.

Valley WRD

The Valley WRD will be specifically engineered as a dyke to provide discharge during normal

flow events and to control and retard high flow events such as may occur following a wall slump into the lake. The Valley WRD will be constructed asymmetrically along the south side of the valley, sloping to the north (fig 2, top right). Where practicable, bench width will be minimised and graded toward the valley floor to prevent water ingress through bench flats during precipitation and snowmelt events. Topsoil placement and revegetation with grasses will also provide a capture and release cover.

Rainfall data and valley stream flow data will be collected over the mine life to provide a good understanding of engineering requirements for the Valley WRD. The Valley WRD will also be specifically engineered as a dyke, with geotechnical and geochemical assessments of all construction materials specifically made to this purpose. It will be engineered to most probable flood and seismic event capacities.

Channel

The low rates of baseflow discharge from the pit lake will primarily be through the fractured rock waste base of the Valley WRD and through the karst system on which the Valley WRD is located. The channel will be constructed along the north side to carry pit lake discharge during flow events greater than baseflow but less than substantial flood events (fig 2, top right). This channel will be armoured with marble and limestone excavated predominantly in the unweathered initial overburden removal.

The channel will serve to reduce lake water level therefore reducing pit wall geologies exposed to direct water contact and wave action. This decreased water level also increases lake freeboard and reduced lake volume, providing further protection from surge waves.

Risk Assessment

A summary of inherent risks, risk management and consequent residual risks is shown below (tab. 1). Following the risk mitigation features incorporated in the revised design, residual risks are as follows:

1. surge waves. Based now upon very low likelihood and medium consequence, this risk is now low.

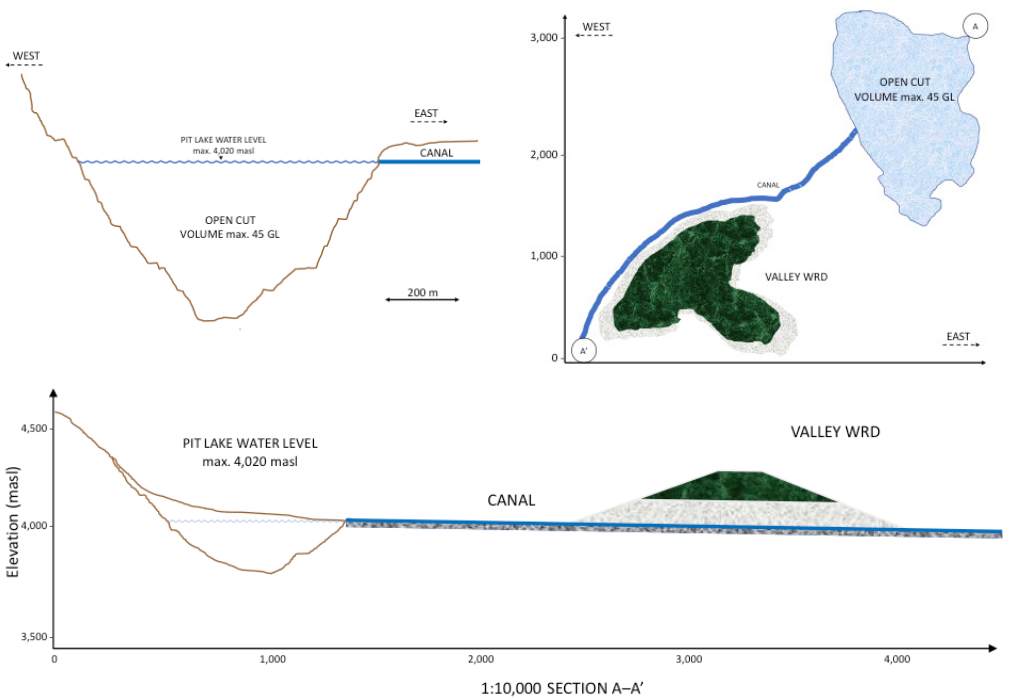

Figure 2 Landform closure design.

2. highwall falls. Based now upon low likelihood and medium consequence, this risk is now low.

Conclusions

Rather than a simple check box exercise, pit lake closure planning should be based upon risk assessments to potential receptors of wildlife, humans and other relevant end uses e.g. local community safety presented in this example. Further, pit lake closure planning should be undertaken with a holistic approach that considers the risk and interaction of other landforms upon each other. In this manner synergisms and efficiencies will often realise better pit lake, and overall, mine closure outcomes (Vandenberg and McCullough 2017).

The greatest risks associated with the case study's pit lake closure were found to be that of surge waves following seismic activity. An appropriate strategy to reduce these risks was developed by having a wet pit void of minimum water level and maximum freeboard and landscape engineering to prevent access and surge wave protection to reduce flood risk. The greatest reduction in wave risk would be achieved by engineering a Valley WRD with a diversion channel.

The updated CMCP was shared with the community technical advisors and stakeholders, receiving positive feedback and finally leading the approval of the environmental certification by the authorities. Therefore, integration of community concerns was another key design factor of this example.

Studies should now further evaluate the identified risks and proposed mitigation and management strategies over life-of-mine for development into a detailed closure strategy. Estimates of closure cost and of potential end use opportunity should also now be made.

References

Castendyk D, Eary T (2009) The nature and global distribution of pit lakes. In: Mine Pit Lakes: Characteristics, Predictive Modeling, and Sustainability Castendyk D & Eary T (eds) Society for Mining, Metallurgy, and Exploration (SME), Colorado, USA, 1-11 pp

Castendyk D, Voorhis J, Kucera B (2020) A Validated Method for Pit Lake Water Sampling Using Aerial Drones and Sampling Devices. Mine Water Environ

Doupé RG, Lymbery AJ (2005) Environmental risks associated with beneficial end uses of mine lakes in southwestern Australia. Mine Water Environ 24:134-138

Gammons CH (2009) Sampling and monitoring of existing pit lakes. In: Workbook of Technologies for the Management of Metal Mine and Metallurgical Process Drainage, Castendyk D & Eary T (eds) Society for Mining, Metallurgy, and Exploration (SME), Colorado, USA, 77-89 pp

Hurst TH, Pacey AJ (2004) New Peruvian mine closure requirements. Latin America Mining Record Aug/Sept:

ICMM (2008) Planning for Integrated Mine Closure: Toolkit. International Council on Mining and Metals London, UK. 86 p

Letient H, Marsland R, Marticorena M, McLeod H (2006) Mine closure planning in Peru. In: Barnhisel RI (Ed.) Proceedings of the 7th International Conference on Acid Rock Drainage (ICARD). St Louis, Missouri, USA, American Society of Mining and Reclamation (ASMR), pp 1051-1064

Table 1 *Risk assessment summary.*

Hazard	Inherent	Management	Residual
Surge wave	Low likelihood and high consequence	Security bund	Very low likelihood and medium consequence
	MODERATE RISK	Valley WRD	**LOW RISK**
		Channel	
Highwall falls	Moderate likelihood and high consequence	Safety berm	Low likelihood and medium consequence
	HIGH RISK		**LOW RISK**

Lund MA, McCullough CD (2011) Restoring pit lakes: factoring in the biology. In: Mine Pit lakes: Closure and Management, McCullough CD (ed) Australian Centre for Geomechanics, Perth, Australia, 83-90 pp

McCullough CD, Marchand G, Unseld J (2013) Mine closure of pit lakes as terminal sinks: best available practice when options are limited? Mine Water Environ 32:302-313

McCullough CD, Schultze M, Vandenberg J (2018) Realising beneficial end uses for pit lakes. In: Drebenstedt C; von Bismarck F; Fourie A & Tibbett M (Eds.), Proceedings of the International Mine Closure 2018 Congress. Leipzig, Germany, ACG, pp 497-504

McCullough CD, Schultze M, Vandenberg J (2020) Realising beneficial end uses from abandoned pit lakes. Minerals 10:133

McCullough CD, van Rooijen A, van Maren B (2019) Process-based shoreline erosion modelling for batter design of a coal mine pit lake. In: Fourie AB & Tibbett M (Eds.), Mine Closure 2019: Proceedings of the Fourteenth International Conference on Mine Closure. Perth, Australia, Australian Centre for Geomechanics (ACG), Perth, Australia, pp 75-87

Puhalovich AA, Coghill M (2011) Management of mine wastes using pit/underground void backfilling methods: current issues and approaches. In: Mine Pit Lakes: Closure and Management, McCullough CD (ed) Australian Centre for Geomechanics, Perth, Australia, 3-14 pp

Read J, Stacey P (2009) Guidelines for open pit slope design. CRC Press Sydney, Australia. 510 p

República del Perú (2008) Guía para la elaboración de planes de cierre de minas. Ministerio de Energía y Minas, República del Perú, Lima, Peru. 62 p

Ross T, McCullough CD (2011) Health and Safety working around pit lakes. In: Mine Pit lakes: Closure and Management, McCullough CD (ed) Australian Centre for Geomechanics, Perth, Australia, 167-181 pp

USGS (2020) Today in Earthquake History on November 10th: M7.3 - Ancash, Peru, 1946, https://earthquake.usgs.gov/learn/today/index.php?month=11&day=10&submit=View+Date, Accessed: June 1, 2020.

Vandenberg J, McCullough C (2017) Key issues in mine closure planning for pit lakes. In: Spoil to Soil: Mine site rehabilitation and revegetation, Nanthi Bolan N; Ok Y & Kirkham M (eds) CRC Press, Australia, 175-188 pp

Tailings Dam Failure: Estimation of Outflow Volume

Amir Keshtgar

Senior Civil Engineer, GHD, 154 Ann Street, Brisbane, QLD 4000, Australia, amir.keshtgar@ghd.com

Abstract

Failure impact assessment is an important activity when considering the potentially disastrous effects of tailings facility failures on human life, environment and the economy. Tailings run out distance, flow depth/velocity and the time to peak are crucial factors when estimating the population at risk and preparing evacuation plans. Dam breach parameters and tailings characteristics are needed to determine the combined tailings and supernatant water breach hydrograph for a hypothetical dam failure. A flood routing model is then required to estimate the run out distance, flow depth, velocity and flow travel time of the released volume. Unlike water storage dams, in which the entire storage sitting above the level of the breach is released, in a tailings dam failure generally a portion of the tailings is released, except in steep valleys or with very low density tailings then a complete entire release is still possible. This volume can be difficult to estimate prior to abreach event.

A new methodology to estimate the released tailings volume and create a breach hydrograph is presented in this study. The method combines supernatant water and tailings volume outflow in order to create the breach hydrograph for input into a non-Newtonian hydraulic model.

The supernatant water in the pool and the dry density of tailings play important roles in defining the sediment concentration and type of outflow fluid. The introduced technique has been applied to estimate the volume of tailings being released in a hypothetical failure event using a conventional three dimensional modeling tool. It is evident that the tailings breach volume is heavily dependent upon the post failure slope of the tailings. The geometry of the facility such as the embankment height and length, the pool volume as well as the breach location effects on the tailings release volume. This study proposes a method to consider the geometrical model of the storage area alongside the geotechnical characteristics and hydraulic of the tailings and sediment concentration for each facility in order to estimate the release volume from the tailings dam rather than using a simplified release volume equation.

Keywords: tailings storage facility, dam breach, failure impact assessment, failure volume estimation

Introduction

Tailings dam break analysis follow five steps: 1) estimation of the release tailings volume, 2) estimation of the water in the tailings (moisture contents) and the free water in the facility (pond size), 3) calculation of tailings concentration, 4) development of the breach hydrograph, 5) routing the hydrograph downstream of the dam.

Unlike dam break analyses undertaken for Water Dams, the failure outflow from Tailings Dams contains a considerable amount of solids resulting in non-Newtonian fluid flow characteristics. Thus, the solid concentration is required to be calculated in the impoundment g to determine the type of fluid immediately prior to the failure. The selection of flood routing package needs to consider the amount of sediment concentration in the impoundment. Many existing dams comprise tailings that may be saturated material encompassing entrained water as well as supernatant water stored above the tailings in the storage facility, which is generated from both mining operations and rainfall. The tailings storage facilities will usually have an emergency spillway structure which is located above the pond elevation to discharge extreme storm events

The water level in the facility in a sunny day condition is identified to be the normal operation level in the pond. For many existing dams, the produced tailings from the mill convey to the tailings storage facility via pipelines laid over the embankment and discharge to the pond by spigots which are located at specific intervals along the pipeline. Therefore, the shape and beach profile is dependent on the tailings flow rate, spigot spacing and tailings characteristics, as well as operational considerations.

Present guidelines do not prescribe a detailed method to assess tailings dam break analyses and downstream hydraulic modelling of the failure flows. The majority of tailings failure assessments use the water storage dam fundamentals, empirical equations and software packages to generate the flood inundation maps. Water dam failure modelling have been widely investigated and there are numerous equations, numerical methods and software packages available to undertake the failure assessment. In contrast the tailings dam failure study has not an established and globally agreed method. The majority of tailings dam failure studies uses the common flood modelling packages to create the flood inundation maps. In many of these studies the run out material is assumed to be water with no consideration of solids concentration and rheological parameters of the tailings.

Rico et al (2008) identified a number of particular characteristics that make tailings dams more vulnerable to failure than water storage dams, namely: (1) embankments formed by locally derived fills (soil, coarse waste, overburden from mining operations and tailings); (2) multi-stage raising of the dam to cope with the increase in solid material stored and effluent (plus runoff from precipitation) released; (3) the lack of regulations on specific design criteria; (4) dam stability requiring continuous monitoring and control during emplacement, construction and operation of the dam, and (5) the high cost of remediation works following the closure of mining activities (Rico et al. 2007).

In a water dam breach it is assumed that the entire pond will release to the level of breach in the piping failure mode. In a tailings facility incident, the released volume depends on characteristics of tailings, amount of free water in the tailings and supernatant water in the pond as well as the liquefaction process. In most cases only a proportion of tailings will be released and the storage are never emptied, except in steep sided valleys and very low concentration tailings.

Rico et. al (2007) studied on 29 tailings dam which failed during 1965 to 2000 around the world. They found out that for tailings dams the height of embankment and runout distance of outflow has poor correlation. Therefore, they produced a relationship between outflow volume and runout distance which resulted in a better correlation. On this basis, they suggested to use an empirical equation that shows tailings outflow volume as a function of total volume of the storage. In their equation approximately one third of tailings and water is released during a failure.

Paulina et al (2018) studied on Rico' methodology considering 35 tailings dam failures based on larger storages and height rather than the original dataset used by Rico. They suggested a new empirical equation to estimate the breach volume as a function of total storage volume; this equation yields smaller release volume compared to Rico's method.

In both methods the released volume was plotted against the total storage volume and a regression line was developed with a correlation of R2 = 0.86% and 88% for Rico and Paulina, respectively. These methods are statistically based and do not take into account the tailings geotechnical or rheological parameters and the geometrical factors of the dam.

Tailings deposition model

Typically, the tailings slurry discharges to the impoundment from a mill via a pipeline network located on the embankment. The tailings deposition model is dependent on the factors like the discharge volume, the frequency of discharge, degree of tailings saturation and dry density of material.

The development of a deposition model is based on the site collected data, site survey and geometric design of the earthen embankments. Basically, the operation and maintenance of the facility, the number and

duration of operating spigots would impact on the beach slope as well as the volume of stored water in the pond. Whilst it is difficult taking into account all the operation and maintenance factors in the tailings deposition model the latest as-constructed survey and bathymetry data would be used to generate a three dimensional model which represents the realistic condition. The bathymetry data inform the volume of water in the pond during a normal operation in a sunny day condition. Where the bathymetry data is not available the normal operating level in the pond can be adopted as an average level; this level should be checked against the historical records of pond level.

In a rainy day situation the water level raises in the pool owning the rainfall and the discharge pump or gravity dewatering system are operational. The dewatering of the pool needs to be done to maintain the beach and keep the water away from the perimeter embankment. However, the dewatering system are considered to be non-operational during a hypothetical dam failure. Thus, the maximum water level in the pool which can occur during a rainy day condition is assumed to be at the emergency spillway structure.

Outflow volume estimation

The post failure slope has substantial effects on the shape, extent, length and the volume of the cone of released tailings from the storage. The post failure residual strength will be estimated using the geotechnical data obtained from site investigation and further stability analysis. On this basis the estimated post failure slope for the tailings facilities can be calculated. Previous historical failures indicate that a dam failure could extend to the full height of the dam.

When the storage facility including the tailings material and supernatant water is modelled, the outflow volume can be estimated by developing a release cone, which starts from toe of the downstream embankment. In order to capture the released tailings volume the breach location is located in the lowest level at the downstream embankment. Figure 1 and Figure 2 show the schematic facility configuration for pre and post failure.

The mechanism of failure is based on the formation of a trapezoidal channel within the embankment as described in Froehlichs study (2008). However the released volume in the impoundment is limited to the failure line and the embankment foundation. The trapezoidal cross section at the embankment is gradually transitioned to a triangle shape inside the impoundment.

The initial breach width can be estimated using the empirical equation of Froehlich and assuming the released volume is equal to a percentage of the total stored volume (say 50%). This base width will be adjusted using the same equation when the more realistic released volume is estimated by the geometric modelling.

The stored tailings within the impoundment may be saturated prior to failure. Whilst the embankment volume

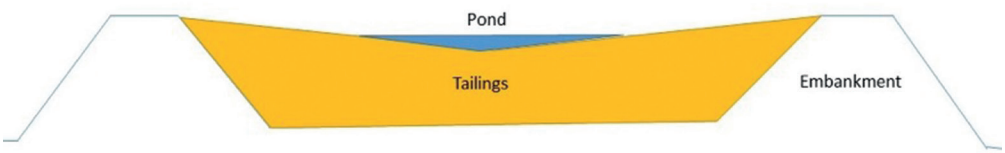

Figure 1 *Tailings Facility – Pre failure.*

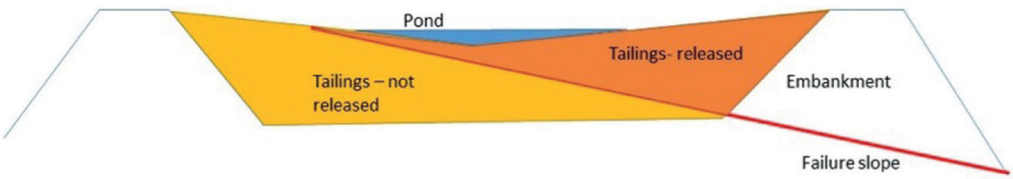

Figure 2 *Tailings Facility – Post failure.*

will be included in the released volume calculation, it has minimal proportion of the total tailings and water volume in the impoundment.

Furthermore, having the geometric model which represents the failure extent and shape in the facility it is possible to determine the encroachment of failure to the pool area. This method can give more realistic volume of released water when the pool is located distant from the failure point.

Tailings Facility – Post failure

Fluid motion is considered to be Newtonian when the shear stress is a linear function of the shear rate or non- Newtonian when viscous behavior is nonlinear and is more complex. The sediment content of the breach outflow is important to classify the flow as water, mud flood, mud flow or landslide. The vast majority of sediment flows fall between 20 to 55 percentage by volume. Very viscous, hyper-concentrated sediment flows are referred to mudflows which are non-homogenous and Non-Newtonian. The mudflow is highly viscous fluid with velocity generally much slower than water on the same slope. Figure 3 shows the flow classification as a function of sediment concentration.

It is required to determine the sediment concentration of outflow and the class of flow prior to selection of the hydraulic modelling package. According to Figure 3 if the volumetric sediment concentration is below 20% the flow could be considered as water. Therefore, the conventional water based flood modelling packages are appropriate to be applied. The water volume inside the water as well as the entrained water are required to be estimated.

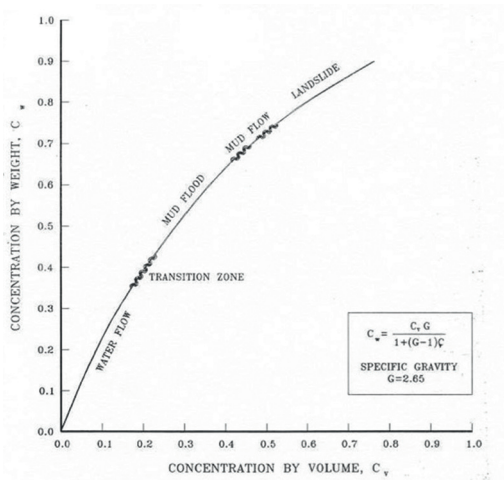

***Figure 3** Flow classification based on sediment concentration (Flo2d-2012).*

Water in tailings

The volume of entrained water can be calculated using the void ratio. Knowing the specific gravity and dry density of tailings the void ratio can be calculated using the below re-arranged equation: $e = \frac{Gs}{Y_d} - 1$

Where,

Gs = specific gravity of tailings solids

γ_d = tailings dry density (t/m3)

Sediment concentration

The volumetric sediment concentration for each failure case needs to be calculated using the supernatant water in the pool above the tailings and the entrained water in the tailings.

The sediment concentration by volume Cv is given by:

$$C_v = \frac{Volume\ of\ sediment\ (Vs)}{Volume\ of\ water\ (Vw) + sediment\ (Vs)}$$

The weight of sediment in the pond can be calculated using the total released weight using the dry density of tailings. The weight of solids shall be converted to volume using the specific gravity of solids.

Having the total released volume which includes the solids and entrained water (Vs + Vw) the sediment concentration by volume in the impoundment can be estimated for the "pre dam break" condition.

In the cases that the failure line encroaches the pool the supernatant water volume stored in the pool needs to be added to the total released tailings volume to calculate the sediment concentration of tailings for "post dam break" condition.

The volumetric sediment concentration is an important input parameter to:

- Determine the flow classification and selection of appropriate hydraulic software.
- Develop a breach hydrograph as an input to a "Non-Newtonian" hydraulic software.

Flood modelling

The breach parameters are required to be estimated to develop the outflow hydrograph

for a failure incident. The breach hydrograph can be developed using the reservoir flood routing models such as HEC-HMS. The parameters of breach width, side slope, formation time need to be calculated and input to the model. There are number of empirical equations (e.g. Froehlich 2008) to estimate the physical breach parameters such as the average width and time of formation.

Volume conservation should be considered in the breach hydrograph development ensuring the released volume is equal to the total hydrograph volume. The peak discharge should occur at breach formation time estimated from empirical equation. Costa (1988) proposed several empirical equations obtained using dam height and volume of reservoir and the resulting peak flow discharge when it failed.

Numerous packages are available to undertake the flood modelling and route the breach hydrograph to assess the run-out distance of tailings and the impact on the environment. Having the sediment concentration of the outflow above 20% it is suggested to use Non-Newtonian package such as Flo2D. The traditional water base modelling packages can be used to evaluate the inundation areas and flow depth.

Conclusions

A methodology to estimate the released tailings volume and create a breach hydrograph is presented in this study. The method combines supernatant water and tailings volume outflow in order to create the breach hydrograph for input into a non-Newtonian hydraulic model if the volumetric sediment concentration is above 20%.

The post failure slope has substantial effects on the shape, extent, length and the volume of the cone of released tailings from the storage. The estimate of post failure residual strength is required using the geotechnical data obtained from site investigation and further stability analysis.

The geometric model which represents the exiting embankments, pond location, failure extent and shape in the facility gives better understanding about the failure length and the possibility of encroachment of failure to the pool area. This method results in more realistic volume of released water when the pool is located distant from the failure point. The pool water would impact on the total released volume particularly in a sunny day failure.

The volume of sediment in the pond can be calculated using the total released volume using the dry density of tailings and specific gravity of tailings. In order to classify the breach outflow at the failure location, the sediment concentration needs to be estimated using the tailings solid volume and total water volume.

In the cases that the failure line encroaches the pool area it is essential to add the supernatant water volume stored in the pool to the total released tailings volume.

Acknowledgements

The author thanks Manoj Laxman for the review and critical comments on earlier versions of this text.

References

Costa, J.E. 1985. "Floods from Dam Failures." U.S. Geological Survey Open-File Report No. 85-560," U.S. Geological Survey, Denver, Colorado.

Froehlich, D.C. 1995a. "Peak Outflow from Breach Embankment Dam," Journal of Resources Planning and Management, Vol. 121, no. 1, pp 90-97.

Froehlich, D.C. 1995b. "Embankment Dam Breach Parameters Revisited," Water Resources Engineering.

Flo-2D. 2012. Simulating Mudflows.

Jeyapalan, J.K., J.M. Duncan, and H.B. Seed. 1982. "Analyses of Flow Failures on Mine Tailings Dams." Journal of Geotechnical Engineering, ASCE, Vol. 109, No. GT2, Feb., pp 150-171.

Rico M., G. Benito and A. Díez-Herrero. 2007. "Floods from Tailings Dam Failures." Journal of Hazardous

Materials. Vol. 154(1-3), pp 79-87.

Tailings Info, 2014. Tailings Related Accidents – Failure, Breaches and Mudflows. Internet accessed on May 12,2015. (www.tailings.info/knowledge/accidents.htm).

Paulina, et.al. 2018. "Tailings Dam Failures: Updated Statistical Model for Discharge Volume and Runout", Environments, 5, 28.

Groundwater Nitrate Bioremediation of a Fractured Rock Aquifer System in South Africa

Paul Lourens[1], Mariana Erasmus[2], Robert Hansen[3], Amy Allwright[1]

[1]*Institute for Groundwater Studies, Faculty of Natural and Agricultural Sciences, University of the Free State, 205 Nelson Mandela Drive, Bloemfontein, 9300, South Africa, lourenspjh@ufs.ac.za, allwrightaj@ufs.ac.za*

[2]*Saense Platform, Department of Microbial Biochemical and Food Biotechnology, Faculty of Natural and Agricultural Sciences, University of the Free State, 205 Nelson Mandela Drive, Bloemfontein, 9300, South Africa, erasm@ufs.ac.za*

[3]*Department of Geology, Faculty of Natural and Agricultural Sciences, University of the Free State, 205 Nelson Mandela Drive, Bloemfontein, 9300, South Africa, hansenr@ufs.ac.za*

Abstract

Due to the importance of groundwater in South Africa, the University of the Free State has successfully developed a zero waste bioremediation technology to treat nitrate pollution in water. Groundwater nitrate pollution of a fractured rock aquifer arose due to the storage of fertilizer effluent in unlined quarries. Numerical model simulations indicates that the proposed remediation removes the nitrate from the aquifer in a shorter timescale than the predicted natural attenuation. Treating the polluted water on site with the zero-waste bioremediation technique, and then re-injecting the treated water into the aquifer provides a holistic and sustainable solution to nitrate pollution.

Keywords: bioremediation, groundwater, fertilizer effluent, numerical groundwater model, nitrate

Introduction

The use of bioremediation, especially denitrification, to remove site contaminants such as nitrate (without the use of filters or ion exchange) is a very complex process with multiple variables. Figure 1 displays the nitrogen cycle with the pathways of interest, namely the anammox, nitrification, ammonification, nitrogen fixation and denitrification. Even though leaching, mineralization, immobilization and volatilization forms part of the nitrogen cycle, it is not the main focus of this report as this system only focus on water treatment. These pathways are driven by various factors including biological, physical and physiological factors. Research has demonstrated that microorganisms have the ability to survive, adapt, and eventually thrive in almost every environment (Stevens et al. 1993; Phelps et al. 1994; Fredrickson & Onstott 1996; Colwell et al. 1997; Onstott et al. 1998; Pedersen et al. 2000; Moser et al. 2003; Kieft et al. 2005; Gihring et al. 2006; Onstott et al. 2009; 2011; Ragon et al. 2013; Lau et al. 2014; Rajala et al. 2015).

Nitrate reduction is a naturally occurring process, which is performed by a large group of heterotrophic facultative anaerobic bacteria, such as *Paracoccus denitrificans, Rhodobacter sphaeroides* and *Pseudomonas spp.* The ultimate by-product is nitrogen gas (N_2) which follows the following reduction pathway: nitrate (NO_3^-) → nitrite (NO_2^-) → nitric oxide (NO) → nitrous oxide (N_2O) → nitrogen gas (N_2) (fig. 1).

The groundwater nitrate pollution arose due to the storage of fertilizer effluent in two unlined dolerite quarries. This resulted in the degradation of the groundwater quality of the underlying fractured rock aquifer. Nitrate may enter groundwater with ease and migrate over large distances from the source due to the high solubility of nitrate, and because soils are largely unable to retain anions (fig. 2).

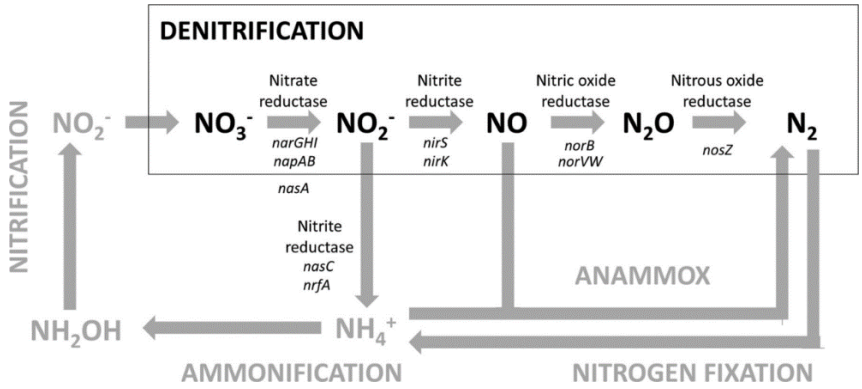

Figure 1 *The Nitrogen Cycle (Taken from Alvarez et al. 2014).*

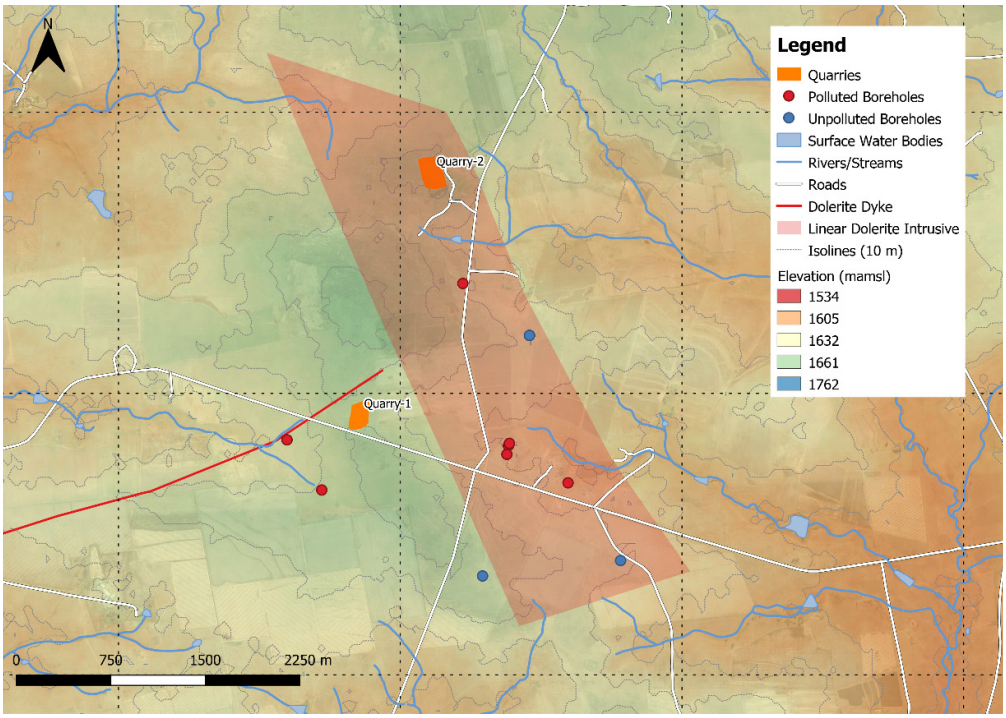

Figure 2 *Study Site Layout Map.*

Materials and Methods

Bioremediation – Proof of Concept

A customary nitrate reduction column was prepared according to standard operating procedures used in the TIA/SAENSE platform. The column consisted of 110 mm PVC pipe with a height of 1 m, containing dolomite as a solid matrix and sealed at both ends to create an anoxic environment. The column was equipped with In/Out valves and connected to a peristaltic pump with silicone tubing. The drainage volume of the column was measured, which was used to calculate the hydraulic retention time (HRT) of the column. Influent water containing an electron donor was introduced at the base of the column at the determined HRT. Before the nitrate contaminated water was added, the column was seeded with the microbial community that consisted of known nitrate reducers and the column was closed until

optimal Oxidation Reduction Potential (ORP) conditions for nitrate reduction (± -150 mV) was reached. Once optimal ORP conditions were obtained, the column ran at a HRT of 24 hours.

The added donor will allow the microbial community to deal with higher amounts of nitrate and this relates to an increased Biological Oxygen Demand (BOD) and will enhance growth. To have maximum growth and denitrification, the electron donor is stoichiometrically balanced with the electron acceptors (oxygen, to promote anaerobic conditions and nitrate, for denitrification). The system therefore creates anoxic conditions by controlling the oxidation reduction (redox) state. Other factors that have an influence on denitrification such as temperature, pH and HRT was also controlled throughout the laboratory column experiment. The column effluent (treated water) was sampled intermittently and analysed for pH, DO, ORP, Temp, EC, NO_3-N, NO_2-N and NH_3-N. These parameters were used to determine if any working conditions could be changed in the column to ensure maximum nitrate reduction. Due to the high concentration of nitrates present in the water, the column first ran on diluted water for 60 days. Thereafter the dilution factor was decreased in order to identify the highest concentration of nitrate that the microbial consortium could tolerate while still reducing nitrate to levels below the SANS 241 class 1 limits.

Groundwater Quality Interpretation

Quarterly groundwater monitoring data for the study site was available from 2015 to 2018. This data was analysed statistically as well as over time to determine the groundwater response of specifically the nitrogen compounds, i.e. nitrate and ammonia in the groundwater.

Groundwater Numerical Modelling

A numerical groundwater model was developed for the study site to achieve the set objectives and the form the base for the numerical groundwater transport models. The FEFLOW software programme (Version 7.1) was used for the numerical groundwater model. The software applies the Finite Element method to approximate differential equations and simulate fluid flow and transport of dissolved constituents in the subsurface with reactive components.

The purpose of the model was to simulate contaminant transport in the groundwater system and to evaluate the remediation strategy for the site. To achieve this aim, modelling scenarios were performed using the developed, calibrated numerical groundwater model.

Remediation Strategy/Approach

The remediation strategy is to pump treated water from a bioremediation plant to the two quarries that initially contained fertilizer effluent water that polluted the underlying aquifer/groundwater. These two quarries are situated on a topographic high (water divide), thus if the quarries are filled with water, it will generate an artificial hydraulic head, recharging the underlying aquifer. The treated water will this be used to flush the underlying aquifer to dilute the nitrate concentrations within the groundwater. It is likely for this treated water to enter the same preferential flow paths of that of the fertilizer effluent initially dumped in the quarries.

Results and Discussion

The results of the Nitrate Reduction Column Tests (fig. 3) are discussed below:

I. Stage One Results (inlet effluent diluted five times)

a. The average nitrate reduction was 88.4% during the first 60 days and was below the SANS241 standards for drinking water.
b. No nitrite or ammonium was produced, indicating that complete denitrification took place, with final concentrations of 0.049 mg/L and 1 mg/L, respectively.
c. The increase of the nitrate concentration in the outlet values during 31/01/2017 and 09/02/2017 happened, because feeding of the donor in the column was stopped to determine if the system (microorganisms) will be able to restore itself once introduction of the donor was again resumed. The system was able to restore itself as can be seen in the graph.

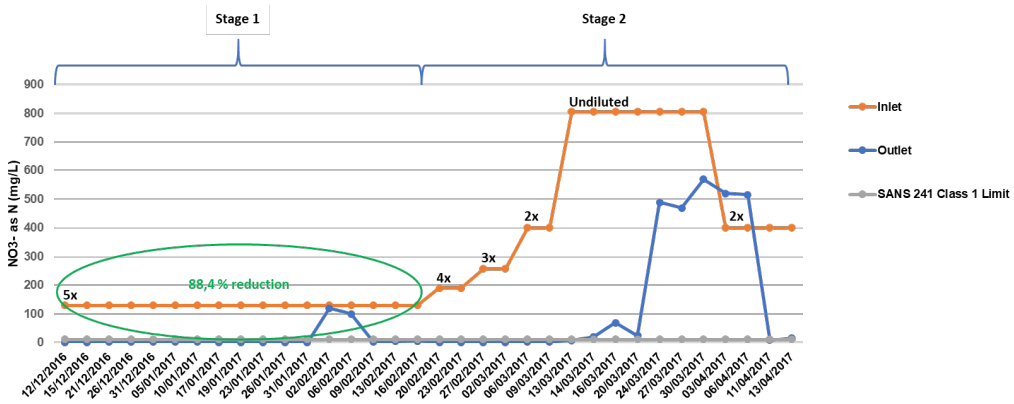

Figure 3 Nitrate (as N) profiles for the influent and effluent water.

II. Stage Two Results (stepwise increase of inlet effluent concentration):

a. On 16/02/2017 the dilution factor was decreased to four times (4×) to contain an inlet nitrate concentration of ~190 mg/L and for the following seven days, the nitrate reduction could be maintained below the SANS241 standards (1.3 mg/L as N, resulting in 99.3% removal).
b. On 23/02/2017, the dilution factor was again decreased to three times (3×) to contain an inlet nitrate concentration of ~258 mg/L and for the following seven days, the nitrate reduction could still be maintained below the SANS241 standards (0.9 mg/L as N, resulting in 99.7% removal).
c. On 02/03/2017, the dilution factor was again decreased to two times (2×) to contain an inlet nitrate concentration of ~400 mg/L and for the following seven days, the nitrate reduction could once again be maintained below the SANS241 standards. The nitrate outlet was 2.1 mg/L (as N), resulting in 99.5% removal. The nitrite and ammonium concentrations were 0.05 mg/L and 0.26 mg/L, respectively.
d. On 09/03/2017, the inlet was pumped undiluted into the column with an inlet nitrate value of 805 mg/L. During the following seven days, the nitrate outlet gradually increased to 24.3 mg/L, the nitrite increased to 3.92 mg/L and the ammonium increased to 0.75 mg/L.
e. From 24/03/2017 to 30/03/2017, the outlet values increased drastically, having nitrate and nitrite concentrations of 570 mg/L and 63 mg/L, respectively. The ammonium remained at 0.27 mg/L.
f. On 30/03/2017, the pump was stopped and the column was closed for five days. The inlet was again diluted two times (2×) to a nitrate concentration of ~400 mg/L before starting the column for another 14 days.
g. During the last week of the experiment (11/04/2017 – 13/04/2017) the outlet values decreased again for nitrate, nitrite and ammonium to 15.2 mg/L, 2.02 mg/L and 1 mg/L, respectively.
d. The highest nitrate inlet value observed in this study, that did not lead to incomplete denitrification, was two times (2×) diluted i.e. ~400 mg/L of nitrate, however nitrate concentrations between 400 mg/L and 800 mg/L remains to be tested.

The most polluted borehole, indicating the highest nitrate concentration over the monitoring period (maximum = 7 692 mg/L as NO_3^-) is also the closest borehole down gradient from Quarry1 along a dolerite dyke that acts as a preferential groundwater flow path for polluted water to flow from the quarry to the borehole. A plot of the time series data from 2015 to 2018 indicates a trend of decreasing nitrate concentrations with time (fig. 4).

A trend line of the average concentration changes throughout the monitoring history is also shown on fig. 4. This trend line can

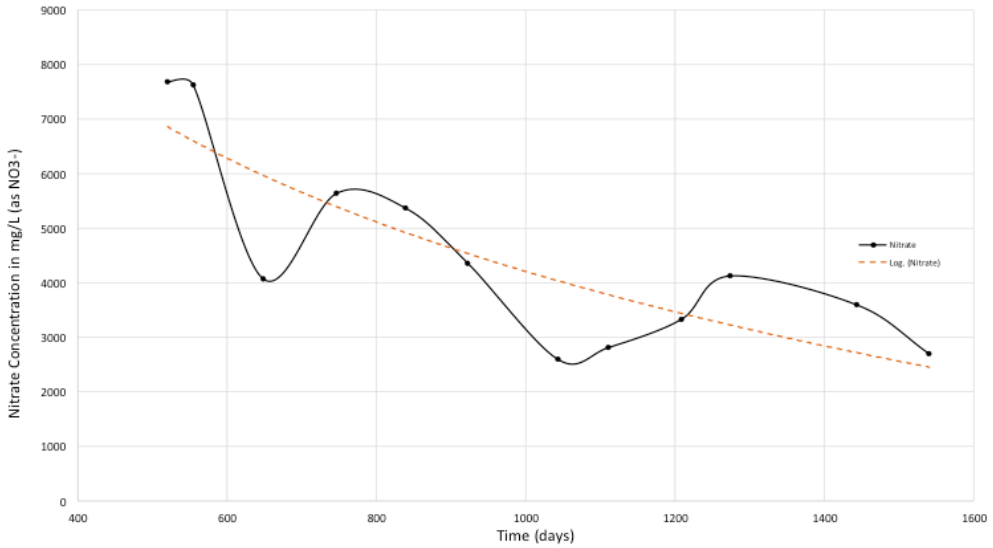

Figure 4 Time Series data of nitrate concentrations in the most polluted borehole down gradient from Quarry-1.

be described by the following mathematical expression:

$y = -4060 \ln(x)+32\,253$

The equation expresses the average behaviour of nitrate concentration (as NO_3^-) over time, where time in fig. 4 is in days. Evaluation of this expression in conjunction with the time series data indicates that the rate of nitrate decrease is such that the nitrate concentration is projected to reach concentrations below the SANS 2015 drinking water limit of 50 mg/L (as NO_3^-) in the year 2024.

The simulations from the numerical model indicates that the proposed remediation removes the nitrate from the most polluted borehole in a shorter timescale (between the year 2021 and 2023) than the predicted natural attenuation (fig. 5).

The analysis above is based on the assumption that the source is totally removed and that the only nitrate present in the system is the nitrate in the groundwater itself.

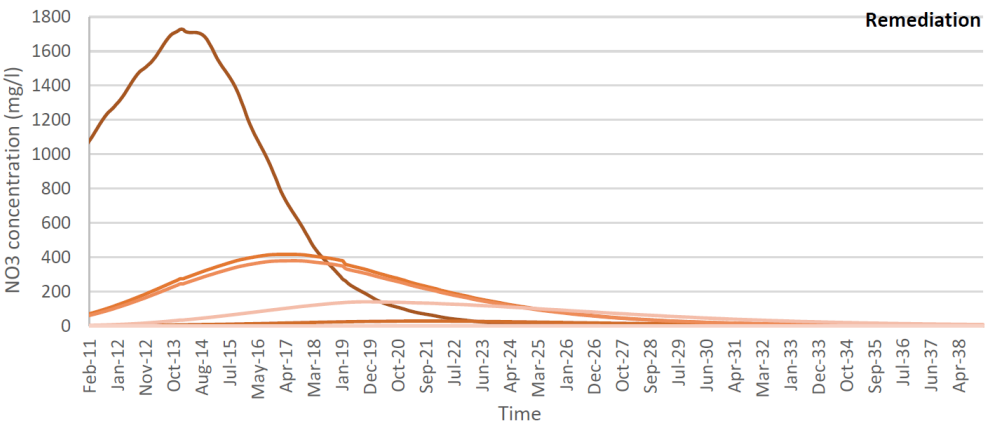

Figure 5 Simulated nitrate concentrations (as N) with the implementation of the remediation strategy.

Conclusions

The results obtained from the laboratory column test indicates that an effective bioremediation strategy can be developed for the complete nitrate reduction in the polluted water. The simulations from the numerical model indicates that a combined remediation strategy of pumping contaminate water, treating it on site with the zero-waste bioremediation technique, and then re-injecting the treated water into the aquifer can provide a holistic and sustainable solution to the nitrate pollution.

References

Alvarez L, Bricio C, Bles, A, Hidalgo A and Berenguer J (2014) Transferable Denitrification Capability of Thermus thermophilus. Applied and Environmental Microbiology. 80:19-28.

Fredrickson JK and Onstott TC (1996) Microbes Deep Inside the Earth. Sci Am. 275:68-73

Gihring TM, Moser DP, Lin L, Davidson M, Onstott TC, Morgan L, Milleson M, Kieft TL, Trimarco E, Balkwill DL and Dollhopf ME (2006) The Distribution of Microbial Taxa in the Subsurface Water of the Kalahari Shield, South Africa. Geomicrobiol. J. 23:415–430.

Kieft TL, McCuddy SM, Onstott TC, Davidson M, Lin L, Mislowack B, Pratt L, Boice E, Sherwood Lollar B, Lippmann-Pipke J, Pfiffner SM, Phelps TJ, Gihring T, Moser D and van Heerden A (2005) Geochemically Generated, Energy-Rich Substrates and Indigenous Microorganisms in Deep, Ancient Groundwater. Geomicrobiol. J. 22:325–335.

Lau MCY, Cameron C, Magnabosco C, Brown CT, Schilkey F, Grim S, Hendrickson S, Pullin M, Sherwood Lollar B, van Heerden E, Kieft TL and Onstott TC (2014) Phylogeny and Phylogeography of Functional Genes Shared Among Seven Terrestrial Subsurface Metagenomes Reveal N-Cycling and Microbial Evolutionary Relationships. Front. Microbiol. 5:531.

Moser DP, Onstott TC, Fredrickson JK, Brockman FJ, Balkwill DL, Drake, GR, Pfiffner SM, White DC, Takai K, Pratt LM, Fong J, Sherwood Lollar B, Slater G, Phelps TJ, Spoelstra, N, DeFlaun M, Southam G, Welty AT, Baker BJ and Hoek J (2003) Temporal Shifts in the Geochemistry and Microbial Community Structure of an Ultradeep Mine Borehole Following Isolation. Geomicrobiol. J. 20:517–548.

Onstott TC, Colwell FS, Kieft, TL, Murdoch L and Phelps TJ (2009) New Horizons for Deep Subsurface Microbiology. Microbe Magazine. 4(11):499–505.

Onstott TC, Phelps TJ, Kieft T, Colwell FS, Balkwill, DL, Fredrickson JK and Brockman FJ (1998) In: Enigmatic Microorganisms and Life in Extreme Environments. Springer Science & Business Media Publishers. ISBN: 9780792354925.

Pedersen K, Motemedi M, Karnland O and Sandén T (2000) Cultivability of Microorganisms Introduced into a Compacted Bentonite Clay Buffer under High-Level Radioactive Waste Repository Conditions. Eng Geol. 58:149-161.

Phelps TJ, Murphy EM, Pfiffner SM and White DC (1994) Comparison between Geochemical and Biological Estimates of Subsurface Microbial Activities. Microb. Ecol. 28:335-349.

Ragon M, Van Driessche AES, García-Ruíz JM, Moreira D. and López-García P (2013) Microbial Diversity in the Deep-Subsurface Hydrothermal Aquifer Feeding the Giant Gypsum Crystal-Bearing Naica Mine, Mexico. Frontiers in Microbiology. 4:37.

Rajala, P., Bomberg, M., Kietäväinen, R., Kukkonen, I., Ahonen, L., Nyyssönen, M. and Itävaara, M. (2015). Rapid Reactivation of Deep Subsurface Microbes in the Presence of C-1 Compounds. Microorganisms. 3:17-33.

Stevens TO, McKinley JP and Fredrickson JK (1993) Bacteria Associated with Deep, Alkaline, Anaerobic Groundwaters in Southeast Washington. Microb Ecol 25:35-50.

The Use of Systematic Sampling and XRF-XRT Based Scanning to Determine Potential Recovery of Metals from Waste Rock

Stefan Sädbom[1], Lotta Sartz[1], Jan-Erik Björklund[2], Mathias Svenlöv[2], Mikael Bergqvist[3], Mattias Bäckström[1,4]

[1]*Bergskraft Bergslagen AB, Fordonsgatan 4, 692 71 Kumla, Sweden, stefan.sadbom@bergskraft.se; lotta.sartz@bergskraft.se; mattias.backstrom@bergskraft.se*

[2]*Lovisagruvan AB, Håkansboda 1, 711 77 Stråssa, Sweden, jan-erik.bjorklund@lovisagruvan.se; mathias.svenlov@lovisagruvan.se*

[3]*Orexplore AB, Box 7527, 103 92 Stockholm, Sweden, mikael.bergqvist@orexplore.com*

[4]*Man-Technology-Environment Research Centre, Örebro University, 701 82 Örebro, Sweden, mattias.backstrom@oru.se*

Abstract

It is difficult to evaluate the potential for reprocessing and extraction of minerals from waste rock with valuable and/or harmful elements.

We suggest a new sampling strategy/protocol for waste rock, specifically developed for historic mining sites, in combination with XRF-XRT scanning with a GeoCore X10 instrument.

Håkansboda historical mine site in Sweden was used as a case study to look at the potential for the combination of techniques.

The combination of the suggested randomized sampling strategy/protocol and the dataset from the GX10 scanning enables prediction of amenability for pre-processing with the use of mechanical sorting or if the extraction of valuable minerals only can be achieved through fine grinding, flotation or leaching.

Keywords: mining waste, secondary resource, sampling, mineral recovery, tomography

Introduction

Mining waste is abundant and poses an environmental problem. It is also possible that some of the mining waste are suitable secondary resources for reprocessing. In order to determine both environmental impact and resource potential detailed characterization is required. However, it is usually not practical to excavate the entire area and sometimes also cultural heritage issues pose a hurdle to extensive sampling. It is therefore important to have methods for sampling considering these problems but still provide useful results.

It is often complicated to sample and determine average concentrations of elements in historical waste rock. This makes it hard to evaluate the potential for reprocessing and extraction of minerals with valuable and/or harmful elements.

Early evaluation of the potential for reprocessing also need to consider the concentrations of relevant elements, their host mineralogy and paragenesis, grain sizes and distribution between different size fractions in the mining rock waste.

In this paper, we present a new sampling strategy/protocol for waste rock, specifically developed for historic mining sites. We also look at the combination of X-ray fluorescence (XRF) and X-ray tomographic (XRT) scanning in order to determine the potential for reprocessing.

Methods

Geological setting

A very quick estimate of the potential for recovery of valuable minerals from waste rock can be obtained by scanning remains of sample preparation pulp from destructive analysis. Håkansboda historical mining site in Sweden was used as a case study to look at the potential for the combination of techniques (sampling strategy and XRF-XRT scanning). Håkansboda mining site has

primarily been mined for copper, but also some cobalt. The mineralization is sulfide based and contains chalcopyrite ($CuFeS_2$), pyrite (FeS_2), pyrrothite ($Fe_{1-X}S$), sphalerite (ZnS), galena (PbS), arsenopyrite (FeAsS) and some cobaltite (CoAsS).

Sampling strategy and chemical analysis

Sampling of mining waste is anything but straightforward. Heterogeneity issues, for instance, make the use of classical statistical methods problematic. It is important to understand the creation of mining waste deposits in order to understand how to sample and suggesting an approach for surveying and sampling mining waste.

In order to collect a fair sample from a mining waste deposit it is crucial to know how the waste has been generated, why it is deposited in different areas and how the handling of the waste has influenced its homogeneity and thus the prerequisite for collecting a fair sample.

The concept of using cumulative moving average (CMA) to determine when enough samples have been collected to establish saturation is described and exemplified with some analytical results from the historical mining site Håkansboda in Sweden.

It is also suggested that several seemingly peripheral, parameters regarding the mining site (shape of the deposit, vegetation cover, vegetation type etc) are recorded in order to increase knowledge about the site.

It is, however, important to remember that every mining site is unique and site-specific information is important in order to be able to revise the sampling strategy.

Before samples are collected it is important to define the waste piles/objects that are going to be sampled. Each object should ideally cover an area with the same or similar properties. Pieces (20-75 mm) was chipped from rocks in different waste piles/objects. Only one chip was collected from each primary piece. 25-50 pieces were collected for each sample (2-5 kg). To be as objective as possible when chip was selected favouring by size, colour, accessibility, shiny or dull minerals were avoided. It is important to remember that dense material generally stay close to the point of disposal and large pieces will tumble down to the base of the slope. Samples should therefore be collected evenly to include the various segregations that may have occurred as a result of dumping.

At vegetated piles vegetation was carefully lifted and samples were collected without doing an excavation.

Collected composite samples were sent to MS Analytical, Stensele, Sweden, for sample preparation (crushed to 70% passing 2 mm). A subsample was split and sent for destructive analysis at MS Analytical in Vancouver. Digestion was performed using aqua regia or a four acid mix for the lithogenic elements while analysis were performed by ICP-OES and ICP-MS.

A compromise between the costs for sampling and, based on empirical evidence from earlier investigations, an estimated absolute confidence error of about 25-50% from the true average. 25% is commonly used as a requirement for pre-feasibility studies.

To find the point of saturation, a study of the cumulative moving average (CMA) value of the EMOI (Element or Mineral of Interest) through a series of samples from the same object (same population) will indicate when saturation has been satisfactorily reached. 36 composite samples were collected from Håkansboda historical mining site. Sample saturation, here defined as the point when additional samples do not significantly change the average obtained by previous samples.

XRF-XRT scanning

Remaining sample pulp after crushing and splitting was wrapped in thin plastic cling film and placed in the drill core sample tube. After scanning, which took less than 20 min, it was possible to study a tomographic image of the scanned sample and get indicative chemistry, measured and mineral stoichiometric calculated bulk density and distribution of the dense particles in the sample.

Drill core scanning by combined XRT (X-ray tomography) and XRF (X-ray fluorescence) was performed using the GeoCore X10 instrument (Orexplore AB, Stockholm, Sweden). For elemental concentrations, the GeoCore X10 utilizes a combination of XRF spectra and attenuation to calculate stochiometric solutions for mineral compositions and final elemental abundances (in wt. % or mg/kg) per unit volume of drill core. Scanning data was imported into the

Orexplore Insight software, to visualize and analyze the obtained digital drill core.

The rendering is reflecting attenuation expressed as metallic aluminum equivalents with the current instrumental setup. Attenuation can not be directly translated to mineralogy, but as a guidance for some case-relevant non-silicate minerals, the theoretical attenuations are estimated to be about: pyrite 3.88, pyrrhotite 4.00, sphalerite 4.17, arsenopyrite 6.52 and cobaltite 6.68.

Results and discussion

Sampling strategy

From a sample set of 36 waste rock samples from Håkansboda the average concentrations were 6.6% sulfur, 10 000 mg/kg dw copper, 410 mg/kg dw cobalt, 4 300 mg/kg dw arsenic, 9 620 mg/kg dw zinc and 10.4% iron.

Individual concentrations for each sample as well as cumulative moving average concentrations (CMA) are presented in fig. 1 for sulfur, copper, cobalt and arsenic. It is clear that the CMA is getting close to the true average values (within 20-25%) for all presented elements after roughly 15 samples. In practice this means that by collecting and analysing around 15 composite samples from a site you will get a good handle about the average concentrations at the site. It is, however, important to note that even if 15 composite samples are often enough at this site another type of mining waste might require another number in order to reach the true

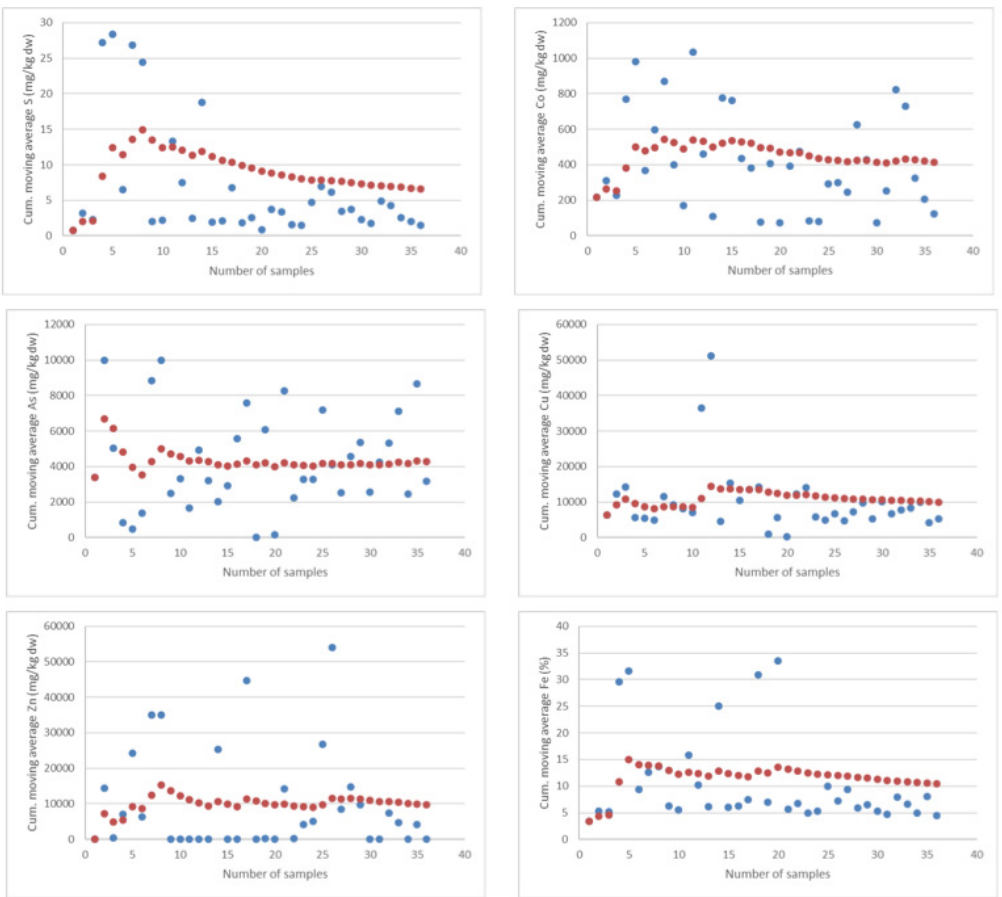

Figure 1 *Cumulative moving average concentrations (mg/kg dw) for sulfur, cobalt, arsenic, copper, zinc and iron at Håkansboda historical mining site in Sweden. Average concentrations are calculated using increasing numbers of samples (from 1+n until all samples have been included). Calculated average (n 36) concentrations for sulfur, cobalt, arsenic, copper, zinc and iron are 6.6%, 410 mg/kg dw, 4 300 mg/kg dw, 10 000 mg/kg dw, 9 620 mg/kg dw and 10.4%, respectively.*

average. Different elements behave differently and have different distribution patterns, some elements are more "nuggety" than others (i.e. compare the distribution of gold versus a rock-forming element like silica).

XRF-XRT scanning

The GeoCore is primarily designed for scanning solid drill cores but has in this experiment been used for small particles. All samples have been scanned, but only results from two samples will be presented. The tomographic image of sample HAK19035 in fig. 2 shows on the left the tomographic image of the total sample length (0.247 m corresponding to 755 g at a measured bulk density of 2.32 g/cm^3) and on the right a 3D-image of a selected 25 mm (88.2 g) subsample (shown in blue to the left). The subsample is estimated to contain 118 visible non-silicate mineral grains.

Another example is HAK19016 in fig. 3. The entire sample is 0.346 m corresponding to 878 g at a measured bulk density of 2.48 g/cm^3 and the subsample (in blue) is 43 mm (108 g). The subsample is estimated to contain 129 visible non-silicate mineral grains.

It is quite clear from both samples that dense minerals containing trace elements are mainly found as discrete particles. These discrete particles consists of the same mineral and from the results it can be concluded that at this liberation minerals and thus the element of interest can be recovered using physical sorting. There is also information about the sulfide presence in the sample. The data can also be used to determine how much of the potential acid generating sulfide minerals are remaining in the waste after reprocessing.

In tab. 1 below a comparison between element concentrations based on the XRF scans from the GeoCore) and conventional wet chemistry (digestion and ICP analysis) are presented. In general the reported concentrations from the GeoCore are after a ca 20 minute scan, in the same order of magnitude as the conventional analysis but somewhat lower. It is, however, important to remember that the concentrations from the GeoCore are based on the entire section while the concentrations from the conventional analysis are only based on a small fraction

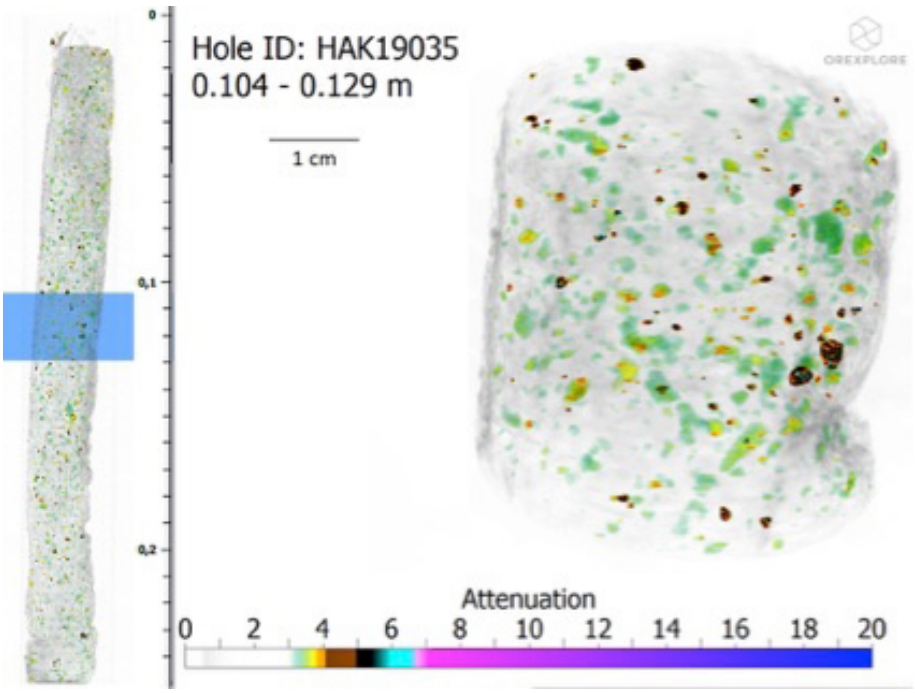

Figure 2 *Attenuation for sample HAK19035. Magnification shows the section 0.104-0.129 m. Minerals with attenuation below 3 has been rendered transparent in the image (carbonates and silicate minerals).*

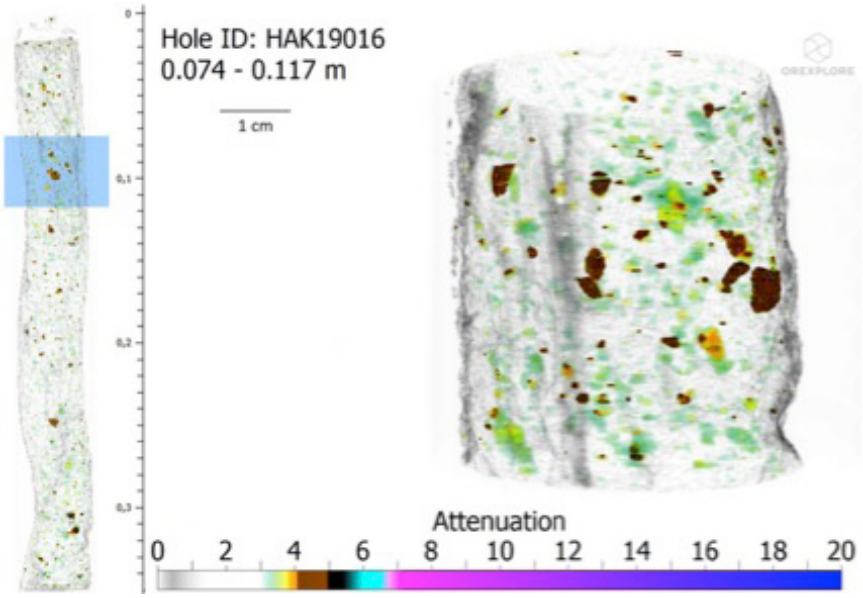

Figure 2 *Attenuation for sample HAK19035. Magnification shows the section 0.104-0.129 m. Minerals with attenuation below 3 has been rendered transparent in the image (carbonates and silicate minerals).*

of the section. It is thus clear that even if the GeoCore is not calibrated for element concentration determination the results are still a very good indication about the presence of trace elements as well as potentially acid generating sulfur. Since also the mineralogy are determined the acid generating potential can quickly be determined for entire sections of waste rock or exploration drill cores.

Conclusions

A quick method has been suggested as an answer to a difficult practical problem. It was found that by using a randomized sampling it is enough to sample approximately 15 composite samples from a site in order to obtain an average within acceptable limits from the "true" average.

Scanning of the crushed waste rock with a XRF-XRT scanner (GX10) provided an indication on elemental concentration, elemental associations and the distribution of grades between particles. This information provided information about the association and clustering of elements within the waste rock and if the mineralization is enough liberated for mechanical sorting at the chosen particle size. The results will also provide an indication about how much of the potentially acid producing sulfides that will be removed from the site when the elements of interest are being recovered.

In summary, the combination of the suggested sampling strategy/protocol and the dataset from the GX10 enables prediction of amenability for pre-processing with the use

Table 1 *Comparison between estimated concentrations of sulfur, iron, zinc, copper, cobalt and arsenic based on the GeoCore scans and conventional wet chemistry (MS Analytical, Vancouver).*

Element mg/kg dw	HAK19016 Conv.	HAK19016 GeoCore	HAK19035 Conv.	HAK19035 GeoCore
Sulfur	244 000	129 000	188 000	97 500
Iron	136 000	73 900	250 000	81 400
Zinc	350 000	89 500	25 300	8 790
Copper	9 290	4 720	15 300	5 890
Cobalt	825	283	776	378
Arsenic	>10 000	2 090	2 010	809

of mechanical sorting or if the extraction of valuable minerals only can be achieved through fine grinding, flotation or leaching.

Sampling of mining waste is impossible, but it can still be done!

Acknowledgements

This study is part of the X-MINE Project funded by the European Union's Horizon 2020 research and innovation program under grant agreement 730270.

References

Sädbom S, Bäckström M (2018) Sampling of mining waste – historical background, experiences and suggested methods. BKBAB 18-109 Rep, Bergskraft Bergslagen AB, 71 pp

The Effects of Using Hydrogen Peroxide to Provide an Improved HDS Process

Jodie Evans[1], Richard Morgan[2], Richard Coulton[3]

[1]*Siltbuster Ltd, Williams Building, Kingswood Gate, Monmouth NP25 4EE Jodie.evans@siltbuster.com*

[2]*Siltbuster Ltd, Williams Building, Kingswood Gate, Monmouth NP25 4EE Richard.morgan@siltbuster.com*

[3]*Materials Recovery Systems Ltd, Unit 48A, Symondscliffe Way, Severnbridge Industrial Estate, Portskewett, Caldicot NP26 5PW Richard.coulton@m-rs.co.uk*

Abstract

HDS treatment plants are effective active AMD remediation processes, comprising of two-stage systems using aeration as the oxidant. In this paper, the practicality of using H_2O_2 as an alternative oxidant to reduce to a single-stage HDS plant was assessed. Comparative trials were conducted (two-stage (conventional HDS) and single-stage processes) on a bench-scale HDS rig, treating a continuous flow of 150 mg/L Fe net alkaline synthetic mine water. Results demonstrate that HDS treatment plants can be modified to a single stage when using H_2O_2 without compromising water quality or dewatering capabilities (42% dewatered solid content) of the HDS process.

Keywords: AMD, HDS, Aeration, H_2O_2

Introduction

Whilst the mining industry is one of the leading markets of the global economy (Rudko 2020), the consequences of mining cause substantial long-term environmental and ecological threats (Ojonimi et al. 2019). Acid Mine Drainage (AMD) is considered a global environmental issue (Balci and Demirel 2017) with strict surface and ground water quality targets driving the development of AMD remediation strategies. Although passive treatment processes are more favourable remedial options for AMD, if the contaminant load is too high, or there are constraints with land availability, then active treatment is necessary (Coulton et al. 2007).

One of the most well-established forms of active AMD remediation involves chemical treatment to oxidise Fe (II) to Fe (III), manipulate pH and subsequently precipitate Fe(III) as oxyhydroxides ($Fe(OH)_3$) (Fan et al. 2019). Fe oxidation and precipitation can also aid in the removal of other dissolved metallic species by co-precipitation. Removing metals in this way chemically entraps large amounts of water, generating a gelatinous Low-Density Sludge (LDS) with a solids content of 2-5% (Coulton et al. 2004). Resulting in poor settling velocities and a voluminous sludge for disposal. Continuous recirculation of LDS back into the process provides sites for crystal nucleation, increasing the solids content to 20-50% (Coulton et al. 2004; Murdock, Fox and Bensley 1993) converting from LDS to High Density Sludge (HDS). Examples of UK based HDS treatment plants include, Wheal Jane (Coulton et al. 2003a), Dawdon Colliery (Bailey et al. 2013), Horden Colliery and Blenkinsopp (Wyatt et al. 2018).

Conventionally the HDS process is undertaken in two stages using air for oxidation. Consequently, the process has high capital costs requiring at least 2 reaction vessels; the sizing of main vessel being determined by the pH and the rate of Fe oxidation. In addition, operating costs are high due to the amount of energy required to break up the air into small bubbles and the consumption of alkali required to maximise the oxygen transfer rate. Theoretically, the HDS process can be reduced to a single-stage system. In this paper the practical feasibility of using a strong chemical oxidant, hydrogen peroxide (H2O2) as an alternative to air, with the aim of reducing the HDS process to a single stage is assessed. H2O2 is considered favourable as the Fe oxidation reaction rate is almost

instantaneous (Leavitt 2010) requires little mixing energy and is less dependent on pH than aeration.

A purpose-built bench scale HDS rig was used to treat a continuous flow (10 L/h) of 150 mg/L Fe circa pH 6 (net alkaline) synthetic mine water for each 10-day run (fig. 1). A fresh supply of mine water was prepared daily and kept under a CO2 atmosphere to prevent atmospheric oxidation, ensuring a representative feed. 1% sodium hydroxide (NaOH) was used as the alkali solution and an anionic polymer (AD985) was prepared at a 0.01% working strength. NaOH addition was managed through a pH-controlled dosing pump.

Table 1 *Parameters of each run and associated campaign.*

Campaign	Run	No. Reaction Stages	Oxidising Reagent	Sludge Recitc	Volumetric Recirc Ration
1	1	1	H_2O_2	No	0%
	2	1	Air	No	0%
2	3	2	H_2O_2	Yes	25–30%
	4	2	Air	Yes	25–30%
3	5	1	H_2O_2	Yes	25–30%
	6	1	Air	Yes	25–30%

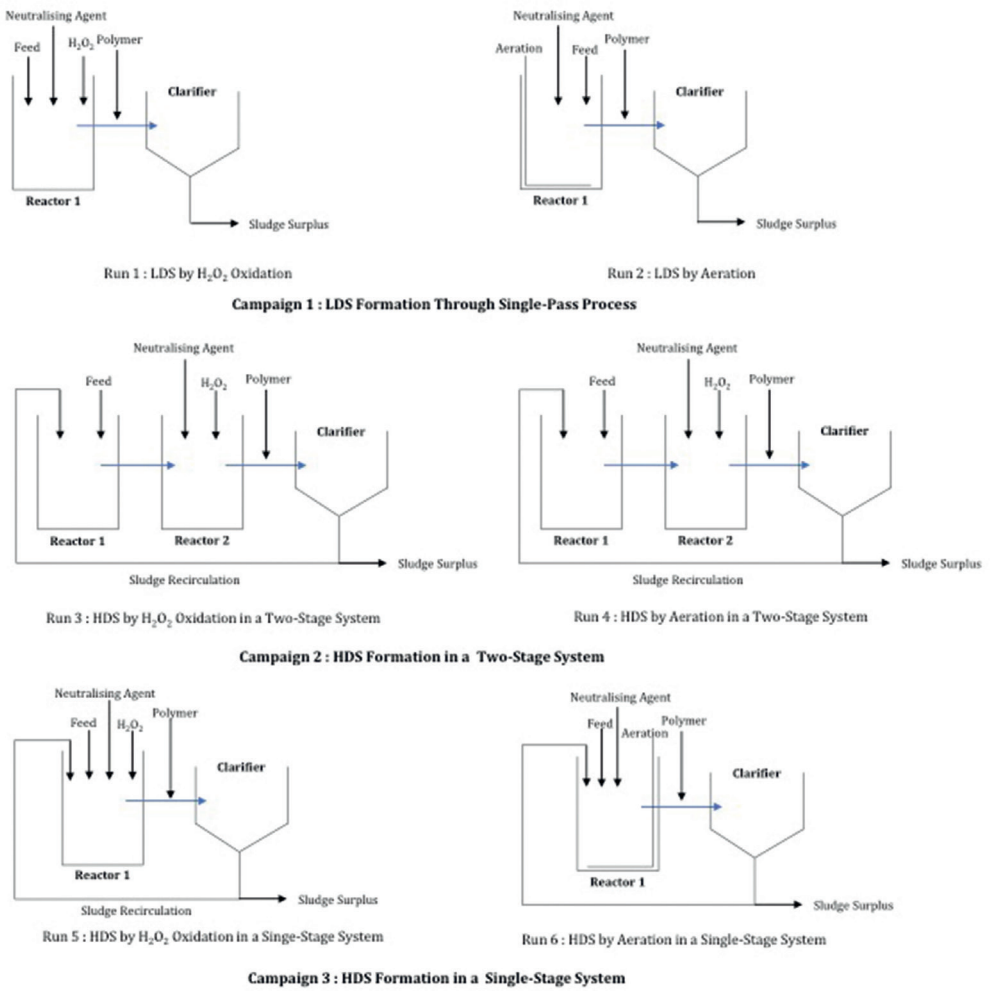

Figure 1 *Structure of Runs 1-6 for the bench scale comparative study*

Reactors used for homogenisation and oxidation hold a volume of ~ 5 L, providing a retention time of 30 minutes. Each reactor was paired with a mechanical mixer to provide sufficient mixing as required to ensure homogenisation of feed water, sludge and dispersal of oxidant and alkali. Following the precipitation reaction AD985 was added to promote flocc formation and aid settlement within the clarifier.

As the rate of oxidation through the aeration process is predominantly pH dependent, every unit drop in pH promotes a decrease in the rate of oxidation by a factor of 100 (Coulton et al. 2003b). Thus, to ensure an optimum oxidation rate of Fe (II) to Fe (III) in the aerated trials, a pH of >8.4 was required and achieved through addition of NaOH. As H_2O_2 is an extremely powerful oxidant, the pH required relates to the solubility of Fe(OH)3. Therefore, for the runs using H2O2 (1% active ingredient), NaOH was added to maintain a pH >5.5 to achieve a discharge Fe limit of <1 mg/L.

For each run, 100ml samples were collected daily from the clarifier inlet and a 1-hour settlement test conducted, providing an initial settling velocity (m/h) and settled solid content (w/v) by mudline analysis. Total suspended solids (TSS) was analysed post settlement test. To establish the mechanical dewatering capabilities, a 50 mL sludge sample was drawn from the bottom of the clarifier daily and dewatered under 1 bar of pressure, providing the dewatered solid content (w/w). Monitoring of reactor pH and reagent consumption was conducted throughout.

Results

Average TSS

For campaign 1, the average TSS concentration of sludge produced was 267 – 289 mg/L (tab. 2). Results compared well to the theoretical value of 286.6 mg/L (equation 1), suggesting that all the Fe (II) was oxidised and precipitated through the system.

$$TSS = \frac{(Fe^{2+}concentration\ in\ feed\ water \times atomic\ mass\ of\ Fe(OH)_3)}{atomic\ mass\ of\ Fe^{3+}} \quad (1)$$

Once conditions stabilised, $Fe_{(total)}$ concentration in the clarifier supernatant was <1 mg/L consistently.

TSS values for the H_2O_2 process (Campaign 2 and 3) were over 6000 mg/L greater than the conventional two-stage aeration process and over 7000 mg/L greater than the single-stage aeration LDS processes (fig. 2).

Initial Settling Velocities

Initial settling velocities in Campaign 1 were 1–1.1 m/h, as expected for LDS. A conversion from LDS to HDS was observed in Campaign 2, where initial settling velocities were more than ten times that of Campaign 1 (tab. 2). In Campaign 3, the H2O2 run had an initial settling velocity of 9.4 m/h compared to the aerated run which only achieved 4.8 m/h.

For Campaign 2 and 3, mudline analysis showed that the H2O2 runs followed a similar pattern to the conventional two-stage aeration run (fig. 3). However, the Campaign 3 aeration run did not, suggesting that this process does not form true HDS.

NaOH Consumption

H_2O_2 runs were operated at pH 5.5 and consumed between 115–125 mg/L NaOH (tab. 2). Aerated runs were operated at pH 8.4 and consumed 298–370 mg/L.

Settled and Dewatered Solid Content

Settled solid content for Campaign 1 was <5% in both runs. Dewatered solid content within the sludge was 30% when using H_2O_2 compared to 16.5% with aeration. For both Campaign 2 and 3, the aerated runs had a higher settled solid content, but a lower dewatered solid content than the H2O2 runs. For the Campaign 3 aerated run, the dewatered solid content was much lower than any other HDS process, indicating once more that true HDS did not form during this run.

Time to form HDS

The conversion of LDS to HDS in the H2O2 runs took 4–5 days compared to 9 days for the conventional two-stage aerated runs (tab. 2). HDS had not formed in the Campaign 3 aerated run after 10 days.

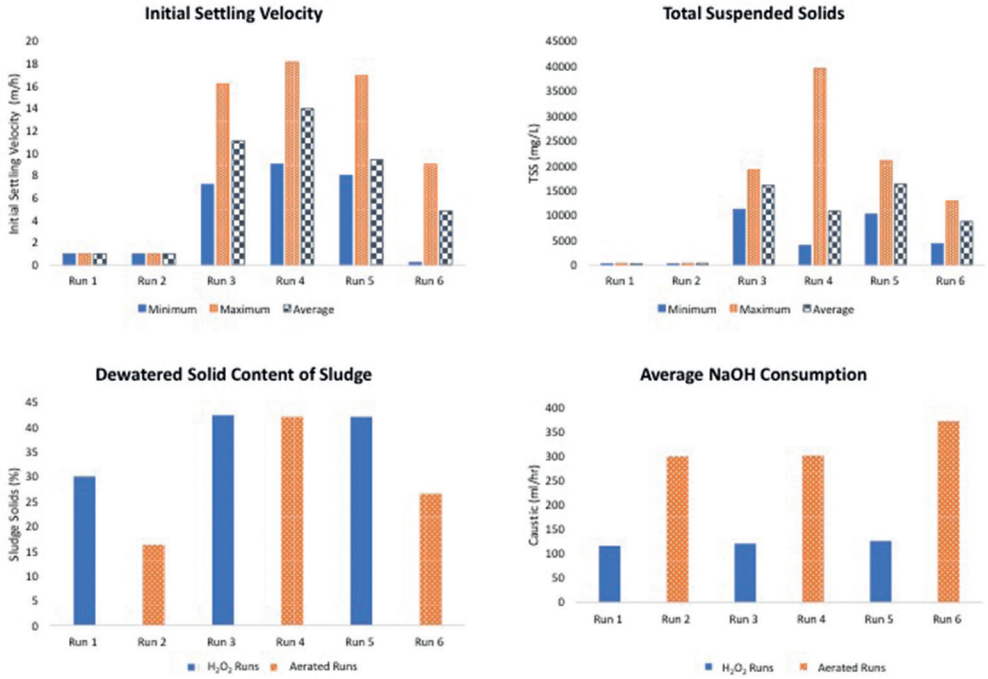

Figure 2 *Results from the bench scale comparative study.*

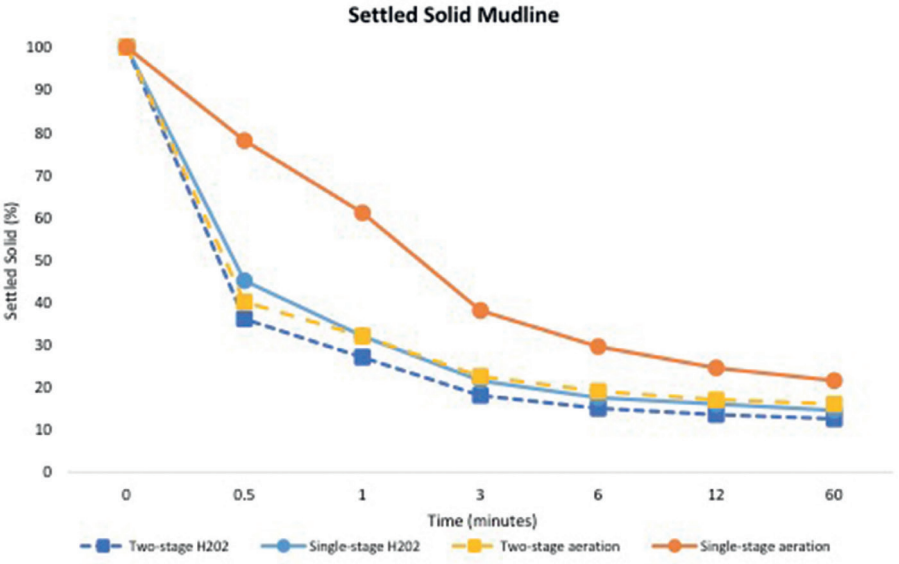

Figure 3 *Settled solid mudline for Campaign 2 & 3 (Run 3–6).*

Table 2 Summary of bench scale results.

Campaign	Run	Operating pH	Average NaOH Dose	Average Clarifier TSS[1]	Mass Recirc Ratio[2]	Initial Settling Velocity	Settled Solid Content (weight/volume)	Dewatered Solid Content (weight/volume)	Time to Form HDS	Sludge Type
1	1	5.5	115 ml	267 mg/L	N/A	1.1 m/h	<5%	30%	N/A	LDS
	2	8.4	298 ml	289 mg/L	N/A	1 m/h	<5%	16%	N/A	LDS
2	3	5.5	120 ml	16021 mg/L	1:56	11.1 m/h	12.5%	42.3%	4 days	HDS
	4	8.4	300 ml	10830 mg/L	1:38	14 m/h	16%	42%	9 days	HDS
3	5	5.5	125 ml	16228 mg/L	1:56	9.4 m/h	14.5%	42%	5 days	HDS
	6	8.4	370 ml	8738 mg/L	1:30	4.8 m/h	26.5%	26.5%	N/A	MDS[3]

Note:

[1]Refers to the Clarifier inlet TSS

[2]Refers to the ration between $Fe(OH)_3$ generated by oxidation/precipitaion to $Fe(OH)_3$ within the recirculated sludge.

[3]Medium Density Sludge (MDS)

Discussion

Reduction of the HDS process to a single stage could not be achieved using aeration. This was demonstrated when comparing the Campaign 3 aerated run with the Campaign 2 aerated run, where settling velocities were 4.8 m/h and 14 m/h, respectively. Sludge produced in Campaign 3 aerated run did not comply to the descriptions of LDS or HDS and in this instance was referred to as medium density sludge (MDS).

However, Campaign 2 and 3 H2O2 runs produced HDS with a low formation time and with improved sludge characteristics, including lower settled solid content. For example, 12.5% versus 14.5% in Campaign 2, showing less voluminous sludge was generated using H2O2. Furthermore, the dewatered solid content of H2O2 HDS in Campaign 2 and 3 was comparable to that of the conventional process. An improvement in dewatered solid content was also seen in Campaign 1, where the H2O2 sludge dewatered to 30% (w/w) compared to 15% (w/w) in the aerated sludge.

Alkali consumption in the H2O2 runs was less than in the aerated runs. Theoretically, 215 mg/L of NaOH was required to completely neutralise Fe oxidation and precipitation, with only an additional 0.23 mg/L required to raise the pH from 5.5 to 8.4.

Increases over theoretical NaOH consumption within the aerated runs were due to the alkalinity buffering change in pH, resulting in a reduction in alkali efficiency. H2O2 runs consumed less than the theoretical value due to the consumption of alkalinity and low reaction pH.

Conclusions

Results from this study demonstrate that the design of the conventional HDS plant can be modified to a single stage system by using H_2O_2 as the oxidant, without compromising water quality or sacrificing the dewatering capabilities of the conventional HDS process. The benefits associated with this include reduction in capital, maintenance, and operational costs due to the simplicity of a single reactor system. Furthermore, the reduced plant footprint and faster HDS establishment time allows the single stage system to become a more widely applicable solution to temporary and permanent treatment of net alkaline AMD.

Acknowledgements

The authors thank Kay Florence for the critical input, Tom Penny for laboratory support and Siltbuster Ltd for allowing the time and facilities to conduct the analysis.

References

Bailey M, Moorhouse A, Watson I (2013) Heat extraction from hypersaline mine water at the Dawdon mine water treatment site. In: Fourie A.B, Tibbett M (eds) Mine Closure Conference 2013, p 1-12

Coulton R, Bullen C, Dolan J, Hallett C, Wright J, Marsden C (2003a) Wheal Jane mine water active treatment plant - design, construction and operation. Land Contamination & Reclamation

11(2):245-252

Coulton R, Bullen C, Hallett C (2003b) The design and optimisation of active mine water treatment plants. Land Contamination & Reclamation 11(2):273-279

Coulton R, Bullen C, Williams C, Williams K (2004) The formation of high density sludge from minewater with low iron concentrations

Coulton R, Froggatt E, McKelvey P (2007) Celtic Copper Herritage project, Avoca Mines: pilot plant treatment trials. Monmouthshire. Unipure Europe Ltd

Fan J, Liu X, Gu Q, Zhang M, Hu X (2019) Effect of hydraulic retention time and pH on oxidation of ferrous iron in simulated ferruginous acid mine drainage treatment with inoculation of iron-oxidizing bacteria. Water Science and Engineering 12(3):213-220

Leavitt B (2010). In situ iron oxidation using hydrogen peroxide. Journal American Society of Mining and Reclamation (1):551-569

Murdock D, Fox J, Bensley J (1994) Treatment of acid mine drainage by the high density sludge process. Journal American Society of Mining and Reclamation (1):241-249

Ojonimi T, Asuke F, Onimisi M Onuh C (2019) Acid Mine Drainage (AMD): an environmental concern generated by coal mining. Journal of Degraded and Mining Lands Management 6(4):1875-1881

Rudko G (2020) The role of mining industry in the world economy and the economy of Ukraine. Mineral resources of Ukraine [in Ukrainian] (4):23-29

Wyatt L, Moorehouse A, Watson I, (2018) Adaptive mine water treatment: modelling to long-term management. In: Wolkersdorfer Ch, Sartz L, Weber A, Burgess J, Tremblay G (eds)11th ICARD IMWA MWD Conference - Risk to Opportunity, p 769-774

Study on Mechanism Analysis and Treatment Measures of Karst Water Disaster in Mines

Weitao Liu[1,2], Lifu Pang[1,2], Yanhui Du[2,3]

[1]*College of Energy and Mining Engineering, Shandong University of Science and Technology, Qingdao, Shandong 266590, China, plf1715@163.com*

[2]*Shandong University of Science and Technology State Key Laboratory of Mine Disaster Prevention and Control, Qingdao, Shandong 266590, China*

[3]*College of Safety and Environmental Engineering, Shandong University of Science and Technology, Qingdao, Shandong 266590, China Abstract*

Abstract

According to the theory of rock mechanics and fracture mechanics combined with the actual geological conditions of the coal seam floor, the coupling of water and rock is analyzed, and it is believed that the karst pore water pressure has a greater influence on the strength of the floor rock. The method of numerical simulation is used to analyze the stress change of the floor and the failure of the plastic zone during mining at a water pressure of 1-8 MPa. It is believed that when the water pressure is greater than 4 MPa, the floor has a greater impact.

Keywords: water-rock coupling, water barrier, karst water, numerical simulation

Introduction

With the development of coal mining technology and detection technology and the location of coal seams gradually concentrated in the deep, the threat of shallow surface water damage and traditional mining water damage has gradually decreased. The main threat in the process of deep mining comes from floor karst water. The floor karst water is in the original equilibrium state with the floor rock under hydrostatic pressure (Wu et al. 2015; Liu 2016). When mining is carried out, the original equilibrium state is broken, the hydrostatic pressure becomes the hydrodynamic pressure, and the water pressure is in a state of fluctuation. At this time, the floor water barrier will be destroyed. The possibility of water inrush (Krzysztof et al. 2016). At present, domestic and foreign experts and scholars have conducted some research on the mechanism and law of floor water inrush caused by karst water. Zhang Peisen et al. used the fluid-solid coupling model of FLAC3D to simulate the whole process from the formation of floor mining cracks, the damage and destruction of hidden faults to the formation of water inrush channels in the coal mining process. It is believed that the coupling effect of mining stress and water pressure causes cracks in the floor rock to initiate and expand until penetration and water inrush (Zhang et al. 2018). Sun Yunjiang et al. used the ESG microseismic monitoring system to monitor the formation process of the water-conducting fracture zone in the floor in real time, and explored the relationship between fault fracture expansion and confined water pressure (Sun et al. 2017). Gao Saihong et al. considered the damage and fracture mechanism of fractured rock mass under the action of water, and deduced the stress intensity factor of the crack under the action of water (Gao et al. 2012). Sun Jian et al. established a three-dimensional fluid-structure coupling model through the secondary development of FLAC3D software. Numerical simulation is used to explore the relationship between the pressure change of confined water in the inclined coal seam floor and the threat of water inrush as the mining proceeds (Sun et al. 2018). Odintsev and Miletenko established a confined hydraulic fracturing model and found that natural hydraulic fracturing is restricted by natural stress and induced stress, groundwater hydrostatic pressure and mining sequence

(Odintsev and Miletenko 2015). Shi Longqing et al. used a non-linear risk evaluation method to evaluate and analyze water inrush from coal seam floor, and optimized the inaccuracy of the water inrush coefficient method. The above experts and scholars lack the research on the damage and destruction of the aquifer caused by mining under different pressures of karst water (Shi et al. 2017). Based on this, the article uses theoretical analysis and numerical simulation methods to explore the damage and treatment methods of the aquifer under the action of karst water (Liu 2015).

Water-rock coupling analysis

According to the actual geological conditions of coal mining, the floor rock during the mining process can be divided into the upper failure zone, the middle semi-humid zone, and the lower complete water-rock coupling zone. The upper area is directly damaged by mining activities, mainly compression and shear damage. As shown in Figure 1(a), it is simplified as a uniform load q, and the inclined cracks as shown in the figure appear under the action of pressure. Starting from the middle area of the floor rock there is water. This part is not only affected by the mining disturbance, but also partly by the pressure of the confined water. The force is shown in Figure 1(b). The part of the area under the floor that is in direct contact with karst water will have slow seepage under hydrostatic pressure. This part is saturated or half-saturated. When mining activities occur, the pressure of the confined water will also change. This part is disturbed by mining, and a large number of secondary cracks will be derived from primary cracks. The karst water penetrates the lower area of the floor under the action of water pressure, and complete water-rock coupling appears. According to some experimental research results, sandstone can lose 15% of its strength when it is close to saturation. In most cases, the biggest influence on rock strength is the water pressure in the voids and fissures.

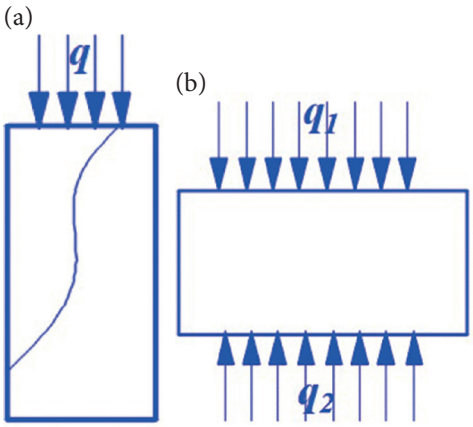

Figure 1 *Types of damage.*

According to the research of many rock mechanics experts, as long as there is a connected fracture system in the rock, Terzaghi's effective stress law can be applied (Xu 1981).

$$\sigma^1 = \sigma - p \tag{1}$$

Where σ is the total stress (MPa), p is the pore water pressure (MPa), and σ1 is the effective stress (MPa).

According to the Mohr-Coulomb strength theory, under the action of pore water pressure, the shear strength of the rock in the complete water-rock interaction coupling region under the floor rock is

$$\tau_f = c + \sigma^1 tg\varphi$$
$$\tau_f = c + (\sigma - p)tg\varphi \tag{2}$$

It can be seen that the pore water pressure in the rock reduces the strength of the rock, and the degree of strength reduction is determined by the pore water pressure.

Influence of karst water pressure

Model establishment

Taking the 1311 working face of Yangcheng Coal Mine as the geological background, a three-dimensional geological model was established (Fig.2). According to the actual geological data, it is determined that the length of the model is 200 m, the width is 200 m, the height is 130m, and the coal seam thickness is 5 m. The model is divided into 80,000 units and 85,731 nodes. The front and back, left and right boundaries of the model are set as horizontal constraints, the upper boundary is free boundary, and the bottom boundary is full constraint. Each step along the strike length is 10m, a total of 10 steps. Considering the boundary effect, the left and right boundaries of the model are both 50m

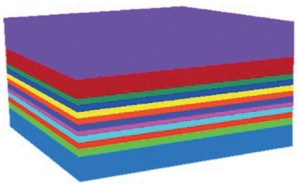

Figure 2 Three-dimensional geological model.

from the open cut and the coal pillars left on the stop line of the working face; the distance between the front and back boundaries of the model for roadway protection coal pillars is both 50m. In the simulation process, the Mohr-Coulomb plastic constitutive model and the Mohr-Coulomb failure criterion are used to calculate the coal seam floor mining failure characteristics. According to the test principle of the controlled variable method, the water pressure is set as a single variable, the water pressure range is 1-8 MPa, and other conditions remain unchanged.

Result analysis

Vertical stress analysis

Set the water pressure to 1-8 MPa, perform excavation simulation on 8 groups of models, and get the vertical stress cloud diagram. Because the number of cloud images obtained by simulation is too large, four sets of simulation results of water pressure of 1 MPa, 3 MPa, 5 MPa, and 7 MPa are selected. Select the stress value of the node (85, 86, 40) to draw the stress curve (Fig. 3).

According to Figure 3, as the working face continues to advance, the vertical stress on the bottom plate first increases and then decreases. The position where the maximum stress appears is basically in the middle of the mining face. After the water pressure is applied, the effect of water pressure is not obvious in the early stage of mining. When the mining face advances for about 30 m, the stress begins to increase rapidly. The greater the water pressure, the faster it will increase. When the water pressure reaches 3 MPa, when the water pressure increases, the magnitude of the stress increase does not change much. Comprehensive analysis suggests that when the karst water pressure of the floor is greater than 3 MPa, stress concentration is likely to occur, and the vertical stress of the floor is increased.

Plastic zone analysis

According to the numerical simulation under the condition of 1-8 MPa water pressure, the following plastic zone failure cloud map is obtained (Fig. 4). Due to the large number of cloud images obtained by the simulation, the cloud images of the plastic zone at the time of excavation 100 m under the conditions of 1 MPa, 3 MPa, 5 MPa, and 7 MPa were selected for display.

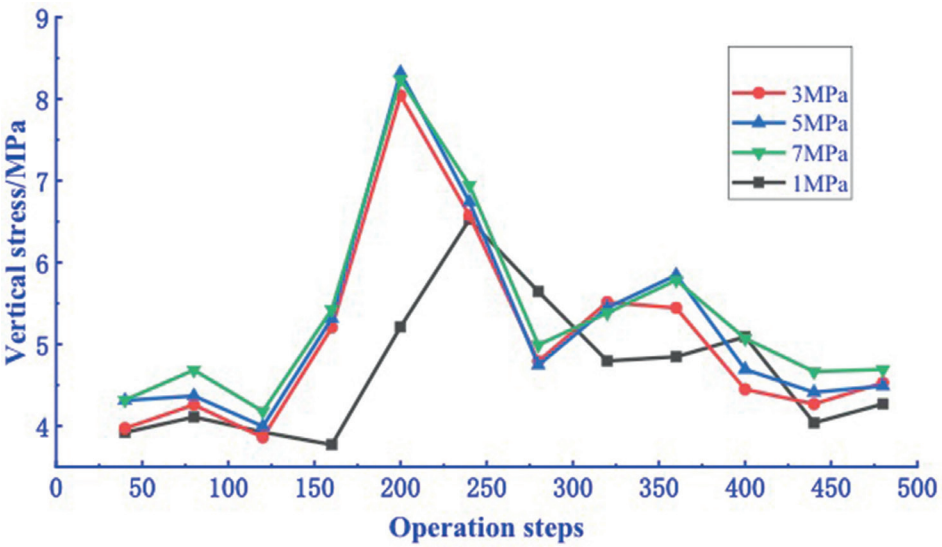

Figure 3 Stress curves under different water pressures.

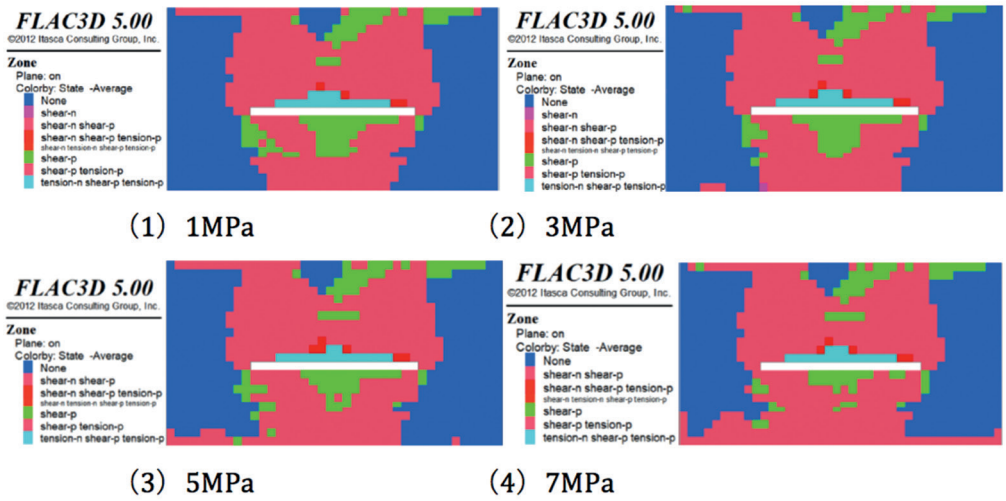

Figure 4 *Cloud map of plastic zone under different water pressure.*

It can be seen from Figure 4 that with the progress of mining, the vertical and horizontal extents of floor damage are increasing. When the working face is mined to 100 m, the damage of the floor shows a hemispherical shape, the closer to the floor, the greater the damage range, and the damage range away from the floor shrinks. When the karst water pressure is small, the impact on the floor failure is small. As the water pressure increases, the damage depth and damage range are increasing. When the water pressure is greater than 3 MPa, the bottom plate begins to be affected by stronger water pressure. When the water pressure reaches approximately 5 MPa, the floor is severely affected by the water pressure while the mining is disturbed.

Water pressure analysis

Set the water pressure to 1-8 MPa, and perform excavation simulation on 8 groups of models, and the water pressure change values of all nodes can be obtained. Because the amount of data obtained by the simulation is too large, the water pressure change values of the nodes (95, 96, 60) when the water pressure is 1 MPa, 3 MPa, 5 MPa, and 7 MPa are selected to draw different water pressure change curves (Fig. 5).

It can be seen from Figure 5 that as the mining progresses, the water pressure changes less in the early stage of mining, indicating that the mining disturbance is weak at this time. When the advancing distance of the working face is about 30 m, the water pressure begins to change suddenly, and the sudden change point is roughly located in the middle of the mining face. When the karst water pressure value is large, the pore water pressure value of the node increases rapidly.

Conclusions

(1) According to the knowledge of rock mechanics, the water-rock coupling between the lower part of the coal seam floor and the aquifer is analyzed. It is believed that the pore water pressure in the rock reduces the strength of the rock, and the degree of strength reduction is determined by the pore water pressure. Water-rock coupling seriously damages the stability of the floor.

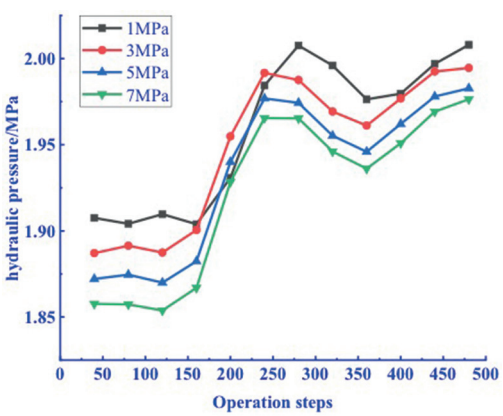

Figure 5 *Variation curves of different water pressures.*

(2) The method of numerical simulation is used to simulate the disturbance of the floor when the karst water pressure is 1-8 MPa. According to the simulation results, it is believed that when the water pressure is less than 4 MPa, the vertical stress on the bottom plate does not change much. Begin to have a strong influence on the damage of the bottom plate. When the water pressure reaches 5 MPa, under the action of mining disturbance, it has a great influence on the plastic damage of the floor, which leads to an increase in the depth and scope of the damage of the floor. When the karst water pressure increases, the pore water pressure of the floor rock will increase accordingly.

Acknowledgements

This research was funded by the National Natural Science Foundation of China (grant 51874192), the National High Technology Research and Development Program (863 Program) of China (grant 2015AA016404-4), the Natural Science Foundation of Shandong Province (grant ZR2019MEE084), the State Key Research and Development Program of China (grant 2017YFC0804108), and the SDUST Research Fund (grant 2018TDJH102).

References

Gao SH, Cao P, Wang SL. Analysis of fracture criterion of and type of crack in rock masses under hydraulic pressure[J]. Journal of Central South University(Science and Technology), 2012, 43(03):1087-1091.

Krzysztof P, Kazimierz R, Piotr C. Causes and Effects of Uncontrolled Water Inrush into a Decommissioned Mine Shaft. Mine Water and the Environment, 2016, 35(2):128-135.

Liu H. Feasibility study on dewatering of Taiyuan limestone water under high pressure in Chengjiao Coal Mine Floor [D]. China University of mining and technology, 2016, 41-67.

Liu WT. Mine water disaster and its prevention and control [M]. Beijing: Coal Industry Press, 2015, pp 70-115.

Odintsev VN, Miletenko NA. Water inrush in mines as a consequence of spontaneous hydrofracture [J]. Journal of Mining Science,2015,51(3).

Sun YJ, Zuo JP, Li YB, et al. Micro-seismic monitoring on fractured zone and water inrush mechanism analysis of deep mining above aquifer in Xingdong coalmine[J]. Rock and Soil Mechanics, 2017,38(08):2335-2342.

Sun J, Wang LG, Zhao GM. Failure Characteristics and Confined Permeability of an Inclined Coal Seam Floor in Fluid-Solid Coupling[J]. Advances in Civil Engineering, 2018, 2018(PT.6):2356390.1-2356390.12.

Xu ZY. Rock mechanics (Third Edition) [M]. Water conservancy and electric power press, 1981, pp 20-56.

Shi LQ, Gao WF, Han J, et al. A Nonlinear Risk Evaluation Method for Water Inrush Through the Seam Floor[J]. Mine Water & the Environment, 2017, 36(4):1-9.

Wu Q, Liu YZ, Zhou WF, et al. Evaluation of Water Inrush Vulnerability from Aquifers Overlying Coal Seams in the Menkeqing Coal Mine, China [J]. Mine Water & the Environment, 2015, 34(3):258-269.

Zhang PS, Yan W, Zhang WQ, et al. Study on factors influencing groundwater inrush induced by backstopping of a coal seam with a hidden fault[J]. Caikuang yu Anquan Gongcheng Xuebao/Journal of Mining and Safety Engineering, 2018, 35(4):765-772.

Scale-up of Electrochemical Units for Mining Waters Treatment

Maria A. Mamelkina[1], Ritva Tuunila[1], Antti Häkkinen[1]

[1]*LUT School of Engineering Science, LUT University, P.O.Box 20 FI-53851, Lappeenranta, Finland*

Abstract

The mining industry is getting more attracted to developing water treatment technologies. The ease with which technology is brought from lab to industrial scale, along with minimizing the time consumption and costs, is influenced by several factors. Some of these depends on the reactor, removal mechanisms, volumes and operating conditions. While others are affected by external factors such as maximum size of the equipment, treatment costs of established or alternative technologies. Scale-up is mainly employed to see if the technology meets the market requirements and expectations. This study focuses on transferring an electrocoagulation process from lab scale to pilot plant.

Keywords: electrocoagulation, scale-up parameters, process development, mining waters

Introduction

Electrocoagulation background

Electrocoagulation, with aluminum and iron electrodes, has been first patented in the US in 1906, while drinking water treatment by electrocoagulation was conducted extensively in the US by 1946 (Chen 2004). However, still nowadays, electrocoagulation of mining waters may belong to TRL 5 to TRL 7, meaning that technology has been already validated, demonstrated and system prototypes already exists. Depending on the mining water content and source, application of electrocoagulation is still hindered and is at the early developing stages (TRL 3 to TRL 5). TRL here refers to the Technology Readiness Level as one of the indicators of a technology maturity level. TRL indicator levels vary from 1 (when basic principles of a process are observed) to 9 (when a technology is proven in an industrial environment). Regarding the mining waters, initially, the suitability of electrocoagulation to remove toxic metals was assessed (Florence 2015,). Later, removal of nitrate and other nitric compounds by electrocoagulation was studied (Lacasa et al. 2011c). One of the latest steps was to develop electrocoagulation for sulfate and cyanide removal by electrocoagulation from mining water (Mamelkina 2020).

Overview of the commercialized electrocoagulation units

While the full-scale industrial application of electrocoagulation for the treatment of mining waters is limited, some pilot units have already been commercialized. One of the latest industrial scale EC-treatment plants was installed in Severnyi Mine, JSC Kola MMC. Iron electrodes were used to remove N-compounds, suspended solids, color and metals (Fe, Cu and Ni). Pilot plants that utilize different electrochemical methods have been designed and tested to remove nitrogen compounds, neutralize water streams and remove toxic metals. Thus, there are several commercialized electrochemical technologies to treat nitrate (NitrEL) and ammonia (AmmEL) rich waters, for example, provided by Current Water Technologies Inc. Also, a solution (AmdEL) to prevent the formation of acid mine drainage using magnesium anodes is also available. The Outotec EWT process is another commercially available technology that is based on electro-oxidation and electrocoagulation for the removal of toxic metals, arsenic, antimony, selenium and other oxyanions. One module's treatment capacity is from 5 to 40 m^3/h, so that the need for the treatment of larger amounts of water can be met by adding more modules. Modular system benefits from the ease of scale-up and reduced

quantity of residues formed, when compared to conventional processes, however, the low conductivity and high solid content of treated water may hinder the process significantly. The Hydro 400 is an electrochemical water treatment unit that is available to treat mining and mineral processing water. One unit is capable of treating 40 m^3/h, and the treatment capacity can be increased by adding more units. When testing the Hydro 400 unit, case studies that were performed proved the suitability of EC-treatment to the removal of phosphorous, suspended solids, lead, iron and aluminum from contaminated water. The application of a Hydro 400 unit to treat mining waters resulted in a 15% cost reduction, compared to chemical coagulation and other conventional treatment methods. The Soneco® water treatment system by Power & Waters is based on the combination of ultrasound and electrolysis for the efficient removal of phosphorous and toxic metals, as well as for the neutralization of the acid mine drainage. Soneco® units benefit from a cleaning-in-place tool that provides electrode cleaning by ultrasonic cavitation, prolonging the lifetime of the equipment and affecting dramatically the operation costs. FCC Aqualia has been recently working on the application of electrocoagulation and bio-electrochemical processes to coprecipitate phosphorus and nitrogen. The main distinction of this process, when compared to the others mentioned, is that it produces biogas as a potential power source and benefits from the possible valorization of generated sludge containing aluminum, phosphorous and nitrogen as a fertilized.

Scale-up and design issues

Electrocoagulation process is classified as difficult but quantifiable or very difficult and rarely quantifiable. On one hand, the reactor geometry makes the process easy to scale-up. On the other hand, the electrochemical principles involved and especially the contaminant removal mechanisms hinder the scale-up of electrochemical water treatment processes crucially.

There are two main rules to consider in the design and scale-up of electrochemical reactors. The first concerns the optimal design of the cell and the other is devoted to the reaction mechanisms involved in the process. Among the most reported and significant scale-up parameters for electrocoagulation process is the relation of the surface area to volume ratio (S/V). The S/V ratio is mainly related to the current density, rate of coagulant dosing and bubble production; however, the flow regime and reactor configuration are not considered.

The cell design used for electrocoagulation processes varies greatly from applying open tanks, parallel plate cells or complex designs with moving electrodes. The choice of electrode material and shape, reactor configuration, operation mode and electrode arrangement are the key parameters, especially at the initial stage of process development. Electrode material affects the amount, and type, of metal ions in the solution, coagulation efficiency and process costs, while the reactor configuration influences the fluid flow regime, bubble paths, mixing/settling characteristics and mass transfer (Chopra 2001). The operation mode influences process performance, energy consumption, while electrode arrangement allows the minimization of energy consumption and improvement in the removal of contaminants (Zhou 2018).

Most of the research to date was performed using a monopolar connection of electrodes, very few studies have been performed using a bipolar connection arrangement. In the latter condition, it is possible to have better performance and lower energy consumption, however, bypassing of electrodes and loss of charge may occur.

The major distinctions between different the electrocoagulation reactors are their configuration and operation mode. A design may be presented as a batch or a continuous system. On one hand, the latter mentioned system has, as advantages, a continuous feed of wastewater and operation under (pseudo) steady-state conditions. One of the key advantages of continuous systems is that the coagulant demands are substantially fixed. On the other hand, a batch system maintains a fixed wastewater volume per treatment cycle. However, the main disadvantage is the change with time of operating conditions within the reactor (Holt 1999). The operation

mode mostly affects the performance, reliability and chemical interaction within the EC-process.

In all cases, the cell design should provide uniform current and potential distributions that promote the optimization of parameters such as energy consumption, coagulant production and process performance. In addition, it is desirable that the equipment should meet the requirements of low cost material for manufacturing, ease of maintanance, installation and operation as well as the possibility for scale-up.

In this paper process development and scale-up stage for electrocoagulation treatment of mining waters are decribed. Different operation modes, various cell designs and process conditions were assessed during the work. This paper contains data on sulfate andcyanide removal, however, the removal of other nitric compounds as well as toxic metals has been evaluated elswhere (Mamelkina 2020).

Methods

Current work focus was on switching from batch operation to continuous, process design and treatment of over 200 L of water. In this work both tank (1 L and 70 L) and parallel-plate flow electrochemical cells were utilized to treat mining waters. With the application of parallel-plate flow cell, both batch-recycle (3 L) and continuous (200 L) single pass modes were tested. The dimensions of electrodes for tank cells were 60×70×2 mm (resulting in total anode area of 168 cm^2) for 1 L reactor and 300×300×5 mm (resulting in total anode area of 3600 cm^2) for 70 L reactor. The dimensions of electrodes for parallel-plate flow cell were 100×100×2 mm (resulting in total anode area of 100 cm^2).

During tests both synthetic and real mining water samples were used. More details about the experimental procedure, operating parameters, contaminants concentrations and analytical procedure can be found (Mamelkina 2020).

Results and discussion

When developing an electrocoagulation process to treat mining waters, firstly, chemical coagulation tests were performed using sulfate and cyanide rich waters. At that stage, the coagulation mechanisms, required amount of coagulant and chemical coagulation performance have been studied. The highest sulfate removal of 81% was observed at pH 2 and iron coagulant , when cyanide removal did not exceed 15% with both iron and aluminum coagulants. Second step devoted to the batch lab scale electrocoagulation using tank (1 L) and parallel-plate flow (3 L) cell. At that stage performances of chemical coagulation and electrocoagulation were compared. Removal mechanisms and kinetics were studied, operation parameters and cell's configurations were evaluated. The highest sulfate removal was 54% when using tank cell at final pH 11, 3 A and iron electrodes. Operation with parallel-plate cell at batch conditions resulted in the highest sulfate of 18% at pH 2. Almost complete cyanide removal was observed using both tank and parallel-plate cells equipped with iron electrodes. The third step in scale-up of electrocoagulation process was performed using 70 L batch tank reactor and parallel-plate cell treating 200 L of real mining

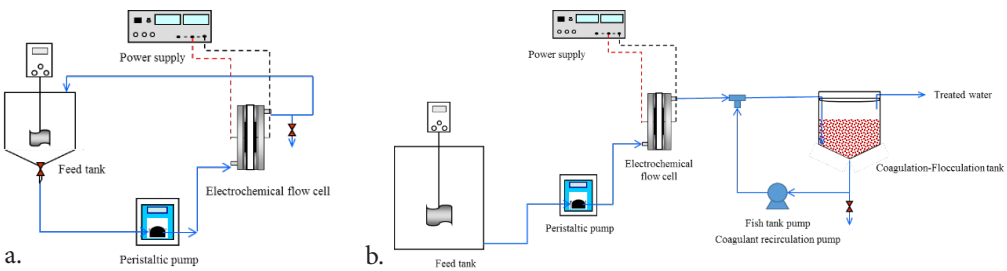

Figure 1 Schematic diagram of electrocoagulation process operating in a. batch and b. continuous modes using parallel-plate cell.

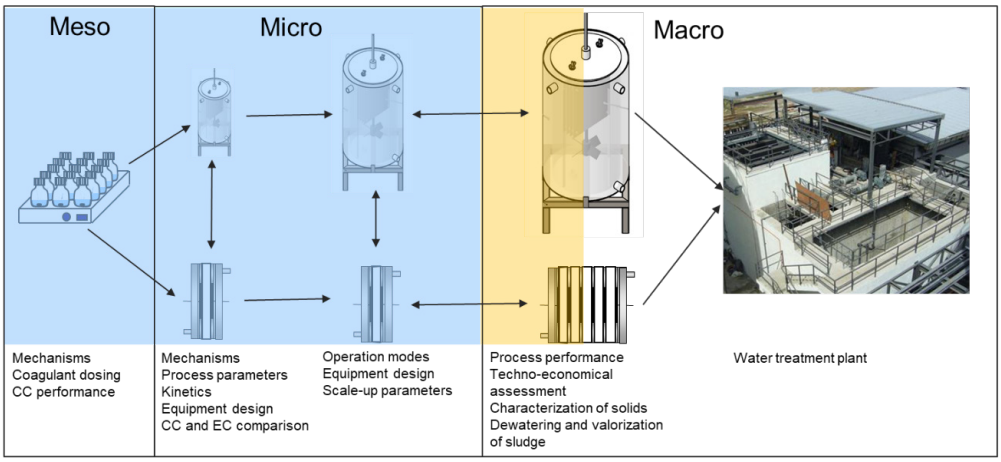

Figure 2 *Stages of process development and scale-up for the electrocoagulation of mining waters at meso. micro and macro levels, blue color – completed stages, yellow color – present stage.*

water. Scale-up parameters were determined, and operation modes were compared at this step. Sulfate was removed up to 50% in 1 L tank cell and up to 30% in 70 L tank cell with aluminum electrodes, using current density as a scale-up parameter. The highest removal of sulfate during continuous operation with parallel-plate cell was 70% at pH 2. The process development and scale-up stages are summarized in Fig. 2.

$$j = \frac{I}{S} \quad (1)$$

$$Q = \frac{j}{q} \cdot S \quad (2)$$

During scale-up of a tank cell, current density was chosen as a scale-up- parameter, however, later it was found that the amount of solids generated was the most reliable scale-up parameter. When developing a novel process design based on continuous operation and solids recirculation, the electric charge passing through the system was switched from batch operation to continuous, and this is proposed as one of the scale-up parameters. It should be highlighted that in this arrangement, electric charge depends on the intensity and flowrate, q, but not on time. The electric charge, Q, has been calculated using Eq. 2 based on the current density, j, (Eq. 1) that was similar for both batch and continuous operations. Where, I – current, S – anode area.

Conclusions

There are several reasons why understanding of scale-up might be needed at different stages of process development, such as studying the economic feasibility (pilot plant, demonstration plant), determination of bottlenecks of the technology (miniplant, pilot plant) and commercializing a new process. All in all, scale-up is mainly employed to see if the technology meets the market requirements and expectations. Even though the electrocoagulation treatment of mining waters has not been yet assessed from techno-economical point of view, the most suitable reactor configuration as well as process operation and scale-up parameters are proposed. Thus, based on the results parallel-plate electrode configuration and operation at continuous mode are recommended. The ease in scale-up of parallel-plate cells makes the utilization of those appealing for industrial application. Electric charge is suggested as one of the main scale-up parameters when switching to different operation modes and when increasing the scale-up level.

Acknowledgements

This work was conducted as part of the EWT-CYNCOR project funded by EIT Raw Materials (European Institute of Innovation and Technology), and the ITERAMS project funded by the European Union Horizon 2020 program.

References

Chen G (2004) Electrochemical technologies in wastewater treatment. SepPur 38:11–41

Chopra AK, Sharma AK, Kumar V (2001) Overview of electrolytic treatment: An alternative technology for purification of wastewater. Arch Appl Sci Res 2:191–206

Florence KM (2015) Mechanisms of the removal of metals from acid and neutral mine water under varying Redox systems

Lacasa E, Cañizares P, Sáez C, Fernández FJ, Rodrigo MA (2011) Removal of nitrates from groundwater by electrocoagulation. Chem Eng J 171(3):1012–1017

Mamelkina MA (2020) Treatment of mining waters by electrocoagulation

Zhou M, Oturan MA, Sirés I (2018) Electro-Fenton Process: New Trends and Scale-Up. Springer Singapore, Singapore

Open Pit-Mine Water Management in Equatorial Area

Yogi Irmas Pratama[1], Fahmi Syaifudin[1], Kris Pranoto[1]

[1]*Senior Engineer – Civil, Mine Planning Department, PT Kaltim Prima Coal, Wisma Rayah, Senior Camp A21/2, Sangatta Utara, 75683 Kutai Timur, Indonesia,*
Yogi.Pratama@kpc.co.id, Fahmi.Syaifudin@kpc.co.id, Kris.Pranoto@kpc.co.id

Abstract

PT Kaltim Prima Coal, currently the largest open-pit coal mining company in Indonesia, is located in East Kalimantan. A province passed by the equator experiences heavy rainfall throughout the year. Annual average rainfall is recorded at 2,152 mm. Controlling water inflow quantity is the most important thing in water management to have decent water quality. Proper design configuration consists of dry dam as flow detention and labyrinth pond for quality adjustment. Water discharge reduction up to 90% in average brings enormous benefit for water management system. Also, the design becomes the most feasible option in post mining.

Keywords: Rainfall, Water Management, Mining, Equator

Introduction

PT Kaltim Prima Coal (KPC) is one of the largest coal mining companies in Indonesia. It is located in the province of East Kalimantan. Geographically, the region is crossed by the equator which leads to weather conditions. In general, Indonesia consists of two seasons, dry and rainy seasons. Rain occurs throughout the year without meaningful seasonal differences.

From 1998 to 2012 the sediment ponds configuration used at KPC was categorized in 2 types. First was a blocking sediment pond with large dead reservoirs on hilly areas and the second was labyrinth type sediment pond which was built in area that tended to be flat and there were no insulated hills. This typical labyrinth pond had a small storage capacity and expensive cost. Looking further into other ponds in other mines, configurations were also commonly used in other coal mines in Indonesia.

Sediment ponds in KPC generally manage catchment in the average range of 1 km^2 to 6 km^2. Combination of a large enough catchment and high rainfall will generate a large water discharge outflow. Such condition causes difficulty on water considering the runoff discharge when it rains is enormous and uncontrolled. Refer to Indonesia regulation of energy and mineral resources ministry 7/2014 concerning the implementation of land reclamation of former settling ponds as part of post-mining. So it can be defined that in the post mining stage sediment pond must be able to be changed into a wetland and does not leave the risk of dam break and or failure in the future. According to status of notifiable and other dams at KPC 2008 report study (Simmons 2008) conducted at KPC, in the construction of dam blocking, the accumulation of sediment that occurred in the ponds increased hazard structure such as overtopping, internal erosion (piping), slope stability, and foundation failure in the long term operation.

Answering the problems, KPC has revolutionized the sediment pond configuration. Starting from the design concept which was developed in 2013 and made changes and improvements to date. The total sediment pond that has been built using this new configuration method is 11 ponds, where the total number sediment ponds that have successfully been transformed into the new configuration are 4 ponds. Configurations includes building 2 types of settling ponds in each KPC managed catchment area which has huge live storage pond system as shown in the scheme in Figure 1 below. Two types of ponds built were (1) the type of dam blocking with a dry dam concept and (2) labyrinth pond. Dry dam ponds function to regulate the outflow and labyrinth ponds function

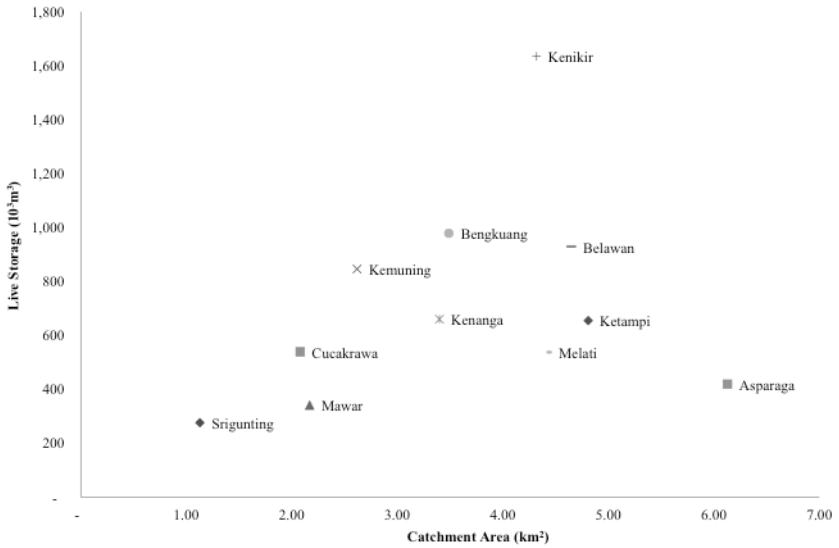

Figure 1 *Registered sediment pond using new configuration system in KPC area.*

as settling ponds. A model example of this detention dam on KPC operation is shown in this paper. Basic principles and methods of such a solution are shown.

Methods

Currently 18 rain stations are actively operated in KPC, with a wide coverage area throughout the mining area of PT KPC. Analysis of the average regional rainfall implemented to calculate the weighing of each rain station uses the polygon Thiessen method. Data consistency test is also carried out to find whether there are environmental changes and or changes in how to measure rain data. If the test results state that the rainfall data is consistent it means that there are no changes to these 2 variables (Haan et. al. 1994). Results of the data processing are then presented in the form of rain design with a certain return period. Where the return period is defined as a hypothetical time where rain or discharge with a certain amount will be equaled or exceeded once in that time period.

Hydrograph is a graphic presentation of one of the flow quantities as a function of time (Chow 1988). Hydrograph shows the overall response of the catchment area to rain inputs. Unit hydrograph is a direct runoff hydrograph produced by effective rainfall evenly distributed in a catchment area with a fixed intensity (taken 1 mm/hour) in a set unit of time (taken 1 hour). For rivers that do not have observable flood hydrographs, synthetic hydrographs that have been developed in other countries are usually used, the parameters of which must be adjusted first to the characteristics of the drainage area under review.

Therefore, building a dry detention reservoir is a very progressive solution nowadays. It is an effective water structure, which has no noisy effects on the environment and can even be an aesthetic part of the countryside. It has to retain the flood wave and prevent an odd amount of water from flowing outside the river bed. Minimizing flood risk can be achieved in three ways (Cipovova 2011):

- Decreasing the accumulated discharge. This can be provided by water structures, weir dams, detention reservoirs or flooding less valuable parts of a region
- Increasing the capacity of a water course
- Instituting corrections and arrangements in the flooded area (e.g. planning, warning, and rescue services).

Rain that occurs throughout the year in the KPC active operational area requires proper methods of management. Analytical methods used in calculating and designing

a structuring point pool include and are not limited to:

- Preliminary Design shall be part of general water management plan based on official version of 5 Years Long Term Water Management Plan.
- Development conceptual design which includes sediment pond control location. Location must be considered to its safe distance from public facilities and main water course. Also in addition for practical reason must refer to ministry decision of energy and mineral resources 1827-2018. Conceptual design shall also follows criteria below:
    - *Pond Configuration*
      Pond configuration consists of two types, control discharge fill embankment and excavated labyrinth pond as settling pond. Discharge inflow run off from catchment area is controlled and the discharge is reduced by using filled embankment. Within low discharge from outflow point of filled embankment, water quality could be settled easily at labyrinth pond.
    - *Type of outlet and emergency spillway*
      Typical of outlet on the embankment and excavated pond is defined by two. Low level intake as main water flow and emergency spillway to cover unplanned rainfall or discharge happen in the future.
    - *Storage capacity and structure examination*
      The examination is including water storage capacity both of dead storage and live storage (temporary). Also the examination of the embankment height refers to Indonesia minister regulations of public works and public housing ministry 27/PRT/2015.
    - *Geotechnical investigation and assessment*
- Development of detail design which includes catchment, rainfall, runoff, all of hydrologic and hydraulic aspect, sedimentation rate, and also maintenance schedule.

Result

Rain data is obtained from rain stations that are scattered in all catchment areas of the pond and there is also an automatic rain station which is useful for getting rainfall events data. Rain data from manual monitoring has been collected since 1985. Based on a study of automatic rain data, the concentration of rain events is 3 hours. The percentage distribution of rainfall events is 22.6% at the first hour, 63.5% at the second hour and 13.5% at the third hour. The average annual rainfall is 2,152 mm, 179 mm monthly and 5.7 mm daily.

For sediment ponds, there are two classifications of storage which are divided into two reservoir levels. Live storage is the reservoir volume that is above the low level intake elevation to the crest dam elevation and functioned as a discharge detention. Dead reservoirs as sediment reservoirs volumes are below the elevation of the low level intake to the bottom of the ground level of water storage. In the use of ponds as discharge detention, volume of live storage must be optimized.

Detention pond construction is carried out by placing an outlet at the bottom of the sediment pond, sedimentation is planned to occur in the labyrinth pond. Sediment pond embankment is maximized to control water discharge. To maximize its function, it is done by installing the outlet capacity in lowest level available and considering the availability of storage that can be provided. In this scheme, the outlet must use a closed channel type such as pipe or concrete box culvert.

Flood event is simulated within 24 hours. Calculation is done by Nakayasu synthesis unit hydrograph. Parameters involved in the synthetic hydrograph analysis using Nakayasu HSS are (1) time to peak magnitude, (2) time lag, (3) time base of hydrograph, (4) catchment area, (5) length of the longest channel, and (6) run off coefficient (Soemarto 1986). If it depictes in the hydrograph scheme, the peak of the flood occurs within the first 3 hours. High incidence of rain and concentrated in a short time raises the potential for flooding if no control of water discharge arises. One option that can use discharge control

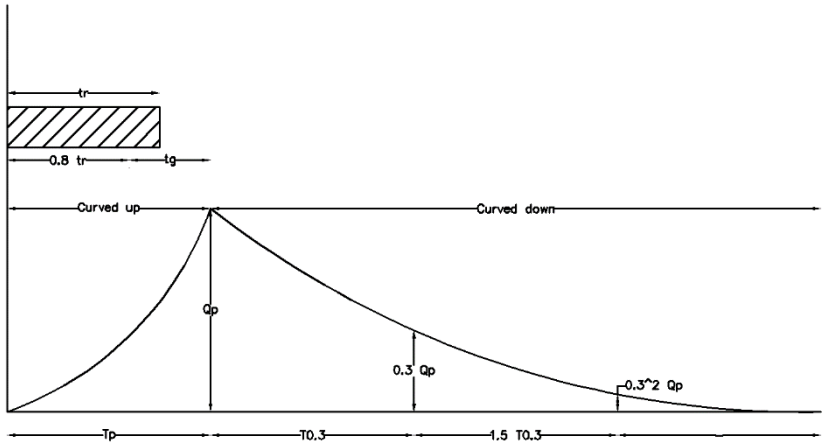

Figure 2 *Hydrograph synthetic scheme of HSS Nakayasu.*

using the detention dam principle. Figure 2 describes the main forming of hydrograph scheme in certain condition.

In the detention pond, discharge reduction that comes out compared to incoming discharge can reach up to 90% in average. In some sediment ponds that have applied the detention pond concept the following discharge decreases are obtained in the table 1. Column (e) describes percentage of total discharge reduction happens in the system. Averagely, the discharge reduction could be optimized above 90% from total peak inflow discharge. Commonly, the low level intake placed as main intake is using HDPE pipe 355 mm with the number of installation line adjusted to meet operational capacities.

Small capacity of the outlet compared to the incoming water discharge makes the water temporarily accommodated in the pond's live storage which will later come out slowly until it returns empty when there are no additional rain events. In this connection the height of the water level in the pond will

Table 1 *Discharge reduction calculation resume.*

Sediment Pond	Peak Inflow Discharge (m^3/s)	Peak Outflow Discharge (m^3/s)	Live storage (m^3)	Discharge Reduction (%)	Low level intake types
(a)	(b)	(c)	(d)	(e)	(f)
Cucakrawa	15.35	6.09	538424.00	60.33%	300mm steel pipe riser
Mawar	14.77	1.05	340341.00	92.87%	3x355mm HDPE pipe
Kemuning	18.42	1.92	845560.00	89.56%	1000mm concrete box culvert
Kenanga	37.33	2.26	659620.84	93.95%	4x355mm HDPE pipe
Kenikir	43.43	1.05	1634000.00	97.59%	3x355mm HDPE pipe
Kecubung	48.18	1.34	2420402.00	97.22%	3x355mm HDPE pipe
Melati	52.28	0.81	537027.00	98.46%	4x355mm HDPE pipe
Ketampi	37.11	0.80	653999.19	97.84%	1x1000 steel pipe
Asparaga	8.31	2.53	418304.00	69.55%	1x355mm HDPE pipe and 1x1000mm steel pipe
Kelayang	91.33	5.20	961019.83	94.31%	3x355mm HDPE pipe

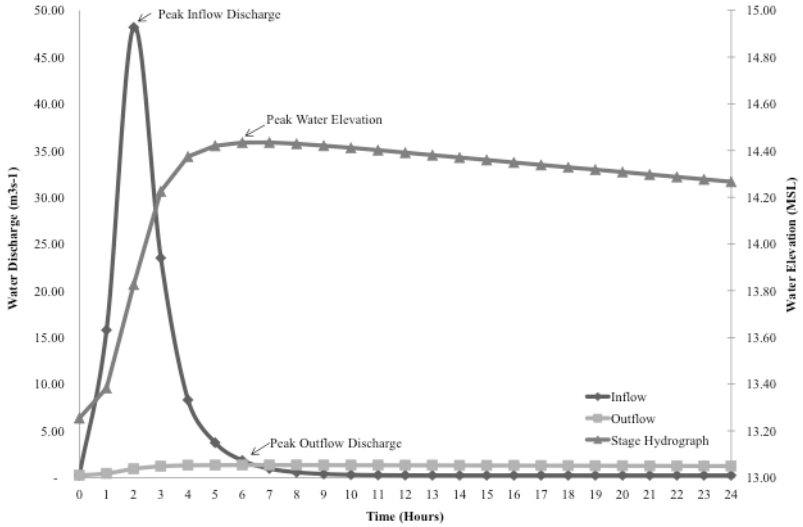

Figure 3 *Discharge routing graph scheme in general.*

rise rapidly and will go down in the span of time according to the capacity of the outlet. Result of such calculation is shown in the table 1 and general scheme applied in the calculation can be found in figure 3.

Topographical conditions greatly affect the possibility of the volume of live storage that can be obtained. It is necessary to choose the right outlet capacity with the volume of storage that can be provided. Calculation of compatibility between outlet capacity and storage capacity is calculated with the water balance between the volume of water entering, the capacity of the outlet and the storage volume. The condition to be achieved is the reduction of outflow compared to the incoming water discharge, it is expected to reach less than 10% of the value of inlet flow and the water can still be accommodated in the detention pond. Determination of the percentage of discharge detention is carried out in this process, the availability of live storage volume is proportional to the percentage of discharge reduction that can be applied.

In the next compartment (labyrinth pond) is a place where sedimentation of dissolved and suspended particle in runoff water is expected. Sedimentation is the process of separating solids from liquids (slurry) by utilizing gravity deposition. Application of this concept has succeeded in reducing the cost of water quality treatment for each cubic meter. Discharge coming out of the detention pond directly decreases the horizontal flow rate in the labyrinth pond. When compared to the absence of discharge control, the ratio of vertical velocity (particle deposition velocity) will be greater than the horizontal velocity (flow velocity) if there is a discharge control pool thereby increasing the potential for settling in the labyrinth pond. With an increase in the natural deposition process, it decreases the need for coagulants to separate dissolved or suspended material in the stream.

If using a larger outlet capacity, it will result in a higher flow velocity or horizontal speed, which will affect the effectiveness of the deposition process. Trash rack is needed to prevent the outlet from clogging. Periodic cleaning must be done on the trash rack. Trash rack is installed in front of the pipe outlet to prevent the entry of trash or other barrier material that can be carried by runoff water.

There are deficiencies in the application of detention ponds, deposition of discrete particles in the upstream part is inevitable. The length of time left makes the flow velocity slowed down so that the process of settling discrete particles will occur naturally. However, when a high flow of discharge occurs, the precipitate will be able to be swallowed by the flow into the next

compartment. In addition to facilitating water quality processing operations, detention ponds directly protect the lives of civil society in the downstream part of the pond by preventing flooding.

Dry dams are much more advantageous than usual impounding dams in the point that sediment is not trapped as much as possible. Detention ponds that do not store sediment will facilitate the decommissioning process of the pond at the end of the mining period. After mining activities are completed, sediment dredging is not necessary, because all sediment entering the pond is channeled downstream for sedimentation and dredging is carried out periodically in the labyrinth pond.

Based on the regulations in force in Indonesia set by the environmental agency, when decommissioning, the company must be able to ensure that the quality of water that will come out of the sediment pond must meet quality standards for a long time even without processing activities. When compared to the weir pond that holds sediment, at the end of the mine there is an accumulation of sediment that must be cleaned before the pond can be decommissioned.

Conclusions

Application of such method has successfully deducted peak of water inflow discharge up to 90% in average from its peak. Low discharges are aimed to diminish cross sectional area of labyrinth since it is linear. Meanwhile, sedimentation process is designed to be occurred on labyrinth.

These schemes successfully bring several advantages for water management system in KPC. Firstly, operation of water treatment facility becomes more effective and more efficient since water flow discharge has been conditioned to be relatively low and constant. Secondly, sediment pond maintenance becomes easier to be managed as several options emerge to recover pond capacity. Also, it becomes the most feasible option in closing the operation in post mining stage; hence, environmental regulatory risk could be eliminated.

References

Haan CT, Barfield BJ, Hayes JC (1986) Design Hydrology and Sedimentology for small catchment. Academic Press, INC, 525 B Street, Suite 1900, San Diego, California, USA

Chow VT, Maidment DR, Mays LW (1988) Applied Hydrology. McGraw-Hill Book Company. Singapore

Cipovová K. Design of a Detention Reservoir. Department of Hydraulic Engineering Faculty of Civil Engineering Slovak University of Technology in Bratislava Radlinského 11813 68 Bratislava. Vol. XIX, 2011, No. 1, 33 – 40, DOI: 10.2478/v10189-011-0005-0

Sumi T, Designing and operating of flood retention 'dry' dams in Japan and USA, Department of Civil and Earth Resources Engineering, Kyoto University Kyoto University Katsura 4, Nishikyo-ku, Kyoto, 615-8540, Japan

Ponce VM (1989) Engineering Hydrology. San Diego State University. Prentice Hall, Englewood Cliffs, New Jersey

Ward RC, Robinson M (1990) Principles of Hydrology. London Mc Graw Hill Company. Singapore

Limantara LM (2010) Hidrologi Praktis, page 147, Lubuk Agung. Bandung

Soemarto CD (1986) Hidrologi Teknik. Usaha Nasional. Surabaya. Indonesia

Status of notiable and other dams at KPC 2008, report number 28001-1 April 2008, Sherwood Geotechnical and Research Services, Corinda, Australia

Water Management Plan 2020-2024 (2020) Internal Publication. East Kutai. Indonesia

Final Treatment Trials on Cwm Rheidol - Ystumtuen mines discharges, Wales, using Sono-electrochemistry (Electrolysis with assisted Power Ultrasound)

Chris Bullen[1], Peter Stanley[2]

[1]*Power & Water, C10 Ashmount Business Park, Swansea, SA6 8QR, UK, cbullen@powerandwater.com*

[2]*Natural Resources Wales, Tŷ Cambria, Newport Rd., Cardiff, CF24 0TP, UK, peter.stanley@cyfoethnaturiolcymru.gov.uk*

Abstract

Results of the successful 2019 Sono-electrochemistry Soneco© final pilot trials using a magnesium electrode are presented. The preferred pH range was 8.8 to 9.0 removing 90.0%, 95.7% and 95.1% total lead, zinc and cadmium.

Full-scale treatment plant would utilise 3.1 kW/m^3/h, a clarification area of 57 m^2 (enabling the lamella to fit in the existing filter beds) generating a sludge volume of 4.8 m^3/day at 2% w/w (further dewaterable by press). CapEx for a comparable high-density sludge process has an appealing ratio of 1:3. Reducing electrode costs will make OpEx more competitive whilst planned process enhancements will lower CapEx and OpEx further.

Keywords: Sono-electrochemistry, electrochemistry, liquid chemical free treatment, Soneco, reactor

Introduction

The Cwm Rheidol metal mine complex comprises of six separate mines including Ty'n y Fron a satellite mine connected by a former tramway. Four mines Ystumtuen, Penrhiw, Bwlchgwyn and Llwynteifi on the upland plateau are hydraulically connected with the Cwm Rheidol mine. Two adits drain mine water towards the Afon Rheidol. It is currently classified as one of the top-ten most polluting mine waters in Wales, discharging highly acidic mine water rich in dissolved metals (e.g. lead, zinc and cadmium) that accounts for almost half of the metals loading into the Afon Rheidol damaging the ecosystem and further adding to water body derogation to the tidal limit some 18 km downstream. The combined metal load is approximately 9 tonnes/year consisting of approximately 4.8 tonnes of zinc, 160 kg of lead, 11 kg of cadmium and 4.0 tonnes of iron. The river is also impacted with yellow ochre staining from the iron rich water (NRW 2016). Adits 6 and 9 are situated at two different heights in the Rheidol valley, Adit 6 is located at approximately 110 m and Adit 9 approximately 60 m above the Afon Rheidol. Both adits serve different mine areas and yield different water quality, flow, heavy metal concentration and metal solubility. **Adit 6** the uppermost on the mountain has a higher volume of metal mine water (30 m^3/h) yet lower concentrations of soluble metals in acidic conditions. **Adit 9** is less elevated in height and of lower volume of mine water (2 m^3/h), but higher concentrations of dissolved metals and more acidic. In 2009, the adit discharges were collected into two pipes that conveyed the discharges safely down the side of the narrow steep sided valley to a manifold before collectively discharging into the existing filter beds at a fairly constant ratio of 14:1.

The original limestone filter beds from the mid 1960's have been ineffective. Cwm Rheidol poses a challenging topology for traditional passive treatment processes or large treatment plants capable of dealing with the varying levels of water which can flow from the mines as they would require considerable area of relatively flat land (0.8 Ha) to operate adequately and cope with both high and low levels of flow to operate effectively. Natural Resources Wales (NRW) has a completed

feasibility study on long-term Mine Water Treatment Plant (MWTP) for Cwm Rheidol. Due to the location and access issues the MWTP will need to be compact and with a small footprint, require minimal operational input, traffic movements and reduced risk to watercourse. Optioneering is the next stage.

Sono-electrochemistry

An alternative to adding hydroxides via traditional liquid chemicals (that can result in increased infrastructure, access requirements for delivery, safety implications, and increased risk to adjacent watercourse through uncontrolled release) hydroxides can be added using sacrificial anode electrochemistry. Here the anode is made from high purity magnesium (>98% Mg). Though the use of liquid magnesium hydroxide is common in mine water treatment the production of magnesium hydroxide via sacrificial dissolution of a magnesium electrode by electrolysis and ultrasound to electro-generate magnesium hydroxide is a novel process.

By combining power ultrasound with electrolysis in the Soneco© (Morgan 2014) sono-electrochemistry system can reduce the build up of the passivation layers (Stern and Helmholtz layers) that can develop on the electrode surface during the operation of conventional electrochemistry systems. Eliminating the formation of the passivation layer lowers the electrical resistance of reactor circuit, reduces the power requirement, increases treatment efficiency and effectiveness (Morgan 2014). This makes the Soneco© a viable alternative to conventional liquid chemical-based systems for the treatment of acid mine water drainage (AMD).

Methods

Original trials were undertaken during March and August 2018 (Rose 2019) that successfully showed the Soneco© is a suitable alternative treatment to liquid chemical dosing for treatment of mine water generated at the Cwm Rheidol - Ystumtuen mines. A third and final set of trials were undertaken during December 2019 and designed to: Re-Confirm that the proposed water limits stated can be achieved by the proposed treatment process, confirm the proposed treatment plants inputs and generate data that can be used to undertake concept sizing of a proposed MWTP.

Materials: Trial Pilot plant treatment system

The pilot plant, shown schematically in Figure 1 and in the photograph presented in Figure 2, was configured as a continuous process to minimise, as far as possible, scale up error, by matching the pilot plant operating parameters with those anticipated for the proposed full-scale plant. The process stream consists of: Mine water feed pumping system, Stage I: Soneco© DB1 Reactor, Stage II: Flocculation tank and Stage III: Lamella Clarifier.

Ancillary equipment comprised of a 50 mm flowmeter and a clarifier de-sludge pump. Conductivity and pH probes were mounted in the feed sump, another pH probe was mounted in the flocculation tank. Two 1m^3 IBC tanks were also positioned on site to store sludge produced.

Mine water was pumped to the pilot plant from a collection tank installed where combined adit flows enter the existing reed bed system. The volume of mine water treated was recorded by a magnetic flow meter on the feed line, with flow rate regulated by a manual diaphragm valve. The operating flow rate varied between 0.95–1.1 m^3/h over the course of the trial. The mine water pH and conductivity were continuously measured in the collection tank.

Stage 1 of the process consisted of a Soneco© DB1 Reactor where magnesium hydroxide was generated electrochemically by applying a current to the magnesium anode. The current (and hence dose rate) was controlled via a pH probe located at the inlet of the Stage II Flocculation Tank. The amount of magnesium released (and hence magnesium hydroxide added) in the Stage I Reactor was controlled via a proportional integral derivative (PID) control loop. The reactor was built from SS316 with: 1No Magnesium Anode, 2No Stainless Steel Cathodes, and 8No ultrasonic transducers for removing passivation layers.

pH corrected mine water overflowed

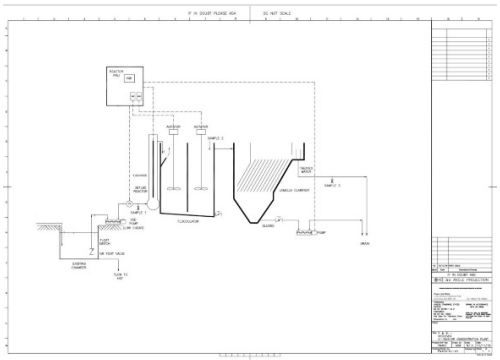

Figure 1 P&ID of Trial System.

Figure 2 Photograph of the Trial System.

from the Stage I Reactor into the Stage II flocculation tank. The 4 m^3 tank was fitted with a top mounted mixer to keep the solids in suspension, degas the metal hydroxide formed and aid floc formation. A pH probe was fitted within the flocculation tank providing a PID feedback loop that would achieve the required treatment via an inputted setpoint.

Flocculated mine water overflowed from the Stage II Flocculator into the Stage III Lamella Clarifier (combined with inlet floc mixer) where metal hydroxide floc settled and thickened. Solids/liquid separation was achieved in a lamella clarifier with an effective settling area of 10.0 m^2. Supernatant water was discharged into the filter beds prior to release to the environment.

Thickened separated solids from the clarifier were transferred via gravity back to sludge holding tanks (1 m^3 IBC tanks) and removed from site to be analysed. Supernatant water from the IBCs were decanted back to the filter beds.

Samples were taken from the: feed pit, DB1 reactor weir overflow and the final treated water. Samples were analysed (by Wheal Jane Laboratories, Truro, Cornwall England) for: pH, TSS, conductivity, sulphate, calcium, magnesium, potassium, chloride, sodium, alkalinity, carbonate, copper, arsenic, aluminium and Total and dissolved: lead, zinc, iron, cadmium, manganese. The following parameters were monitored to assess the performance of the pilot plant: volume of water treated, energy consumption, water quality (influent and effluent), magnesium consumption, sludge generation, and solids settlement characteristics (settling velocity and settled solids).

Results

The operating flow rate varied between 0.95–1.1 m3/h, measured using a magnetic type flow meter, over the course of the trial.

Table 1 presents a summary of the total metal results from the analysis undertaken on the feed mine water. These values show that as the trial proceeded the metal concentrations, i.e. zinc and cadmium, reduced in concentration due to heavy rainfall.

The results of analysis of samples undertaken on Stage 1 (Soneco©) treated water showed that the dissolved metals vary as the treatment pH varies. Once the weir discharge pH was >8.5 the dissolved zinc, lead and cadmium concentrations reduced to 0.10 mg/L, 0.10mg/L and 0.001mg/L respectively and hence this confirms that the use of magnesium electrodes is an appropriate way of raising the pH of the mine water and precipitating the dissolved metals as metal hydroxides.

Table 2 presents a summary of the total metal results from the analysis undertaken on the treated mine water. The results show that the potential treated water limits were met when the pilot plant was operated at a pH of >8.8.

Table 3 presents the total metal removal rates across the whole pilot plant during the trials. Lead, zinc and cadmium removal rates for when the operating pH was >8.8 were >86%, 91% and 90%.

Table 1: Mine water total metal concentrations

	pH	Pb	Zn	Fe	Cd	Mg	Ca	Mn
		mg/L	mg/L	mg/L	mg/L	mg/L	mg/L	mg/L
03/12/2019	2.9	0.47	22.29	2.36	0.041	15.10	35.82	0.930
04/12/2019	3.0	0.62	22.91	2.70	0.041	15.50	----	----
05/12/2019	2.9	0.48	22.28	4.56	0.041	14.85	35.12	0.940
06/12/2019	3.0	0.48	20.80	2.00	0.041	14.43	----	----
09/12/2019	3.0	0.71	15.19	5.65	0.030	10.62	27.68	0.580
10/12/2019	3.1	0.68	14.50	4.22	0.028	10.17	----	----
11/12/2019	3.0	0.89	14.37	4.16	0.028	9.93	26.94	0.510
Max		0.89	22.91	5.65	0.041	15.50	35.82	0.940
95%ile		0.84	22.72	5.32	0.041	15.38	35.72	0.938
Average		0.62	18.91	3.66	0.036	12.94	31.39	0.740
Min		0.47	14.37	2.00	0.028	9.93	26.94	0.510

Table 2 Treated Water Discharge Total Metal Concentrations.

	pH	Pb	Zn	Fe	Cd	Mg	Ca	Mn
		mg/L	mg/L	mg/L	mg/L	mg/L	mg/L	mg/L
03/12/2019	8.8	0.05	0.96	0.87	0.002	42.12	34.97	0.280
04/12/2019	6.1	0.06	5.06	1.22	0.022	38.46	----	----
05/12/2019	5.6	0.09	10.65	2.57	0.034	35.56	35.36	0.820
06/12/2019	5.9	0.06	9.29	1.93	0.031	34.68	----	----
09/12/2019	9.1	0.10	1.32	2.04	0.003	34.80	25.28	0.096
10/12/2019	6.1	0.19	4.91	1.23	0.019	23.86	----	----
11/12/2019	6.0	0.19	6.72	1.29	0.023	24.31	25.48	0.440
Max		0.19	10.65	2.57	0.034	42.12	35.36	0.820
95%ile		0.19	10.24	2.41	0.033	41.02	35.30	0.763
Average		0.11	5.56	1.59	0.019	33.40	30.27	0.409
Min		0.05	0.96	0.87	0.002	23.86	25.28	0.096

The conductivity measurement was recorded during the trial using the on-line meter. Due to an average mine water conductivity of 562 µS/cm the water can be termed as having low conductivity. During the trial the mine water conductivity dropped from an initial 657 µS/cm to a concentration of 437 µS/cm at the end of the trial.

Settlement tests (also termed mudline tests) were undertaken on the clarifier feed (Stage II discharge). The data derived from these tests have been used to calculate: the initial settling velocity and the final settled solids concentration. The settlement velocity of 0.6 $m^3/h/m^2$ was required to ensure a TSS limit of <30 mg/L was met. Using a rise rate of 0.6 $m^3/h/m^2$ and a total treatment flow rate of 9.4 L/s (34 m^3/h) total effective clarification area of 57 m^2 has been calculated.

Figure 3 presents an unedited photograph of the mine water, precipitate generated and treated water off the lamella clarifier.

Table 3 Total Metal Removal Rates.

	pH	Pb	Zn	Fe	Cd	Mn
		%	%	%	%	%
03/12/2019	8.8	90.0	95.7	63.1	95.1	69.9
04/12/2019	6.1	90.3	77.9	54.8	46.3	
05/12/2019	5.6	80.4	52.2	43.6	17.1	12.8
06/12/2019	5.9	87.3	55.3	3.5	24.4	
09/12/2019	9.1	86.1	91.3	63.9	90.0	83.4
10/12/2019	6.1	72.1	66.1	70.9	32.1	
11/12/2019	6.0	78.7	53.2	69.0	17.9	13.7
Max		90.3	95.7	70.9	95.1	83.4
95%ile		90.2	94.4	70.3	93.6	81.4
Average		83.5	70.3	52.7	46.1	45.0
Min		72.1	52.2	3.5	17.1	12.8

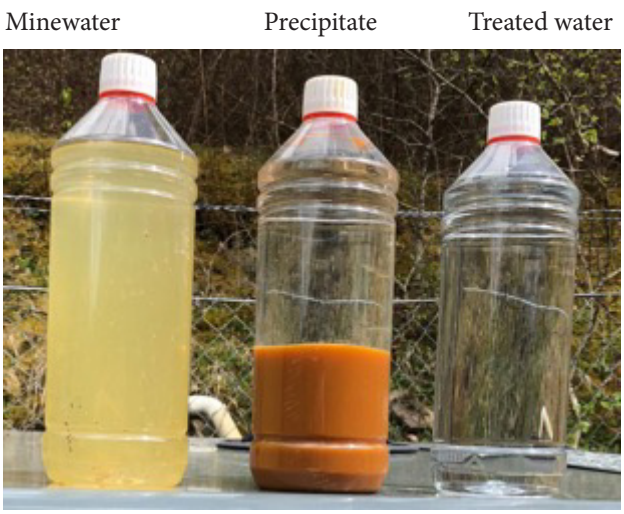

Figure 3 *Photograph of the Mine Water as it passes through the Treatment System.*

Magnesium was added via applying a current to the anode proportional to the pH in the inlet to the floc tank. Due to the chemical reactions this was converted to magnesium hydroxide with the hydroxides then used to precipitate the dissolved metals as metal hydroxides. Using a measured magnesium increase of 27 mg/L the magnesium hydroxide usage was calculated at a dose rate of 64 mg/L, this will equate to a daily plate usage of 22 kg/day of electrode in the full-scale plant when treating 34 m^3/h.

The solids generation rate, mg of solids per litre of mine water treated, has been calculated from the mine water inlet iron concentrations and the percentage of iron in the dry solids removed from the system. This calculated the sludge generation rate was 120 mg/L of water treated. Using 120 mg/L equates to a daily solids production of 98 kg of dried solids per day or 0.93 m^3/day (6.5 m^3/week) of 10% w/w solids (dewatered sludge). Sludge composition as key components as a % of the solids: Iron 17.4%, zinc 10.8%, Hydroxide 29.3%, Carbonate 9.4%.

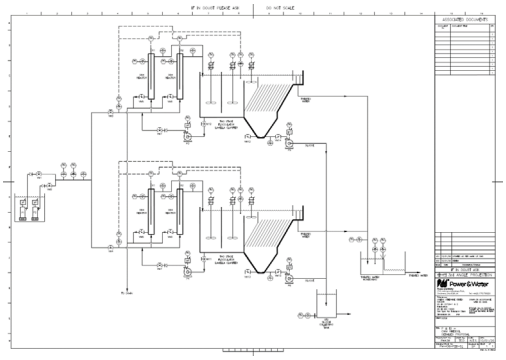

Figure 4 P&ID of Full-Scale System.

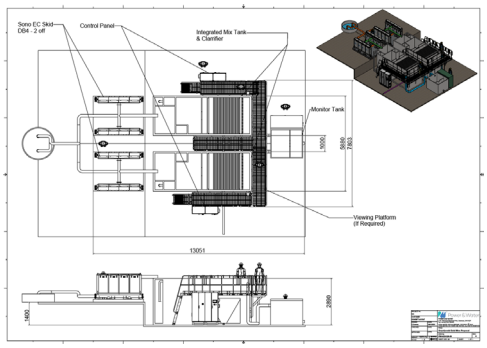

Figure 5 GA of Full-Scale System.

Full Scale Design

The trial has again successfully shown that the sono-electrochemistry process can remove the required metals, e.g. lead, zinc and cadmium, and enabled the proposed full-scale MWTP concept design to be completed. The proposed plant would consist of: a single feed system with overflow to river, two process streams each consisting of 2No DB4 reactors with automated pH control, 1No flocculation tank, 1No lamella clarifiers with 40 m^2 of clarification area and sludge transfer pumps. Common ancillaries will consist of sludge treatment via 1No sludge storage tank, 1No automated filter press, 1No sludge cake skip and treated Water Monitoring equipment, Table 4 presents a summary of the outline concept design parameters. Figures 4 and 5 show the P&ID and general Arrangement of the proposed full-scale plant.

The concept design has enabled the CapEx and OpEx costings to be undertaken enabling a comparison with a traditional high-density sludge (HDS) plant.

Table 4 The Outline Concept Design of the Full-Scale Plant.

	Item	Unit	Valve
System Design	Soneco Reactor	Name	4 No DB4
	Flash Mix	m^3	1
	Floc Mix	m^3	2
	Clarification area	m^2	57
Alkali Dose	Magnesium Hydroxide Dose Efficiency	%	92
	Actual Magnesium Hydroxide Dose	mg/L	67
	Magnesium plate Weight	kg	20
	Plates per year	No	402
Solids generation	Solids generation	mg/L	120
	Waste sludge off clarifier	%ds	2
	Dewatered sludge	%ds	30
	Volume of dewatered sludge	m^3/week	6.5
Required Power	Sono- EC power	kW	77
	Total Power	kW	107

Conclusions

1. This final pilot trial has repeated the excellent removal rates shown in previous trials and confirmed that the Soneco© treatment process is a viable alternative treatment process for AMD.
2. The costed CapEx (excluding groundworks and power supply) for a sono-electrochemistry process is favourable when compared to a traditional HDS process with a ratio of 1:3.
3. Due to existing costs of magnesium electrodes the OpEx of a sono-electrochemistry is less favourable with an HDS plant. Working with the supply chain will, however, reduce electrode costs and make the OpEx applied at Cwm Rheidol more competitive.
4. Further planned process enhancements will halve the required number of units, lowering CapEx, whilst also halving the power demand, hence OpEx. This will make the whole life cost over forty years more favourable for a sono-electrochemistry system enabling consideration during optioneering.
5. Due to the compact design the process is suitable for applications where land availability or access is constrained and landscape, habitat or heritage are sensitive.

Acknowledgements

The authors thank the Welsh Government Water Branch and Innovation team for funding and with NRW the continued project support. We extend thanks and appreciation to all co-organisers for organising the IMWA2020 Conference proceedings and wish them success in progressing IMWA2022 in New Zealand.

References

NRW (2016) Abandoned Mine Case Study: Cwm Rheidol Lead & Zinc Mine.

Rose SA, Matthews, ZN, Morgan G, Bullen CJ, Stanley P (2019) Sono-electrochemistry (Electrolysis with assisted Power Ultrasound) Treatment Trials of discharges from Cwm Rheidol – Ystumtuen mines, Ceredigion, Mid Wales, UK. IMWA 2019: 262-268.

Morgan PG (2014). British Patent No GB 1503638.7 – Method and apparatus for decontamination of fluids (Soneco). International Patent PCT/GB2016/050692 – Method and apparatus for decontamination of fluids.

Morgan SA, Matthews ZN, Morgan PG, Stanley P (2017). Removal of Iron from Dyffryn Adda, Parys Mountain, N. Wales, UK using Sono-electrochemistry (Electrolysis with assisted Power Ultrasound).

Selective Recovery of Copper and Cobalt from Mine Effluent

Esther Takaluoma[1], Tatiana Samarina[1], Gershom Mwandila[2], Leonard Kabondo[2], Kawunga Nyirenda[2], Phenny Mwaanga[2]

[1]*Kajaani University of Applied Sciences, Ketunpolku 1, FI-87100 Kajaani, Finland, esther.takaluoma@kamk.fi*

[2]*Copperbelt University, School of Mines and Mineral Sciences, 4662 Jambo Drive, Riverside, Kitwe, Zambia*

Abstract

Adsorption is a powerful tool to remove contaminants ions from water. In here, two major limitations of adsorption technique (the accumulation of exhausted waste-adsorbent and poor selectivity) are overcome by time-dependent selectivity and cycling of adsorbent by selective desorption. Real mine effluent containing 917 ± 92 mg Cu/L and 36,9 ± 3,7 mg Co/L was used as a real-life sample to demonstrate the ability to separate Cu and Co by means of adsorption on MgO with subsequent recovery copper by leaching and cobalt as sulfide. A brief economic evaluation supports the suitability of the approach.

Keywords: selective adsorption, copper, cobalt, mine effluent, economic evaluation

Introduction

The fast-growing electric vehicle market has increased the need for efficient lithium, cobalt, and nickel containing batteries. It has been estimated, that the cobalt requirements will grow by 15-fold by 2030, as compared to 2019, while the trading of cobalt is often associated with human right violations (Claudiu 2018). However, cobalt, and other critical and valuable materials, can be recovered from industrial side streams and from acid mine drainage, or mine process water. While the concentration is usually low (5 – 40 mg/L for Co, for example) the large flow of water, often hundreds of cubic meters per hour, makes those a substantial source of valuable elements.

Commonly, mine water is treated by applying $CaCO_3$ or $Ca(OH)_2$ to co-precipitate the impurities as faulty cations within the lattice of the forming gypsum or as metal hydroxides by the increase in pH (Geldenhuys 2003). However, this approach has the valuable metals seized in a calcium-rich low metal matrix and requires large storage capacity for tailings. In here, the selective recovery of cobalt and copper from mine effluent is discussed (CCR).

Samples

Mine effluent was received from a mine in Zambia, taken before neutralization process and subsequent flow to environment. Initial parameters are a pH 2,52 and an electric conductivity of 6,82 mS. The samples were analyzed by ICP-OES from accredited laboratory and the results of initial mine effluent shown in Table 1. Synthetic waters with the main constituents was mimicked for initial selectivity tests and for the first eight cycles, with the concentrations depicted in Table 1. After establishing an efficient routine for the recovery path (CCR) the remaining four cycles were repeated with real mine water sample.

Methodology

AAS analysis were conducted with a Perkin Elmer 5000 spectrometer (air-acetylene flame). XRF data was collected with a Panalytical Minipal 4 XRF spectrometer utilizing semiquantitative Omnian parameter. The XRD diffractograms were collected on Panalytical Xpert PRO diffractometer with Co α-radiation at a wavelength of 1.79 Å. Diffractograms were interpreted with Highscore plus and commercial database.

UV-vis spectra were recorded with Specord 50 PLUS from Analytik Jena AG. Deionized water had an electric resistivity of 0.036 mΩ.

Initial tests were conducted with synthetic mine water, prepared according to the concentrations determined by ICP-OES from real mine water, containing the most important contaminants and target elements as shown in Table 1.

Adsorbents

Adsorbent was prepared by calcination of magnesite tailing from local Finnish talcum mine. The main constituents of adsorbent are MgO (58.8%), Fe_2O3 (13.5%), and SiO_2 (21.7%) residues, with MgO being in periclase form. The XRF data of new and copper loaded adsorbent after 10th adsorption cycle is gathered in Table 2.

Iron Removal

Iron is an interfering ion in adsorption and lowers the adsorption capacity by preferential adsorption. The iron in the mine water was removed by pretreatment procedure, without affecting the concentration of the desired cobalt and copper ions. As such, the pH was adjusted carefully to pH 5 by dropwise addition of 5 M NaOH. The precipitated iron hydroxides were filtered through glass powder on filter paper, by means of suction filtration.

Table 1 *Initial concentration of elements from mine water sample and dissolved cobalt sulfide, ICE-OES in mg/L.*

Element	mg/L mine water	synthetic mine water mg/L	mg/L dissolved CoS
Al	114,8		1,61
As	<0,75		< 0,075
B	<1		< 0,1
Ba	<0,25		0,781
Be	0,59		< 0,025
Ca	510	59	41
Cd	<0,1		0,025
Co	36,9	37,552	132
Cr	0,62		0,22
Cu	917	895,05	1,6
Fe	15,4	15,434	0,925
K	66,6		5,75
Mg	953	940	59,5
Mn	264	105,14	475
Mo	<0,25		< 0,025
Na	18,4		30,4
Ni	0,99		3,37
P	5,63		< 0,25
Pb	<0,75		< 0,075
S	2680		242
Sb	<0,75		< 0,075
Se	<0,75		< 0,075
Sn	<0,75		< 0,075
Ti	<0,75		< 0,075
V	<0,25		< 0,025
Zn	2,1	2,36	0,112

Table 2 Adsorbent XRF data.

Element	Adsorbent raw, %	after 10th adsorption, %
MgO	58,8	32,64
SiO_2	21,7	17,53
SO_3	1,28	8,13
K_2O	0,12	0,05
CaO	1,11	0,56
Cr	0,25	0,26
Mn	0,15	0,61
Fe_2O_3	13,58	19,62
Ni	0,16	0,12
Cu	-	11,66

Copper Adsorption and Recovery

To establish selectivity time dependent tests were performed. After iron removal, the solution was divided into 12 aliquots of 200 ml water. MgO-adsorbent was added to the complex water matrix at pH 5 with an overall adsorbent dose of 3 g/L. In appropriate time intervals, the adsorbent was filtered off and the copper and cobalt concentration measured by AAS method. The data from 5 min to 23.5 h is depicted in Figure 2. Copper adsorption is preferential over cobalt adsorption and starts only after complete removal of copper. The study was repeated at lower pH, without pretreatment, and the same overall trend however with slight time delay was observed, most likely due to the slow pH rising effect of MgO to pH 5 – 6, as depicted in Figure 2.

After filtration, copper was recovered by leaching with ammonia solution at 5 % (cycle 1–9) or 10 % (cycle 10–12). The treatment cycle was repeated twelve time and the copper, cobalt, and manganese removal percent is depicted in Figure 3, after each cycle adsorbent mass (loss from filtration, handling and dissolution, less than 10%) reconstituted to 3,00 g/L. Copper was removed selectively with very little effect on cobalt and manganese concentration as can be seen Figure 3. Copper was leached with 5% ammonia, and the adsorption capacity slowly declined to 50% copper removal at

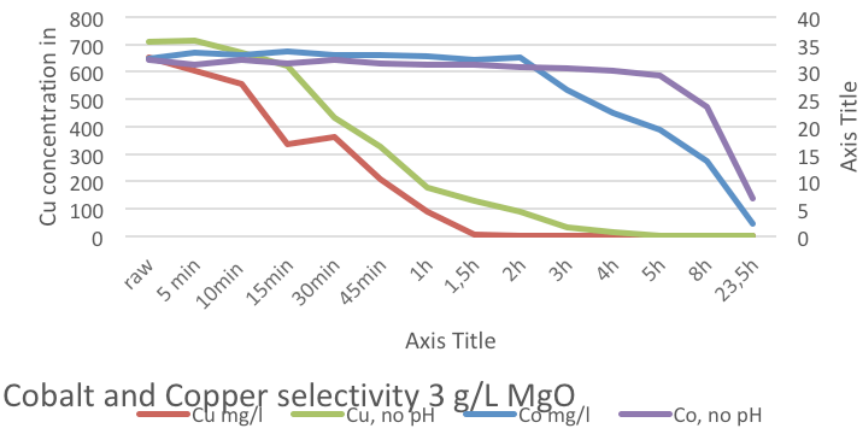

Figure 2 *Time dependent adsorption of copper and cobalt onto MgO, at 3 g/L adsorbent dose at pH 5 and pH 2.5 (raw mine water, no pH and iron removal).*

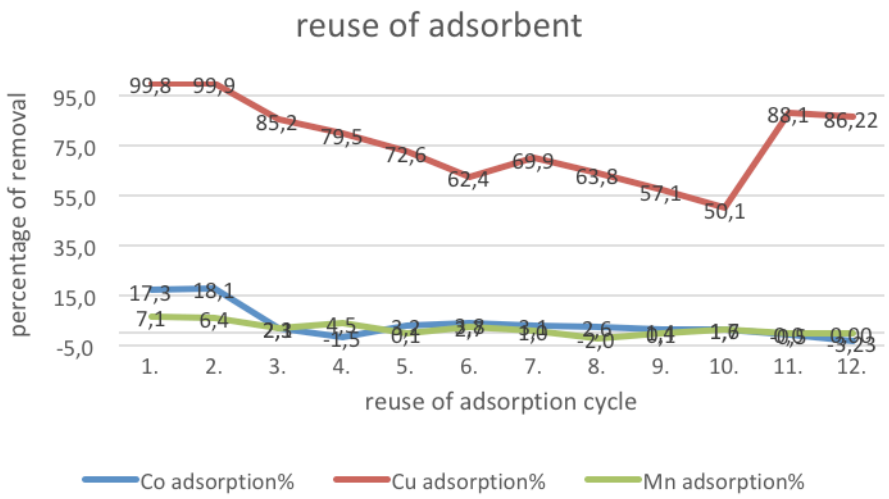

Figure 3 Sorption and desorption of MgO utilizing synthetic mine water, negative datapoints due to measure uncertainty.

tenth cycle, with initial concentration of 895 mg/L Cu and an adsorbent dose of 3 g/L. XRF spectroscopy, refer to Table 2, confirmed the visual analysis of 11% copper loading of adsorbent. Leaching with 10% ammonia removed copper and restored adsorbent capacity, as seen after 11th cycle.

Cobalt Recovery

After copper removal by adsorption, cobalt was precipitated as CoS by dropwise addition of Na_2S upon stirring. Black precipitate formed was filtered off, dissolved in HNO_3, and sent to accredited laboratory for quantitative analysis. The concentration of contaminants in dissolved CoS is combined in Table 1. Manganese (475 ± mg/L) precipitated with the cobalt (132 ± 13 mg/L) to give cobalt/manganese sulfide. Other impurities are coprecipitated magnesium and calcium, and enrichment of less than 1% nickel (3,37 ± 3,4 mg/L). Copper is present in 1.6 ± 0,16 mg/L.

Proposed treatment scheme for copper and cobalt recovery (CCR)

To put the proposed CCR scheme into piloting stage, only mature and commercial technique is required for pH adjustments, filterings, and adsorbent dosage. The process can be overviewed in Figure 1.

Economic Considerations

Three main valuable contaminants are included in mine effluent from Zambian mine: copper, cobalt, and manganese. At the current flow of 800 m^3/h and 19200 m^3/d and the prices for copper, cobalt, and manganese being 4617 USD/t, 29500 USD/t, and 2000 USD/t, respectively, (infomine, June 2020) the mine is losing daily a potential revenue of 2768 USD per day or 1010203 USD per

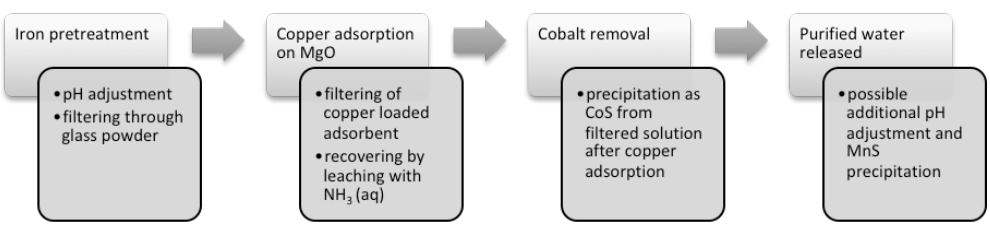

Figure 1 Process-flow of copper and cobalt recovery (CCR).

year, calculated from the metals currently precipitated as hydroxide into tailings, at 100% yield. The present gypsum precipitation has a cost of 12 to 18 USD per day and can be considered as the cheapest practice. Reagent costs in USD for the proposed CCR process (Figure 1) including pretreatment-copper adsorption/desorption-pH adjustment and CoS and MnS precipitation steps are considered in Table 3 and calculated as costs per day. To estimate the costs some assumptions were made, e.g. adsorbent cost was estimated to be 400 USD per ton, taking calcination costs of magnesite tailings into considerations. Reagent prices were averages from common retail vendors. Ammonia was reused 20 times at 10% concentration and the adsorbent 20 times. This results into combined costs of 21,890 USD per day. Certainly, the costs of sulfide concentrate must be correlated to metal prices taking smelting costs into account. At the current process shown, the process appears far from economical (10 times of revenue). Possible optimizations can be considered after breaking down the costs: the largest price was the use of NaOH for pH adjustment, this could be cut by utilizing lime as currently also used, but only with the goal of pH adjustment until pH 5 not for full precipitation of metals. Calcium ions does not influence adsorption properties of MgO. The second largest price is adsorbent and ammonia leaching. Here, a piloting to find out the final number of re-usability of adsorbent and the re-use and optimization of ammonia amount. The left most column in Table 3 considers the optimization parameters such as reuse of adsorbent 40 times, reusing ammonia 40 times, and utilizing lime for pH adjustment.

Conclusions

Calcined magnesite can adsorb over 11% of its weight in copper as determined by XRF. Selectivity of copper over cobalt is obtained by time-dependency. Real mine effluent containing copper in over 10 times excess over cobalt was used as a real-life sample to demonstrate the ability to separate chosen elements by means of adsorption and to recover copper and cobalt, two commercially valuable elements (CCR process). The

Table 3 *Chemical costs for proposed recovery scheme, in USD, 19200 $m^{3/d}$.*

treatment step	chemical	price USD/t	used for 1 m^3 in kg	price per m^3/USD	price per day	pos. optimization
adsorbent	MgO	400	3	0,06	1152	576
pH adjustment	NaOH	400	0,8	0,32	6144	12
filtration	sand or glass	80		0	0	0
ammonia desorption	ammonia 25%	200	30	0,12	5760	1440
Na_2S precipitation	Na2S	400	0,025	0,010	189	189
pH adjustment	NaOH	400	0,8	0,32	6144	12
Na_2S precipitation	Na2S	400	0,181	0,072	1390	1390
pH adjustment	H2SO4	200	0,006	0,001	21	21
Na_2S precipitation	Na2S	400	0,142	0,057	1091	1091
SUM					**21890 USD/d**	**4730 USD/d**
possible revenue					**2768 USD/d**	**2768 USD/d**

composition of sample was complex: iron, calcium, aluminium and magnesium were the major components in concentration 15 ± 1,5 mg/L Fe, 510 ± 51 mg/L Ca, 115 ± 12 mg/L Al, and 953 ± 95 mg/L Mg, respectively. In the first step, iron was removed by pre-treatment to reach maximum capacity of adsorbent and improve selectivity of adsorption. Then, copper was selectively adsorbed onto MgO-containing powdered adsorbent, and selectively removed by extraction. Cobalt was quantitatively precipitated as CoS. The adsorbent was then reused and has been cycled for twelve times. Based on comparison of reagent costs and loss of revenue, the approach is currently more expensive than lost revenue, however politic decisions, tailing storage problems, rising commodity prices and especially optimization of process by piloting and cycling of leaching solution could make CCR process easily feasible in the future.

Acknowledgements

This study was conducted as part of the KAKKU project (number A74868 EAKR, Kainuun Liitto).

References

Claudiu P, Blagoeva D, Alves Dias P, Arvantidis N (2018) Cobalt Demand-supply balances in the transition to electric mobility, Joint Research Centre (European Commission) doi: 10.2760/97710

Geldenhuys AJ, Maree JP, de Beer M, Hlabela P (2003) An integrated limestone/lime process for partial sulphate removal, The Journal of The South African Institute of Mining and Metallurgy, p 345—354.

www.infomine.com, retrieved 15.6.2020.

Human Health and Environmental Risk Assessment for Closure Planning of the Argyle Diamond Mine Pit Lake

Cherie D. McCullough[1], Samantha Sturgess[2]

[1]*Mine Lakes Consulting, PO Box 744, Joondalup DC, WA 6005, Australia, cmccullough@minelakes.com*

2Rio Tinto, Perth, WA 6000, Australia, Samantha.Sturgess@riotinto.com

Abstract

Argyle Diamond Mine (Argyle) is a large open cut and underground mine in Northern Australia preparing for closure with the pit as a water management structure. Water quality will be pH 8-9, with solute concentrations increasing through evaporative concentration. However, poor pit lake habitat quality and restricted access to humans and stock limits exposure to potential receptors.

A risk assessment based on consequence and likelihood, found all risks from the pit lake water to be very low. A risk assessment offers a useful approach to assessing pit lake risk when specific water quality criteria alone may not be appropriate.

Keywords: Mine closure, pit lake, environmental risk assessment, human health, water quality, acid and metalliferous drainage

Introduction

Mine pit lakes are a common feature of open cut mine closures extending below local groundwater levels (Castendyk and Eary 2009). With large water volumes which often contain waters degraded by elevated contaminants of potential concern (COPC), pit lakes can represent a relevant socio-environmental risk at mine closure (McCullough and Lund 2006) and may represent the highest environmental risk closure landform for many mines (Doupé and Lymbery 2005)

Determining acceptable long-term pit lake water quality is a substantial challenge for closure planning because the final lake may not resemble or have intended end use values of a natural lake. Furthermore, some pit lakes take decades to fill with water quality improving or degrading over time, and yet relinquishment decisions need to be made within a much shorter post-closure monitoring period.

Study site

The Argyle Diamond Mine (Argyle) is a large open cut and underground lamproite pipe mine in Northern Australia which is preparing for closure in late 2020. Argyle is located on a State Agreement Mining Lease in the East Kimberley region of Western Australia. It is situated in the headwaters of Smoke and Limestone Creeks, which ultimately drain into Lake Argyle, approximately 35 km to the north-east.

The climate is monsoonal, with potential cyclones and heavy rains during the wet season from November to April, high evaporation rates during dry season months and warm temperatures all year round. The Argyle project area is on a pastoral lease with extensive grazing including access to natural waterways. Long term grazing has led to cattle damage of native vegetation and habitats through direct grazing and associated effects including soil erosion and compaction and weed invasion. These activities are expected to have impacted the suitability and quality of habitats for many native terrestrial vertebrate fauna in particular.

Open pit mining of the Argyle Kimberlite 1 (AK1) pit void commenced in 1985 and was completed in 2013. During open pit mining, waste material was hauled to the waste rock landforms (WRLs), while ore was taken to the processing plant for diamond recovery. The WRLs contain some geological units with the potential to generate acid and metalliferous drainage (AMD) and seepage from the southern WRL has been managed as part of operations since 1999.

The resulting pit void has a maximum depth of approximately 600 m with breakthrough to the underlying block cave in the southern bowl. Following cessation of the underground operations and associated dewatering, the block cave will flood and water will daylight in the base of the open pit within one year. A key closure domain identified as potentially presenting risk at closure was the pit void and associated lake which will form following cessation of dewatering activities.

AK1 Pit lake

A conceptual hydrogeological model was constructed to represent the AK1 Pit Lake including major inflows (predominantly groundwater) and outflows (predominantly evaporation) that form the basis of the design for the water balance model. Pit lake modelling was then undertaken to understand the water levels and water quality that will result in the open pit void for up to 300 y after dewatering and mining ceases (Aquastrat 2020).

Initial modelling predicted that the pit lake would be a terminal evaporative sink. This water balance provided an opportunity for a sustainable and long-term water management approach utilising the pit lake to contain AMD seepage and other mine waters not suitable for release to the environment. As part of Argyle's closure water management strategy, two WRL seepage locations will be directed into the open pit during the dry season and initial drain down of AK1 Tailings Storage Facility (TSF) water will be pumped to the underground leading to the pit lake (fig 1).

Major inflows into the pit lake are from good quality groundwater that mixes with TSF seepage water over the first five years until seepage is less than 15 L/s when discharge to the pit ceases. Groundwater and runoff then dominate pit lake inflows, with only a minor contribution from WRL seepage. Evaporation is the only loss in the (sensu McCullough et al. 2013) pit lake water balance.

Numerical water balance modelling under a median climate regime, predicted a median equilibrium (steady state) pit lake water level with approximately 18 m freeboard below the lowest discharge level, which is the invert point of a waste rock landform seep that will be connected to the underground portal at closure. Groundwater modelling indicated that seepage of the pit lake into regional groundwater, even saline density-driven, was highly unlikely due to low hydrogeological transmissivity around the pit void and the terminal nature of the lake being down-gradient of regional aquifers. Pit lake water balance modelling also indicated that pit lake discharge of water to nearby Limestone Creek was highly unlikely and would only be initiated during extreme storm events concomitantly resulting in extremely high creek flow events.

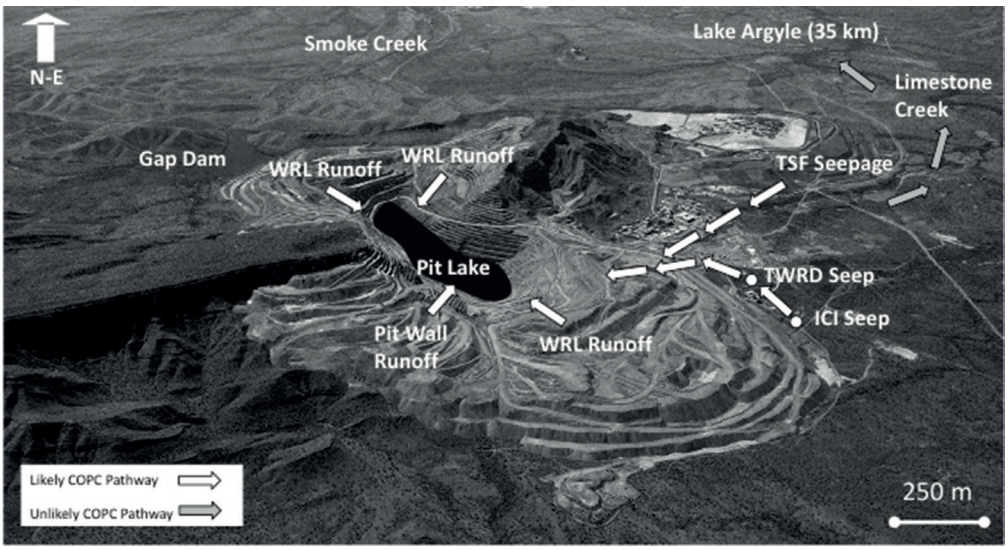

Figure 1 *Argyle Diamond Mine pit lake COPC likely and unlikely pathways.*

Methodology

A Human Health and Environmental Risk Assessment (HHERA) was developed to refine closure planning of the AK1 open cut void and the consequent development of a pit lake therein. Given the interaction of the pit lake with other closure landforms and the need for mine closure planning to be holistic across the project area and greater region, an integrated landform approach was taken across the whole project area. A key objective of this environmental risk assessment was to meet requirements of the Western Australian (DMP & EPA 2015) Guidelines for Preparing Mine Closure Plans for closure risk assessment for pit lakes. The key aspect addressed was consideration of risk to human, native wildlife and stock health primarily from the AK1 pit lake, 150 and 300 years following mine closure (fig 2, left).

Pit lake water balance and quality modelling helped understand COPC sources, trends and concentrations at 300 years following closure. A conceptual Source-Pathway-Receptor (SPR) model linked pit lake water balance and water quality models with fauna and flora studies, and surface and groundwater conceptual models to understand potential COPC transport mechanisms to these receptors. A risk matrix assessed the worst consequence and likelihood of exposure to pit lake water across both spatial and temporal scale following closure planning. Where required, further closure management was used to reduce inherent risks to acceptably low residual levels.

Following international guidance for pit lake closure planning and mine closure risk assessment e.g., APEC (2018); Vandenberg and McCullough (2017), an SPR conceptual modelling approach was undertaken (fig 2, right). As per Commonwealth guidance of (DIIS 2016) *Preventing Acid and Metalliferous Drainage*, all of the SPR model needs to be complete for a risk to be tangible. A workshop of experts and senior staff familiar with Argyle closure planning determined the contaminant hazard sources, pathways and receptors. Risk magnitude was then ascribed in the same workshop from likelihood of a defined consequence occurring. Risk magnitude was further refined from spatio and temporal distribution of the consequence occurring.

The primary intent of the HHERA was to identify:

- the environmental values and their associated human, stock and ecological receptors that need to be protected;
- any further closure management actions planned or required to further mitigate risk; and
- the residual risk to these components, including potential source, pathway and receptors.

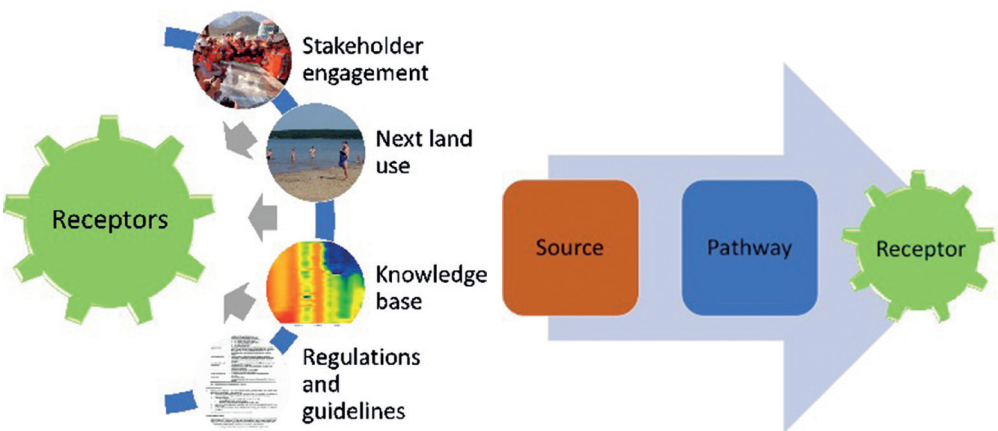

Figure 2 *Data sources for receptor identification (left) and the source-pathway-receptor (SPR) contaminant transfer model (right).*

Risk Assessment

Receptor values

The region surrounding the Argyle lease has agriculture values and is extensively grazed by beef cattle, but also supports ecological and cultural values associated with the land and vegetation, natural waterways and aquatic, terrestrial and bird life. Although the region's environmental values are degraded by grazing, bird life and aquatic ecological functionality and diversity is still high with some conservation listed species likely to be present after closure. Traditional Owners and other people will use the land surrounding the pit lake and therefore may also come into contact with COPC following closure.

Aquatic ecosystem ecotoxicological threshold data was based upon generic guideline values (GVs) relevant to the region (ANZG 2018), or site-specific guideline values (SSGVs) (Warne et al. 2015) developed for Argyle in accordance with Batley et al. (2003). For non-biomagnifying contaminants, SSGV 'Threshold' values were adopted where available.

Drinking water is not the only source of contaminants for terrestrial and semi-terrestrial wildlife. Other sources, typically food, are likely to be more relevant for wildlife, and also need to be considered. Terrestrial and semi-terrestrial wildlife linked to aquatic food chains are at risk from a suite of water-borne contaminants that can bioaccumulate in organisms and biomagnify along the food chain. In these instances, guideline values that protect aquatic species from waterborne contaminants may not convey safety for species that consume aquatic organisms (ANZG 2018). Water quality trigger values of 99% ecosystem protection were chosen for bioaccumulating/bioconcentrating elements risk. This risk was determined through review of ANZG (2018) COPC factsheets and also the primary literature (El-Shenawy et al. 2016).

Water quality guidelines for the protection of aquatic ecosystems were used to screen COPC concentrations. The outcomes of this screening process informed protection of aquatic biota as environmental receptors, but not of waterfowl that might prey upon them as food items. Waterfowl as receptors were screened through considering indirect COPC contact via ingestion of AK1 Pit Lake aquatic biota. These biota may have body burdens of COPC through bioaccumulation and biomagnification (ANZG 2018) and direct contact and ingestion of AK1 Pit Lake COPC as water and sediments. Australasian (ANZECC/ARMCANZ 2000) livestock drinking guidelines were used to screen drinking water specifically for beef cattle. These were complemented by South African livestock drinking guidelines (DWAF 1996). Recreational water quality was determined by a conservative approach of assuming primary contact with ingestion and applying drinking water guidelines (NHMRC/NRMMC 2018).

Results

The HHERA indicated that the AK1 pit lake will present a very low and localized risk (tab. 1). Long-term pit lake water quality would be weakly alkaline but gradually increase in salinity and metalliferous concentrations due to evaporative concentration of tailings and waste rock seepage input and catchment runoff. However, the pit lake is not expected to have similar end use values of natural water bodies for ecological or cultural uses, but instead its primary land use value will be as a water management structure. Furthermore, poor habitat quality meant the lake would not be considered an "attractive nuisance" and restricted access to humans and stock the exposure pathways to potential receptors was limited. The lake is also expected to be hydraulically terminal with very low likelihood of discharge during extreme precipitation events.

Low likelihood high rainfall events would commensurately dilute COPCs in AK1 Pit Lake discharge to relatively low concentrations and resulting low environmental consequence. Pit lake discharge was therefore also very low risk to downstream water quality. However, due to the terminal evapoconcentrating nature of the pit lake water quality, risks from poor quality pit lake water are likely to exist for a very long time. Predominant contaminant pathways were direct contact and drinking of pit lake water and biomagnification from aquatic biota of the pit lake. Transport pathway effectiveness was reduced through a number of factors which are expected to limit biotic

Table 1 Summary of potential AK1 pit lake receptors, pathway and residual risk rating.

Receptor	Pathway	Residual risk rating
Terrestrial native wildlife	May attempt to forage.	Very low
Bats	Direct consumption of pit lake aquatic biota, especially flying invertebrates with aquatic life stages and amphibians.	Very low
	Native terrestrial animal water consumption low but may still be attracted.	Very low
	Direct consumption of pit lake aquatic biota, especially flying invertebrates with aquatic life stages and amphibians.	Very low
Regional birdlife	May use habitat for predator avoidance. May attempt to forage.	Very low
	Direct consumption of pit lake aquatic biota, especially flying invertebrates with aquatic life stages and amphibians.	Very low
Livestock	Direct consumption of pit lake water.	Very low
Humans	People may be attracted to the pit lake for swimming.	Very low

processes including: limited opportunities for organic matter and nutrients to accumulate in the lake, lack of vegetated littoral margins and riparian zones, low nutrient status and water quality issues associated with elevated concentrations of some metals, including salinity.

Waterfowl, ghost bats, terrestrial native wildlife and humans were identified as the most sensitive receptors; particularly through potential bioaccumulation and biomagnification via a food chain with foundations in pit lake aquatic biota. However, both waterfowl and bats were not expected to spend substantial time foraging the low food biomass of the pit lake ecosystem due to steep shaded sides and deep waters, little vegetation and low nutrient and productivity status.

The environmental risk of biomagnification through bushtucker hunting and fishing by Indigenous land users intentionally within the pit lake was not considered of high consequence, and the frequency low and thus of low risk. Risk to both waterfowl and human ingestion of pit lake biota was also inherently assessed as low, due to the presence of nearby Gap Dam as a more productive and diverse water body and therefore preferred alternative aquatic habitat for native wildlife and as a hunting/fishing resource.

Stock risk was considered very low due to very limited access to the steep sided pit lake void and poor climbing ability of cattle as well as poor grazing habitat within the pit lake catchment. Stock risk was further mitigated by the presence of alternative stock watering points and preferential grazing outside of the pit void. Although COPC concentrations will be elevated with water quality deteriorating over many years, COPCs will not be at concentrations to impact human health e.g. from skin absorption or accidental ingestion of water during swimming.

Conclusions

In conclusion, the Argyle pit lake water quality is likely to present a minor risk to key environmental receptors of birdlife, terrestrial wildlife bats, livestock and human ingestion in particular. Furthermore, closure planning risk mitigation activities are expected to reduce these risks to very low and acceptable levels. Consequently, risk to wildlife and humans from the presence of the AK1 pit lake containing elevated solute concentrations is not of material significance. Although environmental risks are low, various closure features and management activities may further reduce inherent risk. These management activities included:

- construction of an engineered abandonment bund to reduce human and animal access;
- deliberate avoidance of revegetation and other habitat creation measures within the pit void catchment; and,
- Stakeholder engagement and pit void perimeter warning signage was also expected to further mitigate human health risk.

Rather than a simple check box exercise, pit lake closure planning should be based upon risk assessments to potential receptors of wildlife, humans and other relevant end uses, including local community health risk. In line with contemporary pit lake closure

planning advice, we recommend a HHERA (or equivalent) be undertaken for all mine closures where pit lakes present as a key final landform, but that explicit consideration is given to developing clear pit lake and associated catchment end use values and closure objectives with stakeholders prior.

Post-closure pit lake water level and quality monitoring data are recommended to validate and calibrate pit lake modelling that underpins risk assessments. These data provided validation and associated assurance that the pit lake is on predicted trajectories for both water balance and quality, whereby there can be confidence that closure risk is appropriately determined for relinquishment and into the future.

Further, pit lake closure planning should be undertaken with a holistic approach that considers risk and interactions between other landforms. These synergisms and efficiencies will frequently realize better pit lake, and overall, mine closure outcomes (Vandenberg and McCullough 2017).

References

ANZECC/ARMCANZ (2000) Australian and New Zealand guidelines for fresh and marine water quality. National Water Quality Management Strategy Paper No 4. Australian and New Zealand Environment and Conservation Council & Agriculture and Resource Management Council of Australia and New Zealand, Canberra. 1,500 p

ANZG (2018) Australian and New Zealand Guidelines for Fresh and Marine Water Quality. Australian and New Zealand Governments and Australian state and territory governments (ANZG), Canberra ACT, Australia. Available at www.waterquality.gov.au/anz-guidelines. p

APEC (2018) Mine Closure Checklist for Governments. Asia Pacific Economic Consortium (APEC), Canada.

Aquastrat (2020) Argyle Diamond Mine Closure Feasibility Study – AK1 pit lake water balance and water quality model. Aquastrat Pty Ltd, Perth, Australia. Unpublished report produced for Rio Tinto. 71 p

Batley GE, Humphrey CL, Apte AC, Stauber JL (2003) A guide to the application of the ANZECC/ARMCANZ water quality guidelines in the minerals industry. ACMER, Brisbane, Australia. p

Castendyk D, Eary T (2009) The nature and global distribution of pit lakes. In: Mine Pit Lakes: Characteristics, Predictive Modeling, and Sustainability Castendyk D & Eary T (eds) Society for Mining, Metallurgy, and Exploration (SME), Colorado, USA, 1-11 pp

DIIS (2016) Leading Practice Sustainable Development Program for the Mining Industry - Preventing Acid and Metalliferous Drainage Handbook Department of Industry, Innovation and Science (DIIS), Canberra, Australia.

DMP & EPA (2015) Guidelines for preparing mine closure plans. Western Australian Department of Mines and Petroleum (DMP), Environmental Protection Authority of Western Australia (EPA), Perth, Australia. 115 p

Doupé RG, Lymbery AJ (2005) Environmental risks associated with beneficial end uses of mine lakes in southwestern Australia. Mine Water and the Environment 24:134-138

DWAF (1996) South African water quality guidelines. 2nd edn, Vol. 5: Agriculture CSIR Environmental Services, Pretoria, South Africa. p

El-Shenawy NS, Loutfy N, Soliman MFM, Tadros MM, Abd El-Azeez AA (2016) Metals bioaccumulation in two edible bivalves and health risk assessment. Environ Monit Assess 188:139

McCullough CD, Lund MA (2006) Opportunities for sustainable mining pit lakes in Australia. Mine Water and the Environment 25:220-226

McCullough CD, Marchand G, Unseld J (2013) Mine closure of pit lakes as terminal sinks: best available practice when options are limited? Mine Water and the Environment 32:302-313

NHMRC/NRMMC (2018) National Water Quality Management Strategy: Australian drinking water guidelines. National Health and Medical Research Council (NHMRC)/Natural Resource Management Ministerial Council (NRMMC), Canberra. Version 3.5. 1,172 p

Vandenberg J, McCullough C (2017) Key issues in mine closure planning for pit lakes. In: Spoil to Soil: Mine site rehabilitation and revegetation, Nanthi Bolan N; Ok Y & Kirkham M (eds) CRC Press, Australia, 175-188 pp

Warne M, Batley GE, Van Dam RA, Chapman JC, Fox DR, Hickey CW, Stauber JL (2015) Revised method for deriving Australian and New Zealand water quality guideline values for toxicants. Department of Science, Information Technology and Innovation, Canberra, Australia. 45 p

Rethinking Hydrologic Design Criteria for Mine Closure

Michael Harvey[1], Krey Price[2], Mark Pearcey[3]

[1]*Principal Geomorphologist, Tetra Tech, 6121 Indian School Road NE, Albuquerque, New Mexico, USA, 87110, mike.harvey@tetratech.com*

[2]*Principal Hydrologist, Tetra Tech, 235 St Georges Terrace, Perth, Western Australia, 6000, krey.price@tetratech.com*

[3]*Principal Advisor Water, Rio Tinto, 152-158 St Georges Terrace, Perth, Western Australia, 6000, mark.pearcey@riotinto.com*

Abstract

Hydrologic design criteria for mine closure landforms in riverine environments commonly specify that landforms need to be stable under extreme, single hydrologic events such as the probable maximum precipitation or probable maximum flood. The cumulative geomorphic effects of multiple, more frequent, and lower magnitude hydrologic events may well exceed that of a single, extreme event. In addition, failure of a closure landform in the riverine environment may be dictated by non-fluvial factors such as settlement, cracking, piping or mass failure of emplaced fill or pit walls. Factors other than extreme hydrologic events need to be considered in mine closure planning.

Keywords: mine closure, design criteria, hydrology, geomorphology

Introduction

Rehabilitation of creek and river corridors remains, arguably, the most challenging aspect of mine closure in the Pilbara region of Western Australia. This is particularly the case where Channel Iron Deposits (CID) in Tertiary-age paleochannels are open pit-mined in spatially coincident modern drainages and the ratio of waste material to extracted ore is very low and thus pit backfill is an on-going challenge.

Closure in the riverine environment can encompass re-establishment of drainage features over fully backfilled pits, partial pit backfill with land bridges to convey sediment and flows, and total or partial hydrologic disconnection between partially-filled open pits and the channel system. Typical closure scenarios for non-backfilled pits are illustrated in Figure 1 (Price 2018).

In general, fluvial processes in the Pilbara tend to be driven by infrequent, high intensity and short duration hydrologic events that are related to the occurrence of Tropical Cyclones (Harvey et al. 2014, Rouillard et al. 2015, Rouillard et al. 2016). Climate change projections suggest that it is likely that intense rainfall in most locations in Australia, including the Pilbara, will become more extreme, driven by a warmer, wetter atmosphere (Department of Industry Innovation and Science 2016).

Regulatory Guidance for Design of Closure Landforms in Australian Riverine Environments

Mine closure guidelines in Western Australia include language requiring post-closure landforms to be physically safe, geotechnically stable, geochemically non-polluting and sustainable in the long term (Western Australian Department of Mines and Petroleum 2015) which is in accordance with the hierarchy of closure needs identified by the Asia-Pacific Economic Cooperation Mining Task Force (APEC Mining Task Force 2018).

The Australian National Council on Large Dams (ANCOLD) defines long term as 1,000 years (ANCOLD 2019) which significantly exceeds the limits of engineering practice, which is generally considered to be between 100 and 200 years, and also exceeds the duration of most human institutions that would monitor and regulate the post-closure landscape (APEC Mining Task Force 2018). Leading practice in Australia dictates that

a post-closure design life of 1,000 years be adopted as being considered 'in perpetuity' (Department of Industry Innovation and Science 2016).

Guidance from Western Australian regulatory agencies on hydrologic design criteria for closure landforms in the riverine environment is either not clear (300 years or longer for landforms, voids and ecosystems to 500-1,000 years for pit lake modelling) or recommends that landforms are constructed to be stable under single extreme events such as the probable maximum precipitation (PMP) or the probable maximum flood (PMF). While extreme events such as the PMP, or the resulting PMF, may be attractive from a perceived regulatory risk reduction perspective, the very low probability of occurrence of such an extreme single design event means that fluvial processes, and hence the dynamics of the closure corridor, will be governed by multiple events with a much higher probability of occurrence. In addition, while a structure may provide a design level of protection when built, subsequent changes in the river environment such as aggradation may lead to conditions in the future where the design level of protection is not provided.

Probability of Extreme Hydrologic Events

Probable Maximum Precipitation

The probable maximum precipitation is defined as the "theoretically greatest depth of precipitation for a given duration that is physically possible over a given size storm area at a particular geographical location at a certain time of the year" (Hansen et al. 1982). Prior to the 1950s, the concept was known as the maximum possible precipitation (MPP). The name was changed to the PMP reflecting the uncertainty surrounding any estimate of maximum precipitation (Wang 1984). There is no known way to develop the PMP from first principles (National Research Council 1994) and proposed estimation methodologies have been the subject of much debate. By another definition, the PMP is the estimated precipitation depth for a given

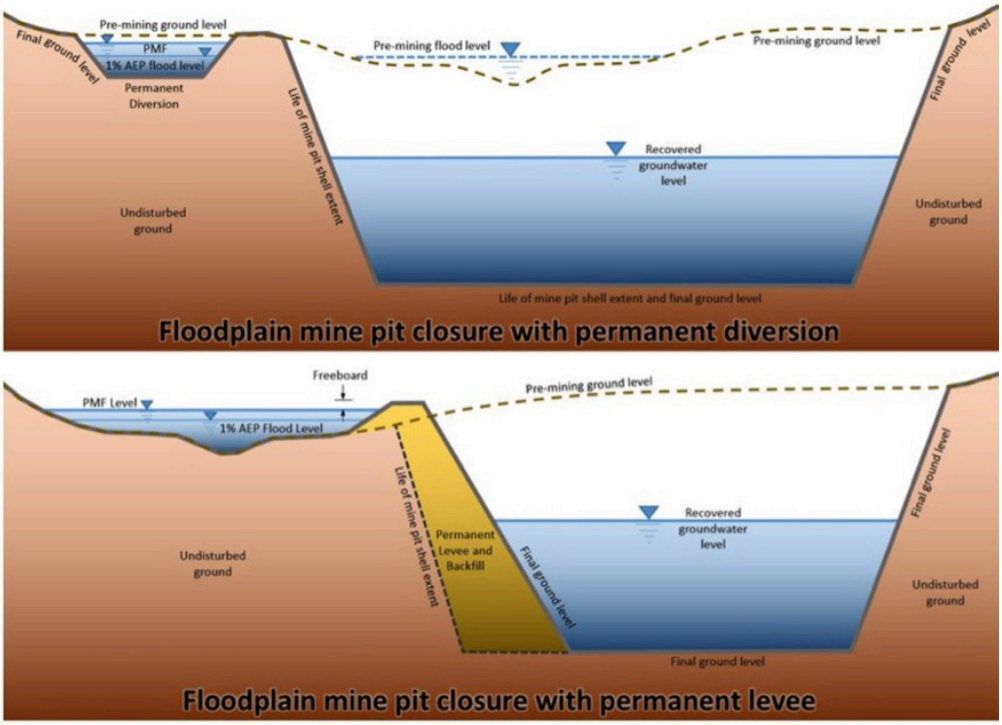

Figure 1 *Typical closure scenarios with permanent diversions and a levee for a non-backfilled pit (Price 2018).*

duration, drainage area, and time of year for which there is virtually no risk of it being exceeded (Wang 1984). However, the fact that measured rainfall depths have exceeded PMP estimates in the past clearly indicates that the PMP approach by no means implies zero risk in reality (Koutsoyiannis 1999).

The PMP estimation methodology makes the inherent assumption that the past climate will be representative of future conditions. As global climate patterns continue to change, PMP estimates from previous analyses may need to be updated. The Mine Closure Checklist for Governments (APEC Mining Task Force 2018) describes some of the challenges associated with climate change and mine closure, including changing rainfall patterns, drier climates, rising temperatures, and rising sea levels. Changing rainfall patterns may quite possibly have the greatest impact as areas have more intense and/or more frequent rainfall events or even more prolonged periods of dry weather than in previous years (IPCC 2007).

Probable Maximum Flood

The probable maximum flood (PMF) is defined as "the largest flood that could conceivably occur at a particular location, usually estimated from the PMP coupled with the worst flood-producing catchment conditions" (Douglas and Barros 2003). The temporal and spatial patterns of the predicted PMP rainfall depths, antecedent soil conditions, and precipitation losses will all impact the estimate of the PMF. Use of the PMP to generate the PMF has become the standard for dam design in many parts of the world including the United States, China, India, and Australia (Svensson and Rakhecha 1998). Estimates of the annual exceedance probability (AEP) of the PMF range from 1 in 10,000 to 1 in 1,000,000 in Canada (Smith 1988) to 1 in 1,000,000 in the eastern USA (Shalaby 1994). However, there is considerable uncertainty in estimating both the PMP and PMF (Salas et al. 2014).

Guidance in Australia (Nathan and Weinmann 2019) states that the absolute upper limit of flood magnitude under consideration is the probable maximum flood, which is a design concept that cannot be readily assigned an annual exceedance probability. However, the AEP of the PMP is considered to vary from 1 in 10,000 to 1 in 10,000,000. The stability of hydraulic features that are included in mine closure plans may be undermined by morphological changes that occur as a result of more frequent events with a higher likelihood of occurrence. Given the extremely low probability of occurrence of the PMP/PMF, designing for it is not pragmatic if the features cannot withstand the impacts of a series of more frequent events.

Fluvial Processes and Geomorphic Change

In general, fluvial processes in the Pilbara, located in the arid subtropics, tend to be driven by infrequent, high intensity and short duration hydrologic events that are related to the occurrence of Tropical Cyclones (Harvey et al. 2014). The morphology of the alluvial sections of the ephemeral-flow, gravel-bed creeks where sediment transport is episodic, tends to be a relic of the last major flow event and results in highly variable channel morphology over both space and time (Graf 1988). Graf (1988) concluded that in arid and semi-arid regions where the flows are ephemeral, infrequent and relatively short-duration hydrological events rarer than the 1 in 100 AEP are the major determinants of overall valley floor morphology, but more frequent events are responsible for defining highly variable channels (macro-channels) within the disturbed landscape. Macro-channel morphology (compound channels) is associated with regions of high hydrological variability (Croke et al. 2013). Macro-channels are characterised by a small inner channel and associated benches set within a much larger channel that operates as a conduit for high magnitude floods (Croke et al. 2016). They have large channel capacities, with bankfull capacities approaching a 1 in 50 AEP, and are laterally stable even during extreme flood events because of the presence of highly erosion-resistant clays (Fryirs et al. 2015) or calcrete and ferricrete-cemented alluvium in their banks (Harvey et al. 2014).

Tooth and Nanson (2004) demonstrated the high variance of morphologic, hydraulic and sediment transport characteristics over

relatively short distances in ephemeral flow channels in central Australia and because of this high morphologic variability, it is very difficult to define either channel-forming discharges (Wolman and Miller 1960, Baker 1978, Wolman and Gerson 1978) or design discharges (Harvey and Mussetter 2005). Consequently, channel dimensions within the ephemeral flow channels are unlikely to be related to hydrologic events of any particular recurrence interval, and as such, existing channel morphology provides a very poor template for post-mining channel reconstruction in the Pilbara (Harvey et al. 2014).

International Approaches to Engineering Design and Long-Term Landform Stability

With the exception of tailings dam design where PMP/PMF criteria are prescribed (ICOLD 2013, Slingerland et al. 2018), the international literature on mine closure generally addresses regulatory goals for reclamation/closure/relinquishment rather than specific hydrologic design criteria. For example, the extensive South African Guidelines for the Rehabilitation of Mined Lands (Chamber of Mines of South Africa and CoalTech 2007) does not specify any hydrologic criteria but rather focusses on achieving post-mining landscape rehabilitation and acceptable future land use.

The U.S. Surface Mining Control and Reclamation Act (SMCRA) of 1977 aims to avoid disturbance of alluvial valley floors and their attendant hydrologic balance (both surface water and groundwater). If stream diversions are required, they must convey the peak runoff from the 1 in 100 AEP, 6-hour precipitation event. There is also an expectation that "good engineering practice" will be employed in design of the diversion structures (Office of Surface Mining and Reclamation and Enforcement 1977).

To accommodate the dichotomy of constructing landforms that are stable over the long-term and the limits of engineering practice, the U.S. Uranium Mill Tailings Radiation Control Act (UMTRCA) of 1978 requires closure measures to be effective for up to 1,000 years to the extent reasonably achievable and, in any case for at least 200 years (Nuclear Regulatory Commission 1978; APEC Mining Task Force 2018) even though they fall short of the full duration of the hazard (Nuclear Regulatory Commission 2002). These timeframes were formulated to cover periods over which climatological and geomorphic processes could be reasonably predicted given current knowledge of earth sciences and engineering (Logsdon 2013).

Canadian practice is encapsulated within the APEC Mining Task Force (2018) document and addresses the problems of prescribing extreme events as hydrologic design criteria as well as acknowledging the practical limits of engineering design

Concluding Discussion

Hydrologic design criteria provided by regulatory agencies for mine closure landforms in the riverine environment in the Pilbara region of Western Australia are not clear or recommend that landforms need to be stable under extreme, single hydrologic events such as the PMP or PMF. These extreme hydrologic design events with annual exceedance probabilities in the order of 1 in 10,000 to 1 in 10,000,000 are not appropriate for designing long-term mine closure landforms in the riverine environment of Western Australia

The use of a single extreme event as a design criterion confuses the low annual exceedance probability of a design event with the desired design longevity of the closure landform (Price 2018). A post-closure design life of 1,000 years can be considered to be in perpetuity (Department of Industry Innovation and Science 2016). However, even a design life of 1,000 years significantly exceeds the limits of engineering practice, that is generally considered to be between 100 and 200 years, and also exceeds the duration of most human institutions that would monitor and regulate closure and relinquishment (APEC Mining Task Force 2018).

Engineering analysis for long-term closure (1,000 years) needs to take into account the impacts of a series of design events that have lower magnitude but higher frequency. The cumulative geomorphic effects of multiple more frequent and lower

magnitude events may well exceed that of the single extreme event.

Failure of a closure landform in the riverine environment may be dictated by non-fluvial factors such as settlement, cracking, piping or mass failure of emplaced fill or pit walls and as such are not explicitly evaluated in a hydrologic risk-based analysis. Even if the overall probability of failure can be reasonably constrained, the consequences of failure of a closure landform will tend to be location-specific, and thus, a generalised approach to establishing risk is unlikely to be particularly useful.

A more realistic approach to hydrologic design for long-term landform closure is provided by the U.S. Uranium Mill Tailings Radiation Control Act (UMTRCA) of 1978. The UMTRCA requires closure measures to be effective for up to 1,000 years to the extent reasonably achievable and in any case, for at least 200 years (Nuclear Regulatory Commission 1978, APEC Mining Task Force 2018). However, this approach also requires the development of a site-specific, long-term surveillance plan that involves annual inspections and maintenance, as required, in perpetuity. This approach would require a program to distribute dedicated funds to those groups assuming responsibility for ongoing maintenance.

References

ANCOLD (2019) Guidelines on Tailings Dams: Planning, Design, Construction, Operation and Closure. Revision 1, July 2019

APEC Mining Task Force (2018) Mine Closure Checklists for Governments. Prepared by Natural Resources of Canada and Golder Associates, Ltd. APEC#218-SO-03.1. Singapore.

Baker VR (1978) Stream channel response to floods with examples from Central Texas. Geol. Soc. America Bulletin 88(8), 1057-1071.

Chamber of Mines of South Africa and CoalTech 2007 Guidfelines for the Rehabilitation of Mined Land. https://coaltech.co.za/surface-environment/guidelines-for-the-rehabilitation-of-mined-land/.

Croke J, Reinfelds I, Thompson C, Roper E (2013) Macrochannels and their significance for flood-risk minimisation: Examples from southeast Queensland and New South Wales, Australia. Stochastic Environmental Research and Risk Assessment 28(1): 99-112.

Croke J, Fryirs K, Thompson C (2016) Defining the floodplain in hydrologically-variable settings: implications for flood risk management. Earth Surface Processes and Landforms 41(14), 2153-2164.

Department of Industry Innovation and Science (2016) Mine Closure: Leading Practice Sustainable Development Program for the Mining Industry. https://www.industry.gov.au/sites/default/files/2019-05/lpsdp-mine-closure-handbook-english.pdf

Douglas EM and Barros AP (2003) Probable maximum precipitation estimation using multifractals: Application in the Eastern United States. J. Hydrometeorology, https://doi.org/10.1175/1525-7541(2003)004<1012:PMPEUM>2.0.CO;2

Fryirs K, Lisenby P, Croke J (2015) Morphological and historical resilience to catastrophic flooding: the case of Lockyer Creek, SE Queensland, Australia. Geomorphology 241, 55-71.

Graf WL (1988). Definition of floodplains along arid-region rivers. In Flood Geomorphology. John Wiley and Sons, New York, 231-242.

Hansen EM, Schreiner LC and Miller JF (1982) Application of probable maximum precipitation estimates, United States east of the 105th meridian. Hydrometeorological Rep. 52, National Weather Service, Silver Spring, MD, 176 pp.

Harvey MD and Mussetter RA (2005) Difficulties of Identifying Design Discharges in Steep, Coarse-Grained Channels in the Arid Southwestern US. Proceedings of the EWRI 2005 World Water and Environmental Resources Congress, Anchorage, Alaska, May 15-19.

Harvey MD, Pearcey MR, Price K, and Devkota B (2014) Geomorphic, hydraulic and sediment transport modelling for mine-related channel realignment- case study: Caves Creek, Pilbara, Western Australia. Hydrology and Water Resources Symposium, Barton, ACT. Engineers Australia, 2014: 259-266.

ICOLD Committee on Tailings Dams (2013) Sustainable design and post-closure performance of tailings dams. Bulletin No. 153, ICOLD.

IPCC (2007) Fourth Assessment Report and Climate Change. https://www.ipcc.ch/pdf/assessment-report/ar4/wg2/ar4 wg2 full report.pdf.

Koutsoyiannis D (1999) A probabilistic view of Hershfield's method for estimating probable maximum precipitation. Water Resources Res., 35, 1313–1322.

Logsdon MJ (2013) What does perpetual management and treatment mean? Towards a framework for determining an appropriate period of performance for management of reactive, sulphide-bearing mine waste. International Mine Water Association, 2013 Conference Proceedings, Golden, Co., 53-58.

Nathan R and Weinmann E (2019) Estimation of Very Rare to Extreme Floods, Book 8 in Australian Rainfall and Runoff - A Guide to Flood Estimation, Commonwealth of Australia.

National Research Council (1994) Estimating Bounds on Extreme Precipitation Events. National Academy Press, 29 pp.

Nuclear Regulatory Commission (1978) Uranium Mill Tailings Radiation Control Act. https://www.nrc.gov/docs/ML1327/ML13274A489.pdf#page=507

Nuclear Regulatory Commission (2002) Remedial Action at the Moab site: Now and for the Long Term. Letter Report. Washington DC. The National Academies Press. https://doi.org/10.17226/10402.

Office of Surface Mining Reclamation and Enforcement (1977) Surface Mining and Reclamation Act. https://www.govinfo.gov/content/pkg/USCODE-2011-title30/html/USCODE-2011-title30-chap25.htm

Price K (2018) Event-based versus duration-based assessment for long-term modelling of mining impacts. Hydrology and Water Resources Symposium 2018, Melbourne, 3-6 December.

Rouillard A, Skrzypek G, Dogramaci S, Turney C and Grierson PF (2015) Impacts of high inter-annual variability of rainfall on a century of extreme hydrologic regime of northwest Australia. Hydrol. Earth Syst. Sci., 19, 2057–2078, 2015.

Rouillard A, Skrzypek G, Turney C, Dogramaci S, Hua Q, Zawadzki A, Reeves J, Greenwood P, O'Donnell AJ and Grierson PF (2016) Evidence for extreme floods in arid subtropical northwest Australia during the Little Ice Age chronozone (CE 1400-1850). Quaternary Science Reviews, 144, 107-122.

Salas JD, Gavilán G, Salas FR, Julien PY and Abdullah J (2014) Uncertainty of the PMP and PMF. Handbook of Engineering Hydrology: Modelling, Climate Change and Variability. CRC Press, Boca Raton, Fl. USA, 575-603

Shalaby AI (1994) Estimating probable maximum flood probabilities. JAWRA v.30, (2), 307-318. https://doi.org/10.1111/j.1752-1688.1994.tb03293.x

Slingerland N, Isidoro A, Fernadez S and Beir NA (2018) Geomorphic analysis for tailings dam design in consideration of a 1000-year closure design life. 2nd International Congress on Planning for Closure of Mining Operations, Santiago, Chile.

Smith CD (1988) The PMF does have a frequency. Canadian Water Resources Journal, V.23 (1)

Svensson C and Rakhecha P R (1998) Estimation of probable maximum precipitation for dams in the Hongru River catchment, China. Theor. Appl. Climatol., 59, 79–91.

Tooth S and Nanson GC (2004) Forms and processes of two highly contrasting rivers in arid central Australia, and the implications for channel-pattern discrimination and prediction. Geological Society of America Bulletin, v. 116, No. 7/8, pp. 802-816.

Wang B-H M (1984) Estimation of probable maximum precipitation: Case studies. J. Hydraul. Eng., 110, 1457–1472.

Western Australian Department of Mines and Petroleum (2015) Guidelines for Preparing Mine Closure Plans. May, 2015.

Wolman MG and Miller JP (1960) Magnitude and frequency of forces in in geomorphic processes. Journal of Geology, v.66, (1), 54-74.

Wolman MG and Gerson R (1978) Relative scales of time and effectiveness of climate in watershed geomorphology. Earth Surface Processes, v.3, 189-208.

Scour Protection Design Criteria for Mine Site Infrastructure

Krey Price[1], David Westwater[2]

[1]*Surface Water Solutions, 57 Bromfield Drive, Kelmscott, WA 6111, Australia, krey.price@surfacewater.biz*

[2]*Superintendent Hydrology, Rio Tinto, Central Park, Perth, WA 6000, Australia, dave.westwater@riotinto.com*

Abstract

This paper challenges velocity-based rock sizing methodologies traditionally applied for mine site infrastructure drainage management and proposes alternative shear-based methods. Standard velocity-based rock-sizing methodologies are considered to have potential to lead to overdesign of rock armour requirements, resulting in higher costs. The relevance of alternative rock sizing methods for a range of scales is presented in this paper in light of the limitations on total energy resulting from depth and velocity thresholds under typical design conditions. A literature review was undertaken to identify the sources that serve as a basis for standard rock sizing approaches. In past practice, shear-based methods for rock sizing have typically been dismissed due to requirements for iterative solutions. Recent advances in computational analyses mean that shear-based analyses can now be readily adopted for previously impractical applications. Published shear-based rock sizing approaches were reviewed for this study; these methods generally show a linear relationship between the critical tractive force and the effective diameter of the particle. In order to assess the typical distribution of shear stress and velocities a range of channel and culvert configurations were assessed by application of the USACE HEC-RAS program. Maximum velocity and shear stress profiles were extracted from the model results and applied in rock sizing criteria. A 1:1 ratio between shear stress in pascals and median rock size (D50) in millimetres was developed based on a range of reviewed data sources and a safety factor of 2.0 was achieved against incipient motion through a 25% increase in diameter. Recommended armour rock gradations were developed using the shear-based method and compared to results from the standard velocity-based approach. The comparison shows that the shear-based method generally results in a smaller rock size than the velocity-based approaches, indicating that there is a fair degree of conservatism in the application of the velocity-based criteria for the simulated scenarios.

Keywords: Drainage, Flood Management, Erosion, Scour, Hydraulics

Introduction

Standard velocity-based rock-sizing methodologies are generally intended for the protection of bridge abutments/piers and other applications with relevant flow depths. Much of the published rock sizing guidance is based on assumed depth-to-stone size ratios that may differ from design conditions at typical mine-site drains and culvert inlets and outlets. Figure 1 presents a graphical representation of one example of velocity-based rock sizing in common use in Australia. The velocity thresholds are compiled from the Austroads Guide to Road Design (2013), which, in turn, is derived from the Main Roads Western Australia Floodway Design Guide (2006). This paper provides a literature review of the sources that serve as a basis for this Australian rock sizing approach and compares velocity-based methods with alternatives that use shear stress.

Background Theory

Velocity vs. shear: Many published sources for rock sizing methodologies include both empirical and derived relationships between hydraulic conditions and the recommended gradation and sizing of armour rock. Empirical relationships typically include safety factors for design, while some derived

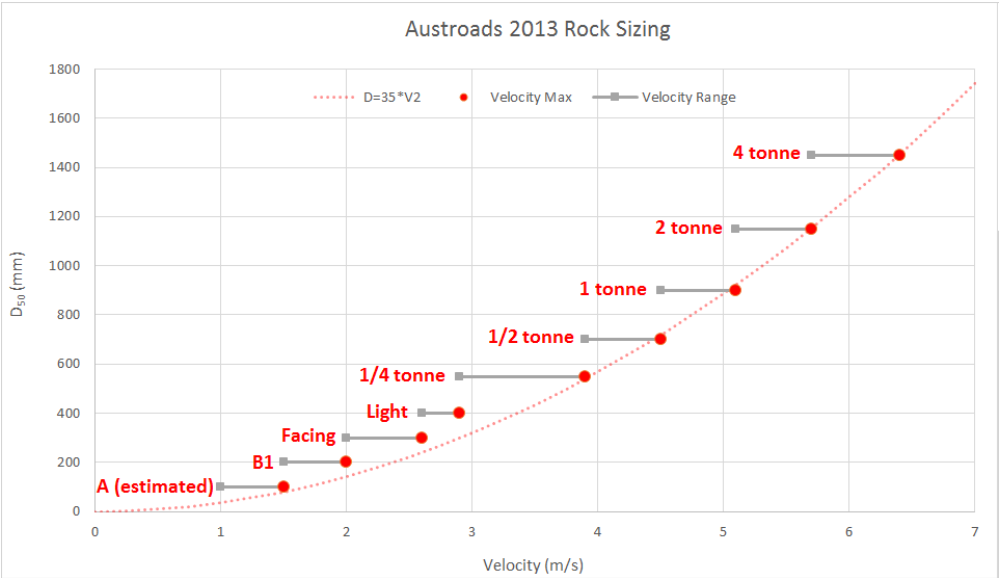

Figure 1 *Rock sizing data compiled from the Austroads Guide to Road Design (2013) and the MRWA Floodway Design Guide (2006).*

relationships predict critical thresholds for incipient motion. Additional considerations are required where characteristics deviate from assumed values and could reduce factors of safety.

Published rock sizing methodologies can typically be separated into two categories:

1. Velocity-based methods which are simplified relationships that recommend an armour rock gradation based on velocity only.
2. Force-based approach methods which may also include the fluid velocity in some form along with the addition of other parameters such as the depth, hydraulic radius, shear stress, or other flow characteristics to account for the tractive forces acting on the stones.

A commonly applied alternative to velocity-based rock sizing is the use of shear stress as the primary indicator of rock size requirements. In simplified form for uniform flow conditions, shear stress is equal to the product of the unit weight of water (γ), the hydraulic radius (R), and the unit-less energy gradient (S):

$$\tau = \gamma R S \qquad \text{(Equation 1)}$$

Figure 2 and Table 1 illustrate an example of two different uniform flow conditions in which the velocities are identical, but the shear stress differs. The scenarios in Figure 2 represent substantially different open channel flow conditions with identical velocities. The smaller channel requires a steeper energy gradient to represent the same velocity; this results in a higher shear than in the larger channel. The results presented are based on a simplified equation for uniform, normal-depth flow; in reality, flow conditions in the vicinity of a bridge or culvert inlet and outlet can be much more complex, and the calculation of shear stress can be highly iterative. In the past, these iterative solutions were difficult to calculate. The U.S. National Cooperative Highway Research Program (NCHRP 2006) compiled previously applied rock sizing methodologies. Referring to computation efforts in the 1970s and 1980s, the NCHRP report states that shear-based methods are preferable to the velocity-based methods, but that velocity-based methods have generally been applied because "most designers prefer velocity-based methods, and shear is difficult to measure and little information regarding shear stress on riprap was available." With the increasing capacity of

Table 1 Comparison of velocity and shear stress for armour rock sizing.

Case	Discharge	Side Slope	Base Width	Top Width	Velocity	Shear from R
	m^3/s	H:V	m	m	m/s	Pa
1	300	2	10	26	4	125
2	35	2	2	9	4	180

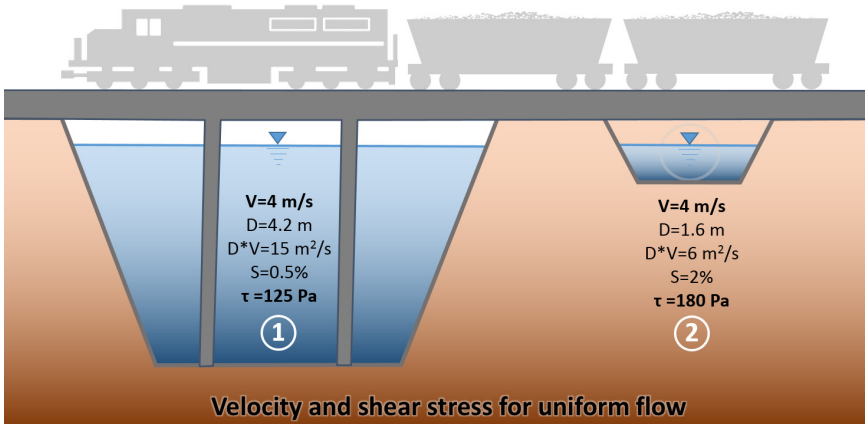

Figure 2 Comparison of velocity and shear stress for armour rock sizing (Indicative scale for reference only).

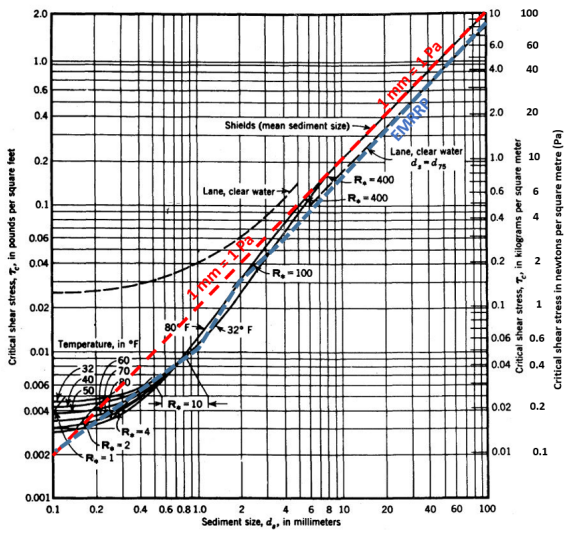

Figure 3 Relationship between shear stress and rock diameter (Annotated from USDA SCS 1983).

two-dimensional (2D) hydraulic modelling applications, previous limitations based on the complexity of iterative solutions may no longer be applicable, and shear-based rock sizing approaches are now viable alternatives to velocity-based approaches.

Incipient motion of a particle occurs when the forces acting on the particle exceed the forces resisting motion. The critical conditions required to produce incipient motion are often represented by equations that make use of the Shields parameter, which is a unit-less number that relates the fluid force on a particle to the weight of the particle. Figure 3 shows the relationship between rock size and critical shear stress based on a study

by Shields (1936), Meyer-Peter and Mueller (1948), and Lane (1955). The added dashed line shows a 1:1 relationship between shear stress in pascals and an equivalent median rock size in millimetres, which corresponds to a typical Shields Number of approximately 0.063. When safety factors are applied to linear dimensions such as the median diameter of the rock, the actual safety factor against motion increases in cubic relationship. A 25% increase in diameter, for instance, increases the particle weight by almost 100%, providing an effective safety factor of 2.0. Based on the studies cited above, for the purpose of this paper, a 1:1 ratio between shear stress and rock size is assumed for incipient motion, with a 25% increase in D_{50} (corresponding to a 100% increase in W50) applied as a safety factor against mobilisation.

Rock Sizing Methods – Literature Review

The following summarises selected rock sizing methodologies and the evolution of the original source data that served as a basis for the criteria currently adopted in Australia. The current Austroads Guide to Road Design Part 5 (Austroads 2013) incorporates velocity thresholds from several previous publications, including the 1994 Austroads Waterway Design guide (Austroads 1994). Some of the limitations cited in the 1994 guidance have not been carried forward into the 2013 version. Specifically, the 1994 guide cites a 1960 California Highways manual (CDPW 1960) as the source for the rock sizing methodologies. A 1.5H:1V batter slope and specific gravity of 2.65 are assumed, along with bank velocities of two-thirds of the average channel velocity in straight reaches and four-thirds of the average channel velocity along bends. The recommended rock size is increased to convert from a numerical count of individual rocks to a recommended median diameter (D_{50}) by total weight in the Austroads manual. The Austroads guidance generally appears to be intended for adoption in large channel designs; as such, the recommendations should be interpreted with caution when applied to smaller-scale applications. Main Roads Western Australia (MRWA) generally follows Austroads guidance for selecting rock class based on velocity, with the addition of several supplemental rock classes, including two sub-facing-class rock specifications.

The Austroads Guide makes frequent reference to the United States Federal Highway Administration (FHWA) series of Hydraulic Engineering Circulars (HEC) and Hydraulic Design Series (HDS) documents that relate to highway design. The documents with the most relevance to scour protection for culvert inlet and outlets are HEC 11, HEC 15, HEC 23, HEC 26, and HDS 5. Some of the shear-based methods presented in HEC 15, HEC 23, and HEC 26 are acknowledged to be iterative in nature. The 1960 CABS method (CDPW 1960) that was originally used as a basis for the Austroads and MRWA velocity-based approaches was superseded by a 1970 edition and the 2000 CABS method (CDT 2000). A 2006 NCHRP report re-examined the CABS methods along with several others rock sizing approaches, and recommended falling back on the 1994 U.S. Army Corps of Engineers EM 1110-2-1601 method (USACE 1994) for riprap sizing, essentially superseding the methods that serve as a basis for Austroads and MRWA. The 1994 U.S Army Corps of Engineers riprap sizing method (USACE 1994) traces back to equations presented in Stephen Maynord's 1988 Stable Rip Rap Sizing for Open Channel Flows (Maynord 1988) and subsequent validation tests performed on very large physical models. The USACE method is presented in the form of an equation that shows riprap size being inversely proportional to the depth for the same velocity.

In general, the application of the rip-rap equation is intended for large channels; for smaller channels, the Corps of Engineers' Ecosystem Management and Restoration Research Program (EMRRP) has adopted shear-based stream stability thresholds that were compiled by the U.S. Soil Conservation Service in the publication Stability Thresholds for Stream Restoration Materials (Fischenich, 2001). The rock sizes presented in the EMRRP publication tables are based on a nearly linear relationship between shear stress and particle size for particles above 10mm in diameter. Nearly identical values have also been adopted

by the U.S. Forest Service (USDA 2008), the U.S. Geological Survey (1986), and the U.S. Federal Highway Administration (2010), which trace their sources to U.S. canal studies conducted in the 1920s. Figure 3 presents the SI unit conversion of the tabulated values along with a comparison to values derived from the use of a typical Shields Number of 0.063 with a 1:1 relationship between critical shear stress in pascals and rock size in millimetres. The 1:1 relationship provides a slightly less conservative rock size than the published values. For the cases shown in Figure 2, application of the 1:1 relationship would result in a recommended median rock size of 200 mm for the large channel and 320 mm for the smaller channel. Applying a 25% safety factor yields a recommended D_{50} of 250 mm for the large channel and 400 mm for the small channel. A comparison to velocity-based rock sizing according to Austroads, the velocities of 4.0 m/s in both channels would yield ¼-tonne class rock with a recommended median rock size of 550 mm. In this case, the shear-based method provides a potential reduction of 30% to 55% in the D_{50} size.

Computational Approach

An assessment of typical shear stress and velocity distributions along drains and at culvert inlets and outlets was performed utilising the USACE HEC-RAS software program for a range open channel and culvert configurations. Recommended rock classes were compiled for each channel and culvert size. Velocity-based criteria were applied using Austroads guidelines in the selection of a recommended D_{50} for armour rock. As a comparison to shear-based methods, a 1:1 ratio between shear stress in pascals and median rock size (D_{50}) in millimetres was applied based on a range of reviewed data sources and field tests. In order to provide a recommended safety factor of 2.0 against incipient motion, a 25% increase in diameter was applied to the critical value of D_{50}. A uniform Manning's roughness coefficient of 0.035 was applied to all channels for consistent comparison of results. Figure 4 summarises the results for the configurations assessed using peak velocities and shear stresses. The velocity-based criteria result in a recommended rock size that exceeds the shear-based recommendations by a factor of approximately 2.6. A comparison of peak results to the average channel velocity and shear stress results is shown in Figure 5. Using the peak values as opposed to the average values results in an average increase of 1.5 times the recommended diameter.

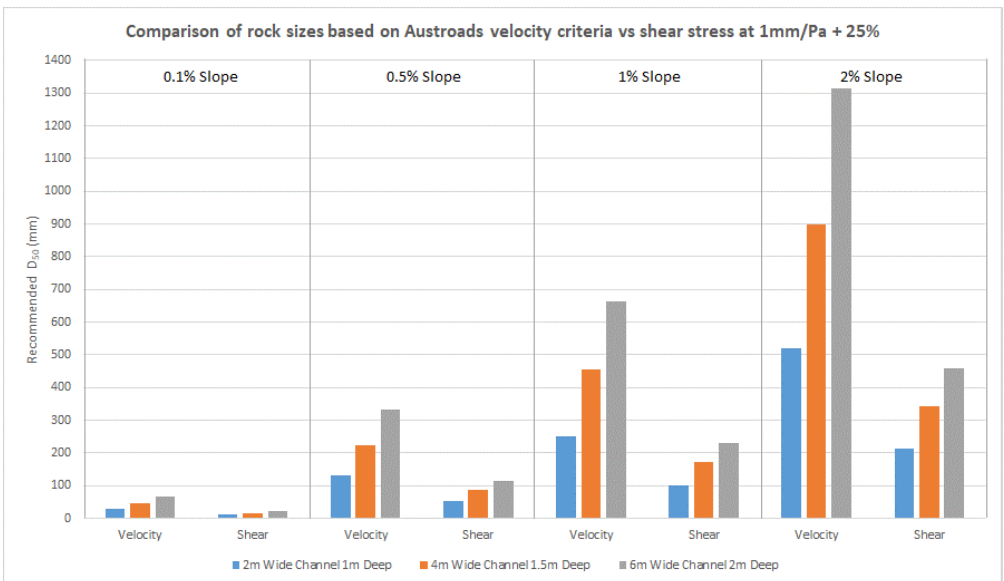

Figure 4 *Comparison of channel rock sizes based on velocity criteria vs shear stress.*

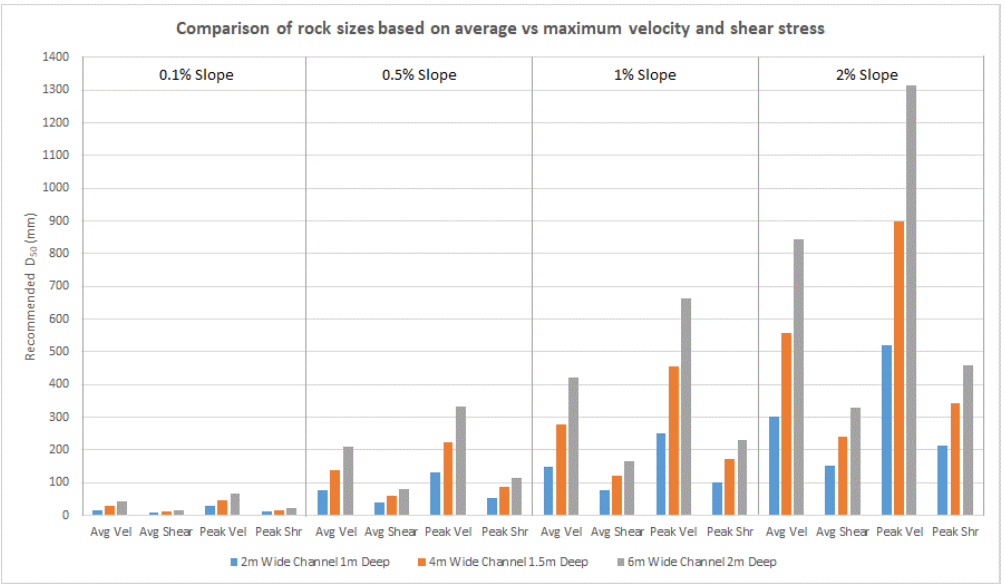

Figure 5 *Comparison of channel rock sizes based on average vs maximum velocity and shear stress.*

Conclusions

Erosion control measures for drain embankments and roadway and rail culverts in the mining sector are typically designed using velocity-based criteria. In Australia, these criteria are published in Austroads and MRWA guidelines. Shear-based criteria have historically been avoided due to computational limitations. Advances in hardware and software allow the application of standardised 2D models to a range of channel and culvert configurations. Velocity-based approaches generally account for the lateral distribution of velocities, and average channel velocities should be applied for riprap sizing under this methodology. The application of localised velocities may cause results to differ from the laboratory or field assessments on which the empirical methods are based. If shear-based criteria are applied, using the maximum channel shear stress is recommended as a conservative approach.

Using the maximum design depths and velocities associated with individual culvert sizes, calculation of maximum shear for application in shear-based rock sizing methodologies generally results in smaller rock size recommendations than the standard velocity-based (Austroads and MRWA) criteria. In order to assess the typical distribution of shear stress and velocities along drains and at culvert inlets and outlets, a range of drain and culvert sizes, configurations, and slopes was entered into the U.S. Army Corps of Engineers (USACE) HEC-RAS program. Average and maximum velocity and shear stress profiles were extracted from the model results and applied in rock sizing criteria. A 1:1 ratio between shear stress in pascals and median rock size (D_{50}) in millimetres was assumed based on a range of reviewed data sources and field tests. In order to provide a recommended safety factor of 2.0 against incipient motion, a 25% increase in diameter was applied to the critical value of D_{50}. A relationship using 1 mm of rock diameter for each pascal of shear stress was applied with a safety factor of 25% on the diameter (resulting in a safety factor of 2.0 by weight or resistance to motion). The proposed shear-based methodology generally results in a reduction of recommended rock sizes in comparison to velocity-based methods. For the range of channel sizes covered in this study (1-2m depth, 2-6m bottom width) the shear-based method resulted in a reduction in the median diameter of approximately 50%. If velocity-based methods are applied for design, shear-based calculations can be presented as a comparison to demonstrate

the level of conservatism or additional safety factors inherent in the velocity-based design parameters.

References

AustRoads. (1994). Waterway Design - A guide to the Hydraulic Design of Bridges, Culverts, and Floodways.

Austroads. (2013). Guide to Road Design: Part 5: Drainage - General and Hydrology Considerations.

California Department of Public Works. (1960). Bank and shore protection in California highway practice.

Chen, Y., & Cotton, G. (1986). Design of Roadside Channels with Flexible Linings. Hydraulic Engineering Circular No. 15. Report No. FHWA-IP-86-5. Federal Highway Administration.

eWater CRC for Catchment Hydrology. (2005). RIPRAP Version 1.01.

Fischenich, C. (2001). Stability Thresholds for Stream Restoration Materials. EMRRP.

Lane, E.W. (1955). Design of stable channels. American Society of Civil Engineers Trans 120, Paper 2776.

Main Roads Western Australia. (2006). Floodway Design Guide.

Maynord, S. T. (1988). Stable Riprap Size for Open Channel Flows. Vicksburg MS: USACE WES.

Meyer-Peter, E., & Muller, R. (1948). Formula for Bed-Load Transport. International Association for Hydraulic Structures Research.

National Cooperative Highway Research Program. (2006). Riprap Design Criteria, Recommended Specifications, and Quality Control. Report 568.

U.S. Army Corps of Engineers. (1994). Hydraulic Design of Flood Control Channels, EM 1110-2-1601.

U.S. Department of Agriculture Forest Service. (2008). Stream Simulation: An Ecological Approach to Providing Passage for Aquatic Organisms at Road-Stream Crossings.

U.S. Department of Agriculture Soil Conservation Service. (1983). National Engineering Handbook Section 3 Sedimentation Chapter 4 Transmission of Sediment by Water.

U.S. Federal Highway Administration. (1989). Design of Riprap Revetment, Hydraulic Eng. Circular No. 11.

U.S. Federal Highway Administration. (2009). Bridge Scour and Stream Instability Countermeasures: Experience, Selection, and Design Guidance. Hydraulic Engineering Circular No. 23.

U.S. Federal Highway Administration. (2010). Culvert Design for Aquatic Organism Passage: Hydraulic Engineering Circular No. 26.

U.S. Federal Highway Administration. (2012). Hydraulic Design of Highway Culverts: HDS Number 5.

U.S. Geological Survey. (1986). Rock Riprap for Protection of Stream Channels near Highway Structures.

Using Data Science and Machine Learning to Improve Site Hydrogeological Conceptual Models

Tim R. Ezzy[1], John Fortuna[1]

[1]*Principal Hydrogeologist, Golder Associates, Milton, Queensland, Australia, TEzzy@golder.com.au, JFortuna@golder.com.au*

Abstract

A key goal of many mining groundwater investigations is to identify the main geological features, hydraulic boundaries and connection pathways that will materially influence: a) operations of a project, and b) the natural resources connected to the groundwater system. Exploratory data science techniques such as machine learning provide the experienced mining hydrogeologist opportunities to accelerate understanding of the role of key features within a site hydrogeological conceptual model (HCM) that may affect groundwater management. This has implications for both regulatory approval processes and operational efficiency.

Keywords: hydrogeological conceptual model, data science, machine learning, groundwater management

Introduction

Data science comprises three overlapping disciplines: 1) statistical modelling and analysis; 2) computer science skills necessary to efficiently store, process and visualise data; and 3) domain expertise in terms of classical training in a subject (VanderPlas 2017). The domain expertise (in this case mining hydrogeology) is necessary to pose the right questions and contextualise the outputs of the analysis.

In this paper we will review a recent mining project where data science techniques were implemented to identify which key geological features that have potential to influence future mine dewatering rates. The authors were engaged by our mining client to undertake a feasibility study (FS) for water management and river realignment for extension of several open cut pits. The mine site is underlain by sedimentary rock aquifers made up of calcareous sediments and dolomite with a porphyry intrusion aquitard. The aquifers are intersected by a dense network of subsurface faults that are situated within a broader pull-apart basin.

Faults have potential to control groundwater flow dynamics via cross-fault juxtaposition and modification of rock properties in the vicinity of the fault (e.g. Caine et al. 1996; Scibek et al. 2016; McCallum et al. 2018; OGIA 2019). Conceptually, there are three categories of permeability structure within a fault zone: barriers, conduits and barrier-conduits (Caine et al. 1996). Barriers tend to reduce groundwater flux, for example, by reducing the permeability along the central fault core. Conduits tend to increase flux either across faults or along fault planes, often through enhanced permeability of the fault damage zone. Barrier-conduits tend to increase fluxes parallel to the fault plane (along the damage zone corridor) while limiting flux across the fault core.

A key water management concern for future development is the potential for connections between the open cut pits and a nearby river through faults and related structural features. The null hypothesis at the mine site was that faulting has no influence on aquifer hydraulic properties. Previous groundwater modelling studies at the site (e.g. the mine prefeasibility study) adopted this hypothesis, and faults were not explicitly differentiated in the model domain. Given the stress regime and geological setting, an alternative hypothesis is that the normal NE-SW faults are oriented favourably with the principal horizontal stresses and are therefore expected to be dilated and could act as regional conduits for groundwater fluxes. Ten regional-scale NE-SW faults have been

mapped in close vicinity to the proposed mine pits. If some, or all of these faults were conduits, then it would have implications for pit dewatering requirements. Further, a number of these faults intersect a major regional perennial river, and the degree of groundwater-surface water connectivity may be a controlling factor in the feasibility of mining in this area.

Aquifer testing undertaken during the FS development was designed to specifically challenge these hypotheses. Aquifer tests were conducted in different rock types that were situated at a range of distances from variably-oriented faults. The objective of the data science approach was to interrogate the thousands of data points that were generated by the field investigations and to challenge the null hypothesis.

Methods

There are 75 estimates of hydraulic conductivity (K) generated from six constant rate pumping tests, including recovery tests, and 37 slug tests undertaken during various stages of project development. These aquifer tests were undertaken at three main hydrostratigraphic units and key geological contact zones. Twenty-three groundwater samples were analysed for major ion chemistry to provide an independent line of evidence on the influence of faults on regional groundwater flow processes. The K data and chemistry data were interrogated using an integrated data science approach that included geological modelling, geospatial analysis and statistical analysis. The integrated data science approach incorporated:

- Geological modelling to visualise the three-dimensional architecture of the hydrostratigraphic units and faults, using Leapfrog software (Seequent).
- Analysing the aquifer testing datasets including time-drawdown derivative analysis to further characterise system boundary conditions and flow system types, using AQTESOLV software (HydroSOLVE, Inc.).
- K data and chemistry data were embedded with geospatial attributes including host rock type and distances to the nearest fault types. QGIS 3.8.3 is an open-source geographic information system (GIS) platform that was used for spatially analysing the outputs from Leapfrog and AQTESOLV.
- Exploratory data analysis (EDA) including statistical analysis and machine learning (ML) were then used to challenge the null hypothesis and seek support for the alternative hypothesis: that the stress regime has enhanced the rock permeability along NE-SW normal faults. Pandas, Numpy, Seaborn and Scikit-Learn are all open source data analysis libraries built on top of the Python programming language. Jupyter Notebook was used to access these Python libraries and clean the datasets and undertake statistical analysis, data visualisation and machine learning.

We also undertook unsupervised, multivariate machine learning analyses of the Project major ion water chemistry dataset. The objective of these analyses was to identify any indicators of groundwater-surface water connectivity during the three constant rate discharge (CRD) tests that targeted specific faults. Two different unsupervised ML algorithms were utilised, namely:

- K-means cluster analysis (KCA); and
- Principal component analysis (PCA).

Data Science Workflow and Results

A geological resource model was built in Leapfrog, using data from the exploration drilling program and targeted hydrogeological investigations. This model contained the main dolomitic and calcareous sedimentary rock formations, as well as the rhyodacite porphyry unit. All of the main geological formations are heavily faulted. In general, the faults tend to be oriented in four main directions: a conjugate pair of N-S striking faults and E-W striking faults; and a separate conjugate pair of NE-SW striking faults and NW-SE striking faults. In total, over 100 faults have been mapped within 10 km of the mine site.

To explore the influence of faults on groundwater inflows to open cut pits, the FS field investigation undertook targeted test pumping at three main fault locations. At each of these three locations, the test

pumping bore and observation bores were constructed to intersect these mapped and modelled fault structures in the near vicinity of the proposed pits. These three CRD tests along faults complemented three previous Pre-FS CRD tests that tested the bulk rock transmissivity and storage properties away from faults.

Confined aquifer analytical radial flow solutions were primarily used in the analysis of the pumping test data. Generally, confined behaviour was observed through the timing and nature of the observation bore responses to pumping, which reflected low values of elastic storage. The approach to the analysis was sequential, starting with a simplified assumption of infinite acting radial flow to the pumped well and adding complexity where necessary. Table 1 summarises the K estimates that were derived for each major rock formation with respect to each aquifer test type. This aquifer testing forms the basis for our subsequent interpretation.

The diagnostic flow plots (time drawdown and drawdown derivative plotted together) aided in confirming the aquifer flow regimes and identifying key boundary conditions at two aquifer test locations (Figure 1). At one test location, barrier boundaries were identified in multiple observation bores at approximately 550 m from the pumped bore, which is the approximate distance to the nearby porphyry intrusion, a site aquitard. At the other test pumping location, a constant source recharge boundary was identified at 250-300 m from the pumping bore, which was the approximate distance to the regional perennial river. The HCM was modified to reflect the aquitard barrier boundary and potential for hydraulic connection with the river.

Table 1 *Summary of K estimates per HSU and Aquifer Test Type*

Test type	HSU	Count	Mean m/day	St.Dev m/day	25th Percentile m/day	75th Percentile m/day	Min m/day	Max m/day
CRD test drawdown	HSU1	1	34	-	-	-	-	-
	HSU2	24	14	17	0.7	19	0.01	56
	HSU3	3	2	3	0.7	3	0.3	5
CRD test recovery	HSU1	1	12	-	-	-	-	-
	HSU2	7	29	34	4	50	1	82
	HSU3	2	2	0	2	2	2	2
Slug test	HSU2	31	12	17	1	14	$3x10^{-6}$	60
	HSU3	6	3	2	2	4	0.	4

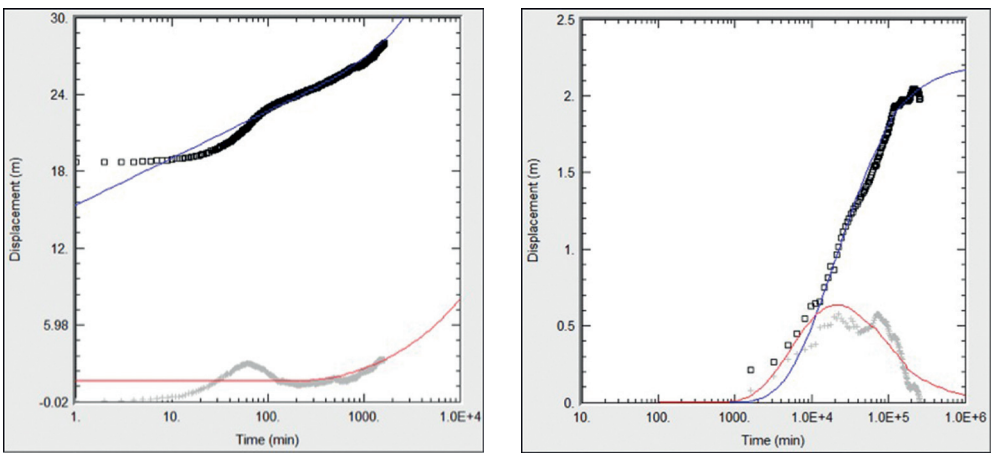

Figure 1 *Characteristic diagnostic flow plots showing: a) presence of no flow barrier associated with porphyry intrusion (Left); and b) presence of constant head recharge boundary associated with hydraulic connection to a regional-scale perennial river (Right).*

To enable spatial analysis of the K data, the solid geology and fault architecture was extracted from the Leapfrog geology model and imported into QGIS. Geospatial analysis included:

- Each fault was characterised based on its broad orientation into one of the four main spatial types and converted from a line to an array of 1m-spaced points.
- The distance between each K data point and the nearest fault point from each of the four fault groups was calculated.

The corresponding K-fault distance dataset was imported into Pandas to create a dataframe for hypothesis evaluation. Figure 2 presents the K distributions for each type of hydraulic test.

Figure 2a presents the K data with respect to the host bedrock geology. This plot shows that the K distributions are similar across different geological formations, except for the contact with the porphyry intrusion which acts as a regional aquitard. Geological formations that are dominantly fine-grained (siltstones and mudstones) have similar K to formations that are expected to be more permeable which highlights the strong influence of secondary porosity through fractures and karst. Also, of note is that the similar ranges of K values from different test types suggests that localised permeability features encountered in slug tests translate to macro-scale features encountered at the pump test scale (i.e. local-scale fracturing is interconnected at the macro scale). Figure 2b presents the K data with respect to geographic location and shows that higher K features are encountered more often at the South Pit area.

Figure 3 presents a series of jointplots showing the relationship of K to distance from each of the four fault type groups. These plots consider the probability distribution for the K data and the distance of that K data from the given fault type. Each of the four fault types have a good representation of nearfield and farfield K data to provide spatial context on whether the faults are influencing the permeability structure within the aquifers. The top two plots present the first conjugate pairs of faults being N-S and E-W orientations. Despite having a high number of data points close to these fault features, the probability distribution shows that a large number of the particularly high K points are situated away from these faults, and only a small number of high K points are within 50-75 m of the fault. It does not appear that these N-S and E-W faults are influencing permeability distribution.

In stark contrast, the NE-SW and NW-SE faults (the bottom two plots in Figure 3) show a much stronger relationship between proximity to faults and higher K. Figure 4 evaluates this relationship by area, and demonstrates that the NE-SW oriented faults (left plot) have higher K values in the South

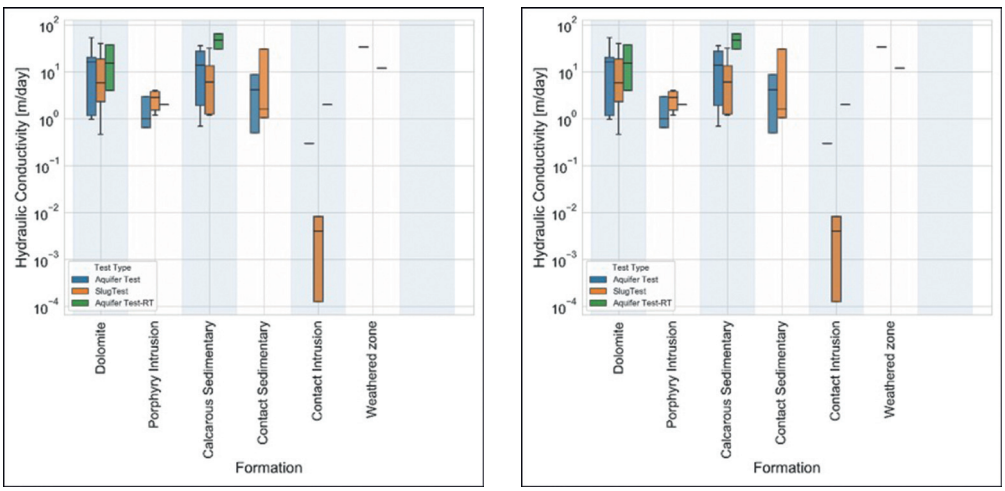

Figure 2 *Boxplots of hydraulic conductivity for each test type: a) categorised by type of bedrock geology (Left); and b) by geographic location with respect to vicinity to the nearest open cut pit.*

Pit and West Pit areas within 50 m of faults, as compared to the background fracture K which tended to be <10 m/day. The NW-SE transfer faults do not exhibit this same relationship and the proximity to these faults is not an explanatory variable for higher K within a reasonable fault damage zone corridor (i.e. <50 m).

As an independent line of evidence, both KCA and PCA were conducted sequentially to interrogate water quality data. Three main groups of groundwater quality were obtained through the KCA, and these groups broadly aligned with the two main hydrochemical facies being Ca-SO4 type water north of the porphyry intrusion and Ca-HCO3 type water south of the intrusion. There are a number of potential surface water-groundwater processes that can be observed from the PCA analysis:

- South Pit observation bore chemistry is similar to the nearby perennial river sample prior to and after the CRD test.
- The Northeast Pit and West Pit bores transition towards the perennial river sample chemistry towards the ends of the tests. This indicates potential for pumping-induced river water recharge, suggesting that the fault systems may be connected to the river.
- The South Pit pumping bore transitions from a water quality that resembles a

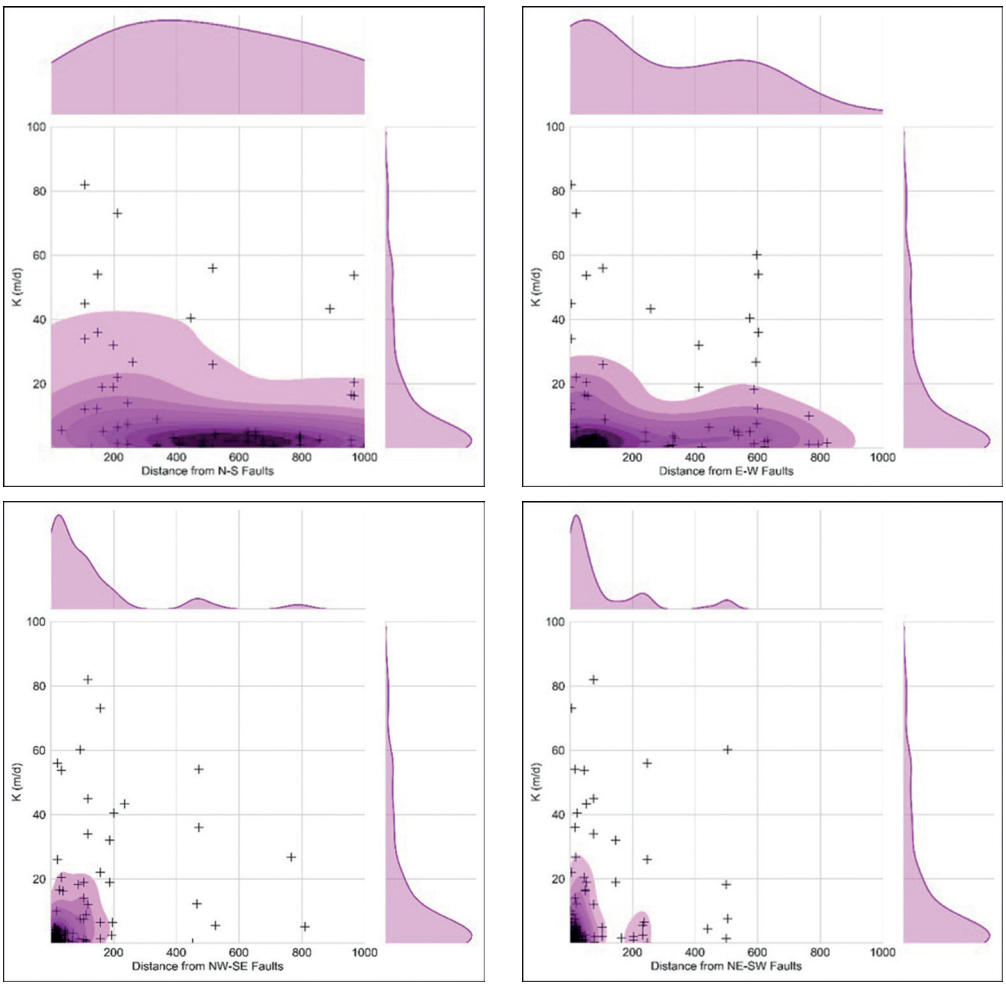

Figure 3 *Jointplots showing the relationship of K to distance from each of the four fault types: a) Distance from N-S faults (Top Left); b) Distance from E-W faults (Top Right); Distance from NE-SW faults (Bottom Left); and d) Distance from NW-SE faults (Bottom Right).*

nearby pit lake to groundwater that is observed in two bores situated more than 1 km to the west.

Conclusions

In our examples, EDA and ML techniques facilitated by Python scripting were used to integrate data from aquifer testing, geological modelling, structural interpretation, and hydrochemistry analysis to achieve a more wholistic understanding of groundwater flow dynamics along structural features and improve both the HCM and resulting estimates of pit inflows and groundwater drawdown distribution. This improved aquifer characterisation has identified which styles of faults are likely to be more transmissive and in doing so provided a more robust basis for estimating ranges of likely groundwater inflows and testing of mitigation measures such as advanced dewatering strategies

Proper application of these techniques is only possible when directed by an experienced hydrogeologist with a keen understanding of the HCMs, through problem formulation directed at specific data gaps.

Acknowledgements

The authors thank fellow Golder hydrogeologists Dr Scott Weeks, Jaco Breytenbach and Nick Coulson for support during the analysis and interpretation of the data.

References

Caine JS, Evans JP, Forster CB (1996) Fault zone architecture and permeability structure. Geology 24(11): 1025-1028.

McCallum J, Simmons C, Mallants D, Batelaan O (2018) Simulating the groundwater flow dynamics of fault zones. Report submitted to Australian Department of Environment and Energy. National Centre for Groundwater Research and Training. 52pp.

Office of Groundwater Impact Assessment (2019) Underground Water Impact Report for the Surat Cumulative Management Area. Department of Natural Resources, Mines and Energy, State of Queensland. 272pp.

Scibek J, Gleeson T, McKenzie JM (2016) The biases and trends in fault zone hydrogeology conceptual models: global compilation and categorical data analysis. Geofluids (2016) 16: 782-798.

Van der Plas J (2017) Python data science handbook: Essential tools for working with data. O'Reilly, Boston, 548 pp.

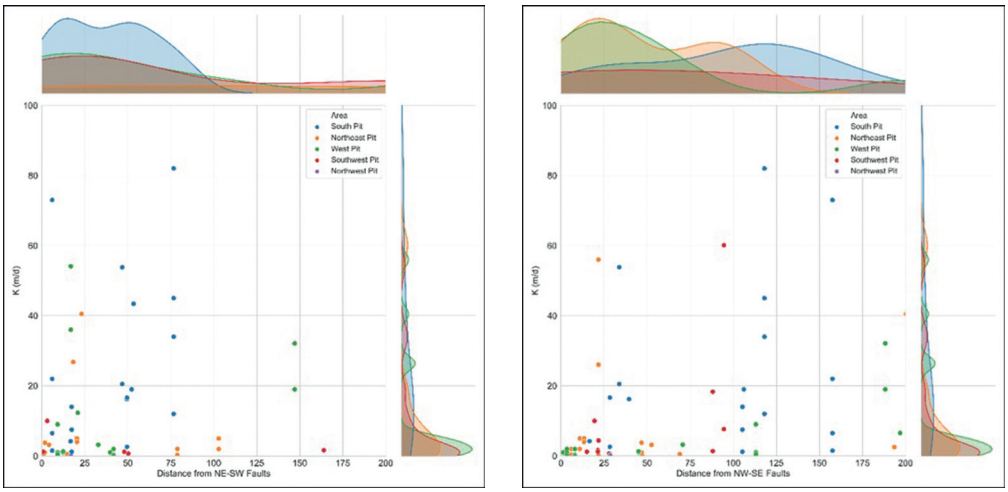

Figure 4 Jointplot showing the relationship of K to distance from: a) NE-SW faults (Left), and b) NW-SE faults (right). Note: only shows K data within 200m of this fault type

Slope Depressurisation at Sishen Mine, Northern Cape, South Africa

Travis White[1], Marnus Bester[2], Richard Carey[3]

[1]*Hydrogeologist, Kumba Iron Ore, Sishen Mine, Hendrick van Eck Street., Kathu Northern Cape, 8446, Travis.White@angloamerican.com*

[2]*Principal Geotechnical & Hydrogeology, Kumba Iron Ore, Corporate Office, 124 Akkerboom Street, Zwartkop, Centurion, 0157, Marnus.Bester@angloamerican.com*

[3]*Section Manager Geotechnical, Kumba Iron Ore, Sishen Mine Hendrick van Eck Street., Kathu Northern Cape, 8446, Richard.Carey@angloamerican.com*

Abstract

Prior to 2014, the dewatering program at Sishen Mine focused exclusively on the deep fractured aquifer and neglected the upper shallow aquifer. In November 2014, increased pore pressures in the shallow aquifer led to slope instability with subsequent slope remediation measures costing more than USD9 million. This initiated the development of an active depressurisation program in its largest pit (GR80), to alleviate pore pressures. The system is an excellent example of the value of an effective depressurisation system which enabled slope design optimisation unlocking substantial value through a 24 million ton reduction in waste stripping and reduced production delays.

Keywords: slope depressurisation, pore pressure, slope design

Introduction

The necessity for Sishen Mine's slope depressurisation system came about due to years of poor surface water management, geological variation in the northern mining area and delayed execution of capital projects. Mining was not affected by water induced slope instability in the past as mining tempos were slower and focussed in the southern part of the mine in areas with thinner clay units. When mining in the northern part of Sishen Mine commenced, where the clay unit is thicker and mining tempos were more aggressive, challenges with water seepage and subsequent bench scale failures began occurring. Exacerbating the situation were elevated water levels in the unconfined aquifer (calcrete). The presence of water within a rock mass reduces shear strength and detrimentally affects slope stability (Read and Stacey 2009). Initial attempts to mitigate the risks associated with water seepage involved the use of vertical drainage wells that would allow the shallow unconfined aquifer to drain into the deeper confined fractured aquifer, but the results were limited and a new approach was required. The new approach entailed four key focus areas:

1. Identify the water source causing the elevated water levels and establish controls to prevent further recharge of the unconfined aquifer.
2. Hydrogeological characterisation of the unconfined aquifer.
3. Review existing system and design a system to depressurise the pit slope more effectively.
4. Develop a monitoring network to establish baseline pore pressure and monitor efficacy of new system.

The outcome of the assessment of the four key focus areas above was as follows:

- The source of the elevated water levels was from the unlined storm water canal and surface water ponds near final pit wall perimeter boundaries.
- The unconfined aquifer has anisotropic hydraulic properties caused by geological heterogeneity.
- The existing system (vertical drainage wells) was not practical nor cost effective

in comparison to shallower wells with a solar pump system.
- The monitoring network gave valuable insight into the efficacy of the new depressurisation system and assisted in delineating potential problem areas that may be encountered in future which enabled proactive deployment in the expansion of the system.

The Sishen Mine depressurisation system has been continually developed since 2016 and is now being implemented in phases according to the mine plan. This paper aims to outline what caused the need for depressurisation, how the problem was resolved and the immense benefits of an effective depressurisation program.

Methods

Identify the source

A series of sample points were selected to determine the water source creating elevated pore pressure in the unconfined aquifer. The sample points were selected according to the spatial distribution of the potential sources. Samples were taken from the unlined canal, boreholes drilled in the unconfined aquifer, seepage ponds at the foot of the high wall and seepage directly out of the high wall.

Hydrogeological characterisation

Quantifying hydraulic conductivity and specific yield is essential when assessing the potential depressurisation techniques to be considered for implementation. A series of ten boreholes were drilled and pump tests were performed on three of the boreholes in the project area. Each borehole was logged noting both primary and secondary lithofacies.

Review depressurisation design

A review of the existing system involved assessing the results achieved to date, possible explanations for the limitations in efficacy, costs incurred, practicality and overall suitability of the design. There are various depressurisation techniques available which include grout curtains, horizontal drainage wells, vertical drainage wells, cut-off trenches and abstraction wells (Beale and Read 2013). Due to the size and complexity of the Sishen mining operation, vertical wells were the only practical and feasible option. With this constraint in mind, the implementation of deep-vertical drainage wells versus shallow-vertical abstraction wells was explored.

Establish baseline & monitoring network

Prior to the review of the previous depressurisation system, there were no grouted vibrating wireline piezometers (VWPs) installed at Sishen Mine. Grouted VWPs are critical monitoring tools that are used to measure transient in situ pore pressures. A monitoring network of VWPs was installed around the project area to obtain a baseline pore pressure, per area, and measure progress of the depressurisation system. Each monitoring point is connected to a data logger which communicates wirelessly to a central gateway and transmits data which is then stored on Sishen Mine's Water Information Management System (WIMS).

Data

Water samples

Fourteen water samples were taken from various locations within the area of study. These include samples from boreholes representing the unconfined aquifer, the unlined canal, seepage from the high wall and seepage ponds at the foot of the high wall.

Hydrogeological characterisation

A series of ten boreholes were drilled at 25 m spacing to 60 m depth. There is little variation in the primary lithofacies with calcrete from 0 m to 50 m and clay from 50 m to end of hole (EOH) but local variations in secondary lithofacies are evident. These variations occur in the calcrete where clay lenses appear erratically throughout the sequence and show no correlation from one borehole to the next. Historically, very little attention was given to the secondary lithofacies in the calcrete as it bears no economic importance. The erratic distribution of clay and sand lenses within the calcrete is noteworthy for depressurisation as this heterogeneity could influence ground water flow. The pump tests on the three wells were conducted over a period of four hours each at a constant discharge rate of 0.5 L/s.

Drawdown of 35 m was achieved in each well after two hours of abstraction and water level recovery (90% of initial water level) in each well varied from six hours to thirty hours.

Shallow wells vs deep wells

Possibly the most important part of the project was to perform a cost analysis on the existing system versus the implementation of a new system. To date, the vertical drainage wells have only achieved a total drawdown of 4 m and drawdown has been stagnant since. The vertical drainage wells used in the initial project area were drilled between 100 m and 150 m depth, through the calcrete, clay and into the banded iron formation (BIF) which forms part of the deeper fractured aquifer system (fig. 1). The clay is thicker in the northern part of the GR80 pit which would require deeper drainage wells to depths greater than 150 m to reach the deep aquifer. The unit cost of a vertical drainage well (>150 m) is approximately USD43,000 while a shallow well (60 m) costs USD14,000. This discernible difference in cost was the primary driver for reassessing the status quo and devising a more efficient and cost-effective system.

Monitoring network

Prior to 2016, Sishen Mine only made use of open standpipe piezometers to monitor water levels. Grouted VWPs were only introduced and used at the mine in 2016 as part of the depressurisation program. A single sensor VWP was installed as a trial in January 2016 after which a number of multi-level VWPs were installed. The multi-level VWPs comprise three sensors installed in an HQ diamond borehole; the lower sensor is installed in the clay, the middle sensor at the calcrete-clay contact and the upper sensor approximately 5 m above the contact.

Results

Water source

Chemistry data for the fourteen water samples was assessed to distinguish different water species and observe any noticeable trends. Similarities in chemistry between the canal (surface water) and ground water samples (boreholes) supports the idea that the unlined canal was responsible for the elevated water levels in the unconfined aquifer. Increased chloride and sodium/potassium for the

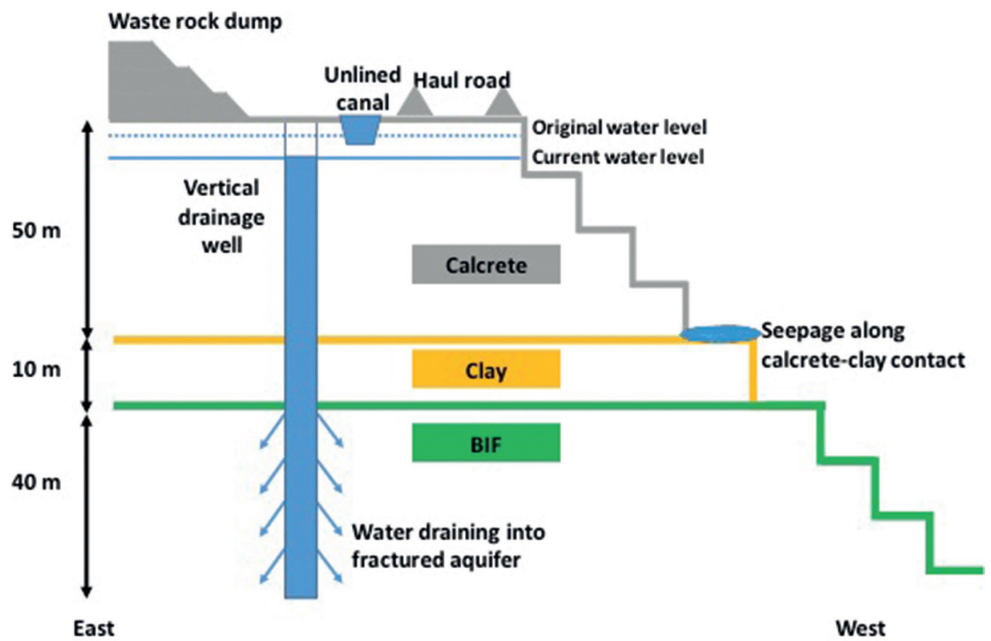

Figure 1 *East-West section through vertical drainage well depressurisation system.*

seepage samples can be explained by water-rock interaction and evaporation within the seepage ponds. The evolutionary trend of the seepage water species is toward the canal and borehole samples which suggests that the water chemistry (before water-rock interaction and evaporation) was similar to that of the source. Additional evidence that also supports the hypothesis are; normal water levels in areas with no canals, seepage more prominent when canal through flow was higher, background water chemistry for unconfined aquifer differs from project area and prominence of seepage issues aligned with timing of canal's construction.

Hydrogeological characterisation

The pump test data from the three wells and heterogeneity in geological logs indicate that the unconfined aquifer is hydraulically anisotropic which is supported by qualitative evidence in the pit. Sporadic and irregularly distributed seepage can be explained by the variations in secondary lithofacies. Though some fracturing is present in the calcrete, the primary control of ground water flow appears to be the presence, or absence, of paleochannels which vary in composition from clay/silt to sand and pebbles/gravel. Seepage is prominent along the calcrete-clay contact and above clay lenses that daylight in the high wall as the clay is an aquitard. The specific yield for each of the depressurisation wells varies from as low as 0.05 to 0.5 L/s with very low hydraulic conductivity (K) in the range of 10-7 to 10-8 m/s in the calcrete.

Cost comparison

Upon reviewing the existing design of the depressurisation system, it was clear that vertical drainage wells would be capital intensive, would take longer to implement and the required reduction in pore pressure was not guaranteed. Taking the above into consideration, the continuation of the vertical drainage well configuration would be futile and the option of using shallow wells equipped with submersible pumps was pursued.

Design

Lining of canal and shallow well solar pump system

To comply with legal and regulatory requirements, the canal was lined with concrete in 2016 which mitigated artificial recharge of the shallow aquifer. Though the water source for the elevated water table was resolved, the calcrete remained saturated and seepage would persist unless the water was intercepted before reaching the high wall.

The pumps for the wells were sized according to the maximum total head (60 m) and specific yield of each well which ranged from 0.05 to 0.5 L/s. The pump set selected for the wells was a Grundfos SQF0,6-2 which has a 0.75 kW motor powered by three 100 W solar panels. The unit cost for the complete solar powered submersible pump set per well (pump, motor, solar panels, switch box, electrical cable, riser pipe, valves, flow meter, well cap and fittings) is USD2,750 which brings the total cost per depressurisation well to USD16,750 which is 60% less than the cost of a vertical drainage well. Figure 2 illustrates the configuration of the solar pump system and VWP installation to monitor performance.

The project area for the depressurisation system covers a linear distance of 5.5 km. Establishing the necessary infrastructure (electrical power lines and pipe work) in an active mining area over such a large distance is challenging and expensive. Recent advances in solar technology has made solar products cheaper, more efficient and easily accessible for both commercial and domestic use. The decision to implement a solar powered submersible pump system was based on the following factors;

1. Solar power would be cheaper than mainline electrical power distribution.
2. The low yields on the wells meant that the effective abstraction duration for each well was 4 to 8 hours per day.
3. Sishen Mine has more than 330 sun days per year which offers excellent potential for exploitation of solar energy.

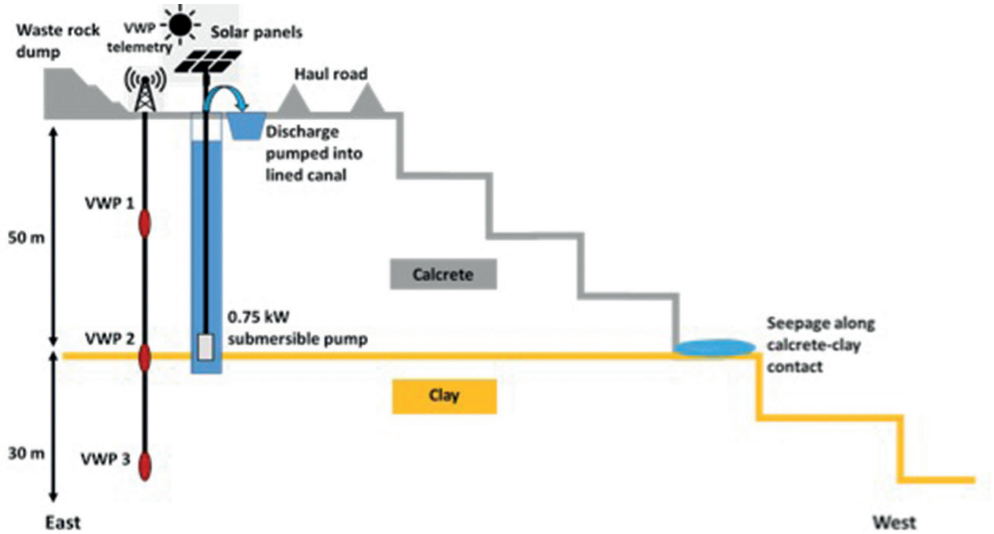

Figure 2 East-West section of solar powered submersible pump system with VWP configuration.

4. Solar systems are modular and manufacturers offer ready built solutions rapid and easy deployment.
5. Modern solar systems require little to no maintenance.
6. Solar powered systems are mobile and offer flexibility in a confined working area.

Implementation

Installation of solar powered submersible pumps

Before full scale implementation of the solar powered system was commissioned, a trial system comprising 7 wells was deployed along the eastern pit boundary of GR80 pit and was monitored over a period of 2 years. Seven wells were equipped and the system delivered approximately 20,000 litres per day. A single sensor VWP with a data logger, for barometric correction and remote monitoring, was used to obtain a baseline and monitor the performance of the trial system. The improved efficiency of the new system was clear upon commissioning and the results are presented in figure 3. Diurnal fluctuations in pore pressure are due to the operating times of the solar system.

With these productive results, the full-scale depressurisation system was deployed and to date there are 36 depressurisation wells in production with 13 multi-level VWPs monitoring their performance. Expansion of the project will continue as mining of the GR80 pit expands to the west of the current mining area.

Discussion and conclusion

The solar powered submersible depressurisation system at Sishen Mine has been incredibly successful in reducing the pore pressure behind the GR80 pit slope. The success of the system is the result of adhering to basic scientific principles with a practical approach in developing and implementing an effective solution. The hydrogeological aspects of the geotechnical model together with the geological, structural and rock mass aspects, proved to be critical in the successful management of geotechnical risk at Sishen Mine.

Successful depressurisation and mine dewatering together with other advancements in geotechnical engineering and operational mine to design adherence, not only led to more effective risk mitigation, but also to the launch of a slope optimisation initiative to unlock value. This is based on the principle that addressing geological uncertainty in potential risk areas, increases the confidence in the slope design. Optimisation initiatives focused on design sectors with favourable interaction of slope geometry with geology, lithologies with favourable strength characteristics where stability analysis indicate optimisation potential as well as

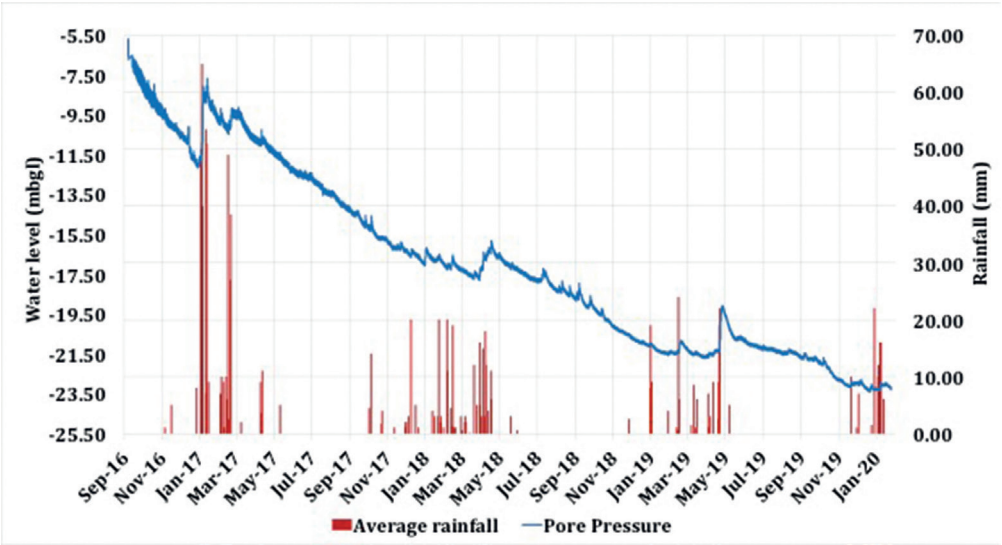

Figure 3 *Data collected by single sensor VWP displaying accelerated drawdown in trial area.*

layout optimisation aspects (geotechnical berms and ramps). Options were evaluated that determine cost saving by decreasing waste stripping for the same amount of ore as well as accessing additional deeper ore at equivalent strip ratios.

Phase 1 of the slope optimisation project was included in the Sishen 2018 Life of Mine (LOM) plan. This work unlocked substantial value for Kumba Iron Ore and was the major contributor to an increase in NPV from 2017 to 2018 of approximately USD720,000,000 from an additional 50 million tons of ore (Anglo American 2019) which would not have been possible without the success of the depressurisation program.

References

Anglo American, 2019. Anglo American Kumba Iron Ore Investors. [Online]

Available at: https://www.angloamericankumba.com/investors/annual-reporting.aspx

Beale, G & Read, J, 2013, Guidelines for Evaluating Water in Pit Slope Stability, CSIRO Publishing, Collingwood Australia.

Read, J & Stacey, P, 2009, Guidelines for Open Pit Slope Design, CSIRO Publishing, Victoria Australia.

Repurposing Mine Sites for the Well-being of Future Generations: Innovative Examples and Case Study of Developing Post Mining Remedial Work in Wales

Peter Stanley[1], Trystan James[1], Bob Vaughan[1], Steven Pearce[2]

[1]*Natural Resources Wales, Tŷ Cambria, Newport Rd., Cardiff, CF24 0TP, UK, geoscience@cyfoethnaturiolcymru.gov.uk*

[2]*Mine Environment Management Ltd., 3A Vale Street, Denbigh, Denbighshire, LL16 3AD, UK, spearce@memconsultants.co.uk*

Abstract

The Well-being of Future Generations (Wales) Act 2015 introduced "sustainability" into legislation for the first time anywhere in the world aiming to improve the social, economic, environmental and cultural well-being of Wales. Seven case studies are described showing how Natural Resources Wales acted "in accordance with the sustainable development principle" revealing how public bodies must act in a manner seeking to ensure the needs of the present are met without compromising the ability of future generations to meet their own needs. Public bodies undertaking substantial capital spending have a duty to ensure they embrace community well-being by applying their Well-being objectives.

Keywords: sustainable, generations, wellbeing, legislation, community

Introduction

Mining has been an active industry in Wales since the Bronze Age, bringing much prosperity during the industrial revolution, however subsequent decline has left a legacy of scarred landscapes and societies. The last lead mine at Parc in the Gwydir Forest (North Wales) closed in 1958 and the copper precipitation ponds at Parys Mountain (Anglesey) were abandoned in 1956. Gold mining has endured and is still practiced at Clogau (North Wales) where processing of mine spoil continues. In relation to coal, only small private mines now exist as large collieries within the extensively worked South Wales Coalfield closed from the mid 1980's.

Many former mining communities that surround the now abandoned mines rank today as some of the poorest in western Europe. The legacy remaining from in excess of 1,300 metal mines, numerous collieries in the South Wales Valleys and those in North East Wales has been one where large reclamation schemes from the mid 1980's were encouraged to help restore impoverished environments and communities, attempting to inject new business opportunities. These restoration schemes accommodated heavily industrialised areas such as Ebbw Vale (the Garden City), Merthyr Tydfil, Llanelli, Wrexham, also at Bwlch and Van lead mines in Mid Wales. Many areas have however, had little development since the cessation of mining, exemplified by the designated landscape of the Blaenavon World Heritage Site (South Wales Coalfield), which contains many original features of the previous mining landscape.

Given this long history of mining in Wales and numerous examples of resultant legacy sites, a valuable long-term opportunity to evaluate the practical application of "sustainability" with respect to mine site remediation has emerged in this Act. Examples of legacy mine site remedial actions are therefore identified and discussed as early stage case studies.

Private and Community Led Repurposing in Wales

Developments utilising former mining landscapes to regenerate local economies have recently used adventure tourism as its base. The development of tourism as an "end

use" at Welsh mines developed from decades of experience with traditional projects like interactive visitor centres, museums and walking trails. A small scale opportunity occurred at the Bedlinog recreation and climbing centre, a former colliery north of Caerphilly. Larger redevelopment of an open cast coal mine occurred at the Ffos Las Horse Racecourse, Carmarthenshire, plus the diversification of a sheep and cattle farm with a cart racing track at Abbey Consols mine, Ceredigion. More recent adventure tourism projects such as the downhill mountain bike center Antur 'Stiniog was established in former slate mines near Blaenau Ffestiniog as a not for profit social enterprise. This followed receipt of over 2,000 support pledges from local residents, each sharing the same vision "To develop the potential of the Outdoor Sector in a sustainable and innovative way for the benefit of local residents and economy". Other examples include aerial zip lines (Zip World) at Penrhyn Quarry near Bethesda, surfing lagoons (Surf Snowdonia) at the former Trefriw aluminium plant and at the Slate Caverns of the Llechwedd Deep Mine, Blaenau Ffestiniog with underground trampoline networks (Bounce Below), cavern exploring plus quarry tours offered. All provide positive community benefits, much needed employment and revenue generation.

Given the history of mining in Wales and the decades of resulting negative socio-economic impact, the developing adventure tourism concept offers an alternative view on what "sustainable" means from the perspective of mine closure.

The Well-being of Future Generations (Wales) Act 2015 (WbFGA)

To maximise the opportunities to progress mine remedial work NRW is looking at recently introduced legislation. The enacting of the WbFGA introduced "sustainability" into legislation for the first time anywhere in the world. This adopts the Gro Harlem Brundtland sustainable development principles (World Commission 1987); and aims to improve the social, economic, environmental and cultural well-being of Wales. This puts in place the following seven goals

1. **A prosperous Wales:** An innovative, productive and low carbon society which recognises the limits of the global environment and therefore uses resources efficiently and proportionately (including acting on climate change); and which develops a skilled and well-educated population in an economy which generates wealth and provides employment opportunities, allowing people to take advantage of the wealth generated through securing decent work.
2. **A resilient Wales:** A nation which maintains and enhances a biodiverse natural environment with healthy functioning ecosystems that support social, economic and ecological resilience and the capacity to adapt to change (for example climate change).
3. **A healthier Wales:** A society in which people's physical and mental well-being is maximised and in which choices and behaviours that benefit future health are understood.
4. **A more equal Wales:** A society that enables people to fulfil their potential no matter what their background or circumstances (including their socio-economic background and circumstances).
5. **A Wales of cohesive communities:** Attractive, viable, safe and well-connected communities.
6. **A Wales of vibrant culture and thriving Welsh language:** A society that promotes and protects culture, heritage and the Welsh language, and which encourages people to participate in the arts, and sports and recreation.
7. **A globally responsible Wales:** A nation which, when doing anything to improve the economic, social, environmental and cultural well-being of Wales, takes account of whether doing such a thing may make a positive contribution to global well-being.

"In this Act, any reference to a public body doing something "in accordance with the sustainable development principle" means that the body must act in a manner which seeks to ensure that the needs of the present are met without compromising the ability of future generations to meet their own needs." A public body like NRW must

consider and balance the short-term needs with those of the long term, particularly if these have a detrimental effect on the long-term effect. This accommodates other public bodies objectives and therefore their involvement or collaboration to enhance well-being deliverables and goals. Thus, for large capital remedial schemes, stakeholder dialogue will accommodate the designated range of national and local public bodies via the Public Services Board (PSB). A Future Generations Commissioner ensures the PSBs fulfill their duties.

This duty requires public bodies to work together with PSBs to enable greater public participation with funded work. For example, by working with the Sports Council of Wales and Public Health Wales NHS Trust, opportunities to encourage enhanced healthy lifestyles can be incorporated into new planning. Similarly, by linking with the Arts Council of Wales, National Museum of Wales or the Higher Education Funding Council for Wales, planned development may leverage additional funds delivering enhanced cultural opportunity for intuitive sensitive public art with communities and schools engaged in design development to educate via nature or social history.

Public bodies undertaking substantial capital spending have a duty to ensure they embrace community well-being and apply their objectives. NRW's objectives link the State of Natural Resources Report (SoNaRR), Natural Resources Policy (NRP) and Area Statements. The NRP, produced by Welsh Government, identifies that NRW will secure nature based solutions, increase resource efficiency to decarbonise and take a place based approach. The NRP focuses upon reversing the decline in biodiversity, reducing pollution and flooding, improving ecological resilience, soil quality and biosecurity, increasing renewables, carbon storage, healthy fish, woodlands, recycling, recovery, maximising recycled aggregate, ensuring sustainable mineral extraction and adapting to climate change. NRW has seven Area Statements, one marine and six land-based that take a place based approach focusing on collaborative working, building on evidence that communities will better deliver behavioural changes to tackle the challenges and priorities. The SoNaRR collates evidence from Area Statements and elsewhere, providing the prime national scale evidence base for Welsh Government to produce the NRP, which develops national priorities where taking action at the right scale will maximise or multiply benefits.

Llynfi Valley Sustainable Redevelopment Case Study

This case study highlights the importance of the socio-economic aspects of mine closure, and how innovation is vital for success. At the former Coegnant colliery and Maesteg Washery in the upper Llynfi Valley (ULV) South Wales, one of the most socially and economically deprived communities in Wales, Welsh Government funded in 2015 a reclamation woodland scheme for community benefit. Although preparatory work preceded the Act, the outputs promoted the principles.

Sustainable woodland planting occurred in ULV that has, based on socioeconomic metrics, higher degrees of limiting long term illness and "General Health Not Good" than those in the nearby communities of Maesteg, Bridgend (14 km away) or Wales as a whole (Powell Dobson Urbanists 2010). Incapacity benefit in the ULV communities is also higher than in both Bridgend and Wales. These socio-economic factors directly effect economic activity within communities as more illness or poor health are an impediment to achieving sustainable positive economic outcomes. For example, there are twice as many people who have never worked here than in Bridgend. Economic mobility is also impaired, comparative analysis revealing car ownership reduced by half in the ULV, resulting in more people traveling to work by bus or taxi and fewer by bike.

Sustainability can be "encapsulated" when development achieves economic, social, environmental and cultural well-being. The planting of 30 ha with 60,000 trees created the Spirit of Llynfi Woodland in an area of 75 ha that demonstrably promotes health and well-being. When initially assessing mine hazards at the site, NRW reviewed typical constraints like crown holes, habitat, drainage and also

the opportunities, for example identifying the potential to exploit mine water enthalpy for community benefit (AECOM 2015). The planting scheme incorporates an off-road cycle route connecting ULV, Maesteg and the national network that provides an obvious improvement to cycle mobility and connectivity. Additional footpaths were introduced, green exercise areas plus trails for people and dogs, a geocache trail. Diversity of habitats was achieved with ponds, marshland, fruit tree orchard, stream bridges with school inspired designs and a lasting artwork was established through the sculpture of Keeper of the Collieries, one of the last working colliers.

Bridgend County Borough Council also introduced the Caerau Construction Skills Centre that linked with the Green Skills Centre at Tredegar to stimulate training in the green economy and increased economic activity in microgeneration and renewable energy installation. Subsequent major Welsh Government investment for community heating from the mine water has occurred.

The Metal (Non Coal) Mine Programme

Following the EU Water Framework Directive (WFD) in 2000, Environment Agency Wales a predecessor body to NRW published the Metal Mines Strategy in 2002 prior to the WFD being implemented into UK law in 2003. This gave an objective to focus on the fifty most polluting metal mines leading to several catchment led assessments of polluting pressures on surface waterbodies. Studies became more site focused leading to remedial intervention actions redirecting surface water away from open cast sites and shafts as entry points.

As part of a review of priority sites, The Coal Authority reviewed monitoring and assessment at ten mines and three Blow Out Potential (BOP) sites (Coal Authority 2016). Prioritisation (Table 1) ranked them according to completeness of monitoring, treatability of the discharges, physical site attributes, constraints of heritage, habitat and landscape, land ownership issues and cost benefit. This review resulted in the least technically complex site at Abbey Consols being ranked top priority, leading to the Teifi Mines of Abbey Consols and Esgair Mwyn progressing to detailed design for treatment and sediment arrest infrastructure to maximise benefits to the Afon Teifi. Feasibility studies are completed at Cwm Rheidol, Cwmystwyth, Dylife and Frongoch-Wemyss mines, whilst at Parys Mountain a cost benefit assessment progresses.

Abbey Consols is located on the opposite side of the river to the 12th century Strata Florida Abbey, whose Cistercian monks were also interested in the mineral resources in the area. Notably the church at the Abbey had been built with a lead roof until a fire attributed to a lightning strike in 1284, caused it to melt and roll off. Culturally the Abbey is nationally important, whilst the mine is the largest contributor of zinc to the River Teifi and impacts some 40 km. NRW used this evidence to pursue design of the

Table 1 *Metal Mine Prioritisation Site Scoring Matrix (from Coal Authority 2016).*

Score Site	Monitoring	Treatment	Physical Site Attributes	Designations	Land Ownership	Cost v Benefit	Total
AC	9	7	7	7	5	9	44
F-W	7	7	7	7	3	7	38
CRh	9	5	7	7	1	7	36
CY	7	7	3	5	7	7	36
Dylife	7	7	7	5	3	7	36
PMtn	9	7	7	5	5	3	36
EM	5	5	3	7	5	7	32

AC=Abbey Consols. F-W=Frongoch-Wemyss. CRh=Cwm Rheidol. CY=Cwmystwyth. PMtn=Parys Mountain. EM=Esgair Mwyn.

Surface Water Management System (SWMS), treatability trials and detailed design with WSP in collaboration with Cardiff University. The favoured treatment design is a semi passive system incorporating $NaCO_3$ dosing and settlement ponds. The discharge rate of 1 L/sec means the footprint of the treatment scheme will be relatively small and capital costs of this scheme are expected to be low circa £1M. The scheme design will transform improvements in water quality using innovative water treatment technology that delivers Public Goods benefitting nationally important cultural heritage, community well-being and offering applied learning opportunities.

Frongoch-Wemyss is in upland Ceredigion on private land located about 3 km from the former mining community of Pont-rhyd-y-groes. Some of the mine buildings are designated Scheduled Monuments (SM's) and of particular note with regard to perception of mine waste, an area of mine spoil is designated a geological Special Site of Scientific Interest (SSSI) for possessing rare supergene mineral formation. Latterly from 1899 to 1903 the site was operated by Belgian company Société Anonyme Minière. The site now benefits a SWMS and has three distinct discharges, one from Frongoch adit that enters the Nant (stream) Cwmnewydion and two much smaller, but concentrated discharges that enter Frongoch stream. NRW pursued innovative sustainable research of contained low energy demand water treatment solutions. Electrochemical coagulation pilot trials on the two concentrated discharges successfully removed the majority of metals and collaboration with Swansea University investigated membrane nanofiltration improving precipitate harvesting to 15–20% solids (Elentec 2019). The electrochemistry trials continue with collaborating partners of LIFE Demine. This site continues to provide opportunities to study the possibilities, and practicality of incorporating sustainable mine water treatment technologies in a remote upland environment that is also a culturally sensitive heritage site.

Cwm Rheidol is in the steep sided Rheidol valley that on the north side of the valley has two adit discharges conveyed to limestone filter beds constructed in the 1960's to address the highly concentrated and ochreous acidic discharges. The filter beds soon passivated, stopped working and now some 9 T/yr of metals enter the Rheidol. The Cwm Rheidol hydro power station, operated by Statkraft UK Ltd, is located downstream where they have a visitor centre and butterfly house. The Rheidol steam railway and Special Area of Conservation (SAC) provide attraction on the valley's southern side. There is no immediate associated community and the location lends itself to incorporation of an active treatment system with a low footprint, which could stimulate economic enterprise. NRW supported Power & Water carrying out sono-electrochemistry trials using the ©soneco process, which proved successful in substantially reducing metal loading and demonstrates the options to utilise renewable energy for mine water treatment (Rose 2019). Trials of Dispersed Alkaline Substrate are planned to provide comparative assessment.

Cwmystwyth has been exploited since the Bronze Age. The stunning landscape setting is located on a steep sided mountain valley 7 km west of Pont-rhyd-y-groes. Treatment of the main discharge, Pugh's adit ochreous discharge, would significantly reduce metal loads to the river by up to 8 T/yr of non iron metals, but not recover the river to good status. It is noted that there are designations for SM's, SSSI and SAC's present identifying a highly sensitive site setting. The Coal Authority has attributed costs of £3M to address discharges from Pugh's adit. Use of onsite hydropower for an active treatment system has been recognised as a potential opportunity and it would be viewed as an exemplar scheme with multiple benefits decarbonising the programme.

Dylife is on the headwaters of the Afon Twymyn and Nant Dropyns about 4 km from the small community of Staylittle in Powys. The Roman fortlet Penycrocbren is situated above the workings and the area has been exploited since Romano British times. The watercourses are intermittent due to loss of water to the mineral workings on the lodes, which strike across the waterbodies. Accordingly, an integrated hydro-scheme to convey water from above the mine workings

to a turbine house beneath the spoil tips is considered favourable. Toe drainage and active treatment of spoil tip discharges will be required as will protection/capping of the dressing floor at the confluence of the tributaries. There are habitat, heritage and biosphere constraints. Costs for the hydro scheme to completion of detailed design are estimated at £700K. Remedial work to convey water over the mine workings would ensure a substantial reduction in metal loading to the river.

Parys Mountain is 3 km from Amlwch and is unique to the UK, being at one time the world's largest copper mine now discharging 231 T/yr of harmful metals into the Irish Sea. Mineral exploitation stretches back to the Bronze Age but huge interest sprang from 1760. Precipitation ponds were also used to extract the copper and a Copper Kingdom visitor centre is based at Amlwch port. There would be interest in mimicking the former cementation method of copper extraction, providing employment with artisanal scale jewellery and manufacture of cookery implements. It could yield educational and tourist interest, particularly if dashboards are made available to schools/institutions with live daily water quality data available. Interest would trigger heritage research at the precipitation ponds and reverberatory furnace. The Coal Authority is undertaking a comprehensive Benefits Assessment considering the newly created North Anglesey Marine SAC and will ensure a recognition of the Natural Capital. Pilot trials of the Dispersed Alkaline Substrate system are planned that may lead to a full scale system, which is currently considered cost disproportionate and provide a test bed for plug and play treatment systems.

NRW has further developed the programme to clean up and restore the 700 km of failing waterbodies impacted by metal mining (Coal Authority 2020). This accommodates the above sites, but also focuses on sites where BOP and mine hazards have been considered. The BOP assessments included Parc, Coed Mawr Pool and Pandora lead mines in the Gwydir Forest on the Welsh Government Woodland Estate. Welsh Government has provided £4.5M capital funding for this financial year 2020–2021 to restore their health and habitat. These mines are centred primarily around Pont-rhyd-y-groes, Gwydir Forest, Llanrwst and Amlwch in Anglesey.

Capital funding received may be used as "match" contribution for other funding mechanisms, like Heritage or Lottery, leveraging more capital delivering well-being betterment to reverse negative socio-economic impacts. Cardiff University has been successful in a SMARTExpertise bid using NRW and Coal Authority remedial programme funds for further collaborative metal mine research, development and innovation. This will focus on Abbey Consols but extend to communications, monitoring devices, stabilisation or valorisation of sediments and precipitates.

Conclusion

The duties imposed by the WbFGA ensure that public bodies like NRW will have to adhere to their well-being objectives enshrined in their Corporate Plans and consider other associated public body interests with a view to collaborating if well-being goals are to be enhanced. The examples described here demonstrate how innovation from private sector led tourism regeneration has empowered communities to utilise former mining landscapes stimulating local economies and developing healthier outdoor lifestyle activities as its base. Furthermore, the case studies highlight opportunities for development of mine water treatment systems as part of remedial works to achieve positive ecological, environmental and economic outcomes. With regard to remedial works that incorporate metal mine water treatment systems, it is recognised that these typically as a minimum will have relatively low capital cost of £1-6M. Whilst this incentivising Act remains in it's infancy, given the setting of the sites, the scale of work with even modest capital outlay can still assist with sustainable area based community benefits, cultural heritage preservation and provide immediate term economic benefit.

Acknowledgements

The authors thank all co-organisers for organising the IMWA2020 Conference proceedings and wish them well in progressing IMWA2022 in New Zealand.

References

World Commission (1987) Report of the World Commission on Environment and Development: Our Common Future.

Powell Dobson Urbanists (2010) Llynfi Valley VARP (Valley Area Regeneration Plan) Baseline Report.

AECOM (2015) Llynfi Woodland Creation Scheme.

Coal Authority (2016) A Review of Priority Metal Mine Sites in Wales.

Elentec (2019) ETEC 17008 – Frongoch Final Project Report.

Rose SA, Matthews Z, Morgan G, Bullen C, Stanley P (2019) Sono-electrochemistry (Electrolysis with assisted Power Ultrasound) Treatment Trials of discharges from Cwm Rheidol - Ystumtuen mines, Ceredigion, Mid Wales.

Coal Authority (2020) Metal Mine Failing Waterbodies Assessment - Overview Report.

Treatability Trials to Remove Zinc from Abbey Consols Mine Water, Wales, UK

Tom Williams[1], Julia Dent[2], Thomas Eckhardt[2], Matt Riding[2], Devin Sapsford[3]

[1]*Natural Resources Wales, Swansea University, Swansea, SA2 8PP, UK, tom.williams@naturalresourceswales.gov.uk*

[2]*WSP Ltd, Willow House, Bristol, BS32 4QW, UK, julia.dent@wsp.com, thomas.eckhardt@wsp.com, matt.riding@wsp.com*

[3]*School of Engineering, Cardiff University, Cardiff, CF24 3AA, UK, sapsforddj@cardiff.ac.uk*

Abstract

Abandoned metal mines are a principal cause of European Union Water Framework Directive (WFD) standards failures in Wales, with 1,300 mines affecting over 700 km of rivers. Abbey Consols lead-zinc mine discharges ≈ 3 kg day^{-1} of zinc to the River Teifi, causing WFD failures for at least 14 km. This paper presents results of laboratory and field trials to identify an effective method to remove zinc from Abbey Consols mine water. Sodium carbonate (Na_2CO_3) dosing to raise pH and facilitate precipitation is shown to offer an efficient and cost-effective treatment solution, achieving >90% reduction in dissolved zinc concentrations.

Keywords: Metal Mine Remediation, Water Framework Directive, Field Trial, Sodium Carbonate Dosing

Introduction

The abandoned Abbey Consols mine, near Strata Florida Abbey, Mid Wales, has been identified as the primary source of zinc to the River Teifi Special Area of Conservation (SRK 1997; ExCAL 1999; Environment Agency Wales 2012). Contaminated groundwater emerges from a pipe in the northeast of the site, approximately 30 m downgradient of the buried deep adit. This flows in a channel around the former dressing floors, receiving seepages and run-off from waste tips, before discharging to the River Teifi. An extensive ground investigation was undertaken in 2019 to improve the conceptual site model, and to locate the buried adit and confirm the origin of the groundwater pipe discharge. The adit was not located but a pronounced groundwater flow in its vicinity was. A standpipe was installed, enabling the adit water to be sampled (Table 1) and collected in bulk for treatability trials.

Table 1 *Selected chemistry of Abbey Consols mine water sampled from adit standpipe.*

Total µgL^{-1}	Min	Mean	Max
Alkalinity (as $CaCO^3$)	23,700	28,667	31,500
Sulfate	28,400	34,800	40,600
pH	6.62	6.92	7.11
Zinc	14,700	16,267	17,700
Lead	594	3,688	6,790
Cadmium	36	40	45
Iron	2,210	20,293	50,700

An hydrochemical assessment (WSP 2019) found that the groundwater pipe discharge contains a combination of adit water and cleaner groundwater. Some of the adit discharge was also found to follow a groundwater pathway into the waste tips. As the adit discharge flows into and interacts with water in the waste tips, and the emerging seepages and run-off from the waste tips flow into the groundwater pipe channel, it is not possible to accurately apportion the metal load from the site between these two main sources. To achieve the WFD zinc (dissolved bioavailable) standard of 13.4 µgL-1 in the River Teifi, zinc load from the site as a whole would need to be reduced by at least 70%. The remediation works being designed by WSP aim to achieve this by separation of the adit water from the waste tips and transfer to a mine water treatment system. The waste tips will be hydraulically isolated through capping

and drainage. This paper presents results from laboratory and field trials to develop the mine water treatment solution.

Laboratory trials: iron dosing with limestone pre-treatment

A treatment options appraisal (WSP 2018) concluded that removal of zinc from the mine water via co precipitation and sorption during iron precipitation may be a suitable solution. In the absence of elevated dissolved iron concentrations in the mine water, chemical dosing would be required. To assess the feasibility of iron dosing, establish optimum removal rates and to refine the likely concentrations required, laboratory trials were undertaken in May 2019. A limestone pre-treatment step was included due to concerns of lowering pH associated with iron dosing. The aim was to identify the optimum contact time between mine water and limestone gravel that resulted in the largest increase in pH and alkalinity. Limestone gravel of 10-14 mm from B&Q DIY store was washed with deionised water to remove fines that could artificially skew the pH. Four 12 L buckets were filled with the gravel and 680 mL of mine water was added to each. The buckets were placed on an orbital shaker for 2, 5, 15 or 45 min and water was carefully discharged for analysis at each interval. The 45 min exposure resulted in an increase in pH from 6.85 to 8.33 and in alkalinity from 23 mgL^{-1} to 374 mgL^{-1} (Table 2). There was also a concurrent reduction in dissolved zinc concentrations of up to 94%. Hydrochemical modelling indicated the formation of a zinc carbonate to be the likely precipitation process.

Following the limestone pre-treatment tests the mine water was discharged from the buckets into beakers for the iron dosing tests. The aim was to establish the affect on zinc removal of dosing with different concentrations of iron (II) (ferrous) sulfate and iron (III) (ferric) sulfate hydrate. At the time of testing the zinc removal results of the limestone pre-treatment tests were unknown, therefore the dosing tests generally produced unrepresentative results as much of the zinc had already precipitated. It is not known how much the test results were affected by iron precipitation; enabling removal of zinc but potentially also enabling zinc carbonates to re-dissolve with the lowering of pH. These first laboratory trials offered a new opportunity for simplifying the mine water treatment solution relative to the original iron dosing and precipitation approach. It was decided further testing should focus on removal of zinc as a zinc carbonate.

Laboratory trials: carbonate sources and multiple contact cycles

A second set of laboratory trials were undertaken in August 2019 to test a range of limestone sources, repeat contact of mine water with the limestone and dosing with carbonate-containing reagents as a substitute for limestone. Chalk (20 mm grain size) and two different types of limestone gravel with grain sizes of 16-32 mm (Abergele) and 20 mm (Penderyn) were tested. The chalk and limestone gravels were pre-washed with tap water in a sieve for 5 min, then rinsed with deionised water to remove fines that could misrepresent the long-term behaviour of the limestone and lead to only temporary effects on pH and alkalinity or produce suspended solids which did not arise from the reaction with mine water. A total volume of 0.0048 m3 of the chalk and two limestone gravels were each placed in 12 L buckets with a 10 mm hole drilled in the bottom and a bung in place. Mine water (750 mL) was added and left undisturbed for either 15 min, 45 min or 2 h. After each exposure period the water was rapidly drained from the bucket into a

Table 2 *Results of different exposure times of mine water to B&Q limestone gravel.*

Contact time	Zinc diss. (μgL^{-1})	Zinc diss. (% removal)	pH	Alkalinity, Tot. as $CaCO_3$ (mgL^{-1})
Raw mine water	15,900	-	6.85	22.8
2 min	9,590	40	6.94	65.0
5 min	6,530	59	7.36	262
15 min	2,940	82	7.77	120
45 min	922	94	8.33	374

Table 3 *Selected results following 45 min and 2 h exposure of mine water to different gravel sources, followed by a 2 h settling time and glass microfiber filtration.*

Treatment	Zinc diss. (μgL^{-1})	Zinc diss. (% removal)	pH	Alkalinity, Tot. as $CaCO_3$ (mgL^{-1})	Weight of precipitate (g)
Raw mine water	16,100	-	6.92	32.9	-
Chalk 45 min	5,520	66	7.86	42.5	0.7448
Chalk 2 h	1,080	93	8.10	50.0	0.7366
Abergele 45 min	9,240	43	7.58	35.0	0.1397
Abergele 2 h	4,280	73	7.77	42.4	0.1052
Penderyn 45 min	9,670	40	7.68	46.5	0.1019
Penderyn 2 h	3,810	76	7.85	50.0	0.1238

glass beaker to ensure all suspended solids, as far as possible, were decanted. To measure settlement rates samples of the decanted solution were gathered 1 cm from the surface 15 min, 45 min and 2 h following decanting. Once the contact and settlement time had lapsed the liquid was drained through a glass microfiber filter and dried overnight to determine the quantity of precipitate. Samples of the filtered water were collected for laboratory analysis (Table 3).

The 2 h exposure to chalk resulted in the largest reduction in zinc concentrations relative to the Abergele and Penderyn gravels, as well as the largest quantity of precipitate. Penderyn gravel resulted in equal alkalinity to chalk over the 2 h exposure period, but a lower pH and more limited zinc precipitation. The B&Q gravel used in the May 2019 laboratory tests resulted in greater alkalinity and zinc removal than any of the three gravel sources used here. Overall, high zinc removal rates (>90%) seem to be achievable within a pH range of 8-8.5, but the mass of precipitate formed may be a concern for a full-size system due to disposal costs.

Chalk gravel was selected to test whether zinc removal efficacy is maintained following multiple cycles of contact between mine water and gravel. Fresh chalk was washed with deionised water to remove fines and was placed into a 12 L bucket with a 10 mm hole drilled in the bottom and a bung in place. Mine water (750 mL) was added and left undisturbed for 45 min, after which the water was drained. The process was repeated a total of ten times with fresh mine water on each occasion. Following the first, third, fifth, seventh and tenth exposures precipitate was measured using glass microfiber filters and the filtered liquid was sent for laboratory analysis (Table 4). The repeat exposure of the chalk to fresh mine water resulted in a steady decline in zinc removal rate from 84% to 61%. pH declined from 8.08 to 7.77 and the quantity of precipitate declined from 0.500g to 0.295g. This suggests that the efficacy of limestone gravel treatment may diminish over time, however, the test would need to be carried out for longer to establish if the removal rates stabilise or continue to reduce.

The final laboratory tests investigated the efficacy of sodium carbonate (Na_2CO_3) dosing at different concentrations on the precipitation of zinc and the associated affect on pH. Mine water (1 L) was placed in beakers on a magnetic stirrer and a stock solution of 2.586 g Na_2CO_3 in 1 L of deionised water was made. The Na_2CO_3 solution was then added to the beakers of mine water at zinc: Na2CO3

Table 4 *Selected results following repeat contact cycles between chalk gravel and mine water.*

Treatment	Zinc diss. (μgL^{-1})	Zinc diss. (% removal)	pH	Alkalinity, Tot. as $CaCO_3$ (mgL^{-1})	Weight of precipitate (g)
Raw mine water	16,100	-	6.92	32.9	-
Cycle 1	2,510	84	8.08	43.5	0.4997
Cycle 3	3,620	78	7.93	40.1	0.3872
Cycle 5	4,450	72	7.97	50.0	0.3696
Cycle 7	4,860	70	7.88	45.0	0.3228
Cycle 10	6,350	61	7.77	43.1	0.2953

Table 5 Selected results following dosing of mine water with Na2CO3 and 2 h standing time.

Treatment zinc:Na_2CO_3 ratio	Zinc diss. (μgL^{-1})	Zinc diss. (% removal)	pH	Alkalinity, Tot. as CaCO3 (mgL^{-1})	Weight of precipitate (g)
Raw mine water	16,100	-	6.92	22.8	-
Na_2CO_3 1:1	6,920	57	7.75	38.5	0.0100
Na_2CO_3 1:2	960	94	8.43	55.0	0.0202
Na_2CO_3 1:2.5	123	99	9.27	63.8	0.0225

ratios of 1:1 (10 mL), 1:2 (20 mL) and 1:2.5 (25 mL). Following reagent addition samples were taken for laboratory analysis. The turbidity of the water and the rate at which settlement of suspended solids occurred was then recorded by visual observations and a photographic record over 2 h. Once the 2 h had lapsed samples were filtered using glass microfiber filters to quantify the amount of precipitate formed, and the liquid was subject to laboratory analysis (Table 5). Standing time during the experiment appeared to have minor beneficial influence on the results and only those following the 2 h period are presented.

Sodium carbonate dosing at a ratio of 1:1 and 2 h standing time resulted in an increase in pH to 7.75 and a reduction in dissolved zinc of 57%. This improved with increased Na_2CO_3 dosing rates to a maximum of 99% at a 1:2.5 ratio, although the resulting pH of 9.27 was greater than the target maximum of pH 9. No visible turbidity was apparent in the water following Na_2CO_3 dosing and the precipitate mass was very low.

The laboratory trials indicated that raising the mine water pH to 8-8.5 via provision of a soluble carbonate source and subsequent precipitation of zinc as a carbonate could be an effective treatment solution. The use of limestone gravel may be a higher risk option due to decreased efficacy over time and the amount of precipitate generated. Dosing of mine water with Na2CO3 may offer a highly efficient, relatively cheap and non-hazardous treatment solution. A non-hazardous reagent is particularly important for a remote and environmentally sensitive setting as Abbey Consols. The treated water has a reduced zinc concentration and its water type is similar to local surface water, lessening any potential effect from the discharge. Treatment volumes in the laboratory were too low to measure settlement behaviour of the zinc carbonate and there was a risk that precipitate could remain suspended in the treatment effluent. It was decided these factors should be assessed through short-term field trials before finalising the design of a large-scale demonstration system.

Field trials: sodium carbonate dosing

A small-scale field trial was designed to test Na_2CO_3 dosing with a continuous higher volume flow of mine water and investigate the settlement rate and characteristics of the precipitate formed. The aim was to generate 1 kg of precipitate, requiring an estimated 40 m^3 of mine water to be processed. The dosing requirements targeted a pH that would provide a maximum zinc removal rate but remained <pH 9 to allow discharge to the environment. The laboratory trials suggested that a dosing ratio of 1:2 (zinc: Na_2CO_3) would provide a pH of ≈ 8.4 and remove ≈ 94% of zinc. The trial commenced on 16th March 2020 but had to be suspended on 24th March due to the implementation of coronavirus restrictions. The trial relied on a simple, temporary facility (Figure 1). Mine water was pumped from the adit standpipe to two intermediate bulk containers (IBCs) to provide the mine water feed. A dosing tank was filled with a 2.6 gL^{-1} solution of Na_2CO_3 made on site by weighing out powdered Na_2CO_3 and mixing with deionised water. The dosing tank and the mine water IBCs were connected to a mixing tank and the flows from each controlled by taps. The mixing tank released the dosed mine water via several outfalls to promote laminar flow into the settling pond (6.6 m × 1.3 m). Treated mine water flowed through the settling pond before draining via an outflow at the far end. The typical volume held in the settling pond during operation was 2.36 m^3 and the typical inflow rate was 0.18 Ls^{-1}, providing a retention time just under 4 hours. The dose of the Na_2CO_3 solution was

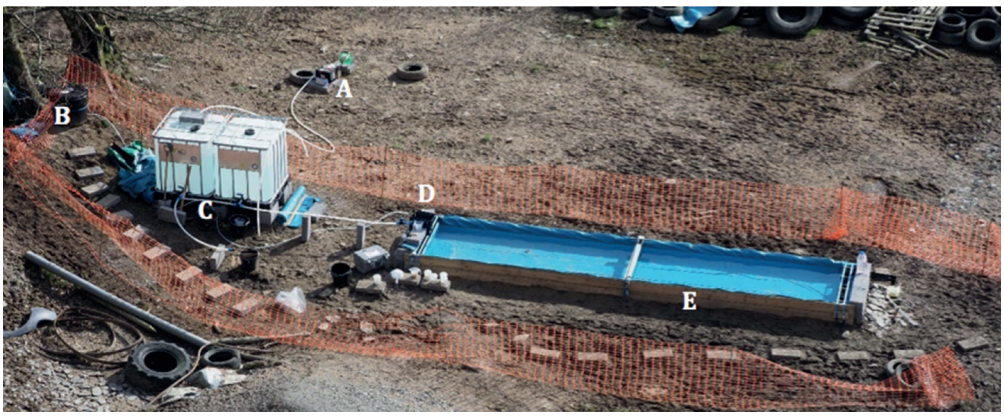

Figure 1 *Arrangement of field trial at Abbey Consols. Adit standpipe (A), dosing solution tank (B), mine water IBCs (C), mixing tank (D) and settling pond (E).*

varied with the tap to maintain the target pH of 8.4 in the settling pond.

Total operation time was 31 h 17 min, treating 19,813 L of mine water with 427 L of Na_2CO_3 dosing solution. The dose equates to between 80 and 100 L day-1, and the ratio of zinc:Na_2CO_3 was on average 1:2.2, but at times reached as high as 1:3.1. Flow measurements were taken from the inflow, dosing tap and outflow using a stopwatch and measuring jug. Water samples were taken from the mine water inflow and the treatment outflow twice per day (Table 6). The zinc removal rate per sample set (one inflow and one outflow taken at the same time) are also presented.

The average mine water inflow pH measured in the field was 7.8, slightly higher than laboratory analyses and also previous field measurements of pH from the adit standpipe (Table 1). The average pH achieved in the settling pond (8.3) was slightly lower than targeted (8.4). This is attributed to the sensitivity of dosing control with the tap installation, including optimisation required following dilution by rainfall. At full-scale the dose control will be finer, managed via an automated system triggered by the settling pond pH. Dissolved zinc removal ranged from 58-91% and total zinc removal ranged from 27-61%, the highest removal rates both coinciding with the highest pH of 9.69. The difference between dissolved and total zinc removal efficiency indicates the settling pond retention time was too short, with precipitate being lost in the outflow. It is also suspected that wind turbulence may have affected how well the precipitate settled.

Three settling pond samples were taken to investigate if standing time affected zinc removal or precipitation overnight (Table 6). On 19th March the settling pond sample showed a much higher dissolved zinc removal rate than total zinc as it was taken following a day of treatment (i.e. no additional settling time). The settling pond samples taken on 20th and 24th March were at the beginning of the day before the treatment system was restarted, indicating the potential removal rate following over 12 h of additional settling time. Although the dissolved zinc removal rates were similar to the operating conditions, the total zinc removal rates were much higher, essentially matching those of dissolved metals, and for the 24th March reached over 80%. The change in removal rates following a longer retention time within the settling pond indicates that the precipitate settling rate is longer than the 3-4 h of the trial. A white precipitate began to form in the settling pond within 1 m of the inflow by the second day of operation and a sample was collected on 23rd March in anticipation of the trial being suspended the following day. The precipitate was allowed to settle in measuring jugs before being filtered with a sieve and paper towel. It was then sealed in a container for transport to the laboratory.

*Table 6 Zinc removal rates between inflow and outflow for individual samples. *settling pond sample.*

Sample date/time	Mine water flow (Ls^{-1})	Zinc:Na_2CO_3 ratio	Mine water inflow field pH	Settling pond field pH	Zinc diss. (% removal)	Zinc tot. (% removal)
17/03/2020 12:00	0.167	1:3.1	7.77	8.10	62	32
17/03/2020 16:00	0.167	1:3.1	7.88	8.10	63	27
18/03/2020 11:00	0.163	1:2.1	7.57	9.69	91	61
18/03/2020 15:55	0.163	1:2.1	7.90	8.12	79	35
19/03/2020 11:00	0.181	1:2.2	7.80	8.60	83	42
19/03/2020 14:50	0.181	1:2.2	7.90	8.10	58	31
19/03/2020 16:20*	-	-	-	8.30	68	20
20/03/2020 10:00*	-	-	-	7.90	69	65
20/03/2020 11:20	0.165	1:1.4	7.83	8.50	75	49
23/03/2020 16:13	0.206	1:2.1	7.77	8.53	86	36
24/03/2020 10:00*	-	-	-	8.16	81	82
24/03/2020 10:00	0.190	1:1.8	7.90	8.46	87	54

The wet weight of the sample measured on site was between 800-900 g and moisture content of the precipitate was 95%. The zinc concentration was 46%, however, the total inorganic carbon was only 1.2%, much lower than expected if a pure zinc carbonate was forming. The ratios of zinc to carbon suggest it's more likely to be hydrozincite ($Zn_5(CO_3)_2(OH)_6$), although potentially with some additional metal precipitate. Hydrozincite is less dense than smithsonite and potentially more easily resuspended, which will therefore benefit from optimisation of the settling time.

Conclusions

Treatability trials identified that dosing with Na2CO3 as a carbonate source and raising pH to ≈ 8.5 can successfully remove >80% of dissolved zinc from Abbey Consols mine water in the field. Over 90% zinc removal was also shown to be achievable, but with a corresponding pH considered too high for discharge to the environment. During the field trial total zinc removal was lower during operation than following overnight standing time in the settling pond, indicating a larger surface area of the pond and protection from turbulence caused by wind are required to settle the precipitate more efficiently for the flow rate treated. The large-scale demonstrator system will target pH 8.5-9 and is being designed to allow comprehensive testing of precipitation and settlement behaviour and to explore the precipitation of hydrozincite versus smithsonite. Mechanisms to reduce the water content of the precipitate will also need to be considered in the design to reduce disposal costs. Although the flow rate from the buried adit is currently unconfirmed, it is considered the mine water treatment, in combination with the mine waste capping works, can achieve the >70% reduction in zinc load required to achieve WFD targets.

Acknowledgements

The Abbey Consols Remediation Project is funded by Welsh Government.

References

Environment Agency Wales (2012) WFD Abandoned Mines Project: Afon Teifi catchment.

ExCAL Ltd. (1999) Metal Mine study: Abbey Consols, Grogwynion and Castell.

SRK (1997) Metal Mines Amelioration Study: Pre-Feasibility Study for the Amelioration of Polluted Drainage Waters from 14 Former Metal Mines in Mid-Wales.

WSP Ltd. (2018) Abbey Consols Treatment Options Appraisal Technical Note.

WSP Ltd. (2019) Detailed Hydrochemical Assessment Technical Note. Appendix E in: Abbey Consols Remediation Study: Ground Investigation Interpretative Report.

Climate Change Adaptation in BHP's Queensland Mine Water Planning and Hydrologic Designs

Weixi Zhan[1], Rory Nathan[2], Sarah Buckley[1], Alan Hocking[1]

[1]*BHP, 480 Queen St, Brisbane, Australia, james.zhan@bhp.com*

[2]*Infrastructre Engineering, University of Melbourne, Victoria, Australia*

Abstract

Little attention has been given to the consideration of climate change in hydrologic designs in the resource industry. As a leading resource company, BHP has a corporate strategy to build water resilience to climate change for long-term business success. This paper describes a set of practical procedures developed for BHP in Queensland that provides guidance to practitioners on how to incorporate climate projections into key hydrologic applications. The developed approaches also provide general guidance on climate data selection, processing and how to incorporate the effects of climate variabilities in hydrologic designs, water management and decision-making.

Keywords: Climate Change Adaptation, Hydrology, Mine Water Management

Introduction

Despite the large body of research that has been undertaken on climate change and its impacts on global and regional water resources and hydrology (Arnell et at. 2011; Gosling et al. 2011), little attention has been given to the practical issues involved in incorporating climate change effects in hydrologic designs and water management.

As a leading resource company, BHP has a corporate strategy based on long-life assets. Building resilience to the physical effects of climate change is essential to long-term business success. The availability of water is regarded as both an asset and a risk to the long-term operations of BHP Queensland. Stretching far beyond the operational phase, hydrology is also a fundamental design input to the closure of BHP's mines. It is thus crucially important to have robust mine water management plans and hydrologic designs that can accommodate the deep uncertainty associated with changes to future climate. The development of procedures that account for a non-stationary climate will facilitate long-term water-related risk assessment and resilient decision making.

Many approaches to selecting climate projection downscaling techniques and data processing methods for hydrologic applications have been described in the literature (Fowler et al. 2007; Maraun et al. 2010) and this presents practitioners with a somewhat bewildering array of options when faced with quantifying the impacts of climate change. The array of choices is partially due to the high uncertainty and variability in climate projections and the ever-evolving nature of climate science investigations.

The procedures described here were developed to provide practitioners with guidance on how best to incorporate future climate projections, including data and downscaling method selection and data processing, into water management and hydrologic applications. While the target audience for these procedures are primarily those undertaking investigations and designs for BHP, the guidelines are of generic relevance to many similar design contexts and hydrologic applications.

Key Hydrologic Applications and Variables

The guidelines are developed to suit the following key hydrologic designs and mine water planning activities:

- Long-term water inventory forecast and balance modelling
- Flood risk assessment for long service life water infrastructure and hydrologic /

hydraulic designs (e.g. diversions, dams, levees, major drainage and floodways)
- Water demand and supply reliability

The key climatic variables relevant to these applications include average annual and seasonal surface temperature, design rainfall intensities, daily rainfall sequences, and average seasonal potential evaporation rates.

Overall Approach

There are four high level steps involved in climate change adaptation in hydrologic assessment:

- *Step 1: Set the effective service life or planning horizon*. Different planning horizons will apply to different assets depending on their expected operational life and legacy arrangements, but if less than 20 years from the baseline then no climate impact assessment is required.
- *Step 2: Review the design standards and criteria relevant to the activity*. For flood overtopping risks the criteria may vary typically between 18% annual exceedance probability (AEP) and 0.1% AEP, whereas water supply and containment criteria typically range between 10% and 1% AEP. Probable Maximum Precipitation (PMP) requires no climate change adjustment as recommended by Australian Rainfall and Runoff (AR&R) (Ball et al. 2019).
- *Step 3: Obtain climate change projections*. There is a considerable body of processed information available on climate change projections that is readily accessible to practitioners. Australia-wide projections are available from CSIRO and Bureau of Meteorology (2020), though region-specific projections are also available. In Queensland, the best source of information is the Queensland Future Climate Dashboard and the Climate Change Scenarios for Biophysical modelling (both accessible from https://longpaddock.qld.gov.au/). The latter is also applicable to the whole Australia.
- *Step 4: Adapt climate projections and undertake hydrologic assessment in planning and design*. Information on projected climate change scenarios are incorporated into the same hydrological modelling tools used for assessing risks under current conditions.

Selection of Climate Projection Parameters, Data and Processing for Key Hydrologic Applications

A flow chart in **Figure 1** demonstrates the steps for climate data selection and processing for hydrologic assessment.

For event-based designs (e.g. flood risk assessment), BHP have adopted the guidance

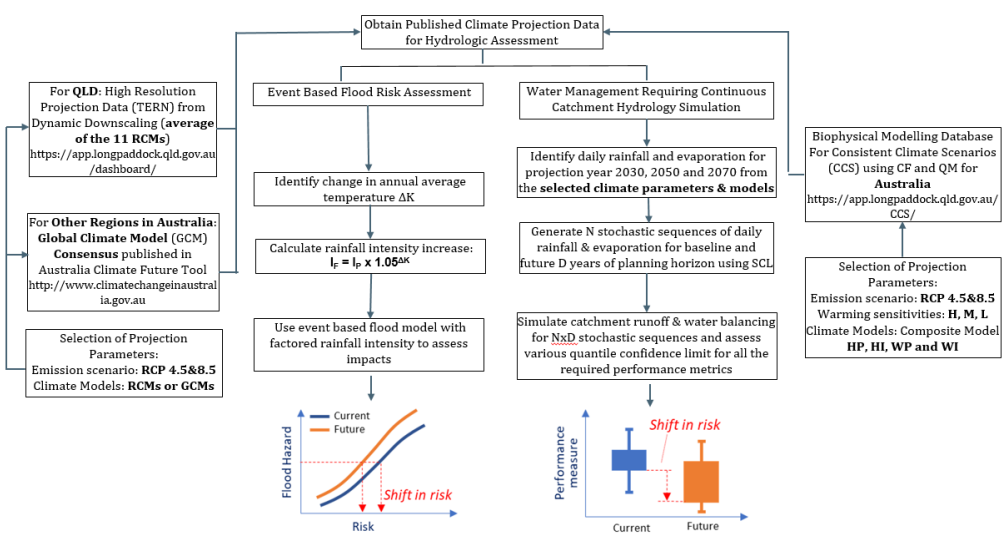

Figure 1 Overview of steps for climate data selection and key hydrological assessments.

provided in AR&R (Ball et al. 2019). The basis of this approach is to increase rainfall intensities by a factor related to the increase in annual mean surface temperature. For Queensland, high resolution (10 km) temperature projections using dynamic downscaling method are adopted; while for wider regions of Australia, the GCMs' consensus method recommended in AR&R can be used. This approach provides conservatively high estimates in that the influence of drying soils and other factors are not considered (Wasko and Nathan 2019), but as yet there are no established procedures for dealing with these other issues.

The approach developed to assess impacts on catchment hydrology and water management is more involved as it is desirable to differentiate between the impacts of climate change and those of natural variability, an important differentiation as it relates to the vulnerability to water availability under change. The key concept involved is to characterise system performance relative to the range of behaviour encountered under current climatic conditions, where the degree to which climate change causes the behaviour of a system to shift outside this baseline range provides an indication of the projected shift in risks due to climate change (Nathan et al. 2019). This concept is illustrated in the lower right panel of **Figure 1**, where the range in performance of the system under current climatic conditions (e.g. volume of water held in storage, or the likelihood that a dam is overtopped) is represented by the blue-coloured box and whisker plot. Under climate change, the range in system performance is altered, as represented by the orange-coloured box and whisker plot. The shift in risk can be assessed for typical (i.e. median) operating measures, or else any performance metric (e.g. 95%ile or 5%ile wet or dry resilience) that is of most relevance.

The assessment of the change in system performance due to climate change can be undertaken using a single climatic sequence obtained from historical records. For example, a baseline period of 1960–2018 is considered representative of current climate, and this provides a 59-year simulation period with which to assess baseline performance. The approaches to assessing climate change is referred to as the "Change Factor" (CF) (or "delta scaling") and Quantile Matching (QM). With CF method, the monthly mean values are shifted by the projected change in for the adopted climate scenario of interest (e.g. a Representative Concentration Pathway Scenario of 8.5 represents a future in which there are little curbing of emissions), at a future year that is relevant to the planning horizon of interest (e.g. 2100). For example, if a monthly mean rainfall is projected to decrease by 10%, then the rainfall of the corresponding month of the 59-year observational record is also reduced by 10%. With QM method, the shape of the probability distributions of future data is altered to provide wider climate variability (Ricketts et al. 2013). The simulation models of catchment runoff and water management are run for these adjusted time series, and the change in performance reported.

However, there is a drawback in the CF/QM approaches. A single sequence altered from historical climate is often insufficient to capture the climatic variability and assess the possible range of system behaviours, especially in those systems with storage volumes that are larger than expected annual inflows. Accordingly, one robust approach to assessing system performance is through the use of stochastic simulation techniques, where a range of suitable techniques are described by McMahon and Adeloye (2005). Practical tools for undertaking this analysis are provided by Srikanthan et al. (2007), and their application to mine water management studies is discussed by Nathan and McMahon (2016).

Guidance on Selecting Climate Projection Parameters, Models and Databases

Detailed descriptions of the selected climate projection parameters, databases and stochastic data processing methods adopted in the Guideline as shown in **Figure 1** are available in Supplementary Materials.

Results & Work Example

The direct outputs included in the Guideline are organised as a "one-stop-shop" for both internal (BHP) and external hydrologists / practitioners to extract the selected projection

data for the target year(s) and location(s) of interest, and use the recommended procedures to process the data for the key hydrologic designs and applications. Due to the large volume of the selected databases, the direct outputs are not included here but summarised in Supplement Materials. They can be accessible for external readers and practitioners with the consent of BHP.

The following worked example demonstrates how to undertake continuous water balance modelling (WBM) and catchment simulations as indicated in Figure 1.

Both mine affected water (MAW) stored on site (e.g. pit storages and dams) and fresh water are crucial sources for production. Understanding future water inventories, shortfalls and demands as well as climate impact on them is critical for infrastructure planning and business decision making. Continuous WBM and catchment simulation with daily time step are adopted in inventory and demand forecast. Key elements included in WBM are the estimation of: 1) direct rainfall and catchment runoff into open pit water storages and dams; 2) evaporation from open water bodies and contributing catchments; 3) MAW and fresh water demands for production and dust suppression (not climate dependent); 4) Controlled MAW releases to downstream receiving creeks.

The Australia Water Balance Model (AWBM; Boughton 2004) was used to relate daily rainfall and evaporation to soil moisture and runoff. Selection of AWBM parameters (e.g. storage capacity, BFI, channel coefficient) is location and catchment specific. Generated stochastic daily rainfalls (single or multiple sites) and repeating pattern of monthly pan evaporation shown in Figure 1 are key inputs for AWBM simulations for calculating inventory, demand and shortfall volumes. The stochastic rainfall and runoff time series are also used in AWBM to produce synthetic river flow conditions which is a key controlling factor for MAW releases.

Step 1: Select SILO data (baseline: 1960–2018) & planning horizon (2020-2039), and recommended model (e.g. 8.5_H_HP_2030_Site) for projected rainfalls and evaporation;

Step 2: Generate stochastic rainfall sequences (500 realisations of 20-year sequences) for SILO and Projected data following the process in **Figure 1** (Detailed in Figure S2, *Supplementary Material*);

Step 3: Generate monthly evaporation patterns as per the process in **Figure 1** (Detailed in Figure S2, *Supplementary Material*);

Step 4: Run the WBM with the 500 realisations (both SILO and Projections) and analyse the impact of climate change on inventory, shortfall and freshwater demand forecasts between "BAU" (baseline) and "BAU+CC" (future climate). Example results are demonstrated in **Figure 2**, **Figure 3** and **Table 1**.

This worked example demonstrates that the cumulative effects from a slight decrease (40-60mm at various quantile levels in **Figure 2**) in annual rainfall and evaporation increase (**Table 1**) can propagate through catchment runoff simulations and may be magnified during back-to-back dry and wet year sequences contained in the stochastic

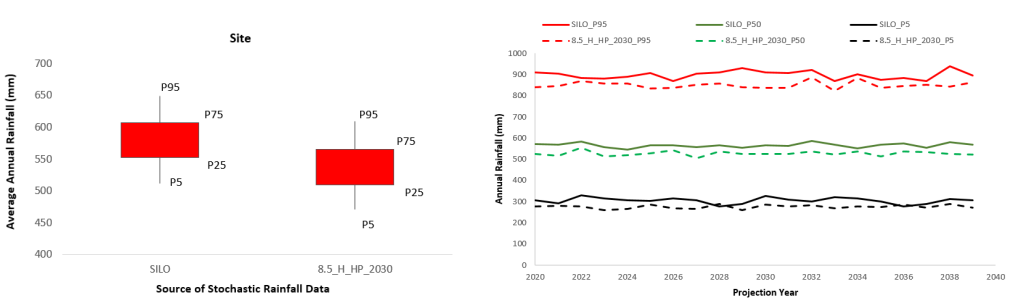

Figure 2 *Comparison of Stochastic Rainfalls SILO vs. Future Projection (A) Quantile distribution of 20-year Average Annual Rainfall; (B) Annual Rainfall Quantile Envelopes (P95, P50, P5) from 2020 to 2039.*

Table 1 Pan Evaporation Change Factor (%) for the "Site".

Jan	Feb	Mar	Apr	May	June	July	Aug	Sep	Oct	Nov	Dec
5.63	5.58	5.79	4.61	4.61	5.06	3.53	3.90	4.20	4.82	4.25	4.35

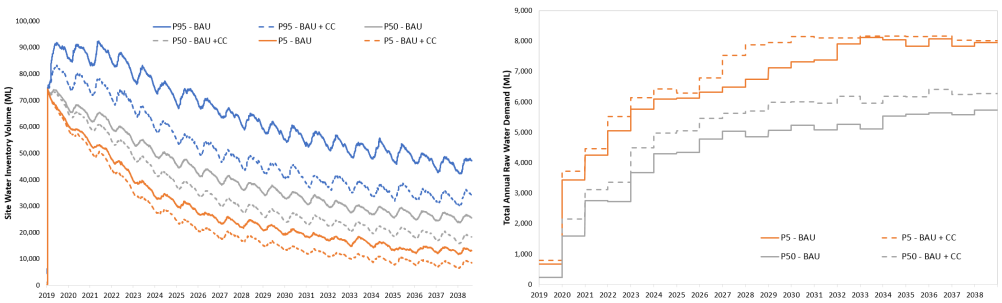

A *B*

Figure 3 Impact of Climate Change on (A) Site Water Inventory Forecast; (B) Fresh Water Demand Forecast (BAU: Simulation with SILO baseline data; BAU+CC: Simulation with Projected Climate Data).

simulations. This could subsequently have substantial effects on water inventory and fresh water demand forecast, and drive change of management and business decisions. For instance, the confidence limit on wet condition (P95 **Figure 3A**) is used for site water storage capacity evaluation and planning purposes, while those representing median and dry conditions (P50 and P5 in **Figure 3B**) are normally adopted for water demand planning and evaluation of water supply reliability.

Conclusions

The developed guideline meet the following key requirements: 1) *Simplicity*: The outcomes produced from the processes are easy to follow and are well suited to facilitate decision making; 2) *Practicality*: the procedures are straightforward for practitioners to follow and replicate; 3) *One-stop data sources*: the procedures take advantage of readily accessible information on baseline and projection data for the key climatic variables; 4) *Consistency and comparability*: The adopted data and means of data processing are consistent for similar types of hydrologic applications (e.g. event-based flood estimate, continuous water balance modelling) and allow comparison between the findings derived from projected climate data and the existing knowledge from the baseline studies.

The guidelines were developed to serve as an internal guidance and criteria for factoring climate projections into BHP's Queensland sites. However, given the generic nature of the guideline, the same or similar databases and approaches (as shown in Figure 1) can be applied to broader hydrologic designs in other regions across Australia.

Acknowledgements

The authors thank BHP, particularly the Water Planning Team at BHP Coal for their financial and managerial support. Special thanks to Jordan Biggs for data collection and processing.

References

Arnell NW, Gosling SN (2013) The impacts of climate change on river flow regimes at the global scale. J Hydrol 486:351–364

Ball J, Babister M, Nathan R, Weeks W, Weinmann E, Retallick M, Testoni I, (Editors), 2019, Australian Rainfall and Runoff: A Guide to Flood Estimation, Commonwealth of Australia. http://arr.ga.gov.au/

Boughton, Walter (2004) The Australian Water Balance Model. The Environmental Modelling & Software, Vol 19, Issue 10: 943-956.

CSIRO and Bureau of Meteorology (2015): Climate Change in Australia Information for Australia's Natural Resource Management Regions: Technical Report, CSIRO and Bureau of Meteorology, Australia. Projection data accessible from http://www.climatechangeinaustralia.gov.au/

Fowler HJ, Blenkinsop S, Tebaldi C (2007) Linking climate change modelling to impacts studies: recent advances in downscaling techniques for hydrological modelling. Int J Clim 27:1547–1578.

Frost AJ, Charles SP, Timbal B, Chiew FH, Mehrotra R, Nguyen KC, Chandler RE, McGregor JL, Fu G, Kirono DG, Fernandez E, Kent DM (2011) A comparison of multi-site daily rainfall downscaling techniques under Australian conditions. J Hydrol 408:1–18.

Gosling SN, Taylor RG, Arnell NW, Todd MC (2011) A comparative analysis of projected impacts of climate change on river runoff from global and catchment-scale hydrological models. Hydrol Earth Syst Sci 15(1): 279–294.

Jeffrey, SJ, Carter, JO, Moodie, KB & Beswick, AR (2001). Using spatial interpolation to construct a comprehensive archive of Australian climate data, Environmental Modelling and Software, vol. 16, no. 4, pp. 309-330.

Kokic Philip, Jin Huidong, Crimp Steven (2013) Improved point scale climate projections using a block bootstrap simulation and quantile matching method. Clim Dyn 41: 853-866.

Maraun, D., Wetterhall, F., Chandler, R.E., Kendon, E.J., Widmann, M., Brienen, S., Rust, H.W., Sauter, T., Themeßl, M., Venema, V.K.C., Chun, K.P., Goodess, C.M., Jones, R.G., Onof, C., Vrac, M., Thiele-Eich, I., 2010. Precipitation downscaling under climate change: Recent developments to bridge the gap between dynamical models and the end user. Rev. Geophys. 48, 1–38.

McMahon, T. A., and A. J. Adeloye (2005) *Water Resources Yield*, 220 pp. CO: Water Resources Publications.

Nathan, R. J., & McMahon, T. A. (2017). Recommended practice for hydrologic investigations and reporting. *Australian Journal of Water Resources*, 21(1), 3–19.

Nathan, R. J., McMahon, T. A., Peel, M., & Horne, A. (2019) Assessing the degree of hydrologic stress due to climate change. Climatic Change, 156(1–2), 87–104.

Ricketts J.H, Kokic Philip, Carter J.O (2013) Consistent climate scenarios: projecting representative future daily climate from global climate models based on historical climate data.

Srikanthan, R, F. Chiew, and A. Frost. (2007) *Stochastic Climate Library*. Catchment Modelling Toolkit. eWater CRC.

The State of Queensland Department of Science, Information Technology and Innovation (2015) Consistent Climate Scenarios User Guide Version 2.2, 2015.

Van Vuuren Detlef P, Edmonds Jae, Kainuma Mikiko, Riahi Keywan, Thomson Allison, Hibbard Kathy, Hurtt George C, Kram Tom, Krev Volker, Lamarque Jean-Francois, Masui Toshihiko, Meinshausen Malte, Nakicenovic Nebojsa, Smith Steven J, Rose Steven K (2011) The representative concentration pathways: an overview. Climatic Change 109 5-31.

Wasko, C., & Nathan, R. (2019) Influence of changes in rainfall and soil moisture on trends in flooding. *Journal of Hydrology*, 575(November 2018), 432–441.

Watterson, IG (2012) Understanding and partitioning future climates for Australian regions from CMIP3 using ocean warming indices, Climatic Change, vol. 111, no. 3, pp. 903-922.

Supplementary Materials

Selection of Climate Projection Parameters, Databases and Data Processing for Key Hydrologic Applications: As part of the guideline development and referenced in Figure 1, this document provides detailed descriptions of the selected climate projection parameters, databases and data processing methods adopted.

Please contact *james.zhan@bhp.com* for acquiring this document.

Cultural Aspects Constraining Mine Water Supply Chain Management in ASAL Areas of Kitui County, Kenya

Nyile Erastus Kiswili[1,2], Joash Kirwah Kibet[2]

[1]*Taita Taveta University, P.O Box 635-80300, Voi, Kenya, nyileras@ttu.ac.ke*

[2]*Jomo Kenyatta University of Agriculture and Technology, P.O Box 62000-00200, Nairobi, Kenya*

Abstract

Kitui County receives low levels of rainfall annually thus considered as Arid and Semi-Arid (ASAL) area. The community has formed many cultural imaginations about water ensuing from scarcity and insufficiency of the commodity in the area. This study sought to establish how community livelihood, beliefs, norms and customs, poverty, rituals and gender involvement constrained mine water supply chain management. The findings showed that there is difficulty in accessing water and the quantity and quality available do not match community domestic needs. Consensus building and factoring in of cultural aspects is key in ensuring success of mining and extraction activities.

Keywords: cultural aspects, mine water, ASAL, water supply chain management

Introduction

Kitui County topography is generally low-lying and it falls in the semi-arid climatic zone. It receives an average rainfall of 900 ml a year. Water as a resource is scarce in the area, and like any other ASAL area, challenges faced affect the performance of the community. The county, which is home to Kamba community, is faced with recurrent drought periods during the dry seasons in the country. During these periods, there is many reported human and animal deaths due to starvation and lack of water, diseases, malnutrition and dehydration (Shelmith 2013). Countywide estimates indicate that 42% of Kitui County's population has access to at least a basic water service (Nyaga 2019). Kitui County has been recently discovered to host several minerals, thus the need for water as a resource to be conserved and managed to promote extraction activities. Mining requires water for the extraction of minerals that may be in the form of solids, liquids or gases.

The demand for adequate water supply in Kitui County is growing daily as the availability and supply of this important commodity becomes very scarce. Population growth and climate change adds pressure to an already stressed watershed in the county. The resulting conflict arising from the shortage of water for both domestic use and industrial use is what is facing most of the regions located in the ASAL areas (Mwaguni, Ruwa, Odhiambo-Ochiewo & Osore 2016). Fernando, Ilankoon, Syed and Yellishetty (2018) argue that mining uses water primarily for mineral processing, dust suppression, slurry transport and employees' needs. In most mining operations, water is sought from groundwater, streams, rivers and lakes, or through commercial water service suppliers. However, often, mine sites are located in areas where water is already scarce and, understandably, local communities and authorities often oppose mines using water from these sources (Abuya 2016). It is no different in Kitui County. Water resource management is an integral part of mining. Despite successful efforts to manage water usage more efficiently, increasingly tougher environmental rules are hiking miners' costs and risks, particularly to those operating in arid regions or close to populated communities (Van & Schreiner 2014). Briefly, Kitui County faces the challenge of insufficient water levels making the community form many cultural imaginations about water, which constrain mine water supply chain.

Methods

The study adopted an explanatory research design. The study required the collection of quantifiable information, which describe the research problem by asking individuals about their opinions and attitude on the cultural aspects constraining mine water supply management. Both primary and secondary data sources were applied in order to achieve the set objectives. Primary data included local views, opinions and perceptions related to mine water supply and the challenges faced. The primary data was obtained through households' visits, field observations and face-to-face interviews from officials in charge of the water sector in the county. Secondary data was obtained from previous studies that were carried out on cultural factors constraining mine water supply management. Relevant publications were other data sources used to relate to the study. Published reports like journals, books and reports also helped to provide information. A total of 300 households were sampled, with medium and low income residential well represented. Selected water bodies in Kitui County being the most focused institutions had a lot to offer in terms of response. Purposive sampling was used to select the households and other actors in the water sector. Data was collected using various methods including questionnaires, oral interviews, field observations and review of literature. Data was analysed using descriptive analysis and presented using statistical techniques. Thematic analysis, which is a data reduction and analysis strategy by which qualitative data are segmented, categorized, summarized and reconstructed in a way that captures the important concepts within the data set, was used.

Findings

Water Scarcity

Respondents were asked to indicate the number of kilometers they walk/travel to get water to estimate the nearness of water sources to the households in Kitui County. Opinions on the sufficiency of water in the county was also sought. This was done in a five level semantic differential questionnaire.

The findings from Table 4.1 indicate that majority of the respondents walk for 30-45 Kilometers to access water, as 18.33% walk for 15-30 Kilometers, 10.67% walk for 1-15 Kilometers and 15% walk for more than 45 kilometers. Only 7.67% walk for less than a kilometer meaning that either they are near the water sources or they have tapped water in their homesteads. This shows that there is difficulty in accessing water in Kitui County making water an important, scarce and valuable resource to the dwellers of the county. On water sufficiency, 47.67% and 43.33% of the respondents indicated that water is extremely scarce and scarce respectively in Kitui County. Out of the 300 households, 0.67% and 3.33% was of the opinion that there is adequate water supply in the region as 5% opted to remain neutral to the enquiry. Views from the water bodies indicate that Kitui County is faced with serious water scarcity challenges. Recurring droughts have diminished water supply, high rates of deforestation have severely reduced water catchment capacity, and population growth and climate change have compounded water shortages. Scarce and coveted, water is a precious commodity and the quantity and quality available in Kitui County often do not match community domestic needs.

Table 1 *Water Scarcity.*

Number of Kilometres	Percentage	Water Insufficiency	Percentages
0-1 Kilometres	7.67	Very adequate	0.67
1-15 Kilometres	10.67	Adequate	3.33
15-30 Kilometres	18.33	Neutral	5
30-45 Kilometres	48.33	Scarce	43.33
Above 45 Kilometres	15	Extremely scarce	47.67
Total	**100**		**100**

Table 2 Monthly Income generated.

Monthly Income (Ksh)	Frequency	Percentage
0-5,000	105	35
5,000-20,000	70	23.33
20,000-40,000	55	18.33
40,000-60,000	45	15
Above 60,000	25	8.33
Total	**300**	**100**

Table 3 Literacy Level of Respondents.

Category	Frequency	Percentage
KCPE and Below	95	31.67
KCSE/O-Level	84	28
Diploma& Certificate	73	24.33
Undergraduate	25	8.33
Postgraduate	23	7.67
Total	**300**	**100**

Poverty Level

According to the information gathered from the questionnaires, the level of income from the residents of the county is low. This made evident that poverty exists in the area, as there were people of percentage 35% who earned less than 5,000 shillings monthly, 23.33% of others earned 5,000-20,000 Shillings, 18.33% earned between 20,000-40,000, 15% earned between 40,000-60,000 as 8.33% of the respondents earned a monthly income of above 60,000 Kenya shillings. The county has high levels of poverty and the local community does not have the available infrastructure and resources to access enough water. Water conservation and storage is challenge to them, as they have no necessary facilities to conserve and access water.

Literacy rate

From the results in Table 3, 31.67% represents the respondents who have schooled up to primary school only as 28% have studies up to secondary school. Few respondents, 24.33% and 8.33% have studied in tertiary institutions earning certificates, diplomas and undergraduate degrees. The rest of the percentage that is 7.67% have studied in universities earning postgraduate degrees. This being evident that the level of education in the area is poor; it brought up a challenge in mine water supply management, as people do not have the knowledge on need for mining activities. There is a lot of illiteracy by the people in the community that makes it difficult to implement mining activities in the region using water as a critical ingredient. The community lacks enough knowledge on good measures to conserve and manage water as a problem. This create stress to the available water resources such as rivers, due to activities such as sand harvesting. The findings also indicate that, women in the county are very much disadvantaged due to the prevailing and past cultural factors that discriminated them. The community believed that women should not go to schools, as their place is the kitchen, a culture that is slowly eroding.

Community Livelihood

Most of respondents concentrated on crop growing (42.66%) as 25% used land for grazing activities; they owned large livestock. A few percentages of 1.67% practices mining and mineral processing which is new to the region. Out of the respondents, 18.67% practiced entrepreneurship and small business as 12% were in formal employment especially from government institutions and local private firms. The entrepreneurship and small business activities includes selling water for a livelihood. The community way of livelihood acted as a hindrance to effective mine water supply management as they do not pay attention to water demanding activities. Much of the water present in the county is directed to livestock management, crop growing and household needs and not for commercialization or industrial use.

Table 4 Community Economic Activity.

Category	Frequency	Percentage
Growing Crops	128	42.66
Livestock keeping & Grazing	75	25
Mining	5	1.67
Entrepreneurship & Small Business	56	18.67
Formal Employment	36	12
Total	**300**	**100**

Table 5 Perceptions on cultural aspects constraining mine water supply.

Respondents' Perceptions On Mine Water Supply	1	2	3	4	5
The Kamba community view water as a precious and scarce commodity thus a great affection to water sources and water use	0%	0%	3.33%	33.3%	63.33%
Mining activities consumes a lot of water leaving little for domestic and agricultural use to locals	1.67%	3.33%	9.33%	66.67%	19%
The livelihood of a community will be destroyed should the water get polluted/quality degrade or water supply fall resulting from use of water in mining	0%	0%	13.33%	46%	40.67%
Water should be reserved for use in the uncertain future as droughts are common and foreseeable in the county	1.33%	12.67%	24.67%	35.33%	26%
Mining companies extract local resources for their profits leaving the community vulnerable than they found them	9.33%	11.67%	21.33%	35%	22.67%
Involvement of the women by miners on matters of water supply is a hindrance to effective implementation and use of water in mining activities	11.33%	12%	30.33%	30.33%	16%
Water supply and Excavation in protected and holy shrine areas cause the local communities to perceive the excavators as the unnecessary evil	20%	20%	20%	24%	16%

Key: 1–Not at all; 2–Small Extent; 3–Moderate Extent, 4–Large Extent, 5–Very Large Extent

The findings of this study indicate that the Kamba community view water as a precious and scarce commodity thus the community has a great affection to water sources and water use. Scarce and coveted, water is a precious commodity and the quantity and quality available in Kitui County often do not match community domestic needs. The community believes that mining activities consumes a lot of water leaving little for domestic and agricultural use to locals. The community believes that water should be reserved for use in the uncertain future, as droughts are common and foreseeable in the county. The community believes that using water in mining pollutes the existing sources of water. Mining can have harmful effects on surrounding surface and groundwater, if proper precautions are not taken. Large amounts of water used for mine drainage, mine cooling, aqueous extraction and other mining processes, increases the potential for chemicals to contaminate ground and surface water, which ultimately has an effect on the health of the local population.

Majority of the households agreed that mining companies extract local resources for their profits leaving the community more vulnerable than they found them. The feeling of not benefiting from the mining activities triggers the unwillingness of the community to facilitate the mines with water supply. Culture of the Kamba community defines the rights, responsibilities and relations between men and women. In Kitui County, the culture is largely patriarchal, giving men dominance over women thus calling for their involvement on mining and water projects. Involvement of females, by miners, on matters of water supply chain management is a hindrance to effective implementation and use of water in mining activities. Men in the county are more involved in decisions. The men are involved in activities that provide them with more access and control of resources, hence decision-making power (Macksembo 2020).

Water supply and excavation in protected and holy shrine areas cause the local communities to perceive the excavators as the unnecessary evil that is a threat to their traditions. This calls for resistance and use of chams for protection. In Kitui County, the communities value their African traditions that is deep rooted in their culture. From the views of the respondents the community had discovered own methods/cultural solutions of managing drought and water problems through traditional customs and rituals. The community believed that lack of rains in the area is a sign of a spiritual imbalances corrected by rites and rituals to appease the gods. Due to the persistent issues of rain unpredictability and lack of modern/Western solutions to prevent drought, the residents of the county had to discover their own methods of managing the environment by invoking traditional customs. Water insufficiency and scarcity forced community members to pull out drums, rattles, whistles, and special dance garbs to invoke the blessings of water spirits

and deities. This justifies the great affection, strong beliefs and value, the community has on water thus responsibly using it for domestic purposes and rarely willing to use water for commercialization or industrial use.

Conclusions

From the findings, it can be concluded that there is difficulty in accessing water and the quantity and quality available do not match community domestics needs in Kitui County; making water, popularly known as Kiw'u, an important, precious and valuable resource to the dwellers of the county. The county has high levels of poverty, illiteracy and the local community has formed several cultural imaginations including beliefs, norms, customs and livelihood, constraining the supply of water for mining activities. The community protects the use of water for mining in the area hindering implementation of mining and extraction activities in the region. Vandalism of mine water supply, opposing supply of water to mining sites is common in the area. There is need for adequate civil education to be undertaken among the resident communities to create awareness that the use of water for mining activities does not mean wastage. Mining companies should also be encouraged to share the water with the residents by undertaking corporate social responsibility activities. The governments, both national and local should work on modalities to ensure that there is sufficient water availability. There is need to build consensus through public participation and factoring in the cultural aspects of the local community before initiating mining extractions and excavations.

Acknowledgements

The authors acknowledge their family for their moral support, continued concern and care of their whereabouts throughout their education life. The authors are also indebted to the entire Taita Taveta University (TTU) and Jomo Kenyatta University of Agriculture and Technology (JKUAT) fraternity for the excellent opportunity granted, relevant support given and the conducive and satisfactory environment created during this research.

References

Abuya WO (2016) Mining conflicts and corporate social responsibility: titanium mining in Kwale, Kenya. *The Extractive Industries and Society*, 3(2), 485-493.

Fernando WA, Ilankoon IS, Syed TH & Yellishetty M (2018) Challenges and opportunities in the removal of Sulfate ions in contaminated mine water: A review. *Minerals Engineering*, 117, 74-90.

Macksembo M (2020) Influence of social cultural factors on implementation of women community projects in Kitui (Unpublished dissertation, University of Nairobi).

Mwaguni S, Ruwa RK, Odhiambo-Ochiewo J & Osore M (2016) Integrated water resources management in a changing climate: the implication of anthropogenic activities on the Tana and Athi/Sabaki Rivers water system for sustainable development. In *Estuaries: A Lifeline of Ecosystem Services in the Western Indian Ocean* (pp. 111-129). Springer, Cham.

Nyaga C (2019) Sustainable WASH Systems Learning Partnership: A Water Infrastructure Audit of Kitui County, University of Oxford.

Shelmith WN (2013) Challenges and Prospects for Effective Water Conservation in Mwingi North District, Kitui County, Kenya.

Van Koppen B & Schreiner B (2014) Moving beyond integrated water resource management: developmental water management in South Africa. International Journal of *Water Resources Development*, 30(3), 543-558.

Author Index

Keyword Index

These Proceedings of the postponed International Mine Water Association 2020 Congress in Christchurch, New Zealand include the submitted papers of the peer-reviewed abstracts of the vibrant community of scholars, practitioners, experts in mine water management, mine water treatment and environmental restoration on the global and local levels. A number of diverse topics are reflected throughout these Proceedings. They all contribute to the theme “Mine Water Solutions” and discuss the most burning issues of finding new solutions and bringing cutting-edge technologies into mine water treatment and preventing damage to the unique environments and ecosystems in different corners of the world. The Proceedings offer an outstanding opportunity to acquire the most advanced methods derived from interdisciplinary research and expertise in the field of mine water worldwide.

ISBN 978-3-00-067297-2